PhD advisor:

Dr. Ir. J. Tramper
Professor Bioprocess Engineering
Wageningen Agricultural University

Co-advisors:

Dr. Dipl.-Ing. G. Schmid
Head Cell-Culture Pilot Plant
Hoffmann-La Roche, Ltd., Basel

Dr. Ir. C.D. de Gooijer
Associate Professor at the Food- and Bioprocess-Engineering Group
Wageningen Agricultural University

Metabolic-flux analysis of mammalian-cell culture

Hendrik P.J. Bonarius

Hendrik P.J. Bonarius

Metabolic-flux analysis of mammalian-cell culture

Proefschrift
ter verkrijging van de graad van doctor
op gezag van de rector magnificus
van de Landbouwuniversiteit Wageningen,
dr. C.M. Karssen,
in het openbaar te verdedigen
op vrijdag 2 oktober 1998
des namiddags te twee uur in de aula.

UB [illegible]

ISBN 90-5485-839-7

Picture: CHO cells on microcarriers. Credits: Ole Skyggebjerg.
Drawings: Flux analysis of cyclic pathways. Credits: Chris de Smidt.

BIBLIOTHEEK
LANDBOUWUNIVERSITEIT
WAGENINGEN

Voorwoord

In 1991, tijdens mijn stage in Basel, fietste ik terug naar huis. Omdat het mooi weer was fietste ik even om langs de Rijnoever. Bij toeval kwam ik een medestudent tegen uit Wageningen. Hij vertelde me dat er een onderzoeksplaats beschikbaar was gekomen bij Hoffmann-la Roche voor een procestechnoloog. De volgende morgen belde ik direkt Hans Tramper en 3 dagen later zat ik bij Georg Schmid in the lab. Nu, in 1998, ligt er een proefschrift. Het is het resultaat van een samenwerking tussen een bedrijf en een universiteit, en later kwam er nog een universiteit bij, en tot slot het ik een groot deel geschreven bij weer een ander bedrijf. Er zijn daarom veel mensen die op verschillende wijze hebben bijgedragen aan de totstandkoming van dit boek.

Georg, it was a pleasure to work with you and I have learnt a lot - and maybe should have learnt more- from your precision and attention for details in scientific writing and working. When I needed something (from an analysis of metabolites to money for traveling), you always helped me to get what I wanted. Thanks a lot for creating the conditions for this work, and I hope we can collaborate some time in the future!
Dr. Leuenberger, thank you very much for giving me the freedom to do research in an exciting industrial environment. Nathalie, I was lucky to share the lab with you, thanks for your patience, helpfulness, and good mood.

Furthermore, I would like to thank many others at the Department of PRP-Biotechnology for their hospitality and their contribution to the work described in this thesis: Dr. Schlaeger, Dr. Weibel, Dr. Wipf, Jean-Marie, Christel, Agnes, Klaus, and Martin. I also received help from people in other departments at Hoffmann-La Roche, and I would like to mention Helga Fitzke, Mr. Oesterhelt and Martine Pozeg.

De hulp van studenten uit Wageningen is heel belangrijk geweest voor dit proefschrift, en hun resultaten zijn direkt terug te vinden in verschillende hoofdstukken. Koen Meesters, José Houtman, René Kesseleer, Ronald Neeleman, Bram Timmerarends, en Geuko Bosker. Dank jullie wel voor jullie inspiratie, inzet, en plezier !

In 1995, I had the opportunity to work in Elmar Heinzle's lab at the Department of Chemical Engineering of the ETH in Zürich. Elmar, it was pleasure to work with you and your experience with mass spectrometry has been critical for the project. Together with Ahmet Özemre, we ran many continuous-culture experiments in a short time. Thanks a lot Ahmet, without your dedication I couldn't have finished Chapter 5. I also would like to acknowledge Dr. Skrabal and Felix Bangert for the NMR experiments and interpretations, Urs Seineke for the design and fabrication of the 100 ml bioreactor, and Evelyn Blochilger for help with the lyophilization apparatus.

In Zürich I could stay at Vassily's place. Thanks Vassily for the collaboration, I enjoyed the long discussions, the tram to the hospital, and the dinners at Boccalino very much.

Hans en Kees, jullie begeleiding vanuit Wageningen is heel belangrijk geweest. Toen ik voorstelde om met fluxanalyse te beginnen, hebben jullie het direkt opgepakt en gestimuleerd om het door te zetten. Hans, dank je voor de vrijheid die je me hebt gegeven en de correcties die ik nodig had om niet te kort door de bocht te gaan. Kees, dankjewel voor je vele tips en handigheden die voorkwamen dat ik het wiel niet voor de tweede keer uitvond.

This thesis has been completed while I was working at Novo Nordisk, where I was generously allowed to use hard- and software. Leif, this is greatly appreciated, tak skal du have !

Papa en mama, jullie hebben vanaf het begin vol achter dit projekt gestaan. Ik heb enorm geluk gehad dat ik van jullie de stimulans en kans heb gekregen om te doen wat ik wil. Ik geniet er heel van en ik hoop dat ik dat in de toekomst nog met jullie kan delen.

Lieve Ellen, ik wil niet anders dan weer bij te zijn.

Aan mijn ouders

Contents

Chapter 1

Flux Analysis of Underdetermined Metabolic Networks: The Quest for the Missing Constraints

Hendrik P.J. Bonarius,
Georg Schmid,
and Johannes Tramper.

ABSTRACT

Metabolic-flux balancing has become an important tool for the quantitative analysis of the physiology of microorganisms and mammalian cells. It has successfully been applied to trace potential sites for metabolic engineering, to determine metabolic capabilities and to design optimal medium compositions and feeding strategies. Traditionally, the intracellular fluxes of complex metabolic networks have been quantified by isotopic-tracer experiments. As this approach has practical limitations 'metabolic-flux balancing' is emerging as a feasible alternative. A fundamental problem of this method is that metabolic networks, and in particular cyclic metabolic pathways, are underdetermined. The search for constraints which can be used to correctly determine fluxes for a range of different conditions offers an exciting challenge.

INTRODUCTION

Microorganisms are widely exploited for the synthesis of proteins or low molecular weight compounds. Their metabolism is used to transform substrates into a wide variety of products. As with chemical-production plants, the flux distribution determines the efficiency of the production process. In biological systems, nutrients are only partly used for biomass and product synthesis and for energy supply. Besides, waste-products accumulate and abundant energy dissipates in futile cycles. In order to optimize the capacity of microbial metabolism, and thus increase yields, the intracellular metabolite flows have to be quantified.

Traditionally, metabolic fluxes have been determined by isotopic-tracer experiments. As the carbon stoichiometry of metabolic reactions is known, it is possible to determine the fluxes at certain branch points by tracing the metabolic fate of carbon-labeled substrates. Although these isotopic-tracer techniques are well established and have been significantly improved, particularly by the application of NMR technology to biological systems (Schulman et al., 1979), they are laborious and expensive to conduct, and cannot be used on an industrial scale. As an alternative, 'metabolic-flux balancing' (Varma and Palsson, 1994) which only requires the measurement of extracellular metabolites (Box 1), has been proposed as a means to determine the flow through primary metabolic pathways (Vallino and Stephanopoulos, 1990).

Data from isotopic-tracer experiments have thus been supplemented with mass-balance equations of the relevant metabolites for the determination of fluxes in entire metabolic networks (Blum and Stein, 1982; Marx et al., 1996; Zupke and Stephanopoulos, 1994; Bonarius et al., 1998d). Additionally, computational methods have been developed to combine these different types of information, allowing the calculation of metabolic fluxes with a minimum of algebraic manipulation (Marx et al., 1996; Zupke and Stephanopoulos, 1994). For industrial applications, however, it is desirable to determine intracellular metabolic fluxes by metabolic-flux balancing alone. Since no isotopically-labeled substrate is required,

the estimation of fluxes from mass balances (see Glossary) can be made in virtually any biological or reactor system regardless of scale.

Box 1

Principles of metabolic-flux balancing

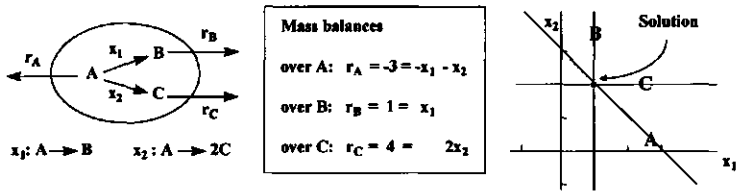

Principles of metabolic-flux balancing. (Numerical values are chosen arbitrarily.)

Metabolic-flux balancing techniques are based on relatively simple linear algebra. If the stoichiometry of the relevant intracellular reactions and the cellular composition are known, and the uptake and secretion rates of the relevant metabolites (for example r_A, r_B and r_C in the figure) have been measured, the reaction rates (x_1 and x_2 in the figure) can be determined using the appropriate mass-balance equations. A reaction network is shown for which one unique solution for the variables x_1 and x_2 can be estimated by least-squares analysis of mass balances A, B, and C. The least-squares method, which is used here because there are more constraints (mass balances) than unknowns (fluxes), is calculated by (pseudo)inverting stoichiometric matrix A (Vallino and Stephanopoulos, 1990);

$$Ax = r \quad \Leftrightarrow \quad A^T Ax = A^T r \quad \Leftrightarrow \quad x = (A^T A)^{-1} A^T r$$

For the stoichiometry and measured metabolic rates given in the figure this equation reads

$$\begin{bmatrix} -1 & -1 \\ 1 & 0 \\ 0 & 2 \end{bmatrix} \cdot \begin{bmatrix} x_1 \\ x_2 \end{bmatrix} = \begin{bmatrix} r_A \\ r_B \\ r_C \end{bmatrix} \quad \Leftrightarrow \begin{bmatrix} x_1 \\ x_2 \end{bmatrix} = \frac{1}{9} \begin{bmatrix} 5 & -1 \\ -1 & 2 \end{bmatrix} \cdot \begin{bmatrix} -1 & 1 & 0 \\ -1 & 0 & 2 \end{bmatrix} \cdot \begin{bmatrix} -3 \\ 1 \\ 4 \end{bmatrix} = \begin{bmatrix} 1 \\ 2 \end{bmatrix}$$

This shows that intracellular fluxes can be quantified by measuring only the uptake and secretion rates of the relevant metabolites.

On-line applications of 'crude' stoichiometric analysis have already been shown to be effective as a means of improving production yields in fermentation processes (Wang et al., 1979). It is theoretically possible to measure and control

Glossary

Balanceable metabolite. A metabolite whose mass balance can be closed.

Condition number of stoichiometric matrix. The condition number of matrix stoichiometric matrix **A** -the ratio of the largest to smallest eigenvalue of **A**- measures the sensitivity of the equation $\mathbf{Ax} = \mathbf{r}$ (Box 1).

Directionality constraint. The demand that a (number of) flux(es) is non-negative.

Linear-dependent metabolite balances. Metabolite balances are linear dependent if (a combination of) the solution planes determined by the metabolite-balances are parallel. (For example, the metabolite balances of A and B in Fig. 2 are linear dependent.)

Metabolite (or 'mass') balance. An equation that describes the accumulation and all relevant incoming and outgoing fluxes of a metabolite pool.

Observability. Here, the extent to which intracellular metabolic fluxes can be determined by the measurement of the extracellular metabolic rates and the biomass composition.

Rank of stoichiometric matrix. The maximum number of linear-independent metabolite balances in a metabolic network is defined as the rank of the stoichiometric matrix. If the rank is smaller than the number of metabolic fluxes (the number of rows of the stoichiometric matrix), the metabolic network is **rank deficient**.

Stoichiometric matrix. Matrix that contains information of the reaction stoichiometry of cellular metabolism (f.e., **A** in Box 1). The rows and the columns of the stoichiometric matrix are associated with the metabolite balances and the metabolic fluxes, respectively.

Underdetermined networks. Rank-deficient metabolic networks are designated 'underdetermined' to indicate that there are insufficient linear-independent metabolite balances to determine the intracellular metabolic fluxes.

metabolic conversions on the level of single enzymatic reactions by metabolic-flux balancing techniques, with the measurement of only a limited number of extracellular metabolites (Van Gulik and Heijnen, 1995). Apart from controlling complex metabolic networks or tracing potential site for metabolic engineering, other applications such as rational medium design (Xie and Wang, 1994), elucidation of metabolic and toxicological effects, location of metabolic control (Kacser and Burns, 1973), determination of maximum theoretical yields (Varma and Palsson, 1993), and a quantitative prediction of biochemical phenotypes from gene data banks (Palsson, 1997), will all benefit from this computational technique. In this review, the fundamental problem that currently hinders the development of such a method is discussed, and various proposed solutions are reviewed. Finally, experiments are suggested to investigate which of these solutions might lead to a method for quantifying metabolic fluxes using only mass balances.

PROBLEM DEFINITION

Two fundamental problems have been identified in applying this technique to large, complex metabolic networks (Vallino and Stephanopoulos, 1990). First, the estimated flux vector, which is calculated by the least-squares method, may be sensitive to slight perturbations in the measured extracellular rates (r_i in Box 1). This sensitivity to error propagation can be checked by calculating the condition number of the system (Vallino and Stephanopoulos, 1990; Savinell and Palsson, 1992a), which depends solely on the reaction stoichiometry of the metabolic network. In Figure 1 the condition number (see Glossary) can be seen to increase with the complexity (Fig. 1a) and the ratio of stoichiometric coefficients (Fig. 2b). A large condition number (>100) indicates that the estimated flux distribution is sensitive to measurement errors. Combinations of reactions that cause network sensitivities can be identified using an algorithm developed by Savinell and Palsson (1992a). The flows through these reactions either have to be determined independently by isotopic-tracer experiments or have to be removed from the network. However, with a few exceptions (Savinell and Palsson, 1992b), the condition number of a metabolic network is generally small (< 100), which

indicates that error propagation is insignificant (Vallino and Stephanopoulos, 1990). Nevertheless, the condition number of the stoichiometric matrix should be determined prior to least-squares analysis.

Figure 1

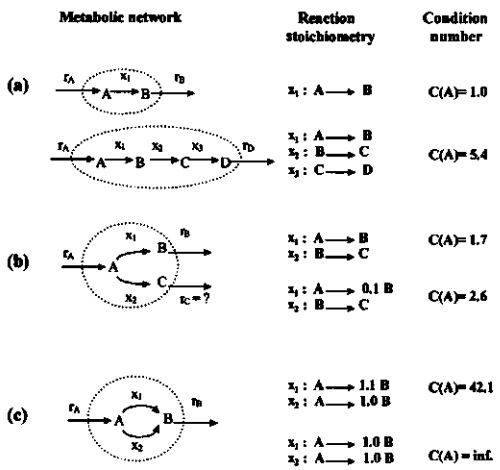

The error sensitivity of a metabolic network is only dependent on the reaction stoichiometry and can be determined by the condition number of the stoichiometric matrix (Vallino and Stephanopoulos, 1990). (a) The condition number increases with growing complexity. (b) If only r_A and r_B are known, the fluxes x_1 and x_2 can be estimated. It is shown that the condition number increases with the ratio of the stoichiometric coefficients. (c) Networks which contain cyclic pathways are error sensitive or not observable ($C(A) = \infty$).

A special case of error-sensitive metabolic networks is reaction dependency (Figure 1c). In contrast to error propagation, this causes observability problems in the determination of the fluxes in the metabolic networks of almost all prokaryotic (Noorman et al., 1991; Savinell and Palsson, 1992a; Vallino and Stephanopoulos, 1993; Van Gulik and Heijnen, 1995; Varma and Palsson, 1993; Sauer et al., 1996) and eukaryotic (Fell and Small, 1986; Savinell and Palsson, 1992a; Bonarius et al., 1996) cells. Reaction dependency occurs particularly due to cyclic pathways, which

are abundantly present in metabolic systems. In Figure 2a the problem associated with a cyclic metabolic pathway is visualized.

Figure 2

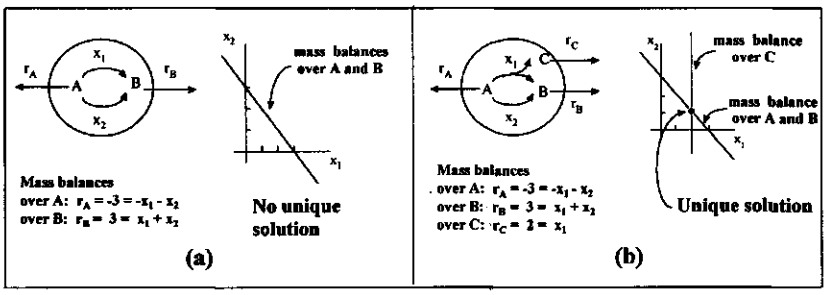

An undetermined (a) and a determined (b) metabolic network. (a) Reactions x_1 and x_2 are linear dependent. (Numerical values are chosen arbitrarily.)

Reactions in metabolic cycles are linear dependent and cannot be derived from the extracellular measured rates. In a metabolic network such reactions cause singularities, as a result of which the set of mass balance equations is underdetermined. It is also apparent that the mass-balance equations of metabolites A and B yield the same information, as a result of which the fluxes 1 and 2 cannot be quantified solely by flux-balancing techniques. In this case, the solution space that contains all admissible solutions for fluxes x_1 and x_2 can be visualized by a single line (Fig. 2a). Underdetermined networks such as that shown in Figure 2a are rank deficient.

THEORETICAL AND EXPERIMENTAL SOLUTIONS

In the last years, various approaches have been proposed to estimate fluxes of large, complex metabolic networks by supplementing the underdetermined network with various theoretical assumptions or constraints (Fell and Small, 1986; Vallino and Stephanopoulos, 1990; Vallino and Stephanopoulos, 1993; Varma and Palsson, 1993; Van Gulik and Heijnen, 1995; Bonarius et al., 1996; Sauer et al., 1996; Pons

et al., 1996). This accounts in particular for fluxes in major metabolic cycles such as the TCA cycle, the pentose phosphate cycle, and the malate shunt (The quantification of fluxes in "futile cycles", where there is no branching off the cycle (Fell, 1990), is not covered in this review). Currently, several research groups are comparing flux distributions estimated on the basis of such assumptions with experimentally determined fluxes using isotopic-tracer methods (Schmidt et al., 1998; Bonarius et al., 1998b). Here, several 'candidate' constraints are reviewed and control experiments are suggested in order to find a method for the determination of intracellular fluxes without using isotopic tracers.

Mass balances of co-factors or co-metabolites as additional constraints

When a co-metabolite is produced or consumed in cyclic pathway reactions, the addition of its mass balance may yield a unique solution. In Figure 2b it is shown that a least-squares solution exists for a cyclic pathway when the mass balance of metabolite C is added to the network. In reality, addition of the mass balance(s) of co-metabolites is generally not sufficient to generate an (over)determined system. In complex networks, co-metabolites are either produced in more than one cyclic pathway, for example carbon dioxide, or are not balanceable, such as ATP. In most organisms, carbon dioxide is produced in the pentose cycle, the TCA cycle and the malate shunt and consumed in the pyruvate carboxylase reaction (Fig. 3). Therefore, the addition of the carbon-dioxide balance to the metabolic network will not allow an independent determination of the fluxes in these cycles. Nevertheless, useful information can be obtained from the carbon dioxide production rate, as it provides a means of checking the consistency of the estimated fluxes with respect to the carbon balance.

By addition of the ATP balance to a metabolic network such as shown in Figure 3, the rank of the stoichiometric matrix increases with one unit. As a result the observability increases, and the split ratio of fluxes at either the glucose-6-phosphate or the pyruvate branch-point can be determined. However, the ATP mass balance cannot be closed due to the fact that both ATP yields and ATP

requirements for maintenance processes can only be estimated (Savinell and Palsson, 1992b; Van Gulik and Heijnen, 1995). It has been suggested that theoretical calculations of ATP yields result in significantly higher levels than can be deduced from experimental data (Verduyn et al., 1990). Moreover, relatively small changes in such estimations will have large effects on the calculated flux distribution (Bonarius et al., 1998b).

Figure 3

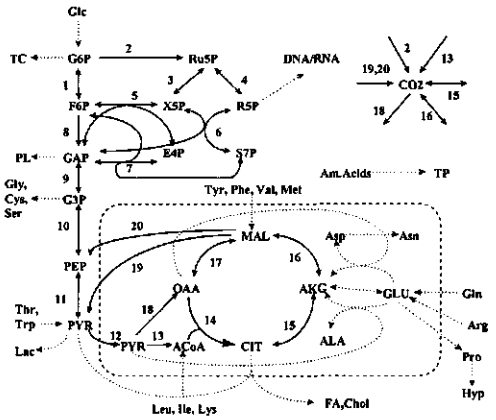

Metabolic pathways of hybridoma cells. Dashed arrows indicate fluxes which can be quantified using mass balances. Solid, numbered arrows represent fluxes that are linear dependent and consequently not calculable using balancing techniques. (The dashed line represents the mitochondrial membrane.) Abbreviations: ACoA acetyl-CoA, AKG α-ketoglutarate, CHOL cholesterol, CIT citrate, E4P erythrose-4-phosphate, GAP glyceraldehyde 3-phosphate, GLC glucose, G6P glucose-6-phosphate, G3P 3-Phosphoglycerate, LAC lactate, MAL malate, OAA plus oxaloactetate, PEP phosphoenolpyruvate, PYR pyruvate, R5P ribose-5-phosphate, Ru5P ribulose-5-phosphate, S7P sedoheptulose-7-phosphate, TC total carbohydrates, TP total protein, X5P xylulose-5-phosphate.

The mass balances of reducing equivalents, for example NADH and NADPH, are often used to determine the split ratio of metabolic fluxes at branch points, such as occur in the metabolism at (phosphoenol)pyruvate or glucose-6-phosphate (Savinell

and Palsson, 1992a; Vallino and Stephanopoulos, 1993; Van Gulik and Heijnen, 1995; Bonarius et al., 1996). However, microorganisms interconvert these co-factors with unknown reaction rates using transhydrogenases. Therefore, in order to estimate fluxes in underdetermined networks, NADH and NADPH should be used as a lumped factor to circumvent the problem of transhydrogenase activity (Bonarius et al., 1996). As a consequence, the split ratio of only one branch point (instead of two) can be estimated. Additionally, it has been shown for liver cells (Fell and Small, 1986), hybridomas (Bonarius et al., 1998b) and *Bacillus subtilis* (Sauer et al., 1996) that the estimated flux distribution is very sensitive to the assumptions made or to small changes in the NAD(P)H balance.

Irreversibility of reactions as additional constraints

Some reactions in metabolic networks are considered irreversible. This additional information allows one to set lower boundaries to these particular reactions and to further constrain the solution space, in which all admissible solutions are situated. Although these constraints do not help to overcome observability problems, they can be used to fine tune the unconstrained solution to equation in Box 1 (Vallino and Stephanopoulos, 1993), if certain fluxes are negative where they should be irreversible, i.e. 0. An algorithm for the determination of all non-negative, admissible fluxes has been described (Schuster and Schuster, 1993). This computational method was applied to describe the basic reaction modes at the corner points of admissible solution space in cyclic pathways (Schuster and Hilgetag, 1994) and to determine optimal flux distributions for the conversion of sugars to aromatic metabolites in *Escherichia coli* (Liao et al, 1996). Further, directionality constraints are essential when applying linear optimization techniques, as will be shown below.

Objective functions as additional constraints; linear optimization

As pointed out above, the mass balances of co-factors such as ATP and NADH can either be closed by mere approximation or not be closed at all, as certain biochemical parameters are not quantifiable. Instead, these mass balances can be used to formulate objective functions. Intracellular pools of co-factors for the transfer of energy or reducing power regulate many enzymatic reactions. Therefore, a surplus of, or a need for, these co-metabolites influences the flux distribution of entire metabolic networks. The metabolic pressure from such needs may be translated into linear objective functions and help to estimate optimal solutions that satisfy various metabolic goals (Fell and Small, 1986). Objective functions that can be applied to estimate fluxes in cyclic routes include, for example, 'maximize NADPH production' (Fell and Small, 1986), 'minimize ATP production' (Savinell and Palsson, 1992a) or 'minimize the sum of the squares of fluxes' (Bonarius et al., 1996).

Figure 4

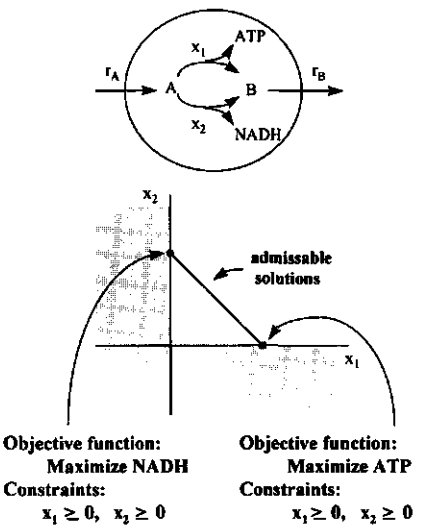

Linear-optimization techniques to estimate fluxes in underdetermined metabolic networks.

Optimal solutions can be calculated using linear-optimization techniques. The principle of applying these techniques to estimate fluxes in underdetermined metabolic networks is shown in Figure 4. By definition, linear optimization results in extreme ('optimal') solutions, i.e., the end points of the stoichiometrically feasible domain (Varma and Palsson, 1994). In some cases certain objective functions have no feasible solutions due to lack of lower or upper boundaries of cyclic routes. In Figure 4 for example, this would be the case if the objective function is 'maximize NADH' and if the flux x_1 is *not* constrained instead of irreversible. Lower boundaries (which are determined by the irreversibility of fluxes) are essential for obtaining a feasible solution by linear optimization, especially because data for maximum reaction rates are not usually available. However, it is unclear whether the end points of the solution space that is constrained by the mass balance equations really represent the true flux distributions. The answer to this question can be found by isotopic-tracer experiments.

Finding the missing constraint

Little research has been carried out to validate the theoretical assumptions that are required to determine fluxes in rank-deficient networks by isotopic-tracer methods. Therefore, it is now desirable to compare the estimated flux distributions on the basis of mass balances and labeling experiments for a large range of growth conditions in order to obtain a fundamental understanding of the effects of different constraints and to investigate whether certain theoretical assumptions are generally valid. There are various methods for inducing drastic changes in the primary metabolism of microorganisms. A limitation of important carbon- or nitrogen sources, or electron acceptors (oxygen), will force microorganisms to rearrange their flux distribution. Alternatively, an increase in the growth rate, which can be induced by raising the dilution rate of cells in continuous culture, would result in an elevated NADPH requirement for anabolic processes. Theoretically, this will result in higher activity of two cyclic pathways, the pentose-phosphate shunt and the malate shunt. Another possible method for specifically stimulating certain fluxes is

the addition of sub-lethal concentrations of toxic compounds with known effects on metabolism. For example, phenazine methosulphate specifically reoxidates NADH and NADPH (Dickens and McIlwain, 1938), resulting in an increase in NAD(P)H-producing reactions. In this case, the constraint 'maximize NADH and NADPH production' would theoretically result in an estimated flux distribution that is similar to the experimentally determined fluxes. Similarly, chemical decouplers of oxidative phosphorylation, such as 2,4-dinitrophenol, will lower the activity of the TCA cycle. Fluxes determined from mass balances supplemented with data from isotopic-tracer methods, combined with fluxes estimated from mass balances supplemented with different theoretical constraints may lead to a fundamental understanding of the validity of the assumptions previously made (Fell and Small, 1986; Savinell and Palsson, 1992a; Vallino and Stephanopoulos, 1993; Van Gulik and Heijnen, 1995; Bonarius et al., 1996; Sauer et al., 1996). In addition, the combined information from mass-balancing techniques and isotopic-tracer experiments will allow to test the consistency of both methods, as their combination renders overdetermined networks. This is relevant, because the use of isotope tracers for the determination of fluxes is not a solved problem (Larrabee, 1989).

In addition, there are some alternatives, that do not require the demanding effort of isotopic- tracer studies, which may help to solve the observability problems of rank-deficient metabolic networks.

Firstly, various studies have already reported quantitative flux data of entire metabolic networks, which were determined using a set of isotopic-tracer sources (Blum and Stein, 1982; Mancuso et al., 1994). From these data (vector **x**), the extracellular metabolic rates (vector **r**) can easily be determined using the equation in Box 1. Subsequently, the constraints determined by the mass balances and the metabolic rates can be calculated and various theoretical constraints can be tested for their ability to correctly estimate the fluxes.

Secondly, the presence of certain single enzyme reactions in metabolic networks causes singularities in the linear set of equations that describes these networks. For example, the pyruvate carboxylase and the transhydrogenase reaction directly cause observability problems. In some cases, however, these enzymes are

not active (Mancuso et al., 1994), a feature which can easily be measured using enzymatic assays. Indeed if no enzymatic activity is found, the particular flux can be deleted and the observability improved.

Thirdly, for several organisms, the estimated flux distribution, and in particular the split ratio at the glucose-6-phophate branchpoint, has been shown to be overly sensitive to the NAD(P)H balance (Bonarius et al., 1998b). As this balance is mainly dependent on the rate of oxygen uptake, improvement in the accuracy of this measurement may lead to completely observable metabolic networks. Additionally, a weighted least-squares solution could be used to account for uncertainties in mass balances such as the NAD(P)H balance.

OUTLOOK

The near future will show whether investigations (such as some of those suggested here) will lead to a universally valid method for the measurement of intracellular fluxes. In the past, it has been regarded as unwise to make generalizations about the metabolic role of futile cycles, because the lack of available experimental flux data under *in vivo* conditions (Fell, 1990). In contrast, this will not be the case for other metabolic cycles such as the pentose shunt, the malate shunt and the TCA cycle. As metabolic pathways have become targets for genetic and biochemical engineers to improve yields of cell lines, the number of isotopic-tracer studies under well-defined conditions will increase. The resulting data may provide a basis for a quantitative understanding of metabolism and help to find missing constraints. Until then, however, isotopic-tracer experiments remain indispensable for the quantification of fluxes in cyclic metabolic pathways.

Other applications, such as rational medium design (Xie and Wang, 1994), elucidation of metabolic and toxicological effects without using radioactive or stable isotopes, rapid quantitative biochemical studies and determination of metabolic-control coefficients (Kacser and Burns, 1973) (For a recent review on the role of Metabolic Control Analysis for rational bioengineering see Westerhoff and Kell (1996)) will benefit from such a breakthrough as well. In addition, it would be

possible to control fermentation processes on the level of intracellular reactions by calculating the metabolic fluxes from on-line measurement data of only a few key metabolites. The experimental validation of theoretical constraints will extend our knowledge of the metabolic strategy of various cell lines. Likewise, such constraints can be used as a link between genetics and physiology (Palsson, 1997), and thus help to predict phenotypes from genome data banks.

ACKNOWLEDGEMENTS

We thank Michael Ibba for critical reading of the manuscript and Bram Timmerarends for the design of Figure 4.

Chapter 2

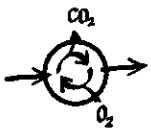

Determination of the Respiration Quotient in Mammalian-Cell Culture in Bicarbonate Buffered Media

Hendrik P.J. Bonarius, Cornelis D. De Gooijer,
Johannes Tramper, and Georg Schmid.

ABSTRACT

The determination of the respiration quotient (RQ = CER/OUR) has so far not been used as a tool for understanding animal cell metabolism. This is due to problems in measuring the carbon dioxide evolution rate (CER) rather than the oxygen uptake rate (OUR). The determination of the CER is complicated by the use of bicarbonate in the medium. Using liquid and gas balances we have derived an equation for continuous culture to quantify the amount of CO_2 that comes from the bicarbonate in the feed. Under cell-free conditions values predicted by this equation agree within 4 % with the experimental results. In continuous culture using hybridoma cells the CO_2 from the feed as determined by an IR-gasanalyzer was found to represent a significant amount of the total measured CO_2 in the off-gas (50 % in a suboptimal and 30 % in a high-growth medium). Further, the problem of CO_2 loss from the medium during medium preparation and storage was solved using both a theoretical and an experimental approach.

For two different growth media RQ values in continuous culture were evaluated. Small but significant differences in RQ were measured, which were matched by differences in specific antibody rates and other metabolic quotients. In a medium with Primatone RL, an enzymatic hydrolysate of animal tissue that causes a more than two-fold increase in cell density, the RQ was found to be 1.05, whereas in medium without Primatone RL (but containing amino acids equivalent in composition and concentration to Primatone RL) the RQ was found to be 0.97. We suggest the RQ to be a useful parameter for estimating the physiological state of cells. Its determination could be a suitable tool for both the on-line control of animal cell cultivations and the understanding of cell metabolism.

INTRODUCTION

Organisms in aerobic fermentations consume oxygen and produce carbon dioxide with rates called the oxygen uptake rate (OUR) and the carbon dioxide evolution rate (CER), the ratio of which (CER/OUR) is called the respiration quotient (RQ). In yeast fermentations RQ's have a value around unity during oxidative growth and correlate with ethanol formation (Wang et al., 1977) as well as nucleic acid and protein content (Nyiri et al., 1975). The RQ value is a key metabolic parameter, that is independent of cell number and can be measured on-line. It reflects the physiological state of cells and varies inevitably with the nature of substrates and products. By means of RQ measurements it has been possible to close mass balances and to determine metabolic flux distributions for prokaryotes and yeast (De Kok and Roels, 1980; Papoutsakis and Meyer, 1985; Roels, 1983; Vallino and Stephanopoulos, 1993). RQ data can also be used for on-line bioreactor control, for example to minimize glucose effects (Wang et al., 1979) or to optimize substrate consumption in yeast (Wu and Wang, 1993).

To our knowledge the respiration quotient has never been determined in bicarbonate buffered animal cell cultures. The reason for this lies in difficulties in measuring the CER rather than the OUR; the use of a bicarbonate buffer system in cell culture media complicates the measurement of the CER. By measuring CO_2 in the culture or in

the outlet gas of the bioreactor a substantial amount of CO_2 from the buffer system will be measured, and not only the CO_2 that is produced by cells.

Basically, there are two ways to solve this problem. The first option is to adapt cells to a bicarbonate-free medium. When replacing bicarbonate by other buffer systems like HEPES and additional NaCl (Schmid et al., 1990), it should be possible to determine the CER simply by measuring the CO_2 concentrations in the inlet and outlet gases (Heinzle, 1992; Royce, 1992), when liquid phase accumulation and relatively high solubility of CO_2 is taken into account. However, not all cell lines adapt to other buffer systems and high inoculation levels and also high cell densities throughout the cultivation are required to cultivate cells in bicarbonate-free medium. Recently we were able to grow cells in a commercially available bicarbonate-free organic buffer system. This was only possible at high cell densities (Bonarius et al., 1995b). Under similar conditions at low cell densities pCO_2 levels are not sufficient for further proliferation. Either CO_2 has to be added or k_la values have to be reduced to maintain required pCO_2 levels. A different buffer system (which causes differences in pCO_2) also influences cell metabolism. For example, it was found that fibroblasts grown in HEPES buffered medium took up a five-fold amount of glucose, when 50 mM bicarbonate was added to the medium (Amos et al., 1976). It has been shown that bicarbonate is required for intracellular pH regulation via two HCO_3^- transporters (Ganz et al., 1989). Therefore, cultivation in bicarbonate-free media can cause experimental bias.

We have chosen an other approach to determine the CER under commonly used (i.e. bicarbonate buffered) culture conditions. The total amount of CO_2 (the sum of CO_2 from the medium and from the cells) in the outlet gas is measured and the amount of CO_2 that is coming from the medium is calculated. To validate this calculation the CO_2 in the outlet gas in continuous culture under cell-free conditions is measured. Furthermore, due to CO_2 evaporation from the medium during medium preparation and storage the amount of CO_2 and bicarbonate in the ingoing medium was not constant. It is also shown how this problem can be solved both theoretically and experimentally.

THEORY

The respiration quotient can be defined as the carbon dioxide evolution rate divided by the oxygen uptake rate:

$$RQ = \frac{CER}{OUR} \qquad (1)$$

Oxygen Uptake Rate

At steady state conditions (pO_2 constant) the OUR of a continuous culture can be calculated from the mass transfer coefficient for oxygen $k_l^{O2}a$ and the fraction of oxygen in the inlet gas under the assumption that the gas and the liquid phase are ideally mixed and that the gasflow is high so that $x_{O2}^{\ i} = x_{O2}^{\ o}$ (Van 't Riet and Tramper, 1991). At reasonable cell densities, the dissolved oxygen in the inlet and outlet liquid phase can be neglected.

$$OUR = k_l^{O_2}a\,(C_{O_2}^{*}(t) - C_{O_2}(t)) \qquad (2)$$

Carbon dioxide Evolution Rate

In contrast to the determination of the OUR, CER measurements are hindered by several causes. Carbon dioxide that is produced by the cells will be hydrated and subsequently dissociated into bicarbonate and carbonate. Hence, the solubility of carbon dioxide will be much higher than the solubility of oxygen and it will accumulate to a significant extent in the liquid phase. Also, the solubility will change as a function of pH. Therefore, either accumulation kinetics have to be included or the experimental set-up has to exclude (liquid phase) accumulation. Typically, a continuous culture can be applied to require steady state pCO_2 levels. However, three problems concerning CER measurements will remain in continuous mammalian cell culture. First, the concentration of CO_2 (species) in the liquid phase has to be determined accurately to complete the CO_2 balance. Second, as discussed above, the bicarbonate in the ingoing medium will potentially be released into the gas phase. This other source of

CO_2 has to be quantified separately in order to determine the carbon dioxide that is produced by the cells. When we carried out continuous culture experiments we encountered a third obstacle. Carbon dioxide evaporates during medium preparation and storage from the medium tank into the surrounding atmosphere. Therefore, the contribution of the bicarbonate buffer from the medium to the carbon dioxide in the outlet gas will not be constant. The problem of CO_2 loss from the medium occurs beyond the bioreactor system and will be discussed separately below.

Bicarbonate controls the pH as result of the following equilibria:

$$CO_2 + H_2O \Leftrightarrow H_2CO_3 \Leftrightarrow H^+ + HCO_3^- \Leftrightarrow 2H^+ + CO_3^{2-}$$

It should be noted that only CO_2 can be exchanged with the gas phase. Under standard cell culture conditions this reaction scheme can be simplified. Because the reactor pH has a value of 7.0 - 7.2, the amount of H_2CO_3 and CO_3^{2-} in the liquid phase is less than 1% of the number of moles of HCO_3^- and CO_2 (Bailey and Ollis, 1986):

$$CO_2 + H_2O \Leftrightarrow HCO_3^- + H^+$$

This simplified equilibrium is used for deriving all necessary balances for the bicarbonate system in a continuous culture as is depicted in Figure 1.

In our further analysis for the liquid phase the concentrations of CO_2 and HCO_3^- will be combined to define the lumped parameter C_A as the sum of C_{CO2} and C_{HCO3} ($C_A = C_{CO2} + C_{HCO3}$). For the gas phase only CO_2 will be used in the mass balance. This approach is pivotal for the theoretical correction for bicarbonate in the measurement of the CER.

When the pH is kept constant, CO_2 and HCO_3^- are in equilibrium (equilibrium constant $K_1 = (C_{HCO3}C_H)/C_{CO2} = 4.21*10^{-7}$ mol l^{-1}) according to:

$$C_{CO_2}(t) = \frac{C_A(t)}{1 + \frac{K_1}{10^{-pH}}} \qquad (3)$$

Figure 1

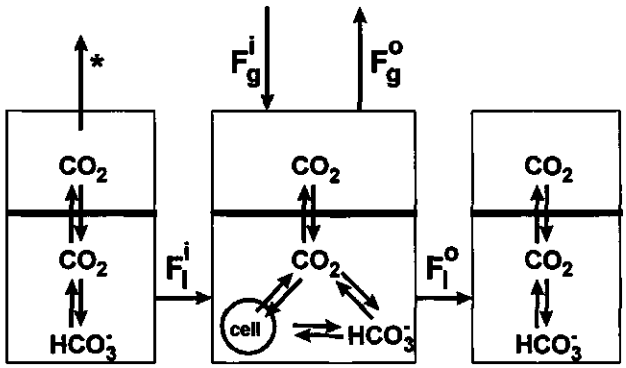

Schematic representation of bicarbonate buffer system in a continuous mammalian-cell culture system. The gas liquid interface is shown by the bold line. The marked arror (*) indicates the carbon dioxide loss from the medium.

For the liquid phase the A (=CO_2+HCO_3^-) balance for a continuous culture ($F_l^i = F_l^o = F_l$) becomes:

$$V_l \frac{d(C_A(t))}{dt} = F_l(C_A^i - C_A(t)) +$$

$$k_L^{CO_2} a\left(\frac{C_A^*(t)}{(1+\frac{K_1}{10^{-pH}})} - \frac{C_A(t)}{(1+\frac{K_1}{10^{-pH}})}\right)V_l + n_v q_{CO_2} V_l \quad (4)$$

The gas phase balance for CO_2 can be written as:

$$\frac{p}{RT}\frac{d(x_{CO_2}^o(t)V_g)}{dt} = x_{CO_2}^i F_g^i - x_{CO_2}^o(t) F_g^o - k_l^{CO_2} a\left(\frac{C_A^*(t)}{(1+\frac{K_1}{10^{-pH}})} - \frac{C_A(t)}{(1+\frac{K_1}{10^{-pH}})}\right)V_l \quad (5)$$

Assuming that accumulation in the liquid phase and in the gas phase is negligible at steady state conditions ($dx_{CO2}^{o}(t)/dt = dC_A(t)/dt = 0$), equations 3, 4 and 5 give:

$$n_W q_{CO_2} V_l = -F_l(C_A^i - (1 + \frac{K_1}{10^{-pH}}) C_{CO_2}(t)) - (x_{CO_2}^i F_g^i - x_{CO_2}^o(t) F_g^o) \quad (6)$$

C_{CO2} can not be calculated by assuming equilibrium between gas and liquid phase ($C_{CO2} \gg C_{CO2}^*$) (Heinzle, 1992), since a partial gradient for desorption is required (Royce and Thornhill, 1991). Royce and Thornhill (1991) calculate the maximum possible C_{CO2} by assuming that oxygen and carbon dioxide transfer rates are equal. This is not the case for continuous mammalian cell culture due to the use of bicarbonate buffered medium. Recently, Oeggerli and Heinzle (1994) showed that a gas phase balance can be used to calculate the liquid phase concentration of volatile compounds in bioreactors. Similarly, C_{CO2} can be determined using the CO_2 gas phase balance. Under the conditions described here there is no accumulation in the gas phase and $x_{CO2}^i = 0$. This results in the following CO_2 gas phase balance:

$$0 = x_{CO_2}^o(t) F_g^o - k_l^{CO_2} a (C_{CO_2}^*(t) - C_{CO_2}(t)) V_l \quad (7)$$

The concentration of CO_2 in the gas liquid interface equilibrium (C_{CO2}^*) can be calculated according to Henry's law:

$$C_{CO_2}^*(t) = x_{CO_2}^o(t) \frac{P}{H^{CO_2}} \quad (8)$$

The mass transfer coefficient for CO_2 is difficult to determine by the dynamic method. pCO_2 Electrodes suffer from poor response times and gas backmixing has to be taken into account (Royce and Thornhill, 1991). Further, C_{CO2} changes with pH and transfer kinetics will be influenced by pH control (Royce, 1992). However, the ratio of $k_l a$ values for CO_2 and O_2 is proportional to the ratio of their liquid-phase diffusivities. From this relation it follows that $k_l^{CO2} a = 0.89\ k_l^{O2} a$ (Royce and Thornhill, 1991). Using this equality Equation 7 and 8 yield:

$$C_{CO_2}(t) = x_{CO_2}^o(t) (\frac{P}{H^{CO_2}} + \frac{F_g^o}{0.89\ k_l^{O_2} a\ V_l}) \quad (9)$$

Under the assumption that the volume of CO_2 originating from the medium and the cells is negligible with respect to the total gas flow ($F_g^o = F_g^i$) and when $x_{CO2}^{\ i} = 0$, Equations 6 and 9 give:

$$n_V q_{CO_2} V_l = x^o_{CO_2}(t) F^i_g \; - \; F_l [C^i_A - x^o_{CO_2}(t)(1 + \frac{K_l}{10^{-pH}})(\frac{P}{H^{CO_2}} + \frac{F^i_g}{0.89\ k_l^{O_2} a\ V_l})] \qquad (10)$$

Finally, it is possible to determine the specific CER (i.e., the CER per cell or the q_{CO2}) by only measuring the fraction of CO_2 in the off-gas $x_{CO2}^{\ o}$, the inlet gas flow $F_g^{\ i}$, and the viable cell number n_v in a bicarbonate buffered continuous culture (other parameters are kept constant or are physical constants):

$$q_{CO_2} = \frac{x^o_{CO_2}(t)[F^i_g + F_l(\frac{P}{H^{CO_2}} + \frac{F^i_g}{0.89\ k_l^{O_2} a\ V_l})(1 + \frac{K_l}{10^{-pH}})] \; - \; F_l C^i_A}{V_l n_v} \qquad (11)$$

The above equation (11) is derived assuming that the ingoing concentration of A ($C_A^{\ i}(t)$) is constant. However, as discussed above and as shown by the marked arrow (*) in Figure 1, the medium tank is an open system that causes loss of CO_2. Therefore, $C_A^{\ i}$ changes with time.

Carbon dioxide loss from the medium

For a complete CO_2 balance the loss of CO_2 from the bicarbonate buffered medium during medium preparation and during medium storage has to be taken into account. This CO_2 loss causes a significant drop in the concentration of CO_2 and HCO_3^- in the feed with time. From now on the term $C_A^{\ i}$ will therefore be referred to as $C_A^{\ i}(t)$. There are two different approaches to solve this problem, a practical and a theoretical one: (*i*) The feed can be equilibrated with an appropriate N_2/CO_2-gas mixture just before it enters the bioreactor so as to maintain a constant bicarbonate level in the feed and (*ii*) the amount of CO_2 loss can be determined by measuring the pH of the medium.

i. Correcting for CO_2 loss by remixing CO_2 in the feed.

The experimental approach to adjust for CO_2 loss with time is to remix CO_2 in the feed just before it enters the bioreactor. In a mixing chamber a N_2/CO_2 gas mixture with a defined fraction of CO_2 gas is continuously remixed with the medium. This fraction is in equilibrium with the original amount of CO_2 in the medium containing sodium bicarbonate. In our case (2.73 $g.l^{-1}$ $NaHCO_3$ and 25 °C) this corresponds to a fraction of 11.43 % (see Appendix A). Thus by constantly equilibrating a 11.43% CO_2/N_2 gas mixture with the medium $C_A^i(t)$ will be maintained constant at 2.73 $g.l^{-1}$.

ii. Correcting for CO_2 loss by measuring the pH of the ingoing medium.

Due to the CO_2 loss the pH of the ingoing medium ($pH^i(t)$) will increase with time. Because a bicarbonate buffer system is concerned, this increase in $pH^i(t)$ can be used to calculate the amount of CO_2 that has been evaporated from the medium and subsequently to estimate the residual amount of HCO_3^- and CO_2. However, two points have to be taken into account before it is possible to calculate the residual amount of C_A^i from the pH only. First, when the $pH^i(t)$ is > 7.6, contrary to reactor conditions the amount of CO_3^{2-} in the medium tank can not be neglected anymore. C_A^i has to be extended to $C_A^i = C_{CO2}^i + C_{HCO3}^i + C_{CO3}^i$ and the equilibrium constant K_2 for the conversion of HCO_3^- into CO_3^{2-} has to be included also to calculate the $C_A^i(t)$. Secondly, in these calculations it can not be assumed that the medium is buffered by bicarbonate only. The buffer capacity is also the result of other components in the medium rather than by bicarbonate alone. By knowing the buffer capacity of both the bicarbonate and the (bicarbonate containing) medium, it is possible to recalculate the $pH^i(t)$ and to determine the CO_2 loss from the medium. The theoretical value that the $pH^i(t)$ would reach if the medium were to be buffered by bicarbonate only and not also by other components will be referred to as $pH^{i,\varepsilon}(t)$. This $pH^{i,\varepsilon}(t)$ is calculated from the measured $pH^i(t)$ by using the ratio of the buffer capacities of the medium and the bicarbonate. This ratio symbolized by e is determined as described in Appendix B. The value for $pH^{i,e}(t)$ can be calculated by $pH^{i,\varepsilon}(t) = pH^i(0) + \varepsilon\,(pH^i(t) - pH^i(0))$.

If CO_2 evaporates from the medium tank the pH^i will increase due to the conversion of protons according to two chemical equilibria:

$$CO_2 + H_2O \Leftrightarrow HCO_3^- + H^+ \quad (I)$$

$$HCO_3^- \Leftrightarrow CO_3^{2-} + H^+ \quad (II)$$

For a certain amount of CO_2 loss it is possible to calculate the amount of protons that have been converted through both equilibrium reactions. However, to calculate this amount of protons the changed equilibrium concentrations of CO_2 species have to be known. These concentrations are a function of the pH^i, i.e the amount of protons. Therefore, an iterative procedure is required to determine the CO_2 loss as a function of pH^i. First it is assumed that L mol CO_2/l evaporates from the medium. The residual concentration of A ($CO_2 + HCO_3^- + CO_3^{2-}$) at t=t will be:

$$C_A^i(t) = C_A^i(0) - L \quad (12)$$

The residual $C_{CO2}^i(t)$ can be calculated using the equilibrium constants K_1 and K_2:

$$C_{CO_2}^i(t) = \frac{C_A^i(t)}{1 + \frac{K_1}{10^{-pH^i(t)}} + \frac{K_1 K_2}{10^{-2*pH^i(t)}}} \quad (13)$$

Where $K_2 = (C_{CO3}C_H)/C_{HCO3} = 5.62*10^{-11}$ mol/l and K_1 as defined before. The residual concentration of the other CO_2 species, $HCO_3^- + CO_3^{2-}$, can be calculated by using Equation 13 and 14:

$$C_{HCO_3+CO_3}^i(t) = C_A^i(t) - C_{CO_2}^i(t) \quad (14)$$

The number of moles of $HCO_3^-+CO_3^{2-}$ that has been converted to CO_2 equals the number of moles of H^+ that has been converted in equilibrium I, and can be calculated by:

$$\Delta C_{H^+,I}^i(t) = C_{HCO_3+CO_3}^i(t) - C_{HCO_3+CO_3}^i(0) \quad (15)$$

Also, the protons that have been converted in equilibrium II have to be taken into account. Similarly to Equation 13 the HCO_3^- is in equilibrium with $HCO_3^- + CO_3^{2-}$ according to:

$$C^i_{HCO_3}(t) = \frac{C^i_{HCO_3+CO_3}(t)}{1+\frac{K_2}{10^{-pH^i(t)}}} \qquad (16)$$

And similarly to Equation 14, the residual concentration of CO_3^{2-} equals

$$C^i_{CO_3}(t) = C^i_{HCO_3+CO_3}(t) - C^i_{HCO_3}(t) \qquad (17)$$

The amount of protons that have been converted through reaction II can be calculated by

$$\Delta C^i_{H^+,II}(t) = C^i_{CO_3}(t) - C^i_{CO_3}(0) \qquad (18)$$

For each L the sum of $\Delta C_{H,I}{}^i + \Delta C_{H,II}{}^i$ and the resulting change in pH^i (that will change the equilibria as described by Equation 13 and 16) have to be in agreement. The resulting increase in pH^i can be found by iteration for each L. Finally, for a range of different L's this gives the fraction β that is defined by

$$\beta = \frac{C^i_A(t)}{C^i_A(0)} = f(pH^i(t)) \qquad (19)$$

Figure 2 gives β as a function of $pH^i(t)$. As mentioned before the buffer capacity of other components than bicarbonate in the medium has to be taken into account as well. A method to correct for this extra buffer capacity is given in Appendix B. In Figure 2 the fraction β is given for bicarbonate as a function of $pH^i(t)$ and for DHI medium (containing bicarbonate) as a function of $pH^{i,E}(t)$.

The steady state assumption in a continuous culture is violated because the $C_A{}^i(t)$ can not be regarded constant anymore. However, the major CO_2 loss and change in $C_A{}^i(t)$ will occur during medium preparation, sterilization and storage. Therefore, during cultivation a pseudo steady state can be assumed since the $pH^i(t)$ (and the $C_A{}^i(t)$) will not change significantly in time intervals of several hours (approximately 0.2 % per day). Rewriting Equation 11 and introducing β and $C_A{}^i(0)$ gives:

$$x^{o}_{CO_2}(t) = \frac{n_v q_{CO_2} V_l + \beta F_l C^{i}_{A}(0)}{F^{i}_{g} + F_l\left(\frac{P}{H^{CO_2}} + \frac{F^{i}_{g}}{0.89\, k_l^{O_2} a\, V_l}\right)\left(1 + \frac{K_l}{10^{-pH}}\right)} \qquad (20)$$

Figure 2

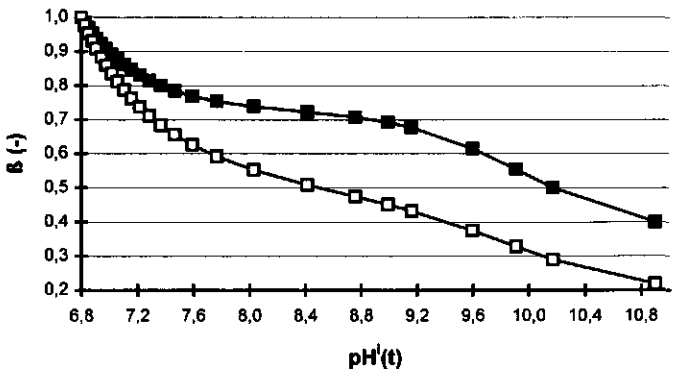

The residual amount of A in the ingoing medium expressed as a fraction of its original value (β), as a function of $pH^i(t)$. The function for a bicarbonate solution (closed symbols) and for a DHI medium (corrected by ε; Appendix A) (open symbols) are given.

Which demonstrates that the fraction of CO_2 that is measured in the outlet gas comes from two sources, the cells ($n_v q_{CO2} V_l$) and the ingoing bicarbonate ($\beta F_l C_A^{i}(0)$). The specific CER (q_{CO2}) can be calculated by measuring this CO_2 fraction in the off-gas (x_{CO2}^{o}), the cell density (n_v), the pH of the ingoing medium (pH^i) and the culture (pH) and the inlet gas flow (F_g^{i}), using:

$$q_{CO_2} = \frac{x^{o}_{CO_2}(t)\left[F^{i}_{g} + F_l\left(\frac{P}{H^{CO_2}} + \frac{F^{i}_{g}}{0.89\, k_l^{O_2} a\, V_l}\right)\left(1 + \frac{K_l}{10^{-pH}}\right)\right] - \beta F_l C^{i}_{A}(0)}{V_l n_v} \qquad (21)$$

MATERIALS AND METHODS

Cell line and culture medium

A murine hybridoma cell line that produces an IgG_{2A} antibody directed against human ferritin was grown in serum-free low-protein lipid-free medium. A mixture of Dulbecco's, Ham's F12 and Iscove's powdered media (DHI; 1:1:2) (Gibco, Grand Island, NY, USA) was used as the basal medium and was supplemented with 5 mg/ml insulin (Sigma, St.Louis, MO, USA), 6 mg/ml transferrin (Boehringer Mannheim, Mannheim, FRG), and 0.35 % (w/v) Synperonic F68 (Serva, Heidelberg, FRG). The medium contained 5 g/l glucose, 5 mM glutamine and 2.73 g/l sodium bicarbonate. Four steady states were examined, two with and two without using 1 % (w/v) Primatone RL (Sheffield Products, NY, USA), an enzymatic hydrolysate of animal tissue. In the medium without Primatone RL amino acids equivalent in composition and concentration to those in Primatone RL are added to the medium (Ajinomoto Co., Tokyo, J). The amino acid composition of Primatone RL and amino acid consumption rates were determined by HPLC.

Cell culture bioreactor

A bench-scale Biostat MD bioreactor with a 1 l working volume (B.Braun Diessel Biotech, Melsungen, FRG) was operated in a continuous mode. Temperature, stirrer speed and pH value were maintained at 37 °C, 150 rpm, and 7.20, respectively. The pH during the continuous experiments with and without cells was controlled by 0.5 M NaOH and 0.5 M HCl, respectively. Oxygen transport was via surface aeration only and the medium dissolved oxygen concentration was controlled at 40 % air saturation by changing the oxygen fraction in a nitrogen/oxygen gas mixture. This fraction was measured by mass flow meters and used to calculate the OUR (see Equation 2). The total gasflow was kept constant at 1.0 l $min.^{-1}$. The dilution rate was controlled at a value of 0.70 d^{-1} using an appropriate balance and a Sartorius dosing system (Sartorius GmbH, Göttingen, FRG). In the continuous experiment without cells different gas flow and dilution rates were applied (Figure 3). The 200 ml remixing

chamber was made of glass, aerated with a CO_2/N_2 gas mixture (11.43 % CO_2) (Garbagas, Bern, CH) and stirred at 800 rpm with a magnetic stirrer for ideal mixing.

Analysis

Viable cell concentrations and viabilities were determined by the trypan blue exclusion method using a haemacytometer. Antibody levels were quantified by a standard ELISA. CO_2 in the outlet gas was measured by an infrared gasanalyzer (Rosemount, Baar, CH). Values for $k_l^{O2}a$ were determined in both fresh medium and medium containing dead cells using the dynamic method (Van 't Riet and Tramper, 1991). No significant differences were found and $k_l^{O2}a$ was determined to be 63.35 d^{-1} at a stirrer speed of 150 rpm and a gas-flow rate of 1.0 l min^{-1}.

RESULTS

Control experiments without cells

It is desirable to determine the respiration quotient (RQ) in animal cell culture. However, accurate CO_2 balancing is difficult to do due to the bicarbonate buffer commonly used in cell culture media. It has to be taken into account that the CO_2 in the outlet gas is coming from two sources: the cells and the bicarbonate in the medium. In the numerator of Equation 20, which is derived in the theory section, these are expressed by the terms $n_v q_{CO2} V_l$ and $F_l C_A^i$, respectively. Further, in continuous culture the sum of CO_2, HCO_3^- and CO_3^{2-} (= A) entering the bioreactor will not be constant due to CO_2 loss from the medium tank. By measuring the pH of the ingoing medium, however, it is possible to calculate the residual amount of CO_2, HCO_3^- and CO_3^{2-} (Equations 12-19). To indicate that A in the ingoing medium is not constant and can be calculated by the method described in the theory section, the second term in the numerator of Equation 20 is changed into $\beta F_l C_A^i(0)$.

To verify the assumptions described in the theory section the bioreactor was operated as a CSTR without cells under different gas flow rates and dilution rates. In this par-

ticular case without cells $n_v = 0$ in Equation 20 and only the second term in the numerator ($\beta F_l C_A^l(0)$) has to be considered.

Figure 3

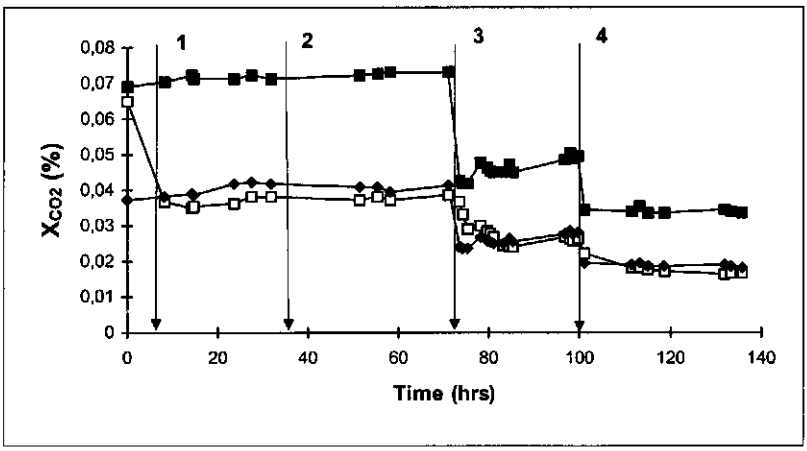

Fraction of CO_2 in the outlet gas at four different steady states (without cells in the bioreactor). The measured values are indicated by black diamonds. The theoretical values are calculated using Equation 20 without (black squares) and with (open squares) using the correction term β for CO_2 loss from the ingoing medium. The gas flow and feed rates at the four steady states are F_g^i = 28,3 mol.d^{-1}, F_l^i = 0,70 L.d^{-1} (1 and 2), F_g^i = 28,3 mol.d^{-1}, F_l^i = 0,49 L.d^{-1} (3), F_g^i = 32,3 mol.d^{-1}, F_l^i = 0,49 L.d^{-1} (4). Medium with (1) and without (2, 3, 4) Primatone RL.

Figure 3 shows the measured and two calculated values for the fraction of CO_2 in the outlet gas under four different conditions. The two calculated values represent Equation 20 ($n_v = 0$) with and without using the correction term β for CO_2 (Equation 19). The use of β calculated by measuring the $pH^i(t)$ of the feed, gives a substantial reduction in the difference between measured and calculated values. The average difference between predicted and measured values without and with using the correction for CO_2 loss in the medium tank are 48.5 % and 4.6 %, respectively. The theoretical values appear to agree well with the measured values provided the correction for CO_2 loss (β) is applied.

It has to be emphasized that the $pH^i(t)$ has to be determined already at the moment of bicarbonate addition and not at the start of the cultivation. Typically, pH values at t=0 are 6.80, increasing after pH adjustment to 7.20 and after filtration to 7.35-7.40, after medium storage to 7.55-7.60 and during long term cultivation to 7.65 (also see Appendix B). As the main CO_2 loss occurs before the start of the continuous cultivation, within time intervals of several hours a pseudo-steady state assumption for the $pH^i(t)$ is justified.

To test whether Primatone RL contains bicarbonate or influences the fraction of CO_2 in the outlet gas the medium is changed from DHI with to DHI without Primatone RL after 35 hours as indicated by arrow nr. 2 in Figure 3. Since no difference in x_{CO2}^o is observed this medium switch can be carried out in continuous culture without influencing CER analysis.

Continuous culture with theoretical correction for CO_2 loss

From the above it is clear that it is possible to correct for the portion of CO_2 that is coming from the bicarbonate in the medium at an error of less than 5 %. Therefore the specific CER (q_{CO2}) can be calculated from Equation 21 by measuring the fraction of CO_2 in the outlet gas and subtracting the theoretical amount that is coming from the bicarbonate medium ($\beta F_l C_A^i(0)$).

In Figure 4A the concentration of viable and dead cells is given for different media. During two steady states in DHI medium with Primatone RL and with the amino acid composition and concentration equivalent to Primatone RL, the viable cell concentration is 3.10 and 1.35 $*10^6$ cells.ml^{-1}, respectively, and the viability > 80 %. Not only the cell density and the specific Mab production is significantly higher (Table I) in the medium with Primatone RL, other metabolic quotients also indicate a more effective metabolism induced by unknown components in Primatone RL (see below).

Figure 4

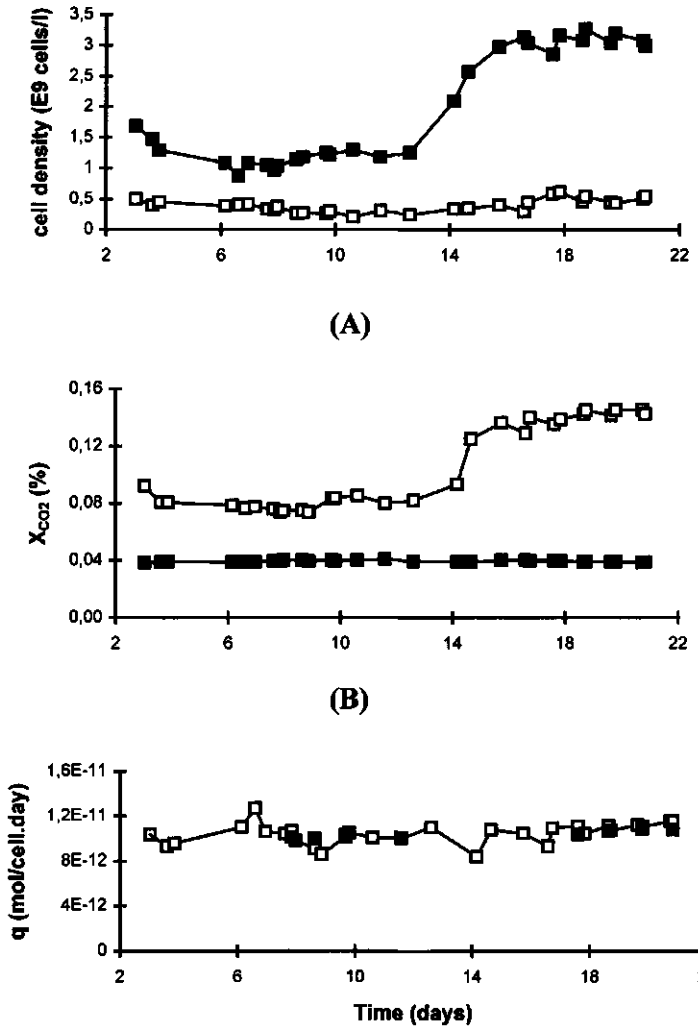

(A) Viable (closed symbols) and dead (open symbols) cell concentrations of hybridomas in continuous culture at constant gas flow and feed rates (F^i_g = 28,29 mol.d^{-1}, F^i_l = 0,70 L.d^{-1}), medium without (Day 0-12) and with (Day 12-21) Primatone RL. (B) The measured fraction of CO_2 (open symbols) in the outlet gas and the calculated fraction of CO_2 *only coming form the medium* (closed symbols). The latter was calculated using Equation 20 with $n_v = 0$. The

difference between both curves indicates how much CO_2 is produced by the cells. (C) The specific CER (open symbols) and specific OUR (closed symbols) from the same experiment. Only the last eight and nine data points of the first and second steady state, respectively, are used for the calculation of the specific metabolic rates, because in the used equations liquid phase accumulation is not taken into account.

Figure 4B shows the measured fraction of CO_2 in the outlet gas and the theoretical fraction coming only from the medium. This theoretical fraction was calculated from Equation 20. The two sources of CO_2 in an animal cell culture can be seen very clearly. A significant amount of the measured x_{CO2} is coming from the medium, 30 % and 50 % for steady states with and without Primatone RL, respectively. The difference between both lines visualizes the CO_2 in the off-gas that is produced by the cells. Figure 4C gives the CER and OUR per cell. For the specific CER only the steady state values are valid, since the calculations assume no accumulation in the liquid and gas phase. Therefore, only the last 8 and 9 datapoints of the first and the second steady state, respectively, are used for the mean values as presented in Table I. By adding Primatone RL to the medium the viable cell density, the specific Mab production rate and the RQ values increased. Student's *t* analysis for a two-group experiment (Youmans, 1973) was applied to test whether RQ data of the two steady states belong to the same population. A *t*-value of 3.62 (6 degrees of freedom) was found indicating that at a (probability of > 0.95) RQ values in medium with Primatone RL are significantly higher. Although the differences are small, this suggests that the determination of the RQ might be a useful indicator for the physiological state of the cells.

Continuous culture with experimental correction for CO_2 loss

CO_2 loss from the medium tank was corrected for experimentally by remixing CO_2 in the feed as described above. In this pertinent experiment there is no need for a (theoretical) correction for CO_2 loss, since the concentration of A (CO_2 + HCO_3^- + CO_3^{2-}) in the ingoing medium was held constant. Figure 5B shows the calculated fraction of CO_2 from the medium and the measured CO_2 in a continuous culture at D = 0.70 d^{-1} for different media. The fraction of CO_2 in the off-gas before inoculation remains constant because the ingoing medium was equilibrated with a 11.43 % CO_2 gas mixture.

To verify the theoretically corrected specific CER values as given in Figure 5C, the bioreactor was inoculated at day 5. The concentration of bicarbonate in the feed is still being kept constant by mixing it with the CO_2/N_2 gas mixture. As shown in Figure 5A the viable and dead cell concentrations in both DHI media are similar to the previous experiment (Figure 4A). Again a significant fraction of the measured x_{CO2} is coming from the medium: 45 % and 67 % for steady state with and without Primatone RL, respectively (Figure 5B). Both values are higher than in the previous experiment shown in Figure 4B because the CO_2 loss during medium preparation and storage and the resulting decrease in C_A^i is experimentally compensated for. This results in different values in C_{CO2} that can be calculated using Equation 9 (Table I).

Figure 5C shows the corresponding specific OUR and CER for the two steady states calculated from Equations 2 and 11. In this particular case $F_l^i C_A^i = 0$ and the measured (constant) fraction of CO_2 before inoculation (0.0915 %) is subtracted from the x_{CO2}^o values after inoculation. Table I gives the mean values of the specific CER in medium with and without Primatone RL that are calculated using the last 6 and 5 data points, respectively. Similar to the RQ determinations with theoretical correction for CO_2 loss a student *t*-value of 4.18 (5 degrees of freedom) was found indicating that RQ values in medium with Primatone RL are significantly higher than in medium without Primatone RL.

Figure 5

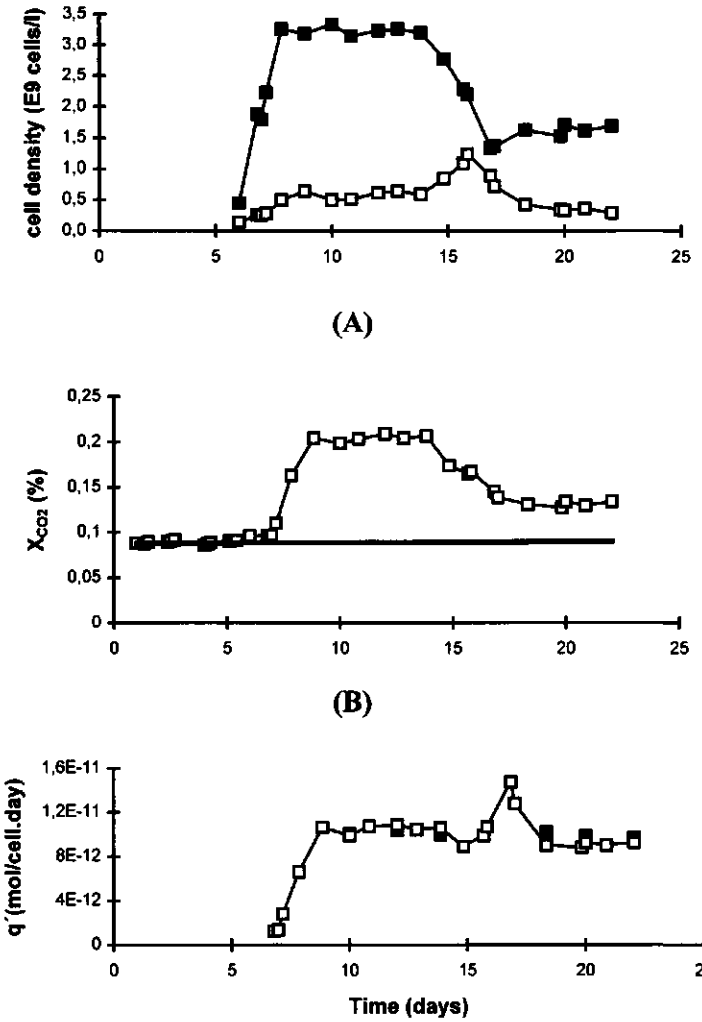

(A) Viable (closed symbols) and dead (open symbols) cell concentrations at constant dilution rate of 0,70 $L.d^{-1}$ (Fi_g= 28,29 $mol.d^{-1}$) with and without cells. [(Day 0-5) Cell-free steady state, (Day 0-14) medium with Primatone RL, (Day 14-22) medium without Primatone RL.] (B) The fraction of CO_2 in the outlet gas (open symbols) before and after inoculation (Day 5). The amount of CO_2 which comes from the medium alone (horizintal line) is kept constant by equilibration of the in-

going medium with a CO_2/N_2 gas mixture. (C) The specific CER (open symbols) and OUR (closed symbols) in the same experiment.

The results in Table 1 demonstrate that the RQ, the specific OUR and CER and the q_{MAB} values as well as the effect of Primatone RL on these metabolic rates agree well between both methods. Because of the high correlation we suggest that the method in which the CO_2 loss from the medium is calculated by measuring the $pH^i(t)$ can be applied for continuous cell culture. Using this method it is possible to determine the RQ in bicarbonate buffered systems without extra devices for controlling the bicarbonate level in the feed.

Table 1

Viable cell numbers, the viabilities, the specific CER and OUR, the RQ and the q_{MAB} values are presented. Mean values for two steady states are given. The numbers in parentheses indicate standard deviations.

Steady state	n_V (10^9cells.l^{-1})	Viability (%)	C_{CO2} (mM)	spec.CER (pmol.cell^{-1}.d^{-1})	spec.OUR (pmol.cell^{-1}.d^{-1})	RQ (-)	q_{MAB} (pg. cell^{-1}d^{-1})
Theoretically corrected for CO_2 loss using pH^i measurements (Figure 4).							
DHI + Primatone RL	3.10	85.6	0.78	11.1 (±0.40)	10.7 (±0.21)	1.04 (±0.02)	12.6
DHI + amino acids	1.35	83.3	0.43	9.92 (±0.67)	10.1 (±0.13)	0.98 (±0.04)	8.7
Experimentally corrected for CO_2 loss by equilibrating with a gas mixture (Figure 5).							
DHI + Primatone RL	3.23	84.8	1.02	11.0 (±0.56)	10.2 (±0.25)	1.07 (±0.03)	12.1
DHI + amino acids	1.68	82.7	0.65	9.90 (±0.21)	10.2 (±0.15)	0.97 (±0.02)	9.1

DISCUSSION

Respiration quotients and primary metabolism

Differences in RQ between the steady states in medium with and without Primatone RL are matched by differences of other metabolic quotients. The specific glutamine and glucose uptake rates in medium with Primatone RL are 45 and 38 % lower and the specific production rates of alanine, lactate and ammonia are 73, 55 and 58 % lower, respectively. The apparent yield of lactate from glucose decreases from 0.72 to 0.49 $mol.mol^{-1}$ after addition of Primatone RL. As will be discussed below, the increase of RQ is mainly a result of the increase in specific CER whereas the OUR remains unchanged. Therefore, the found differences are probably due to higher metabolic conversion rates through reactions catalyzed by decarboxylating enzymes that are not stoichiometrically linked to NADH production and oxidative phosphorylation.

In medium with Primatone RL the RQ is found to be slightly higher than unity. In contrast to yeast fermentation, where ethanol formation causes higher RQ values than unity (Wang et al., 1977), the reason for this is not clear. In mammalian cells all major metabolic pathways where CO_2 is produced (citric acid cycle, pentose phosphate cycle) are proportionally, directly or indirectly linked to NADH production. In these pathways the production of 1 mole CO_2 is accompanied by the production of 2 moles NADH. A surplus of NADH will be oxidized by 0.5 moles of O_2 per mole NADH. The specific OUR will therefore increase proportionally to the specific CER. Higher activities in these metabolic routes can therefore not result in higher RQ values. Maybe higher specific fatty acid synthesis rates could explain RQ values above unity. For example, when 1 mol palmitate is synthesized out of 4 moles glucose 8 moles CO_2 and 16 moles NADH are produced. This should result in an equal specific CER and OUR because NADH oxidation requires 0.5 moles of O_2. However, 8 moles of NADH are required to transport the fatty acid precursor Acetyl-CoA into the cytosol. Under these circumstances synthesis of 1 mole palmitate would require 4 moles of O_2 and co-produce 8 moles of CO_2 (Stryer, 1988). Therefore, enhanced specific fatty

acid biosynthesis could cause higher RQ values than unity. Further investigation into the overall metabolism is needed to elucidate the causes for the differences between the found RQ values and for the fact that RQ values above unity occur.

Volumetric oxygen uptake rates and respiration quotients as on-line measurable parameters

By using two different methods to correct for bicarbonate in the culture medium we determined that the RQ was around 10 % higher after addition of Primatone RL, a medium additive that improves growth and antibody production rates. This increase in RQ is mainly caused by a higher specific CER, whereas the specific OUR remained almost constant. Hu and Oberg (1990) also measured a linear increase in volumetric OUR with increasing cell concentrations. At different steady states the specific OUR will only increase at very low levels of glucose and is independent from glutamine concentrations (Hu and Oberg, 1990; Miller et al., 1989).

In our case we found a linear relationship between cell density and (volumetric) OUR at a high correlation ($r^2 = 0.9264$, $n = 11$) in continuous culture with residual glucose concentrations > 0.6 mM. We suggest that, under certain well-defined conditions, the volumetric OUR and the RQ might be useful parameters as an indication of both the cell density (volumetric OUR) and the physiological state of the cells (RQ). As on-line measurable parameters independent of cell number a combination of volumetric OUR and RQ data might prove useful in medium optimization for continuous culture and potentially also for the development of rational feeding strategies in batch cultures. Likewise, CER data are necessary for closing mass balances when attempting to model cell metabolism.

ACKNOWLEDGEMENTS

H.P.J.B. thanks J.-M. Vonach and Ch. Deuer for excellent technical support. Also, the reviewers comments are very much appreciated.

APPENDIX A

Determination of the CO_2 fraction in the correction gas

The CO_2 concentration of the correction gas that is used for the equilibration of the feed just before it enters the bioreactor has to be determined accurately. It depends on the original bicarbonate concentration ($C_A^i(0)$), the temperature, and the medium composition.

The temperature correction for the Henry's coefficient is carried out according to Royce (1991), who derived from Schumpe et al. (1982):

$$H^{CO_2}_{H_2O,25°C} = \exp(11.25 - \frac{395.9}{(T-175.9)}) = 3.016*10^6\ Pa.l.mol^{-1} \quad (22)$$

At $T = 298.15$ K

$$\log\frac{\alpha}{\alpha_0} = 1.74*10^{-2} = \log\frac{H_{H_2O}}{H_{DHImedium}} \quad (23)$$

The influence of the medium composition can be calculated using the Bunsen coefficient (Schumpe et al., 1982): It follows for $H^{CO2}{}_{DHI,25°C} = 2.897*10^6$ Pa.l.mol^{-1}

Therefore the CO_2/N_2 gas mixture used for the equilibration of the feed contains 11.43 % CO_2, according to

$$x^{equilibration\ gas}_{CO_2} = \frac{H^{CO_2}_{DHI,25°C}}{P}\frac{C^i_A(0)}{(1+\frac{K_1}{10^{-pH^i}})} = 0.1143 \quad (24)$$

Where $C_A^i(0) = 2.73$ gr.l^{-1} $NaHCO_3 = 3.250*10^{-2}$ M and $pH^i = 7.20$.

APPENDIX B

Determination of the buffer capacity ratio (ε)

Figure 6 shows the increase of the pH^i in bicarbonate containing medium and in bicarbonate only. The titration curves are assumed to be linear within the pH range of 6.8 to 8.2. The correction factor e is determined by dividing the slope of the bicarbonate line by the slope of the medium line. The corrected $pH^i(t)$, e.g., the pH that the medium would have if it were to be buffered by bicarbonate only, is calculated by $pH^{i,\varepsilon}(t) = pH^i(0) + \varepsilon (pH^i(t) - pH^i(0))$. For DHI medium with Primatone RL and DHI medium with only the Primatone amino acids e is 3.32 and 3.29, respectively.

Figure 6

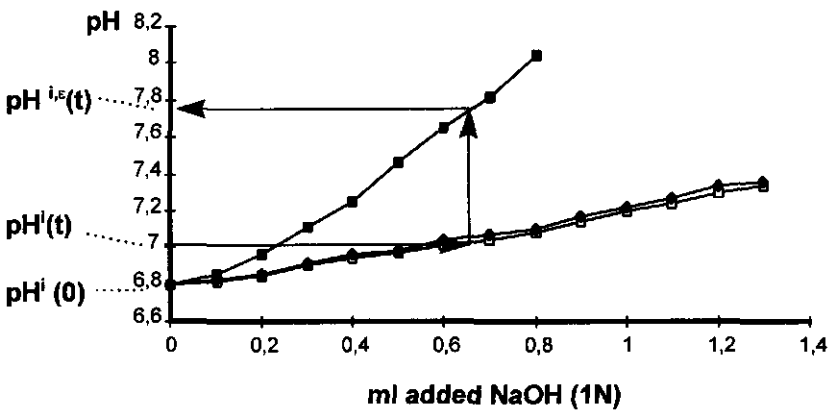

Titration curves of bicarbonate (2.73 $g.l^{-1}$) (black squares), DHI medium + amino acids (black diamonds) and DHI medium + Primatone RL (open squares). When the $pH^i(0)$ in DHI medium equals 6.80 and the $pH^i(t)$ = 7.00, the corrected $pH^{i,\varepsilon}(t)$ = 7.76.

Chapter 3

Error Analysis of Metabolic-Rate Measurements in Mammalian-Cell Culture by Carbon and Nitrogen Balances

Hendrik P.J. Bonarius, José H.M. Houtman,
Georg Schmid, Cornelis D. De Gooijer,
and Johannes Tramper.

ABSTRACT

The analysis of metabolic fluxes of large stoichiometric systems is sensitive to measurement errors in metabolic uptake and production rates. It is therefore desirable to independently test the consistency of measurement data, which is possible if at least two elemental balances can be closed. For mammalian-cell culture, closing the C balance has been hampered by problems in measuring the carbon-dioxide produc-tion rate. Here, it is shown for various sets of measurement data that the C balance can be closed by applying a method to correct for the bicarbonate buffer in the culture medium.

The measurement data are subsequently subject to measurement-error analysis on the basis of the C and N balances. It is shown at 90 % reliability that no gross measurement errors are present, neither in the measured production- and consumption rates, nor in the estimated in- and outgoing metabolic rates of the

***sub*network, that only contains the glycolysis, the pentose-phosphate, and the glutaminolysis pathways.**

INTRODUCTION

Intracellular metabolic fluxes can be determined from extracellular uptake and secretion rates of relevant metabolites using mass-balancing techniques (Vallino and Stephanopoulos, 1990; Varma and Palsson, 1994). A major problem of this method which applies particularly for large, complex networks is that the estimated fluxes are sensitive to errors in the measured extracellular rates. It is therefore desirable to test measurement data on possible errors independent of the flux-balance equations (Noorman et al., 1991). Alternative conservation equations that are independent from flux balances can be derived from heat or elemental balances.

Elemental balances have been used to test fermentation data for prokaryotes and yeast (Roels, 1983; Ferrer and Erickson, 1980; Wang and Stephanopoulos, 1983; Noorman et al., 1991). For mammalian-cell culture however, an error analysis based on elemental balances is hampered by the fact that relatively few balances can be closed. In contrast to fermentations of yeast or prokaryotes (Von Stockar et al., 1997), the heat balance cannot be used because mammalian cells generate only a fraction of the energy that is required to control the cell-culture bioreactor at the desired temperature. The elemental balances for hydrogen and oxygen can not be closed, since (mammalian) cells secrete or take up water at negligible rates compared to the water balance of the bioreactor system. In addition, it is not possible to quantify the H^+-production rate at sufficient accuracy for error analysis due to the presence of buffer systems. Therefore, only the nitrogen and carbon mass balance may be suitable tools for tracing measurement errors in mammalian-cell culture.

A prerequisite to close the carbon balance is the correct measurement of the carbon-dioxide evolution rate. In mammalian-cell culture this is hampered by the use of a bicarbonate-based buffer system in the culture medium. Methods to determine the carbon-dioxide production rate of mammalian cells cultured in bicarbonate-buffered

media have recently been described for continuous (Bonarius et al., 1995a) and batch (Zupke and Stephanopoulos, 1995a) cultures. Here, it is shown that when such methods are used the carbon balance of mammalian-cell culture can be closed within an acceptable probability range. Together with the nitrogen balance, the two constraints that are determined by these elemental balances theoretically allow the detection of gross measurement errors within the set of measured uptake and production rates. The method to detect gross measurement errors, described by Ripps (1965) and developed by Wang and Stephanopoulos (1983) for data from microbial metabolism, is applied for mammalian-cell culture under 7 different culture conditions. Various sets of measurements that are used to estimate the intracellular fluxes are subjected to this particular test.

MATERIALS AND METHODS

Culture conditions and analyses

A detailed description of the various experimental procedures was published before (Bonarius et al., 1996). Briefly, hybridoma cells were cultured in a lab-scale bioreactor (B. Braun Diessel Biotech, Melsungen, Germany) in a continuous mode at a dilution rate of 0.7 d^{-1}. The fraction of CO_2 in the outlet gas was measured using an infrared gasanalyzer (Rosemount, Baar, Switzerland). Glucose and lactate were determined with automated enzymatic assays, ammonia using an ion-selective electrode, and amino acids by HPLC (Amino Quant 1090, Hewlett-Packard, Palo Alto, CA).

The cellular composition was measured as follows (Xie and Wang, 1994b): the total lipid fraction was determined by weight after chloroform/methanol extraction, total carbohydrates were analyzed by the phenol-reaction method, and total cellular protein was estimated using the Biuret assay. Cell size and number were determined using a Casy 1 instrument (Schärfe System, Reutlingen, Germany) and dry-cell weight was determined after dehydration under vacuum. Antibody titers were measured by a standard ELISA. Free intracellular amino-acid pools were extracted

by perchloric acid as described by Schmid and Keller (1992). After neutralization and lyophylization, the fraction of free amino acids of the intracellular pools were quantified by HPLC. The values for intracellular protein-bound amino acids were taken from measurements of hydrolyzed protein (1 N HCl, 125 °C, overnight) of the same cell line, grown under the same medium conditions (Bonarius et al., 1996). The used elemental compositions for C and N of the measured macro-metabolites is shown in Table 1.

Table 1

Elemental composition of measured macromolecules.

	C	N	Source
Protein			
Measured composition[a]	4.879	2.475	Bonarius et al., 1996
Composition literature	4.743	2.411	Creighton et al., 1984
Composition Mabs literature	4.840	2.378	Edelman et al., 1964
RNA/DNA	9.50	3.75	Stryer, 1988
Lipids[a]	18.45	0	Bonarius et al., 1996

[a] Refers to measured amino acids in cellular total protein from cells cultured with Primatone RL in the medium.

Statistical analyses

From the law of mass conservation it follows that when all (produced and consumed) metabolites that significantly contribute to the total mass of an element are determined, the residual value of the elemental balance (ε) can be used as the estimated measurement error for the elemental balance. Wang and Stephanopoulos (1983) used a statistical test function to judge whether the residual values deviate significantly away from their expected distribution of zero means. In this function, h_ε, the residuals are weighted according to their accuracy (or standard deviation of the measured production and consumption rates). In the case of two elemental balances (here, carbon and nitrogen), a lower value of h_ε than 4.61 indicates with a confidence level of

90 % that no gross measurement errors are present. The value of 4.61 for h_ε has been justified by Wang and Stephanopoulos (1983) for all microbiological systems: If the residuals (ε) are assumed to have identical and independent (ϕ, the variance-covariance matix for ε, is diagonal) normal distributions around 0, then the test function h_ε ($= \varepsilon^T \phi^{-1} \varepsilon$) follows a χ^2-distribution with m degrees of freedom, where m is the number of constraint equations.

In this work, each data point is an average of a double measurement at three time points during each steady state (the last three days of each condition). Here, a 'steady state' is obtained when the difference in viable cell density from the average value is smaller than 10 %. Variances are estimated from these six experimental data points. Both the extra- and intracellular free amino-acids pools were measured. The total-lipid assay was only carried out once for each set of measurements. This assays requires relatively large amounts of cells because is a weight measurements. The sampling of large volumes disturbs the steady-state conditions, and samples for the total-lipid assay were therefore only taken at the end of each steady state. The variance of this measurement is therefore not determined experimentally, but assumed to be 10 % of the measured value. Further, due to lack of material from the second, third, and fourth steady state, the average value of the lipid and the DNA measurement of the first and fifth steady state was used for the first five steady states (Table A1a, Appendix A).

Similarly to Wang and Stephanopoulos (1983), it is assumed that the errors are uncorrelated. In reality some correlation in measurements are unavoidable. For instance, the amino-acid measurements may be correlated because all amino-acid concentrations are determined simultaneously by HPLC. Errors that occur in dilution of samples for HPLC or calibration errors are correlated. However, when (non-negative) co-variances are taken into account the test function h_ε will decrease. So, when it is assumed that the measurements are not correlated, the upper limit of h_ε is determined, which implies that for a value of 4.61 the confidence level is equal or greater than 90 %.

Certain fluxes, in particular fluxes in cyclic pathways, cannot be determined by mass-balancing techniques alone, because their reaction stoichiometry is linear dependent (Vallino and Stephanopoulos, 1990; Bonarius et al., 1997). In the metabolic network that describes mammalian-cell metabolism, a subsystem remains therefore underdetermined (See also Figure 1).

Figure 1

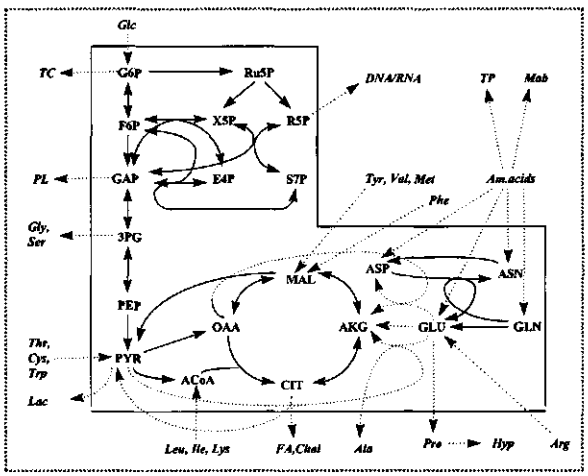

Fluxes that can be quantified by mass balances alone are indicated as dashed lines. To measure the remaining fluxes (solid lines) additional constraints are required. The two networks of which the measured in- and out-going metabolic rates are subject to error analysis, are shown: (i) the entire metabolic network (dotted line) and (ii) the underdetermined sub-network (L-shaped box). Abbreviations: ACoA acetyl-CoA, AKG α-ketoglutarate, CHOL cholesterol, CIT citrate, E4P erythrose-4-phosphate, GAP glyceraldehyde 3-phosphate, GLC glucose, G6P glucose-6-phosphate, 3PG 3-Phosphoglycerate, LAC lactate, MAL malate, OAA oxaloactetate, PEP phosphoenolpyruvate, PYR pyruvate, R5P ribose-5-phosphate, Ru5P ribulose-5-phosphate, S7P sedoheptulose-7-phosphate, TC total carbohydrates, TP total protein, X5P xylulose-5-phosphate.

The fluxes in this subnetwork need to be quantified by isotopic-tracer experiments. If this is not possible, which is for example the case for large-scale cell culture, the fluxes of this smaller network can only be estimated using additional assumptions. In order to prevent that such assumptions affect the determinable fluxes (dashed lines in

Figure 1), the non-determinable fluxes (solid lines in Figure 1) are estimated separately as described elsewhere (Bonarius et al., 1998a, 1998b). Here both metabolic systems are subject to gross measurement error analysis:

(i) the entire metabolic network, and

(ii) the underdetermined network.

By the determination of h_e for the smaller network, both the measurement data (Table A2) and the stoichiometric equations required for the calculation of the in- and out-going flows of the underdetermined network are tested for gross errors.

RESULTS AND DISCUSSION

Hybridoma cells were cultivated in a continuous stirred-tank reactor under different conditions. The pO_2 was varied and in another experiment PMS was added to the culture medium. Viable-cell density, viability, and dilution rate are shown in Figures 2a and 2b.

Figure 2a

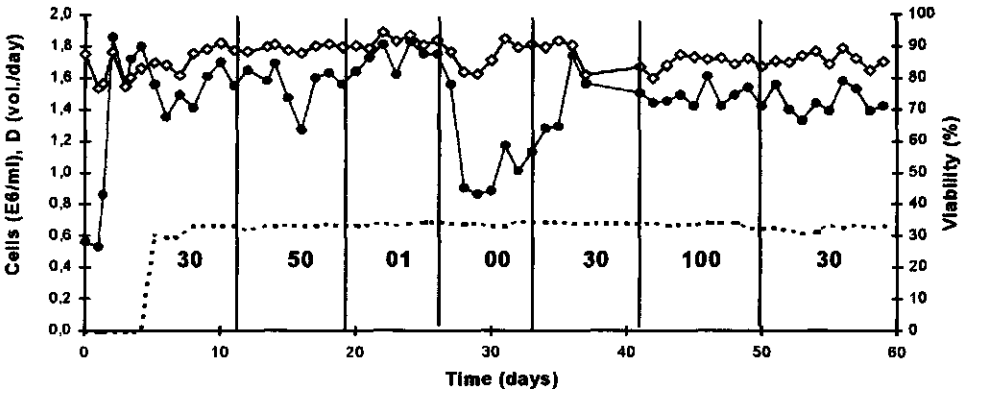

Viable-cell numbers (closed circles), viability (open diamonds), and dilution rate (—) are shown for 60 days continuous culture. The 2-digital numbers indicate set points for dissolved oxygen (% of air saturation). Samples for metabolite analyses were taken during the last three days of each steady state.

The extracellular production and consumption rates of amino acids, glucose, ammonia, lactate, carbon dioxide and monoclonal antibody were determined. Also, the intracellular concentrations of amino acids, lactate, total cell protein, DNA, RNA, and the total lipid and carbohydrate contents were measured. After changing to new parameter settings at least four days of continuous culture were used to dilute remaining metabolites produced during the previous steady state and to allow the viable cell density to stabilize. Steady-state conditions were obtained in all experiments, except during the oxygen limitation experiment ("00" in Figure 2a) in which 'pseudo steady-state' conditions were obtained.

Figure 2b

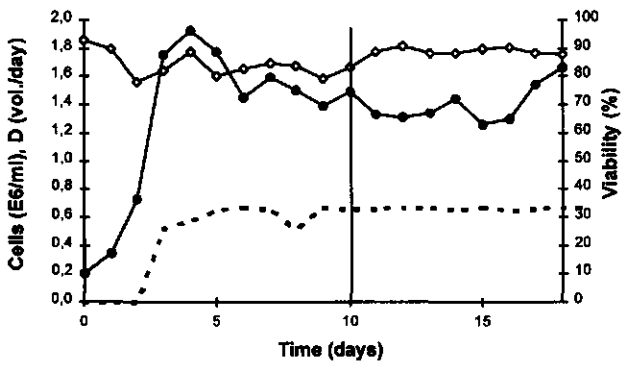

PMS experiment. Symbols as in legend Figure 2a. PMS was continuously added after day 10. Samples for metabolite analyses were taken at day 14, 15 and 16.

Table A1 and A2 (Appendix) show the average measured metabolic rates and their standard deviations for the entire network (i) and the smaller, underdetermined network (ii), respectively. The average viable-cell numbers and implications of these results for the cell physiology and metabolism of hybridoma cells are reported elsewhere (Bonarius et al., 1998d).

In Table 2 the residual values for carbon and nitrogen are given for the various sets of measured uptake and production rates (in 10^{-12} C-mol.cell^{-1}.day^{-1} and 10^{-12} N-mol.cell^{-1}. day^{-1}, respectively.) A positive value indicates either an overestimation of the produced carbon or nitrogen, or an underestimation of the consumed carbon or

Table 2

Residual values (estimated errors) of measured carbon (ε_C) and nitrogen (ε_N) metabolized in hybridoma cells. The total carbon (C_{tot}) and nitrogen (N_{tot}) turn-over, the relative residual values (C_{rel}, N_{rel}) and the test function h_ε, are also shown. In addition, the test function is determined for the same measurements, without taken the bicarbonate buffer into account for the determination of the CO_2 production rates. The erroneous r_{CO2}'s (10^{-12} mol.cell^{-1}.day^{-1}) are given as well.

	pO_2 30	pO_2 50	pO_2 1	pO_2 0	pO_2	pO_2 30	PMS
2a. Values for the entire metabolic network.							
ε_C	-2.59	-1.99	-3.10	-6.52	-1.60	-0.94	0.35
ε_N	-0.25	0.20	0.45	-0.39	-0.22	0.50	0.20
C_{tot}	122.40	101.99	125.26	179.98	111.92	99.73	102.97
N_{tot}	14.86	12.28	10.82	12.38	18.30	13.65	16.98
C_{rel}	-2.12	-1.96	-2.47	-3.62	-1.43	-0.94	0.34
N_{rel}	-1.71	1.60	4.12	-3.18	-1.18	3.67	1.20
h_ε	2.96	0.66	15.25	1.87	1.45	0.55	0.31
2b. Values for entire metabolic network, in the case that the bicarbonate buffer in the culture medium has been neglected for the determination of the CO_2 production rate.							
r_{CO2}	21.81	19.68	14.89	13.30	19.45	18.35	20.71
C_{rel}	5,67	5,35	2,18	0,86	5,33	6,16	7,78
h_ε	7.47	2.54	13.96	4.87	13.10	8.44	4.93
2c. Values for the underdetermined subnetwork.							
ε_C	2.30	1.78	3.91	-4.11	2.94	2.54	0.98
ε_N	-1.33	-0.96	-0.45	-1.12	-1.20	-0.17	-1.34
C_{tot}	106.11	87.92	110.25	171.60	97.78	82.04	78.91
N_{tot}	6.82	4.61	4.31	6.12	5.58	4.98	6.08
C_{rel}	2.16	2.01	3.55	2.40	3.00	3.10	1.24
N_{rel}	19.53	20.71	10.49	18.28	21.57	2.937	23.00
h_ε	4.58	1.16	1.14	0.82	3.66	0.20	2.30

nitrogen. The total turnover rate (the sum of all produced and consumed metabolites) is shown for comparison. In addition, the relative residual value for carbon (C_{rel}) and nitrogen (N_{rel}) is given as percentage of the turnover rate.

Carbon balance and carbon-dioxide production rate

In Table 2a is shown that the carbon balance can be closed for all steady states. In all cases, the relative error for carbon (C_{rel}) is less than 5 % of the total carbon turnover. In order to close the C balance, it is critical to take the bicarbonate in the culture medium into account. If this factor is neglected in the determination of the carbon-dioxide production rate, C_{rel} increases to more than 5 % in most cases. Further, the test function h_ε (in the determination of which the N balance is also included) increases significantly in all cases (except for the set for the steady state at pO_2 = 1 %, which will be discussed below), and to values above 4.61 in 5 out of 6 cases. This gives independent support for the fact that the method that was developed to determine the carbon-dioxide production rate in bicarbonate-containing medium (Bonarius et al., 1995) is sound and can be used for the analysis of cellular physiology and flux analysis of mammalian-cell culture.

Test for gross measurement errors

For 6 sets of measurement data the test function h_ε is lower than 4.61, which shows that with more than 90 % confidence these data are consistent with respect to both the carbon and the nitrogen balance. Only in one case (pO_2 = 1 %, Table 2a), the performance index h_ε is higher than 4.61, indicating that there is a significant measurement error in this set of measured metabolic rates. The relative residual values implies that the measurement of one or more N-containing metabolites are erroneous (Table 2a). The fact that ε_N is positive indicates that either the consumption rate of a (N-containing) metabolite is underestimated or the production rate of a metabolite is overestimated. Comparison of metabolic rates of N-containing metabolites between the different steady states shown in Table A1a, suggests for example that it is unlikely that the measurement of the total protein (TP) at pO_2 of 1

%, is overestimated. It is more probable that either the glutamine-consumption rate is underestimated, or the NH_3-production rate is overestimated, or a combination of both.

Location and identification of measurement errors

In some cases, gross measurement errors can be located by the serial elimination method (Ripps, 1965; Wang and Stephanopoulos, 1983). With this method it is attempted to locate the source of an error by the recalculation of h_ε for a set of measurement data that has been reduced by the removal of data that are suspected to be unsound or erroneous. The removal of the TP, GLN, and NH3 measurement from the data set shown in the third column of Table 2a (pO_2 = 1%) yields a h_ε of 1.67, 1.34, and 0.72, respectively, which indicates that the probability that the ammonia measurement is erroneous is relatively high compared to the likelihood that the total-protein or glutamine determination is incorrect. However, the differences between these h_ε values are relatively small, and combinations of measurement errors cannot be ruled out as simultaneous deletion of two measurements is not possible due to the limited number of constraint equations (elemental balances) available.

Van der Heijden and co-workers (1994) recently classified error types in biochemical reaction systems into three categories. When an error is detected by analysis of conservation equations it can either be a measurement error (i), an incorrect system definition (ii), or a result of a too sensitive χ^2-test due to too small variances (iii). It is not likely in that the error in the third set of data (pO_2 = 1 %, Table 4a) is an error in system definition. At a probability of at least 90 %, six different measurement sets (and other data sets (Bonarius et al., 1996, Bonarius et al. 1998a)) do not contain gross errors. This suggests that -at the same probability- the system definition is sound for the metabolites that are relevant for the carbon and nitrogen balance. Another possibility is that the variances of the data set for pO_2 = 1% are too small. Compared to the other steady states shown in Table A1b (Appendix A), the standard deviation of the NH_3 measurement in the data set for pO_2 = 1% is relatively small. When the standard deviation is increased to $0{,}202*10^{-12}$ mole $cell^{-1}$ day^{-1} (which

corresponds to the highest estimated standard deviation for the NH_3 measurement in Table A1b) the test function h_ε decreases from 15,25 to a mere 4,68, which suggests that it cannot be ruled out that the present error in the data for $pO_2 = 1\%$ is an error of the third kind. In conclusion, the production and uptake rates of mammalian cells shown here can be tested for the presence of gross errors at a probability of at least 90 %, but it is neither possible to locate nor to identify the error(s).

Error analysis of metabolic rates for *sub*network

Table 2c shows the (relative) residual values for carbon and nitrogen and h_ε for the smaller, underdetermined network. The set of metabolite flows (Table A2a) calculated from the reaction stoichiometry and the measured production and consumption rate are consistent with respect to the carbon and nitrogen balance. The fact that the test function for each steady state are all below the value of $\chi^2(0.9) = 4.61$ supports that not only the measurements, but also the stoichiometric equations that have been used for the determination of the in- and outgoing flows of the subnetwork are free of gross system errors (at a probability of at least 90 %), and can be used for flux analysis.

It is further noteworthy that in contrast to the ε_N values corresponding to the entire network (Table 2a), *all* ε_N values associated with the underdetermined subnetwork (Table 2c) are negative. In other words, according to the N balance some of the N-producing fluxes in the other reactions in cell metabolism than those of the subnetwork are overestimated (or N-consuming reactions are underestimated). Because this seems not to be the case for C-containing metabolites, a possible explanation for this small though systematic difference is either that a reaction in which NH_3 is consumed has incorrectly been neglected, or that a NH_3-producing pathway has incorrectly been added to the network. Examples of the latter could be the degradation pathways of amino acids such as cysteine and threonine (Figure 1), which both yield NH_3.

CONCLUSIONS

The carbon balance can be closed in continuous mammalian-cell culture, provided that the bicarbonate buffer in the culture medium is taken into account for the determination of the CO_2 production rate. Together with the nitrogen balance, this allows to test the measurement data of metabolites that are relevant for flux analysis on the presence of gross errors.

The carbon and nitrogen balances over the metabolic subnetwork that consists of the glycolysis, the TCA cycle, the pentose phosphate pathway, and the glutaminolysis, can be closed within the 90 % confidence interval.

APPENDIX A

Table A1a

Average measured metabolic rates of metabolites of entire metabolic network for seven steady states (Values in 10^{-12} mol. $cell^{-1}.day^{-1}$). Abbreviations as in Figure 1. Amino acids are given with the standard three-letter codes.

	PO_2 30	pO_2 50	pO_2 1	pO_2 0	pO_2 100	pO_2 30	PMS
ASP	-0.088	-0.06	-0.044	-0.002	-0.078	-0.173	-0.078
GLU	-0.071	-0.027	-0.054	0.011	-0.029	-0.208	-0.074
ASN	-0.061	-0.068	-0.055	-0.037	-0.047	-0.013	-0.093
SER	0.041	-0.025	-0.113	-0.097	0.023	-0.023	0.080
GLN	-2.102	-1.618	-1.442	-2.025	-1.941	-1.823	-2.140
HIS	-0.072	-0.058	-0.047	-0.054	-0.068	-0.054	-0.059
GLY	-0.094	-0.108	-0.103	-0.094	-0.106	-0.115	-0.135
THR	-0.148	-0.121	-0.102	-0.102	-0.137	-0.134	-0.161
ARG	-0.119	-0.096	-0.084	-0.085	-0.112	-0.158	-0.198
TYR	-0.082	-0.070	-0.065	-0.070	-0.077	-0.075	-0.088
CYS	-0.122	-0.091	-0.090	-0.133	-0.099	-0.101	-0.118
VAL	-0.221	-0.184	-0.14	-0.123	-0.209	-0.198	-0.226
MET	-0.124	-0.101	-0.088	-0.107	-0.112	-0.101	-0.135
TRP	-0.02	-0.021	-0.019	-0.014	-0.009	-0.029	-0.038
PHE	-0.073	-0.068	-0.061	-0.061	-0.067	-0.066	-0.102
ILE	-0.360	-0.313	-0.221	-0.210	-0.313	-0.377	-0.427
LEU	-0.595	-0.501	-0.347	-0.328	-0.524	-0.596	-0.691
LYS	-0.201	-0.164	-0.137	-0.149	-0.19	-0.189	-0.233
PRO	0.120	0.154	0.204	0.237	0.162	0.103	0.078
HYP	0.322	0.244	0.212	0.304	0.254	0.253	0.345
ALA	1.230	0.976	0.773	1.151	1.13	1.232	1.360
GLC	-6.341	-5.374	-18.53	-12.31	-5.825	-4.685	-4.025
LAC	7.480	5.279	10.69	19.08	7.031	4.784	3.432
NH3	1.220	0.717	0.748	0.878	1.072	1.141	1.423
CO2	13.12	11.79	8.920	7.382	11.71	10.83	12.41
RNA	0.062	0.058	0.063	0.057	0.058	0.052	0.062
DNA	0.012	0.012	0.012	0.012	0.012	0.029	0.042
TP	2.421	2.494	2.002	2.243	2.275	2.543	2.769
TC	0.056	0.068	0.053	0.079	0.062	0.079	0.081
LIP	0.151	n.d.	n.d.	n.d.	0.174	0.155	0.139
MAB	0.138	0.112	0.109	0.116	0.115	0.121	0.176

Table A1b

Standard deviations of measured metabolic rates of metabolites of entire metabolic network (Values in 10^{-12} mol. $cell^{-1}.day^{-1}$).

	pO_2 30	pO_2 50	pO_2 1	pO_2 0	pO_2 100	pO_2 30	PMS
ASP	0.0014	0.0067	0.0034	0.0114	0.0015	0.0176	0.0047
GLU	0.0035	0.0019	0.0069	0.0147	0.0034	0.0160	0.0012
ASN	0.0020	0.0063	0.0079	0.0186	0.0015	0.0597	0.0077
SER	0.0012	0.0035	0.0062	0.0237	0.0031	0.0136	0.0093
GLN	0.0492	0.2145	0.0524	0.2030	0.0779	0.2180	0.1470
HIS	0.0022	0.0060	0.0034	0.0070	0.0021	0.0088	0.0028
GLY	0.0063	0.0110	0.0071	0.0222	0.0049	0.0135	0.0074
THR	0.0024	0.0123	0.0073	0.0192	0.0040	0.0179	0.0095
ARG	0.0011	0.0090	0.0034	0.0202	0.0032	0.0200	0.0119
TYR	0.0007	0.0083	0.0017	0.0115	0.0023	0.0094	0.0060
CYS	0.0078	0.0012	0.0103	0.0061	0.0041	0.0127	0.0075
VAL	0.0043	0.0217	0.0037	0.0213	0.0051	0.0249	0.0102
MET	0.0104	0.0121	0.0033	0.0117	0.0041	0.0116	0.0109
TRP	0.0041	0.0028	0.0017	0.0087	0.0009	0.0004	0.0030
PHE	0.0028	0.0083	0.0033	0.0153	0.0019	0.0073	0.0095
ILE	0.0139	0.0414	0.0053	0.0363	0.0086	0.0431	0.0391
LEU	0.0221	0.0654	0.0094	0.0595	0.0131	0.0688	0.0657
LYS	0.0075	0.0168	0.0025	0.0310	0.0054	0.0188	0.0231
PRO	0.0202	0.0404	0.0246	0.0340	0.0311	0.0069	0.0109
HYP	0.0148	0.0323	0.0098	0.0199	0.0089	0.0404	0.0323
ALA	0.0436	0.1518	0.0223	0.0556	0.0377	0.1780	0.0839
GLC	0.345	0.216	0.435	0.133	0.172	0.284	0.605
LAC	0.640	1.000	0.824	1.610	0.449	0.499	0.208
NH3	0.110	0.142	0.051	0.131	0.121	0.202	0.099
CO2	0.299	1.090	0.167	0.596	0.643	1.220	0.367
RNA	0.006	0.017	0.014	0.025	0.012	0.063	0.004
DNA	0.001	0.001	0.001	0.001	0.001	0.001	0.001
TP	0.019	0.007	0.066	0.102	0.030	0.012	0.071
TC	0.003	0.003	0.002	0.001	0.001	0.001	0.002
LIP	0.016	0.016	0.016	0.016	0.016	0.016	0.014
MAB	0.004	0.005	0.005	0.010	0.001	0.011	0.017

Table A2a and A2b

2a. Average measured metabolic rates of metabolites in underdetermined network. Values (in 10^{-12} mol. $cell^{-1}.day^{-1}$) are calculated as described elsewhere (Bonarius et al., 1996). The standard deviations associated with these rates (Table 3b) are linear combinations of the standard deviations of the cellular uptake and production rates, and are calculated accordingly (Box et al., 1978). Abbreviations as in Figure 1.

	pO_2 30	pO_2 50	pO_2 1	pO_2 0	pO_2 100	pO_2 30	PMS
G6P	-6.28	-5.30	-7.21	-12.22	-5.758	-4.75	-4.09
R5P	0.62	0.60	0.59	0.55	0.628	0.55	0.65
GAP	0.17	0.17	0.17	0.17	0.172	0.14	0.14
G3P	0.41	0.33	0.21	0.19	0.350	0.34	0.48
PYR	8.07	5.58	10.77	19.54	7.474	5.14	3.96
ACo	-0.77	-0.58	-0.35	-0.37	-0.673	-0.76	-0.93
CIT	1.46	1.46	1.46	1.46	1.467	1.25	1.25
AKG	-0.65	-0.62	-0.64	-0.94	-0.610	-0.65	-0.63
MAL	0.41	0.42	0.42	0.36	0.423	0.37	0.40
CO2	12.02	10.72	7.48	6.31	10.605	9.52	11.10
ASP	0.13	0.16	0.16	0.20	0.135	0.06	0.20
ASN	0.03	0.02	0.03	0.03	0.040	0.10	0.01
GLU	1.01	0.93	1.00	1.36	0.914	1.02	0.71
GLN	-1.87	-1.39	-1.19	-1.80	-1.696	-1.28	-1.87
NH3	1.20	0.67	0.70	0.84	1.059	1.10	1.39

2b. Standard deviations of metabolic rates of metabolites in underdetermined network (Values in 10^{-12} mol. $cell^{-1}.day^{-1}$).

	pO_2 30	pO_2 50	pO_2 1	pO_2 0	pO_2 100	pO_2 30	PMS
G6P	0.347	0.218	0.437	0.134	0.172	0.301	0.790
R5P	0.007	0.018	0.018	0.026	0.014	0.063	0.001
GAP	0.035	0.035	0.035	0.035	0.035	0.030	0.030
G3P	0.012	0.017	0.025	0.065	0.014	0.034	0.031
PYR	0.892	1.019	1.053	1.863	0.734	0.954	0.497
ACoA	0.050	0.134	0.033	0.162	0.034	0.142	0.153
CIT	0.147	0.147	0.147	0.147	0.147	0.125	0.125
AKG	0.109	0.309	0.074	0.268	0.124	0.355	0.199
MAL	0.020	0.036	0.024	0.053	0.018	0.083	0.024
CO2	0.514	1.305	0.382	0.811	0.858	1.481	0.628
ASP	0.003	0.008	0.008	0.018	0.004	0.027	0.009
ASN	0.003	0.007	0.010	0.023	0.003	0.061	0.011
GLU	0.153	0.395	0.128	0.371	0.176	0.452	0.265
GLN	0.055	0.225	0.065	0.230	0.083	0.238	0.162
NH3	0.114	0.155	0.063	0.157	0.127	0.222	0.114

Chapter 4

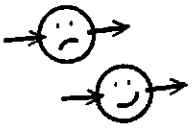

Metabolic-Flux Analysis of Hybridoma Cells in Different Culture Media Using Mass Balances

Hendrik P.J. Bonarius, Vassily Hatzimanikatis,
Koen P.H. Meesters, Cornelis D. De Gooijer,
Georg Schmid, and Johannes Tramper.

ABSTRACT

The intracellular fluxes in the primary metabolism of hybridoma cells in continuous culture have been calculated using mass balances over relevant metabolites. The uptake and production rates of amino acids, CO_2, glucose, lactate, NH_4, Mab, and the intracellular amino acid pools have been determined for two different steady states. The cellular composition (total protein and protein composition, total lipids and fatty acid distribution, total carbohydrates, DNA and RNA) has been measured to calculate the requirements for biosynthesis.

Fluxes of linear metabolic pathways have been determined by measuring the substrate concentrations or the accumulated end products. For the analysis of cyclic metabolic pathways it is shown to be essential to determine the carbon dioxide and ammonia production rates. In mammalian cells both carbon dioxide and ammonia are waste-products of cyclic metabolic pathways. Only by measuring

their accumulation, the fluxes of such pathways can be determined. Other co-metabolites in cyclic pathways, like NAD(P)H, and ATP are not used to estimate the fluxes of primary metabolism. Their mass balances can not be closed because these metabolites are involved in biochemical processes (transhydrogenase, maintenance and oxidative phosphorylation) that are not measurable. However, without these mass balances the set of linear equations that is used to calculate the fluxes is underdetermined. A solution to this problem is the introduction of an additional constraint.

The metabolic fluxes in hybridoma cells in continuous culture at a specific growth rate of 0.83 day^{-1} are estimated for a medium with (optimal medium) and without (sub-optimal medium) Primatone RL, an enzymatic hydrolysate of animal tissue that causes a more than two-fold increase in cell density. It is concluded that:

1. In rapidly proliferating cells, such as investigated here, the majority of glucose (> 90 %) is channeled through the pentose-phosphate pathway, probably to provide NADPH for biosynthesis.
2. Pyruvate oxidation and TCA cycle activity are relatively low, i.e. 9 %, of the glucose uptake in sub-optimal and 17 % in optimal medium, respectively. Under both conditions, only a small fraction of pyruvate is further oxidized to CO_2 due to the small flux from citrate to α-ketoglutarate.
3. Higher carbon dioxide evolution rates in optimal medium are concomitant with increased lipid synthesis rates and with high glucose/glutamine oxidation ratios.
4. The flux from glutamate to α-ketoglutarate (catalyzed by glutamate dehydrogenase) is almost zero in medium with and even slightly reversed in medium without Primatone RL. Almost all glutamine enters the TCA cycle due to the action of transaminases.
5. Proline synthesis does not occur to enable nucleotide synthesis by providing a means to reoxidize NADPH, as has been suggested before. It is more likely that the energy-wasting proline synthesis in hybridoma cells is a redundant pathway, originating from the intercellular proline cycle in mammalian organisms.

INTRODUCTION

Mammalian cells are used for the production of vaccines, recombinant proteins and antibodies. The maximum amount of (recombinant) protein being secreted is relatively low; about 10-20 % of the total cellular protein (Reff, 1993). To increase the capacity of cells to secrete more product and improve space/time yields a better quantitative understanding of cell metabolism is needed. Several studies have already been carried out to proceed in this direction (Mancuso et al., 1994; Sharfstein et al., 1994; Petch and Butler, 1994; Zupke and Stephanopoulos, 1995). By quantifying the intracellular fluxes it might be possible to (i) analyze the nutrient requirements for both anabolic and catabolic processes, and subsequently redesign the culture medium, (ii) tracing metabolic pathways that limit growth, production, or product quality, or pathways that are redundant and energy-consuming and, most important, (iii) understand the bio-chemistry of the cell at a quantitative level, so that the relation and control between different metabolic pathways within the cell can be understood.

The kinetics of animal cell metabolism and the response of animal cells to changes in medium composition and to inhibiting compounds have already been studied extensively (Glacken et al., 1988; Levering et al., 1992; Miller et al., 1989; Miller et al., 1989b; Ozturk and Palsson, 1991; Ozturk et al., 1992). All these studies only concern the extracellular uptake or production rates of primary metabolites, like oxygen, glucose, ammonia, lactate and amino acids. The analysis of these rates can not be used to quantify and understand metabolism at a level of (intracellular) metabolic fluxes. More data are required to calculate the flux distribution in a complex metabolic network like that of mammalian cells (Savinell and Palsson, 1992). These data have in the past been obtained from scintillation counting of the end products of radiolabeled substrates (Fitzpatrick et al., 1993, Katz and Wood, 1993; Petch and Butler, 1994; Reitzer et al., 1980) or from *in vivo* ^{13}C-NMR analysis (Jeffrey et al., 1991; Mancuso et al., 1987; Portais et al., 1993; Sharfstein et al., 1994). Both methods can provide the missing information for the determination of intracellular fluxes because the concentrations of enriched (end)products can be determined.

Due to a practical limit on the number of measurements that can be made by scintillation counting, the information on metabolic activity provided by carbon isotope studies is limited. For example, the citric acid cycle activity is often assessed by simple measurement of $^{14}CO_2$ release (Fitzpatrick et al., 1993), without accounting for the effect of competing pathways (Jeffrey et al., 1991). In contrast, by *in vivo* ^{13}C-NMR analysis different metabolites can be quantified from a single spectrum. Not only different labeled species but also different labeled sites in a molecule can be distinguished. The prevailing metabolic routes that lead to certain end products can therefore be traced (Jeffrey et al., 1991). Moreover, experimental artifacts that might occur during extraction procedures to analyze intracellular metabolites can be avoided (Mancuso et al., 1994; Sharfstein et al., 1994). However, the use of *in vivo* ^{13}C-NMR spectroscopy has some shortcomings as well. Only labeled substrates, intermediates and products can be measured by ^{13}C-NMR analysis. Further, the unsolved concept of metabolic channeling in mitochondria by enzyme complexes might mislead interpretation of ^{13}C-NMR spectrograms for rotationally superimposable intermediates, like succinate and fumarate (Srere, 1990; Portais et al., 1993).

More important, ^{14}C scintillation counting and ^{13}C-NMR analysis require an experimental set-up that causes different culture conditions than standard homogeneous bioreactors. Only in inhomogeneous systems, like hollow fiber reactors, sufficient cell densities can be attained to obtain quantifiable signals for a NMR spectrometer (Mancuso et al., 1994). Studies with ^{14}C labeling techniques or *in vivo* ^{13}C-NMR spectrometry have only been carried out in bioreactors with cells having a very low biosynthesis/maintenance ratio. In hollow-fiber reactors, perfusion chambers or T-flasks where cells are confluent, cells grow at low (specific) rates (μ) close to zero. This is not the case in homogeneous bioreactors, like chemostats, where the cell growth rate and, consequently, the requirement for NADPH is much higher (Stryer, 1988). As will be shown here, this can have a dramatic influence on the metabolic flux distribution. The experimental set-up required for studies with labeled substrates might change the metabolism to such an extent, that another method is needed to determine metabolic flux distributions of mammalian cells in the bioreactors that are widely applied in in-

dustry. This can either be done by the use of labeled substrates in similar (homogeneous) systems or by "metabolic flux balancing" (Varma and Palsson, 1994).

In this paper the metabolic flux distribution of animal cells in continuous culture as determined by the latter method is described. By applying the known cell stoichiometry and by measuring the relevant metabolites the intracellular fluxes can be estimated by linear regression (Papoutsakis and Meyer, 1985; Vallino and Stephanopoulos, 1993; Jorgensen et al., 1995). In comparison to earlier studies on the primary metabolism of hybridomas (Glacken et al., 1988; Hiller et al., 1991; Levering et al., 1992; Miller et al., 1989; Miller et al., 1989b; Ozturk et al., 1992), an additional set of metabolic rates needs to be measured to be able to determine the intracellular fluxes. Recently, Zupke and Stephanopoulos (1995) showed by ^{13}C *in vitro* NMR that metabolic fluxes can be calculated using mass balances. Here, three additional considerations are taken into account to determine metabolic fluxes in mammalian cells.

Figure 1

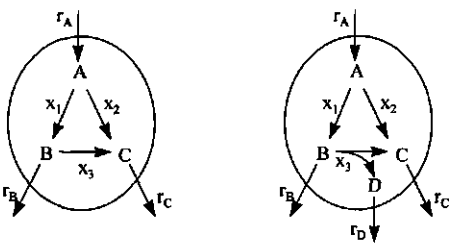

(A) (B)

Fluxes within cyclic pathways can only be determined when measurable and balanceable cometabolites are produced or consumed. The fluxes in network A cannot be calculated by using the measured uptake and production rates r_A, r_B and r_C. There are infinitely many possible combinations for x_1, x_2 and x_3 for each set of metabolic quotients. Only when measurable cometabolites are produced or consumed, as is the case in stiochiometric network B, there is one unique solution for each **r**.

First, the (high-molecular) end products of primary anabolism, i.e., (total) protein, nucleic acids, sterols, lipids, and total intracellular carbohydrates, need to be quantified to

determine the metabolic flux distribution of animal cells. Since a significant amount of the consumed metabolites is converted into biomass, these end products have to be determined accurately for different cell lines and for the same cell line under different conditions.

Second, as will be shown later, the mass balances of co-metabolites (like ATP, NAD(P)H, O_2, CO_2 and NH_3) are necessary to calculate fluxes within *cyclic* pathways. The fluxes in such pathways are *by definition* linear dependent, as a consequence of which the individual fluxes cannot be calculated (See Theory section and Figure 1).

Only by including mass balances of metabolites that are co-produced or co-consumed in these metabolic reactions, the fluxes in cyclic metabolic pathways can be calculated. However, some metabolites can not be used for flux analysis since their mass balances can not be closed. The mass balances of NADPH, NADH, and ATP can not be closed since some biochemical processes, in which these metabolites are involved, are not measurable, e.g. the requirement for ATP in cell maintenance, the activity of transhydrogenase and the P/O-ratio. Therefore, including these mass balances will obviously give biased results and this approach should not be used for the determination of metabolic fluxes. In the metabolic network that is used in our approach, the only co-metabolites of which the mass balances can be regarded as closed, are CO_2 and NH_3. The mass balances of NAD(P)H, O_2 and ATP can only be applied to quantify the mentioned biochemical processes, once the fluxes of primary metabolism (glycolysis, glutaminolysis, pentose phosphate pathway, citric acid cycle and biomass synthesis) are known. The accurate measurement of the CO_2 evolution and the NH_3 production rate is of critical importance.

Third, the carbon dioxide evolution rate (CER) was not measurable in mammalian cell culture due to bicarbonate in the medium. However, we recently developed a method to determine the CER in bicarbonate-buffered cell culture, by applying gas and liquid phase mass balances for carbon dioxide and bicarbonate, respectively (Bonarius et al., 1995a).

Here, the metabolic flux distribution of hybridoma cells for two different culture conditions is determined by the use of mass balances, taking into account the above considerations.

THEORY

The principle of quantifying the intracellular fluxes of biological systems by applying mass balances has been used for almost a decade (Roels, 1980; Papoutsakis and Meyer, 1985; Noorman et al., 1991; Roels, 1983; Vallino and Stephanopoulos, 1993; Varma and Palsson, 1994). For each relevant metabolite a mass balance can be derived in which both the transport rates over the cell membrane and the intracellular reaction rates are included. This results in a set of linear equations (i.e., mass balances for each of the metabolites) with a certain number of unknowns (i.e., fluxes). The set of linear equations that describes the metabolism of mammalian cells is underdetermined; the number of mass balances is smaller than the number of fluxes. To solve such an underdetermined network either some fluxes have to be determined experimentally (Savinell and Palsson, 1992) or extra constraints have to be added. In this article a method is proposed applying this latter strategy.

Equations

The intracellular accumulation of metabolites has to be included in the mass balance of metabolites over a CSTR, as cells that contain a certain amount of a metabolite leave the bioreactor via the outgoing medium. For metabolite A the mass balance thus reads:

$$\frac{dC_{I,A}(t)(n_v+n_d)}{dt}+\frac{dC_{E,A}(t)}{dt} = DC_{E,A}^{med} - DC_{E,A}(t) - DC_{I,A}(t)(n_v+n_d) + r_{tot,A}n_v \quad (1)$$

where n represents the (viable or dead) cell number (cell.l^{-1}), D the dilution rate (day^{-1}) and r the production rate (mol.cell^{-1}.day^{-1}). The indices I and E represent intracellular and extracellular concentrations, respectively. It should be noted that the dimension of $C_{E,A}(t)$ and $C_{E,A}^{med}$ is mol.l^{-1}, whereas the dimension of $C_{I,A}(t)$ is mol.cell^{-1}.

From the total cell balance (Miller et al., 1987) it can be derived that:

$$D(n_v + n_d) = \mu n_v \qquad (2)$$

Under steady state conditions Equations 1 and 2 give:

$$r_{tot,A} = \mu C_{I,A}(t) + \frac{D(C_{E,A}(t) - C_{E,A}^{med})}{n_v} \qquad (3)$$

$r_{tot,A}$ is redefined to discriminate between intracellular production rate and extracellular production rate:

$$r_{tot,A} = r_{I,A} + r_{E,A} \qquad (4)$$

The above equations, that are used the calculate r_{tot}, consider the pertinent mass balances over the bioreactor. The cells are regarded as a black box system. In contrast, to calculate the metabolic fluxes, mass balances are derived over the cell, and the intracellular reaction conversion rates are included.

The conversion rate of a metabolite A in a biological system is given by the stoichiometry and by the metabolic flux through the concerned reactions:

$$r_{tot,A}(t) = \Sigma_j \alpha_{j,A} x_j(t) \qquad (5)$$

where $\alpha_{j,A}$ is the stoichiometric coefficient of A in reaction j (dimensionless), and x_j the metabolic flux through reaction j (in mole reaction product.cell^{-1}.day^{-1}). A negative value of $\alpha_{j,A}$ indicates that metabolite A is a substrate in reaction j, whereas a positive value indicates that metabolite A is produced.

The set of linear equations obtained from mass balances over each relevant metabolite in the cell is represented in matrix notation by

$$r(t) = Ax(t) \qquad (6)$$

where **A** is an n x m matrix of stoichiometric coefficients, **x**(t) an m-dimensional flux vector and $\mathbf{r}_{tot}$(t) an n-dimensional production rate vector.

The flux vector $\mathbf{x}(t)$ can be estimated by the least-squares method, where $\mathbf{x}(t)$ is that value of $\mathbf{x}(t)$ which minimizes the sum of squared deviations of fitted values from the observed values. The least-squares solution, which is denoted by $\mathbf{x}(t)$, can be found by (pseudo)inverting the stoichiometric matrix **A**. Depending on the dimensions and the rank of the matrix, different algorithms can be applied to (pseudo)invert **A**.

Least-squares solution and directly calculable fluxes

In principle, there are two approaches to estimate the fluxes in a metabolic network. Either all fluxes are estimated by the least-squares method (Zupke and Stephanopoulos, 1995) or the fluxes are calculated directly by deriving equations for each flux (Ferrance et al, 1983). This second approach is not possible in rank deficient networks. Here, a combination of both approaches is applied: Only those fluxes that are not directly calculable - because they are part of a sub-network that contains less constraints than fluxes or a sub-network that contains linear dependent fluxes - are estimated by the least-squares method in combination with an additional constraint. The fluxes that are directly calculable are determined by measuring the r_{tot} belonging to them. For example, the alanine transaminase flux (x_{26}) (Table A1 in Appendix A) is determined by the measured alanine production rate and the measured alanine requirement for biomass. After determination of all calculable fluxes a smaller network remains that is rank deficient and is solved by the least-squares method as described above. Figure 2 gives the network that is used to calculate the flux distribution in mammalian cells. The dotted lines represent the fluxes that are directly calculable from the measured $\mathbf{r}_{tot}(t)$ and the measured requirements for biomass and product. The solid lines represent the fluxes that are estimated by the least-squares method.

The input vector $\mathbf{r}_{tot}(t)$ for the remaining network (Appendix B) is calculated using the net catabolic rate vector $\mathbf{r}_{nc}(t)$ for each metabolite. The net catabolic rate for metabolite A is the production rate of A corrected for its biomass synthesis rate (See also Appendix C). The use of the net catabolic rates substantially reduces the complexicity of the equations in Appendix B.

Rank deficiency in metabolic networks

When the (remaining) stoichiometric matrix **A** is rank deficient (rank(**A**) < m and/or n < m), the least-squares problem has infinitely many solutions. From a biochemical point of view there are two possible causes for a network that is not full rank. In a complex biochemical system, like that of mammalian cells, fluxes within sub-networks can be linearly dependent. Particularly, fluxes that form part of cyclic pathways make up rank-deficient sub-networks (rank(**A**) < m). Second, rank deficiency occurs when the number of mass balances is smaller than the number of fluxes (n < m). In both cases an infinite number of solutions can be found for the flux vector **x**(t) for each set of measurements **r**(t).

The measurement of balanceable co-metabolites, like CO_2 and NH_3, is essential for estimating fluxes in cyclic pathways.

Some metabolic pathways are cyclic, as a consequence of which the fluxes within these pathways can not be estimated by measuring the uptake and production rates of the main metabolites only. The metabolites A, B and C in Figure 1a could circulate through the pathway without any accumulation of one of the metabolites. However, when (measurable) co-metabolites are involved that accumulate, the activity of the cyclic pathway is known. In Figure 1b a simple example of a cyclic pathway is given, which shows that without co-metabolites the individual fluxes within the cyclic network can not be calculated. Provided that the metabolite is measurable and its mass balance can be closed, the pertinent co-metabolite is suited to quantify the individual fluxes within the cyclic pathway. This will be discussed in more detail below.

Table 1 gives four examples of cyclic pathways that occur in animal cell metabolism. In contrast to CO_2 and NH_3, the mass balances of NAD(P)H, and ATP can not be closed. They contribute to other biochemical processes that can not be measured. The P/O ratio, the ATP and NADH requirement for maintenance processes are not quantifiable. Also the activity of transhydrogenase, that catalyzes the reversible conversion of NADH into NADPH, is not known. Therefore, these co-metabolites can not be used for estimation of fluxes within cyclic pathways. Although the mass balance of O_2 can

be closed, the determination of the O_2 uptake rate (OUR) cannot be used to estimate metabolic fluxes, because O_2 is stoichiometrically connected to other metabolic pathways via NADH. Only when the fluxes within the mentioned cyclic pathways are known, the mass balances of ATP, O_2, NADH and NADPH can be used to estimate these biochemical processes i.e., P/O ratio, ATP and NADH requirement for maintenance, and transhydrogenase activity.

Table 1

Some cyclic pathways in mammalian cell metabolism.

Metabolic pathway	Balanceable Co-metabolites	Unbalanceable Co-metabolites
Pentose Phosphate Pathway	CO_2	NAD(P)H, ATP, H_2O
Glutaminolysis	NH_3	NAD(P)H, ATP
TCA Cycle	CO_2	NAD(P)H, ATP, $FADH_2$, H_2O
Pyruvate carboxylase-Malic enzyme-Pyruvate kinase	CO_2	NADPH, ATP

Rank deficiency can be avoided by adding extra constraints

When a (sub)network is still rank deficient (i) either the number of fluxes has to be reduced or (ii) extra constraints have to be added to the system.

(i) The number of fluxes can be reduced by lumping reactions. However, this is only allowed when the lumped fluxes are independent from the overall network, otherwise the output vector **x** will be affected.

(ii) Another option is the addition of an objective function by which one unique solution is found out of the infinitely many solutions of the least-squares method in rank deficient networks. Different numerical computations are available to find unique solutions in rank deficient linear systems (Thisted, 1989). In a theoretical study, Savinell and Palsson (1992a; 1992b) used the simplex algorithm to calculate metabolic fluxes in hybridoma cells using different "biochemically meaningful" objective functions. An alternative objective function is the *miminum-norm constraint*. The (Euclidian) norm of a vector is the square of its length, and is found by applying the *Moore-Penrose pseudo-inverse* of **A** (Golub and Van Loan, 1989). This pseudo-

inverse can be calculated by Singular Value Decomposition (SVD) (Thisted, 1989). Out of the infinitely many solutions of the least-squares method, there is only one vector $\mathbf{x}$ for each set of measured $\mathbf{r}_{tot}$'s, that has the smallest Euclidian norm. The Moore-Penrose pseudo-inverse gives this solution for each $\mathbf{r}_{tot}$ (Golub and Van Loan, 1989; Thisted, 1989). (It is outside the scope of this article to describe the SVD algorithm. For a detailed description of this numerical procedure the reader is referred to Thisted (1989).) Here, the minimum-norm constraint is used to calculate the fluxes of a rank deficient ($m = 22$, $n = 21$, rank(A) = 19) network.

Stoichiometric matrix

A metabolic network with the significant metabolic pathways for proliferating animal cells is constructed (Savinell and Palsson, 1992a; Stryer, 1988). Figure 2 shows the metabolic model that is used here for flux analysis. The assumptions that were used to obtain the network are given below.

Since catabolism of high-molecular end products (for instance fatty acid oxidation) does not occur to a significant extent in rapidly growing cells when sufficient nutrients for energy production are available, only pathways that are involved in the catabolism of low-molecular metabolites (amino acids and glucose) and in the biosynthesis of macromolecules are considered.

To reduce the complexity and the number of metabolic equations, reactions in converging pathways that occur in fixed proportions and in complex unbranched biosynthesis pathways with negligible intermediate concentrations are lumped. An example of the first is DNA synthesis and of the latter cholesterol synthesis.

For the metabolic flux analysis all lipids are lumped into one fraction of fatty acids and one fraction of sterols. The fraction of fatty acids is assumed to consist only of oleic acid (C18:1). As will be shown later, this is allowed because C18:1 is the largest fraction and the fractions of fatty acids shorter and longer than C18 are approximately equal. The measured distribution of fatty acids of hybridoma cells is given in the results section. The sterols cholesterol and desmosterol are separated from the fatty acids

into one different fraction (CHOL) because the stoichiometry for their biosynthesis is different (see also Appendix A).

Figure 2

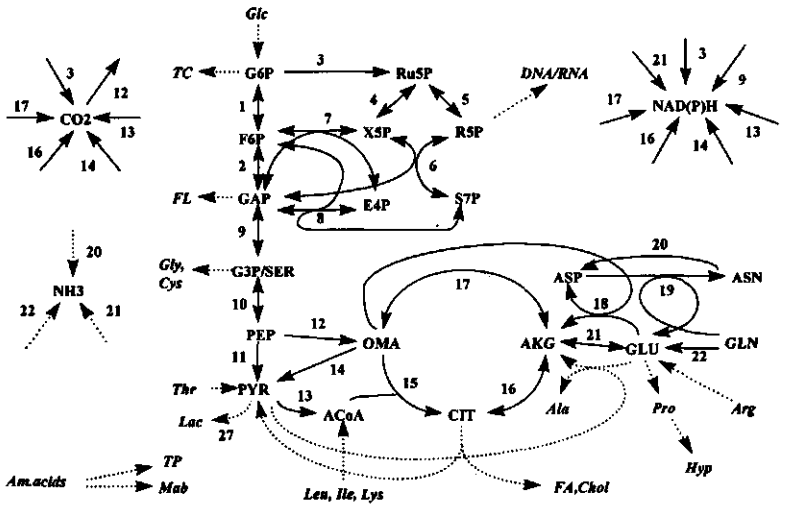

Network used for the determination of metabolic fluxes in hybridoma cells. The dotted lines represent fluxes that are determinable by measuring the end products or substrates. The remaining fluxes (1-21) are solved by the least-squares analysis of the mass-balnce equations complemented with the minimum-norm constraint. The elements of the production rate vector $\mathbf{r}^{LS}(t)$ (Eq. 5) are calculated according to the equations in Table 6.

The citric acid cycle intermediates are lumped into citrate (CIT), α-ketoglutarate (AKG), and oxaloacetate and malate (OMA). These are the metabolites at the key branch points of the cycle (Sharfstein et al., 1994). Oxaloacetate and malate are lumped together because the conversion into oxaloacetate does not yield a balanceable co-metabolite (like CO_2). Neglecting this flux (oxaloacetate to malate) can therefore not influence the estimated values of other fluxes.

The nucleotide synthesis pathway is lumped into two pathways: DNA and RNA synthesis. These have to be regarded as two different fluxes because the stoichiometries for DNA and RNA synthesis are different, and also because of the fact that RNA is de-

graded constantly, whereas DNA is stable. The actual rate of RNA synthesis is higher than its measured intracellular production rate ($\mu C_{I,RNA}$), due to the high RNA turnover. This turnover rate is estimated on the basis of literature values for rRNA and mRNA half-life, as described by Savinell and Palsson (Savinell and Palsson 1992a). By measuring the intracellular RNA concentration, the $r_{I,RNA}$ can be corrected for by the RNA turnover rate.

The fractions of nucleotides in DNA and RNA are given by Zubay (1983): dATP 28.9 %, dGTP 21.7 %, dCTP 20.7 %, dTTP 28.7 % for DNA; and ATP 29.4 %, GTP 19.8 %, CTP 21.4 % and UTP 29.3 % for RNA, respectively.

We found that the measurement of total carbohydrates is of critical importance to close the C balance in hybridoma cells (Bonarius et al., 1998e). It is assumed that the majority of this biomass fraction consists of carbohydrate chains in glycoproteins. Since these are mainly formed from G6P (Stryer, 1988) the "total carbohydrate flux" is G6P + 3.46 ATP → TC (Savinell and Palsson, 1992a).

Mammalian tissue is *ureotelic*, which means that the excess NH_3 is converted into urea and then excreted (Stryer, 1988). However, in tumor cells the urea cycle is often not active (Coleman and Lavietes, 1981). Indeed, as will be shown later, we could not detect urea in the culture medium for the cell line under investigation. Therefore, the urea cycle is not considered in the metabolic flux analysis.

MATERIALS AND METHODS

Cell line and culture medium

A murine hybridoma cell line that produces an IgG_{2A} antibody directed against human ferritin was grown in serum-free low-protein lipid-free medium. A mixture of Dulbecco's, Ham's F12 and Iscove's powdered media (D:H:I = 1:1:2; Gibco, Grand Island, NY, USA) was used as the basal medium, which was supplemented with 5 mg/ml insulin (Sigma, St.Louis, MO, USA), 6 mg/ml transferrin (Boehringer Mannheim,

Mannheim, FRG) and 0.35 % (w/v) Synperonic F68 (Serva, Heidelberg, FRG). The medium contained 5 g/l glucose, 5 mM glutamine and 2.73 g/l sodium bicarbonate. Two steady states were examined, one with and one without using 0.3 % (w/v) Primatone RL (Quest Int., Erftstadt-Lechenich, FRG), an enzymatic hydrolysate of animal tissue. In the medium without Primatone RL amino acids equivalent in composition and concentration to those in Primatone RL were added to the medium (Ajinomoto Co., Tokyo, J).

Cell culture bioreactor

A bench-scale Biostat MD bioreactor with a 1 L working volume (B.Braun Diessel Biotech, Melsungen, FRG) was operated in continuous mode. Temperature, stirrer speed and pH were maintained at 37 °C, 150 rpm and 7.20, respectively. The pH was controlled by 0.5 M NaOH. Oxygen supply was via surface aeration only and the medium dissolved oxygen concentration was controlled at 40 % air saturation by adjusting the oxygen fraction in a nitrogen/oxygen gas mixture. This fraction was measured by mass flow meters and used to calculate the OUR. The total gas flow was kept constant at 0.50 L $min.^{-1}$. Mass flow meters were calibrated using an ADM 1000 Intelligent Flowmeter (J & W Scientific, Koeniz, CH). The dilution rate was controlled at a value of 0.70 d^{-1} using an appropriate balance and a Sartorius dosing system (Sartorius GmbH, Göttingen, FRG).

Cell density, size and viability

Viable cell concentrations and viabilities were determined by the trypan blue exclusion method using a haemacytometer. The total cell concentration and the cell size distribution was determined using a Casy 1 instrument (Schärfe System, Reutlingen, FRG) that is based on the Coulter counter principle.

Carbon dioxide evolution and oxygen uptake rates

Since the medium contains bicarbonate, the measured CO_2 in the outlet gas comes from two sources: the medium and the CO_2 producing cells. Also, the accumulation in

the liquid phase has to be taken into account. The liquid phase concentration can not be calculated by only applying Henry's law, as a partial gradient for desorption is required (Royce and Thornhill, 1991). Moreover, during medium preparation and storage carbon dioxide evaporates from the bicarbonate-buffered medium. A method was developed to determine the carbon dioxide evolution rate under these conditions, by applying appropriate mass balances (Bonarius et al., 1995). It has been shown previously that the CO_2 evolution rate (CER) can be determined by

$$CER = x^o_{CO_2}(F^i_g + F_l(\frac{P}{H^{CO_2}} + \frac{F^o_g}{k_l^{CO_2} a V_l})(1 + \frac{K_l}{10^{-pH}})) - \beta F_l C^i_A(0) \quad (8)$$

where x_{CO2}^o is the measured CO_2 fraction in the outlet gas. The other parameters are defined in the Nomenclature Section. The CO_2 in the outlet gas was measured by an infrared gasanalyzer (Rosemount, Baar, CH).

The O_2 uptake rates were calculated from the mass transfer coefficient $k_l^{O2}a$ and the fraction of oxygen in the inlet gas, as described before[1]. Values for $k_l^{O2}a$ were determined in both fresh medium and medium containing dead cells using the dynamic method (Van 't Riet and Tramper, 1991). No significant differences were found and $k_l^{O2}a$ was determined to be 63.4 d^{-1} at a stirrer speed of 150 rpm and a gas flow of 0.50 L min^{-1}.

Analysis of metabolites

Acid extraction of intracellular metabolites was done as described elsewhere (Schmid and Keller, 1992). Cells were cooled, washed in cold phosphate buffered saline solution (PBS), collected by centrifugation and extracted on ice using perchloric acid (Merck, Darmstadt, FRG). After neutralization with KOH solution, the supernatant was lyophilized and the freeze dried samples were taken up in 1 ml PBS for subsequent analysis of metabolites.

Glucose and *lactate* concentrations were determined with a YSI analyzer (YSI, Yellow Springs, OH, USA). *Ammonia* was measured with an ion-selective electrode (Orion,

Boston, MA, USA). Primary and secondary *amino acids* were determined by HPLC as described elsewhere (Schmid and Keller, 1992). Samples were treated with orthophthal-aldehyde and 9-fluorenylmethyl chloroformate, and the resulting amino acid derivatives separated by HPLC on a RP-18 column (Amino Quant 1090, Hewlett-Packard, Palo Alto, CA).

Fatty acids and *sterols* (cholesterol and desmosterol) were determined by gas chromatography (GC). Cells were harvested at 1.0-1.5 x 10E6 viable cells/mL, washed twice with ice-cold phophate-buffered saline (PBS) and the biomass stored at -70°C under N_2 atmosphere. Frozen cell samples were taken up in 0.25 M sucrose and homogenated by sonication. 1 mL of the homogenate was lyophilized. To the residue 0.1 mL of methanol containing 10 µg pentadecanoic acid (standard) and 1 mL 1 N sodium methylate were added and heated for 45 min to 70°C. After cooling, the solution was neutralized by 1 N hydrochloric acid and extracted with 2 mL hexane (Uvasol, E. Merck, Darmstadt, FRG). The hexane phase was evaporated to 50-100 µL. A solution of diazomethane was then added and concentrated again to ~ 50 µL. The concentrated solutions containing fatty acid methyl esters and sterols were analyzed by GC using a 15 m fused-silica capillary (DB-1) coated with a methyl silicon.

The *total lipid fraction* was determined by weight after chloroform/methanol extraction as described by Xie and Wang (1994b). *RNA* and *DNA* were purified according to Chomczynski (1993) using Trizol Reagent (Gibco, Paisley, Scotland, UK). DNA was quantified at A_{260} using a quartz cuvette (1 cm pathlength) and an A_{260} of 1.0 indicated 50 mg/ml DNA. Total RNA was quantified by measuring the absorbance at 260 nm with yeast tRNA (Fluka, Buchs, CH) being used as a standard. The intracellular *glycogen* was measured after enzymatic breakdown using amyloglucosidase (Fluka, Buchs, CH) as described by Lust et al (1975). *Total carbohydrates* were analyzed by the phenol (Gibco, Paisley, Scotland, UK) reaction using glucose as standard as described by Xie and Wang (1994b). *Total cellular protein* content was quantified using the Biuret assay. Briefly, after cell disruption in lysis buffer (1 mM ethylenediaminetetraacetic acid (EDTA), 0.2 mM phenylmethanesulfonyl fluoride (PMSF) and 0.5 % Triton) cell

fractions were incubated in Biuret reagent and the absorption at 595 nm was determined using a bovine serum albumin (BSA) standard curve.

The *amino acid composition* of total cell protein was determined by HPLC after acid hydrolysis under non-oxidative conditions in a Pierce ReactiTherm Heater (Pierce Europe, Oud-Beijerland, NL). During acid hydrolysis glutamine and asparagine are converted to glutamate and aspartate, respectively. Therefore, only the total amount of glutamate and asparate was used to calculate the amino acid composition. The glutamine/glutamate and asparagine/aspartate ratios as reported in the literature (Creighton, 1984; Savinell and Palsson, 1992a) were used to correct for this deamidation. The value of the cysteine fraction in total cellular protein was obtained from the literature, because of cysteine degradation during acid hydrolysis.

Antibody titers were quantified by a standard ELISA. *Urea* was quantitated by the indophenol color reaction using a detedtion assay of Sigma Diagnostics (Kit nr. 640, Sigma Diagnostics, St.Louis, MO). *Dry cell weight* was measured after centrifugation of 50 ml culture volume and drying the cell pellet at 60 °C under vacuum overnight.

RESULTS AND DISCUSSION

Three conditions need to be fulfilled to determine metabolic fluxes in mammalian cells by flux balance analysis: (i) In the metabolic network all the relevant fluxes should be included and the non-balanceable metabolites should be excluded. (ii) To estimate fluxes in underdetermined networks, additional constraints are required apart from the constraints that are determined by the mass-balance equations. Here, the minimum-norm constraint is used. (iii) The cellular composition has to be determined independently for at least each different cell line, and as will be shown here, also for the same cell line under different (medium) conditions.

Cell densities

By cultivating cells in medium with and without semi-defined components like yeast extract or meat hydrolysates it is possible to create different conditions for an efficient and a non-efficient cell metabolism. By adding Primatone RL, a protein free enzymatic meat hydrolysate, to the medium, cell densities increased more than two-fold in a continuous culture at $D = 0.70\ d^{-1}$ compared to a culture without Primatone RL (but containing amino acids equivalent in composition and concentration to Primatone RL) (Bonarius et al., 1995a). In Table 2 mean viable cell densities are given for three different experiments, each performed using DHI medium with and without Primatone RL, respectively. Samples for flux analysis were taken from Experiment 1.

Table 2

Mean viable cell densities (10^6 cells.ml^{-1}) and respiration quotients (dimensionless) for six steady states. Experiments 1 and 2 were described before (Bonarius et al., 1995a).

	DHI + standard amino acids of Primatone RL		DHI + Primatone RL	
	n_v	RQ	n_v	RQ
Exp.1	1.35	0.98	3.10	1.04
Exp.2	1.68	0.97	3.23	1.07
Exp.3	1.48	0.95	3.51	1.02

Cell size

Cells in medium containing Primatone RL had a significant (14 %) larger volume than cells in medium without Primatone RL according to Coulter Counter analysis (Table 3). Apart from the initial response to osmotic changes that can be described by the Boyle-Van 't Hoff equation, hybridoma and CHO cells attain in steady state larger volumes at high osmolarities (Cohen et al., 1989; Ozturk et al., 1991). The osmolarity in the culture medium with Primatone RL was in fact, though only a fraction, smaller.

Therefore, the changes in cell size can not be caused by a difference in osmolarity. It also seems unlikely that the increase in cell size is caused by differences in cell cycle

Table 3

Cellular composition. Values are given in 10^{-5} mg/cell and as % of dry cell weight (DCW). Values for cell size are given in fl.cell^{-1} (10^{-15} l.cell^{-1}). Numbers between parentheses indicate the number of datapoints used per steady state. RNA values are corrected for degradation rates as described in by Savinell and Palsson (1992). The values for the hybridoma cell line that was investigated by Xie and Wang (1994b) are given in comparison.

	w/o Primatone RL.			w/ Primatone RL.			Xie and Wang (1994b)	
	Absolute value		Fraction of DCW	Absolute value		Fraction of DCW	Absolute value	Fraction of DCW
	10^{-5} mg/cell		%	10^{-5} mg/cell		%	10^{-5} mg/cell	%
TC	3.32	(3)	7.1	3.56	(3)	7.0	0.88	3.5
TP	33.2	(2)	70.6	34.2	(2)	67.1	18.2	72.9
Lipids	4.60	(1)	9.7	5.05	(1)	10.0	3.38	13.5
RNA	2.70	(3)	5.8	3.01	(2)	5.3	0.95	3.8
DNA	0.67	(2)	1.4	0.74	(2)	1.5	0.35	1.4
DCW	47.0	(1)		50.5	(1)		25.0	
Cell size	1760	(3)		2005	(3)		-	

distribution (Martens et al., 1993), since at both steady states cells were growing at virtually the same specific growth rate. Probably differences in energy metabolism influenced cell size for the following reasons. It was found by others that starved cells increased their volume after nutrient repletion. This was ascribed to an energy-dependent response that supports cellular osmotic activity (Cohen et al., 1989) and subsequently leads to an enhanced capacity to regulate cell volume (Hoffmann, 1983). The same might occur after the addition of Primatone RL in that unknown components of the meat hydrolysate enhance the availibility of energy, resulting in a higher os-

motic activity. In any event, to compare the metabolic flux distribution at both steady states, a correction for differences in cell volume has to be applied.

Cellular composition

In Table 3 the cellular composition of cells for the two different conditions are given as determined by the assays described in the Materials and Methods section. The relative fractions are significantly different from other cell lines (Kirkman and Allfrey, 1972; Xie and Wang, 1994b; Zupke and Stephanopoulos, 1995). Also under the two different culture conditions investigated, the total cell mass, and the relative fractions vary. More research is needed to determine whether the cellular composition has to be determined not only for each cell line but also under each different culture condition. If the cellular composition remains equal upon changes in culture conditions, and the cell size varies, only one parameter (for instance total protein content, dry cell weight or cell size) will be sufficient for the determination of metabolic fluxes. The cellular composition of the used hybridoma cell line under a variety of (medium) conditions is currently under investigation.

Since background glucose concentrations were equal to glucose concentrations after treatment with amyloglucosidase, it can be concluded that the hybridoma cells under the conditions described here do not contain any glycogen.

Lipids

Figure 3 shows the distribution of fatty acids and sterols as determined by gas chromatography. For flux analysis the fatty acids are lumped into one fraction of oleic acid (C18:1), which is more than 55 % of total lipids. The amounts of fatty acids with shorter and longer chain lengths than C18 are approximately equal. Therefore, we can assume that the overall stoichiometry for fatty acid synthesis is 8 ATP + 9 ACOA + 16 NADPH $\rightarrow$ FA. The distribution of fatty acids as determined by gas chromatography is similar for both culture conditions, but the total amount of lipids as determined by weight after extraction is significantly different on a per cell basis.

Figure 3

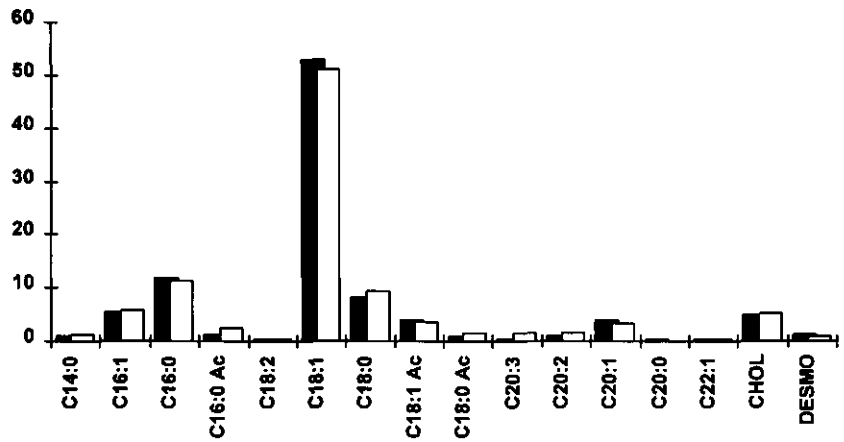

Distribution of fatty acids and sterols of hybridoma cells cultured in medium without (black columns) and with (open columns) Primatone RL as determined by gas chromatography. Values are given as a percentage of the total fatty acids and sterols.

Extra- and intracellular metabolic rates

In Table 4 the sum of extracellular and intracellular production rates (r_{tot}) of hybridoma cells cultured in a sub-optimal and in an optimal medium are shown. The intracellular production rates are calculated from the intracellular pools. The net catabolic rates, that are calculated using the cellular (Table 3) and amino acid (Table 5) composition, the net catabolic rates (Equation 9, Appendix C) are shown as well.

A positive value for the net catabolic rate of an amino acid indicates that the pertinent amino acid is produced in the primary metabolism. Theoretically, the net catabolic rates of essential amino acids (indicated by an asterix in Table 4) can not be positive, because they can not be synthesized in mammalian cells. This is indeed the case for all essential amino acids within the range of their error intervals (the standard deviations of the uptake rates of HIS and VAL for the medium with Primatone RL are 0.0049 and 0.0154 $*10^{-12}$ mol.cell^{-1}.day^{-1}, respectively). Only the net catabolic rate of THR in the medium with

Table 4

Total production rates (r_{tot}) and net catabolic rates (r_{nc}). The net catabolic rates for amino acids (in order of chromatographic separation) and glucose are calculated by Equation 8. The stoichiometric coefficients Θ are determined from the cellular composition (Table 3), the determined amino acid composition in cellular protein (Table 5) and the known amino acid composition of Mab (Table 5) (Edelman et al., 1969). A positive net catabolic rate indicates that the pertinent metabolite is produced in primary metabolism. Mean values of three data points in each steady state (each data point *in duplo*) are given in 10^{-12} mol.cell^{-1}.day^{-1}. Essential amino acids are indicated with an asterix (*). Metabolites that are not integrated in biomass are denoted $r_{nc}=r_{tot}$.

Metabolite	Total production rate (r_{tot}).		Net catabolic rate (r_{nc})	
	w/o Prim.	w/ Prim.	w/o Prim.	w Prim.
GLC	-6.874	-4.716	$r_{nc}=r_{tot}$	$r_{nc}=r_{tot}$
NH3	1.216	0.505	$r_{nc}=r_{tot}$	$r_{nc}=r_{tot}$
CO2	9.924	11.06	8.184	9.090
LAC	8.849	4.873	$r_{nc}=r_{tot}$	$r_{nc}=r_{tot}$
ASP	-0.066	-0.103	0.184	0.159
GLU	-0.079	-0.159	-0.200	-0.287
ASN	-0.018	-0.057	0.053	0.016
SER	-0.080	-0.132	0.089	0.044
GLN	-1.809	-0.997	-1.525	-0.699
HIS*	-0.049	-0.022	-0.025	0.004
GLY	-0.089	-0.087	0.124	0.137
THR*	-0.134	-0.089	-0.013	0.038
ALA	0.680	0.390	0.928	0.640
ARG	-0.133	-0.089	-0.079	-0.068
TYR	-0.063	-0.059	-0.026	-0.020
CYS	-0.085	-0.050	-0.064	-0.027
VAL*	-0.180	-0.145	-0.039	0.003
MET*	-0.066	-0.057	-0.039	-0.013
TRP*	-0.028	-0.027	-0.015	-0.013
PHE*	-0.058	-0.073	-0.007	-0.020
ILE*	-0.168	-0.160	-0.084	-0.071
LEU*	-0.226	-0.303	-0.089	-0.159
LYS*	-0.148	-0.174	-0.077	-0.100
PRO	0.198	0.095	0.294	0.196
HYP	0.177	0.095	$r_{nc}=r_{tot}$	$r_{nc}=r_{tot}$

Table 5

Amino acid composition. The amino acid distribution as determined by HPLC after hydrolysis of total cell protein. For both steady states mean values of three datapoints are given in % mol/mol. Literature values for cell protein and (Savinell and Palsson, 1992a) MAB (Edelman et al., 1969) are given as well. Values for ARG and GLN are corrected as described in the Material and Methods section. The measured values for CYS are given here, but are not used to calculate the net catabolic rates.

Amino acid	W/O Prim.	W Prim.	Savinell and Palsson (1992a)	Mab (Edelman et al., 1969)
ASP	5.3	5.3	5.5	4.0
GLU	5.8	5.9	4.6	5.0
ASN	4.2	4.2	4.4	3.4
SER	5.9	5.9	7.1	5.3
GLN	4.9	5.0	3.9	5.5
HIS	1.9	1.7	2.1	1.5
GLY	8.1	8.1	7.5	6.8
THR	4.7	4.7	6.0	7.9
ALA	7.6	7.7	9.0	6.5
ARG	5.4	5.5	4.7	4.4
TYR	2.4	2.3	3.5	4.1
CYS	0.7	0.6	2.8	2.4
VAL	5.3	5.5	6.9	8.6
MET	2.3	2.6	1.7	1.4
TRP	0.2	0.3	1.1	1.5
PHE	3.9	3.9	3.5	3.6
ILE	4.3	4.4	4.6	4.5
LEU	8.2	8.4	7.5	6.9
LYS	8.9	8.2	7.0	7.0
PRO	6.2	6.8	4.6	6.5
HYP	4.1	3.0	-	-

Primatone RL is slightly positive. Although no gross measurement errors could be detected, this might be due to a small underestimation of the protein content of cells during the steady state with Primatone RL.

Urea could not be detected by the colorimetric urease assay. Therefore, the overall reaction of the urea cycle is not considered here.

Respiration quotients

It was already suggested that fatty acid biosynthesis can cause a respiration quotient (RQ) above unity (Bonarius et al., 1995a). For the biosynthesis of 1 mole of oleic acid 9 moles of CO_2 are co-produced but only 4.5 moles of O_2 are required. In the cholesterol and desmosterol biosynthesis pathway the CO_2 production is also higher than O_2 consumption (Zubay, 1983). Using the stoichiometry in Table A2 (Appendix A) for fatty acid and sterol synthesis (reaction 29 and 30), the intracellular lipid fraction (Table 2), a molar weight of 282 and 386 for oleic acid and cholesterol respectively, the CO_2 produced during biosynthesis of total lipids is $1.74 * 10^{-12}$ and $1.97 * 10^{-12}$ $mol.cell^{-1}.day^{-1}$ for medium without and with Primatone RL, respectively. The differences in RQ values as determined in both media, could thus (partially) be a result of different lipid synthesis rates. The net catabolic rates for CO_2, i.e., the CO_2 produced in metabolic pathways other than the biosynthesis of fatty and nucleic acids, are $8.17 * 10^{-12}$ and $9.07 * 10^{-12}$ $mol.cell^{-1}.day^{-1}$ for medium without and with Primatone RL, respectively (Appendix B). This indicates that the differences in experimentally determined RQ are therefore also a result of changes in catabolism. Complete oxidation of glutamine and glucose results in a RQ of 0.833 and 1.00, respectively. In medium without Primatone RL a relatively high fraction of glutamine is catabolized compared to the amount of oxidized glucose. Assuming that only the oxidation of these substrates determines the RQ, the RQ values for medium without and with Primatone RL would be 0.936 and 0.961, respectively. This reflects the difference between the measured RQ values as well (Table 2). Therefore, it seems that the differences in RQ, as reported before (Bonarius et al., 1995a), are partially a result of lipid anabolism and partially of differences in the ratio of glucose/glutamine oxidation.

Flux Analysis

Before flux analysis was carried out, the data were analyzed for the presence of measurement errors using elemental balances. A statistical method to detect gross measurement errors in fermentation data (Wang and Stephanopoulos, 1983; Bonarius et al., 1998e) was applied to the carbon and nitrogen balances for the data shown here. The

used test function, h_ε, that has a value of 4.61 at a 90 % confidence level, was 0.58 and 0.10 for the measurement data of the experiment without and with Primatone RL, respectively. This indicates that at a confidence of more than 90 % no gross measurement errors were present according to the elemental balances for C and N.

In Appendix A (Table A1) the fluxes of hybridoma cells in continuous culture are given for medium without and with Primatone RL (10^{-12} mol produced metabolite. $cell^{-1}.day^{-1}$). Figure 4 shows the relative values of the estimated fluxes normalized with respect to the glucose uptake rate. The values are expressed as C-mol produced metabolite. For example, flux 4, which has an absolute value of $3.26*10^{-12}$ mol X5P.$cell^{-1}$. day^{-1} in medium with Primatone RL (Table A1), is relative to the glucose uptake (Table 4), $5/6* 3.26*10^{-12} /4.72*10^{-12} *100$ % = 58 %. The factor 5/6 is used to express the fluxes in Cmol. By expressing the fluxes on a combined glucose uptake rate and Cmol basis, the relative magnitude of the different fluxes can be compared.

Glycolysis

In the optimal medium (supplemented with Primatone RL) glycolytic fluxes (x_9 and x_{10} in Table 2a) are significantly lower. The low glycolytic activity in this medium is probably the result of the lower residual glucose concentration. Because the cell density is more than two-fold higher the residual glucose concentrations in the culture medium are lower (1.7 and 9.9 mmol/l for optimal and sub-optimal medium, respectively). Tumor cells, in contrast to normal cells, do not show the Pasteur effect to a significant extent and use almost all glycolytic capacity regardless of intracellular ATP/ADP ratio and the need for energy (Eigenbrodt et al., 1985). Because tumor cells have lost the control over glucose uptake, the extracellular concentration mainly determines the glycolytic flux. The high glycolytic activity and concomittant high lactate production rates in medium without Primatone RL are therefore probably a result of higher residual glucose concentrations.

Figure 4

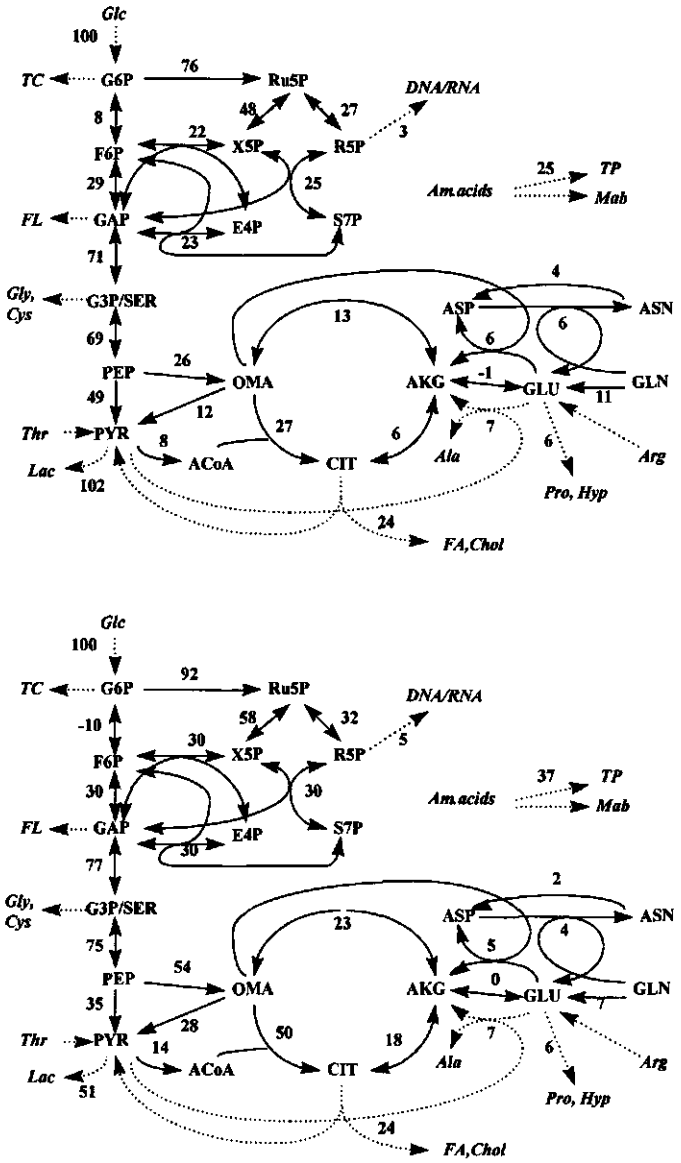

Metabolic flux distribution of hybridoma cells in medium without (top) and with (bottom) Primatone in the culture medium. Fluxes are normalized with respect to glucose uptake rates and expressed as Cmol reaction product.

Glutaminolysis

To glutaminolysis the same applies as to glycolysis. Residual glutamine concentrations are higher in the medium with lower cell density. This results in a higher glutamine uptake rate and more waste products from glutaminolysis. Not only alanine is produced to prevent ammonia accumulation (Glacken et al., 1988), other amino acids can serve as an ammonia sink as well. It appears that the flux through glutamate dehydrogenase (x_{21}) is close to zero (in medium with Primatone RL) or even slightly reversed (sub-optimal medium). These results are in agreement with Jenkins et al. (1992) who found very low glutamate dehydrogenase activity in hybridoma cells during batch culture, as measured by enzyme assay. Thus, under certain conditions α-ketoglutarate is even partly reconverted into glutamate. This might be influenced by relatively high ammonia levels.

The chemical equilibrium of the reaction catalyzed by glutamate dehydrogenase strongly favors glutamate production in the presence of ammonia and α-ketoglutarate (Satlach and Fahien, 1969). In normal proliferating cells these products are rapidly metabolized by carbamyl-phosphate synthetase and α-ketoglutarate dehydrogenase, respectively. Therefore it is very unlikely that in normal cells the glutamate dehydrogenase flux is reversed. Tumor cells, however, are deficient in carbamyl-phosphate synthetase as a consequence of which they form no urea (Coleman and Lavietes, 1981). This is consistent with our results since we could not detect urea in the culture medium. Therefore, it is plausible that glutamate is produced by glutamate dehydrogenase due to ammonia accumulation. Indeed, Ozturk et al. (1992) found higher glutamate production rates under higher initial ammonia concentration in batch cultures of hybridoma cells. This shows that the mechanism for phenomena such as high glutamate production rates, can be elucidated by metabolic flux analysis.

(Hydroxy)Proline synthesis

Another feature of high glutaminolytic activitity is proline and hydroxyproline synthesis. The synthesis of proline is energy dependent; it costs 1 mole of ATP and 2 moles

of NADPH. Eigenbrodt et al. hypothesized that tumor cells produce proline to regenerate NADP from NADPH that is generated in the pentose phosphate pathway (Eigenbrodt et al., 1985). This would allow cells to produce ribose-5-phosphate for nucleotide synthesis. However, according to flux analysis the extent of nucleotide synthesis is too low to explain the energy wasting proline generation. In the most unfavourable case, for the inefficient medium, only 0.22 $*10^{-12}$ mol.cell^{-1}.day^{-1} NADPH would be produced to provide ribose-5-phosphate as a precursor for nucleotides. Fatty acid synthesis, in contrast, requires much more NADPH, i.e., 16 * 0.15 $*10^{-12}$ = 2.4$*10^{-12}$ mol.cell^{-1}.day^{-1}. Therefore, it seems to be more likely that proline synthesis is a result of either (i) a high intracellular glutamate concentration or (ii) a high NADPH-/NADP^{+} ratio that is a result of other pathways than nucleotide synthesis. Indeed, in our laboratory it was found for the same hybridoma cell line that at higher glutamine concentrations the intracellular glutamate concentration was highly correlated to increased proline production rates (Schmid and Keller, 1992). In the light of the reversed glutamate dehydrogenase flux, as discussed above, the proline synthesis might be another mechanism to prevent high ammonia levels.

Another explanation for proline synthesis in hybridoma cells is the following. The proline synthesis machinery might be a rudimentary enzyme system that originates from the intercellular proline cycle (Phang et al., 1981). The principle of this intercellular biochemical interaction is shown in Figure 5. The intercellular proline cycle, a cyclic pathway that was observed for the first time in erythrocytes and hepatocytes, is present in different mammalian tissues. Proline is originally produced by erythrocytes. It is then oxidized by proline oxidase by hepatocytes into pyrroline-5-carboxylate. Erythrocytes, that lack proline oxidase, re-reduce pyrroline-5-carboxylate into proline. Although the advantage of this cycle for hepatocytes (and cells in other tissues, like kidney, heart and brain) is obvious, i.e., NADH-independent ATP generation, the advantage for erythrocytes or other plasma cells remains unclear. However, we speculate that lymphocytes are also involved in the intercellular proline cycle. Consequently hybridoma cells, that originate from these blood cells, possess pyrroline-5-carboxylate reductase and produce proline whenever glutamate, NADPH and ATP are available.

Figure 5

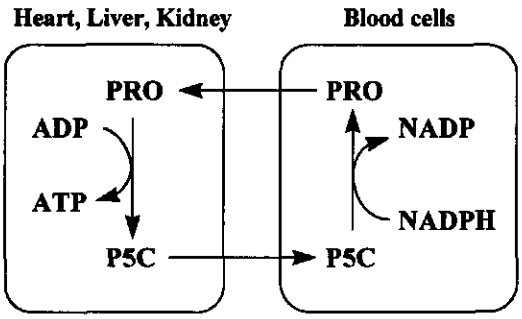

Intercellular proline cycle (Phang et al., 1981). P5C = pyrroline-5-carboxylate.

It is currently under investigation to determine whether (hydroxy)proline synthesis is meaningful for cell metabolism (for the generation of NADPH or as an ammonia sink) or only a redundant and energy wasting metabolic pathway. Hybridoma cell metabolism, like the metabolism of other tumor cells, might be disturbed by the high glutamine uptake rates. Consequently (tumor) cells waste energy without any 'metabolic policy'. If this is indeed the case this pathway might be of interest to inhibit or re-engineer for higher NADPH and ATP availability.

Citric Acid Cycle

The pyruvate oxidation rate in tumor cells is, in contrast to normal cells, independent of cell proliferation. In both fast and slow proliferating tumor cells the amount of pyruvate that is oxidized to CO_2 is small. Eigenbrodt et al. (1985) hypothesized that low pyruvate oxidation rates are a metabolic strategy for survival under extreme (low and high) oxygen conditions or under glucose limitation and for conserving acetyl-CoA for lipid synthesis. This is consistent with our data. The net pyruvate oxidation rate is approximately equal in both media and independent of biomass synthesis and residual glucose concentration (See flux 13 in Table A1). Although a significant fraction of pyruvate is converted into acetyl-CoA and subsequently into citrate, further oxidation in the TCA cycle hardly occurs. The majority of citrate is converted into fatty acids and

sterols with concomitant production of pyruvate (See reaction 29 and 30 in Appendix A, Table A2). To further study this hypothesis in depth for hybridoma cells, the effect of oxygen and glucose levels and the addition of fatty acid precursors on the metabolic flux distribution is currently under investigation.

This concept of the 'truncated citric acid cycle' in tumor cells in relation to lipids biosynthesis has been reviewed by Coleman and Lavietes (1981). In tumor cells the flux from citrate to α-ketoglutarate is found to be much lower than the other citric acid cycle fluxes due to the efflux from citrate to lipid biosynthesis. By anaplerotic reactions, like the transformation of glutamate into α-ketoglutarate, citric acid cycle intermediates are replenished. Using *in vivo* ^{13}C NMR Sharfstein et al. and Mancuso et al. found that the flux from citrate to α-ketoglutarate was only 10 % of the citrate synthase flux (x_{14}) in hybridoma cells cultivated in a hollow fiber system (Mancuso et al., 1994; Sharfstein et al., 1994). Here, the flux from citrate to α-ketoglutarate as determined by mass balancing was indeed low in the sub-optimal medium (3 %), but the difference was smaller in the case with Primatone RL (15 %).

Pentose-Phosphate Pathway

It was found in different cell lines that the percentage of pyruvate formed by the pentose-phosphate pathway is relatively small, i.e., between 0.7 and 11 % from the total glycolytic flux (Katz and Wood, 1963; Reitzer, et al. 1980; Loreck et al., 1987; Portais et al., 1993; Mancuso et al., 1994; Petch and Butler, 1994). Using mass balances to determine the flux distribution of hybridoma cells in continuous culture we found a much higher activity in the pentose phosphate pathway than was found by others: more than 95 % of the glucose is channeled towards pyruvate via flux 3 under both culture conditions (Figures 4a and 4b). The difference between the activity of the pentose phosphate pathway as determined here and measured by labeling techniques as described by others (Katz and Wood, 1963; Reitzer, et al. 1980; Loreck et al., 1987; Portais et al., 1993; Mancuso et al., 1994; Petch and Butler, 1994), is either a result of the use of metabolite-balancing techniques in combination with the minimum-norm constraint, or a result of differences in cultivation methods. In all earlier studies cells were cultured *adherently*, as monolayers in T-flasks (Katz and Wood, 1963; Rietzer, 1980; Petch and Butler,

1994), in the abdominal cavity of young adult Swiss mice (Loreck et al., 1987) or in hollow fiber bioreactors (Mancuso et al., 1994; Sharfstein et al., 1994). In all these studies cells grew at low specific growth rates. The energy metabolism of these cells is therefore focused on maintenance rather than growth. However, the requirement for NADPH, which is consumed in biosynthetic reactions, is much higher in rapidly proliferating cells than in confluent cells. In continuous culture at a μ of 0.83 d^{-1}, as investigated here, the pentose-phosphate pathway operates very similar to what we observe: when much more NADPH than ribose-phosphate is required, the lion's share of glucose-6-phosphate is converted into pyruvate via the oxidative branch of the pentose-phosphate pathway. The flux from glucose-6-phosphate to fructose-6-phosphate is almost zero or reversed. This 'fourth mode' of the pentose-phosphate pathway is described by Stryer (1988). This is consistent with the fluxes found using mass balances. In medium with Primatone RL, the flux through the pentose-phosphate shunt is higher than in sub-optimal medium, because more NADPH is required for biomass synthesis.

Recently, it has been shown for the same cell line and the same medium (with Primatone RL) using 1-^{13}C-glucose and detection of $^{13}CO_2$ by on-line mass spectrometry for exponentially growing cells that a large fraction of glucose is channeled through the pentose-phosphate pathway (A. Oezemre and E. Heinzle, personal recommendation). It is therefore suggested that the minimum-norm constraint is an appropriate constraint that can be used to calculate fluxes in rank deficient networks like that of mammalian cells. It is stressed that if only one flux in the glucose metabolism is validated, the values of the other fluxes in glucose metabolism will be predicted correctly as well, provided that the network is complete. It is hypothesized that the minimum-norm constraint correctly assumes that the total flux activity is minimized in order to fulfill the cells' strive for an efficient flux distribution. A more detailed study of the activity of the pentose-phosphate pathway and the TCA cycle, using different ^{13}C-labeled glucose isotopes is currently in progress. Experimental validation of the values of the fluxes estimated here will show whether the (i) theoretical approach and (ii) the assumed stoichiometry are appropriate tools for the calculation of metabolic fluxes in mammalian cells.

CONCLUSIONS

1. The metabolic fluxes in hybridoma cells can be calculated using mass balances when the metabolic rates of the amino acids, glucose, lactate, ammonia and carbon dioxide are measured and when the cellular composition (fatty acids, sterols, nucleotides, and total protein and carbohydrates) is known. The determination of the NH_3 and CO_2 production rates is essential to estimate fluxes in cyclic pathways. Further, an additional constraint is necessary to estimate the fluxes by the least-squares method.
2. For each different cell line the different fractions of biomass (protein, lipids, nucleotides and carbohydrates) have to be determined in order to estimate the intracellular fluxes of rapidly proliferating cells. More experiments are needed to determine whether these fractions have to be measured also for the same cell line under different culture conditions.
3. In non-efficient medium overflow metabolism of both glucose and amino acids is higher: the net catabolic rates of amino acids are higher, resulting in the synthesis of alanine, lactate, (hydroxy)proline, higher activity of aminotransferases and higher degradation rates of leucine, isoleucine, valine, lysine, and methionine.
4. Pyruvate oxidation is low in both media. Entry of pyruvate in the TCA cycle via pyruvate dehydrogenase in medium with and without Primatone RL is 9 % and 17 % of the glucose uptake rate, respectively. Only a small fraction of pyruvate is further oxidized to CO_2 due to the small flux from citrate to α-ketoglutarate. This flux is smaller in medium without Primatone RL (3 % of the glucose uptake rate) than in the medium with Primatone (15 %).
5. Higher respiration quotients in medium with Primatone RL are concomittant with increased lipid synthesis rates and with high ratios of glucose/glutamine oxidation.
6. The flux from glutamate to α-ketoglutarate, catalyzed by glutamate dehydrogenase is almost zero and even slightly reversed in medium with and without Primatone RL, respectively. Almost all glutamine enters the TCA cycle due to the action of transaminases.
7. In hybridoma cells (hydroxy)proline synthesis does not occur to enable nucleotide biosynthesis (by regenerating NADPH into NADP). The amount of

NADPH that is co-produced in the nucleotide biosynthesis is too small to explain the energy-wasting proline biosynthesis.

ACKNOWLEDGMENTS

H.P.J.B. thanks G. Oesterhelt and M. Pozeg for the fatty acid determination, C. Deuer for the ELISA analysis, H. Fitzke for making available the cell counter, N. Schaub-Wild for help with the amino acid determination, Dr. N. Draeger for help with the analysis of the amino acid composition of cellular protein, and J-.M. Vonach for technical assistance.

APPENDIX A

Table A1

Stoichiometry of the reactions in the underdetermined network that are estimated by the least-squares method and the minimum-norm constarint. Although NAD(P)H and ATP are shown here in the stoichiometric equations, they are not used in the calculation of the metabolic fluxes. The flux values for two steady states are given in 10^{-12} mol product.cell^{-1}.day^{-1}.

	w/o Prim.	with Prim.
1. G6P → F6P	0.37	-0.27
2. F6P + ATP → 2 GAP	3.97	2.92
3. G6P → Ru5P + CO2 + 2 NADPH	6.39	5.00
4. Ru5P → X5P	4.02	3.26
5. Ru5P → R5P	2.27	1.74
6. X5P + R5P → S7P + GAP	2.06	1.63
7. X5P + E4P → F6P + GAP	1.86	1.64
8. S7P + GAP → F6P + E4P	1.93	1.64
9. GAP → G3P/SER + NADH + ATP	9.78	7.36
10. G3P/SER → PEP	9.51	7.18
11. PEP → PYR + ATP	5.87	4.31
12. PEP + CO2 → OMA + ATP	3.60	2.87
13. PYR → ACoA + NADH + CO2	1.81	2.33
14. OMA → PYR + NADPH + CO2	2.26	1,44
15. ACoA + OMA → CIT	2.03	2.68
16. CIT → AKG + NADH + CO2	0.22	0.82
17. AKG → OMA + 2NADH + FADH + ATP + CO2	1.08	1.39
18. GLU + OMA → ASP + AKG	0.45	0.30
19. GLN + ASP + 2 ATP → ASN + GLU	0.52	0.24
20. ASN → ASP + ATP + NH3	0.35	0.13
21. GLU → AKG + NADPH + NH3	-0.06	0.01
22. GLN → GLU + ATP + NH3	0.87	0.37

Table A2

Directly calculable fluxes. Reactions 23 to 44 can be determined by mass-balancing techniques alone.

23. GLC + ATP → G6P
24. F6P + 3.46 ATP → TC
25. PYR + NADH → LAC
26. PYR + GLU → ALA + AKG
27. R5P + 1.3 ASP + 1.9 GLN + 0.49 GLY + 8.9 ATP → 0.79 OMA + 1.7 GLU + RNA + 0.71 NADH + 0.015 CO2
28. R5P + 1.3 ASP + 0.3 SER + 1.9 GLN + 0.2 GLY + 1.2 NADPH + 8.9 ATP → 0.8 OMA + 1.7 GLU + DNA + 0.7 NADH
29. 9 CIT + 9 NADH + 8 ATP + 7 NADPH → FA + 9 PYR + 9 CO2
30. 18 CIT + 16 NADH + 11 NADPH + 11 O2 + 18 ATP → CHOL + 27 CO2 + 18 PYR
31. GAP + 6 ATP + NADH + FA → PL
32. MET + AKG → OMA + GLU + NADH + ATP
33. AKG + LEU → GLU + ACCOA + 2NADH
34. AKG + ILE → GLU + ACCOA + 2NADH
35. AKG + LYS → GLU + ACCOA + 2NADH
36. PHE + GLU → ACoA + OMA + GLN
37. ARG + AKG → 2 GLU
38. GLU + ATP + 2 NADPH → PRO
39. PRO → HYP
40. G3P/SER → GLY
41. CYS → PYR + NH3
42. THR → PYR + NH3
43. Am.Acids + 4.15 ATP → PROT
44. Am.Acids + 4.15 ATP → MAB

The stoichiometries of reactions 29 and 30 are derived by adding up the stoichiometry of the conversion of citrate into Acetyl-CoA (CIT + NADH → ACCOA + PYR + NADPH + CO2) to the net stoichiometry of fatty acids synthesis (29a) and cholesterol synthesis (30a):

29a. 8 ATP + 9 ACCOA + 16 NADPH → FA.
30a. 18 ACCOA + 29 NADPH + 11 O2 + 18 ATP → CHOL + 9 CO2 + 2 NADH

Table A3

List of metabolites.

Metabolites in the small network (Table A1), which is solved by least squares analysis in combination with the minimum-norm constraint.

1. G6P	7. G7P	13. CIT	19. ASN
2. F6P	8. E4P	14. ACCOA	20. CO2
3. GAP	9. G3P/SER	15. AKG	21. NH3
4. Ru5P	10. PEP	16. GLU	
5. X5P	11. PYR	17. GLN	
6. R5P	12. OMA	18. ASP	

Metabolites in the extended network (Table A2).

22. GLC	28. ARG	34. TRP	40. PRO	46. FA
23. HIS	29. TYR	35. PHE	41. HYP	47. CHOL
24. GLY	30. TYR	36. ILE	42. PROT	48. PL
25. THR	31. CYS	37. LEU	43. MAB	
26. ALA	32. VAL	38. LYS	44. DNA	
27. ARG	33. MET	39. PRO	45. RNA	

APPENDIX B

Table B1

Equations for the remaining smaller network. These mass balances finally give the input vector $\mathbf{r_{tot}(t)}$ (1 x n, where $n = 20$) for the small matrix (m x n, where $m = 21$ and $n = 22$). The metabolites corresponding to the numbers are given between parentheses. The input values for medium without and with Primatone RL are given as well. A negative value indicates that a metabolite flows into the network.

	- Prim.	+ Prim.
1. $r(G6P) = -x_{23}(GLC)$	-6.874	-4.716
2. $r(F6P) = x_{24}(TC)$	0.078	0.088
3. $r(GAP) = x_{31}(PL)$	0.187	0.207
4. $r(Ru5P) = 0$	0	0
5. $r(X5P) = 0$	0	0
6. $r(R5P) = x_{27}(RNA) + x_{28}(DNA)$	0.116	0.122
7. $r(S7P) = 0$	0	0
8. $r(E4P) = 0$	0	0
9. $r(G3P/SER) = r_{nc,SER} + r_{nc,GLY}$	0.213	0.181
10. $r(PEP) = 0$	0	0
11. $r(PYR) = x_{25}(LAC) + r_{nc,ALA} + r_{nc,THR} + r_{nc,CYS} - 9*x_{29}(FA) - 18*x_{30}(CHOL)$	6.249	3.420
12. $r(ACoA) = r_{nc,LEU} + r_{nc,ILE} + r_{nc,LYS} + r_{nc,PHE}$	-0.258	-0.350
13. $r(OMA) = 0.8*x_{27}(RNA) + 0.8*x_{28}(DNA) + r_{nc,PHE} + r_{nc,MET}$	0.046	0.049
14. $r(CIT) = 9*x_{29}(FA) + 18*x_{30}(CHOL)$	1.686	1.864
15. $r(AKG) = r_{nc,PHE} - r_{nc,LEU} - r_{nc,ILE} - r_{nc,LYS} - r_{nc,ARG} - r_{nc,ALA} - r_{nc,MET}$	-0.552	-0.237
16. $r(GLU) = r_{nc,GLU} + r_{nc,LEU} + r_{nc,ILE} + r_{nc,LYS} + 2*r_{nc,ARG} + r_{nc,MET} + r_{nc,ALA} - r_{nc,PHE} + r_{nc,HYP} + r_{nc,PRO}$	0.871	0.253
17. $r(GLN) = r_{nc,GLN} + r_{nc,PHE}$	-1.532	-0.699
18. $r(ASP) = r_{nc,ASP}$	0.184	0.159
19. $r(ASN) = r_{nc,ASN}$	0.053	0.016
20. $r(CO2) = r_{CO2} - (9*x_{29}(FA) + 27*x_{30}(CHOL) + 0.015*x_{27}(RNA))$	8.166	9.067
21. $r(NH3) = r_{NH3} + r_{nc,THR} + r_{nc,CYS}$	1.142	0.480

APPENDIX C

Net catabolic rates

The input vector $\mathbf{r}_{tot}(t)$ for the smaller remaining network is calculated using the net catabolic rate vector $\mathbf{r}_{nc}$ [*1)] for each metabolite. The net catabolic rate of metabolite A ($r_{nc,A}$) gives the amount of A per cell per unit of time that is converted into metabolites other than biomass end products. Similar to Xie and Wang (1994a), who used the stoichiometric coefficients of amino acids for biomass and product to rationally redesign the culture medium, we use the stoichiometric requirements for biomass and product to calculate the net catabolic rates. The net catabolic rate for metabolite A (mol.cell^{-1}.day^{-1}) is the production rate of metabolite A corrected for its biomass synthesis rate and can be calculated by

$$r_{nc,A} \equiv r_{tot,A} - (\theta_{TP,A} r_{TP} + \theta_{DNA,A} r_{DNA} + \theta_{RNA,A} r_{RNA} + \theta_{MAb,A} r_{Mab} + \theta_{TC,A} r_{TC} + \theta_{FA,A} r_{FA}) \quad (9)$$

where $\Theta_{B,A}$ denotes the number of moles of metabolite A that is needed for the biosynthesis of one mole biomass. For the sake of simplicity Equation 9 is rewritten into

$$r_{nc,A} = r_{tot,A} - r_{biom,A} \quad (10)$$

where $r_{biom,A}$ is the sum of all biomass requirements rates for metabolite A. Table B1 gives the equations that are used for the calculation of the input vector **r(t)** for the calculation of the 20 remaining fluxes.

[*1)] Note: The net catabolic rates give a first indication for optimizing the medium composition. A negative r_{nc} indicates that a fraction of the pertinent metabolite is converted without being used for biosynthesis. When such a metabolite does not have a function in the primary metabolism, like ATP or co-factor (re)generation, it is considered as redundant. This can be investigated by metabolic flux analysis. When r_{nc} is negligible compared to the uptake rate, the metabolite is regarded as "balanced" (Ferrance et al., 1993) and its medium concentration is considered to be optimal. These metabolites will not be used further in the flux analysis of the remaining primary metabolism. When r_{nc} is positive its medium concentration might be lowered. In this case the pertinent metabolite is not produced from other metabolites. Thus, by metabolic flux analysis it is possible to investigate the medium requirements for the cell catabolism. As shown by Xie and Wang (1994a, 1994b) the medium requirements for anabolism, that probably dominates the final medium composition, can be determined by analyzing the biomass composition.

Chapter 5

Metabolic-Flux Analysis of Continuously Cultured Hybridoma Cells using $^{13}CO_2$ Mass Spectrometry in Combination with NMR Spectroscopy and Metabolite Balancing

Hendrik P.J. Bonarius, Achmet Özemre,
Bram Timmerarends, Peter Skrabal,
Elmar Heinzle, Georg Schmid, and Johannes Tramper.

ABSTRACT

The estimation of intracellular fluxes of mammalian cells using only mass balances is not possible because the set of linear equations defined by these mass balances is underdetermined. Either additional theoretical constraints or additional experimental flux data, which can be obtained by isotopic-tracer studies, are required to quantify fluxes in particular in cyclic metabolic pathways. Here, metabolic flux analysis is carried out using isotopic tracers. Hybridoma cells are grown in medium containing either 1-^{13}C-, 2-^{13}C- or 6-^{13}C-glucose. The fractional labeling of lactate and CO_2 is determined using ^{1}H-NMR spectroscopy and mass spectrometry, respectively. Data from five different steady states are evaluated to determine metabolic fluxes of carbon metabolism. Various evaluation methods, in which bi-directional reactions are assumed to be

negligible, are used for to determine net fluxes in continuously cultured hybridoma cells.

It is concluded for continuously cultured hybrodoma cells, that
(i) 1-^{13}C-glucose (and 6-^{13}C-glucose) experiments reveal that at least 17 to 23 % of glucose is channeled through the pentose shunt.
(ii) On average 17 % of the consumed glucose is metabolized in the TCA cycle, according to 6-^{13}C-glucose experiments.
(iii) Pyruvate-carboxylase activity is insignificant under the condition investigated here.
(iv) Although the NAD(P)H balance can theoretically be used to quantify the metabolic fluxes at the glucose-6-phosphate branchpoint, the resulting values are substantially different from flux values determined using isotopic-tracer studies.
(v) The pentose-shunt flux determines how much glucose is minimally required. The cells investigated here require 1.5 mole glucose cell^{-1}.day^{-1}. Higher amounts of glucose will unnecessarily result in higher lactate production rates.

INTRODUCTION

In the last 3 to 4 years, intracellular-flux analysis of industrially relevant mammalian-cell lines has received considerable interest in an attempt to investigate bottlenecks in cellular physiology. Metabolic-flux analysis has already been proven a useful tool to analyze the requirements for energy and biomass synthesis. Using linear optimization techniques to analyze data of hybridoma-cell metabolism, Savinell and Palsson (1992a) showed that neither the maintenance demand for ATP nor the antibody production rate limit the growth rate of these cells. They also showed that a cell uses its nutrients for growth with only 57-78 % efficiency. In order to improve this low efficiency, Xie and Wang successfully redesigned the culture medium, first on the basis of cellular stoichiometry (1994a) and later on the basis of intracellular-flux estimations (1994b). Doing so, they were able to

significantly decrease production of waste metabolites and increase Mab titers with more than one order of magnitude.

Intracellular-flux analysis has also successfully been applied to evaluate metabolic mechanisms and environmental effects on mammalian-cell metabolism. Zupke and co-authors analyzed the effect of dissolved oxygen on hybridoma cells, giving a fundamental basis for controlling physiological processes through manipulation of the oxygen supply (Zupke et al., 1995). We analyzed the effect of Primatone RL, a semi-defined medium component that promotes both growth and production, on the intracellular-flux distribution in hybridoma cells, in order to investigate metabolic differences between optimal and sub-optimal conditions (Bonarius et al., 1996). Recently, we used metabolic-flux analysis to show how hybridoma cells reduce ammonia accumulation by increasing their glutamate dehydrogenase activity (Bonarius et al., 1998a).

In all of the above-mentioned studies, far-going assumptions with respect to certain metabolic pathways had to be made in order to quantify the intracellular fluxes. The linear network, that is a product of stoichiometric equations and uptake and production rates of the relevant metabolites, is underdetermined without such assumptions. This problem in the science of "metabolic-flux balancing" is an inherent consequence of the presence of cyclic metabolic pathways (Vallino and Stephanopoulos, 1990; Bonarius et al., 1997). Only by adding theoretical assumptions or by carrying out isotopic-tracer experiments, the fluxes in cyclic pathways can be determined.

There is a need for experimental evidence to verify the various assumptions or theoretical constraints (Fell and Small, 1986; Savinell and Palsson, 1992; Bonarius et al., 1996), in particular with respect to fluxes in cyclic metabolic pathways. Several studies have already been carried out to proceed in this direction. Jenkins and co-workers (1992) examined glutamine metabolism of hybridoma cells by following the metabolic fate of ^{15}N-glutamine and showed the relative importance of glutaminase. Zupke and Stephanopoulos (1994) used 1-^{13}C-glucose as isotopic tracer to determine

the malic-shunt flux in hybridoma cells. Mancuso et al. (1994) and Sharfstein et al. (1994) used *in vivo* NMR to measure metabolic fluxes of hybridoma cells in hollow-fiber bioreactors. This technique however, is relatively insensitive as a result of which it can not be used to study the metabolism of mammalian cells in homogeneous cultures, which are widely applied for the production of monoclonals, vaccins and recombinant glycoproteins. Cells growing in perfusion systems, such as hollow-fiber bioreactors, typically grow at low specific rates, resulting in low biosynthesis to maintenance ratios. This difference in cultivation method may significantly influence the metabolic-flux distribution.

Here, intracellular flows of glucose metabolism in continuously cultured, suspended hybridoma cells, growing at almost maximum specific growth rates, are investigated using both experimental and computational methods. Various methodologies are applied and compared. $^{13}CO_2$ yields from 1-^{13}C- and 6-^{13}C-glucose, measured on-line by mass spectrometry, are determined to evaluate the pentose-shunt activity (Katz and Wood, 1963; Larrabee, 1989). The fractional labeling of extracellular lactate secreted by 1-^{13}C-, 2-^{13}C- and 6-^{13}C-glucose-fed cells is determined in order to quantify the pentose- and the malic-shunt activity (Mancuso et al., 1994; Kingsley-Hickman et al., 1990; Willis et al., 1986). A numerical method to determine metabolic-flux distributions from both isotopic-tracer data and metabolite balances, based on atom-mapping matrices (Zupke and Stephanopoulos, 1994), is used to supplement the underdetermined metabolic network. An advantage of this method, in which both mass balances and isotopic-tracer data are combined, is that a large number of metabolic fluxes in one single experiment can be determined, as a result of which errors due to interexperiment variability become irrelevant. In addition, both extraction of intracellular pools and the separation of metabolites for NMR analysis are not required. This can only be achieved when $^{13}CO_2$- and CO_2-production rates are determined in addition to measurement of the fractional labeling of lactate. Measurement of $^{13}CO_2$ and CO_2 yields are essential for the determination of the pentose-shunt activity, when 1-^{13}C-glucose is used as isotopic source. Here, it is shown that, under the assumption that bi-directional fluxes do not influence scrambling of labeling in pentose-shunt intermediates, the net fluxes of the pentose

shunt, the glycolysis, the pyruvate carboxylase, the TCA cycle and the malate shunt can be determined in one single 1-^{13}C-glucose experiment.

A comparison of the experimentally obtained metabolic-flux data with flux analysis estimated using mass balances and various theoretical constraints, is described elsewhere (Bonarius et al., 1998b).

THEORY

Metabolic network

Figure 1

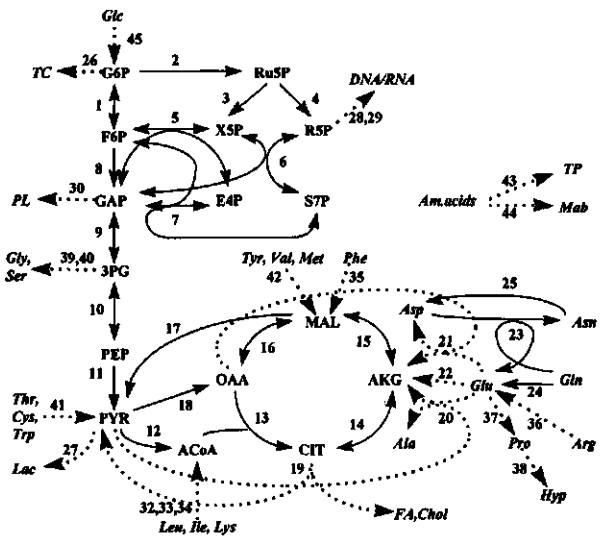

Figure 1. Network of mammalian-cell metabolism. Fluxes that can be quantified by mass balances alone are indicated as dashed lines. To measure the remaining fluxes (solid lines) additional constraints are required. These can either be obtained by isotopic tracer experiments, or as theoretical assumptions.

Figure 1 shows the metabolic network that is used to estimate intracellular metabolic flows with mass-balance equations. The majority of the intracellular fluxes in

mammalian cells can be determined without isotopic tracers, i.e. using the measured extracellular metabolic rates and the cellular composition only. These fluxes are indicated by dashed arrows. To experimentally determine the remaining fluxes of thenetwork, indicated by the solid lines (fluxes 1-18 and 23-24), isotopic-tracer studies are required. The metabolic network in Figure 1 contains three sets of linear-dependent fluxes. These are:

1. The pentose shunt, glycolysis and TCA cycle (Flux 1 to 16)
2. The malate/pyruvate/oxaloacetate cycle (Flux 16, 17 and 18)
3. Glutaminolysis (Flux 23, 24, 25)

In order to quantify these fluxes at least one flux out of each of these three cycles has to be measured independently. Here, particular effort is made to measure the pentose shunt (flux 2) using several isotopic-tracer methods. In addition, all fluxes of the TCA cycle, glycolysis, pentose and malate shunt are determined simultaneously by combining metabolite-balance equations and ^{13}C-lactate and $^{13}CO_2$ measurements. The singularity that is caused by cycling in glutaminolysis (fluxes 23 to 25) is removed by assuming that the flow through asparagine synthetase (flux 23) is negligible, for reasons described elsewhere (Bonarius et al., 1998a). It is stressed that this assumption to estimate the fluxes 24 and 25 does not influence the calculations of fluxes that feed from glutaminolysis into the TCA cycle (fluxes 20, 21 and 22): the fluxes through the reactions catalyzed by glutamate dehydrogenase (flux 22) and alanine and aspartate aminotransferase (flux 20 and 21) can be determined independently. Table A1 (Appendix A) shows the equations required to determine the in- and outgoing metabolic flows of the 'underdetermined' subnetwork with fluxes 1-19.

Pentose-Phosphate Shunt

The pentose-shunt activity in mammalian cells or tissue can be determined by analyzing the production of labeled CO_2 (Katz and Wood, 1963; Larrabee, 1989) or lactate (Kingsley-Hickman et al., 1990; Willis et al., 1986; Mancuso et al., 1994) after incubation of carbon-labeled glucose. Different interpretations of how to

evaluate isotopic-tracer measurement data to quantify the pentose-shunt flux (Larrabee, 1989; Kingsley-Hickman et al., 1990) will be discussed below and compared in the Results Section.

Recently, it was shown that the labeling state of intermediates in the glycolysis and pentose-phosphate pathway are influenced by reversible reactions catalyzed by transaldolase (flux 7) and transketolases (flux 5 and 6) (Wiechert et al., 1997). In the methods applied here, fluxes in the pentose shunt are assumed to be unidirectional, as the labeling in intermediates of the pentose-phosphate pathway has not been measured. All fluxes are therefore given as net values.

The net flux through the oxidative branch of the pentose shunt (flux 2) is underestimated when the reversed reaction catalyzed by phosphoglucose isomerase (reaction 1) is neglected. Here, the amount of flructose-6-phosphate (F6P) that recycles in flux 2 is estimated by a method proposed by Larrabee (1989). From the sedoheptulose-7-phosphate (S7P)- and erythrose-4-phosphate (E4P)-mass balance it follows that the pentose shunt produces 2/3 mole of F6P for each mole of glucose-6-phosphate (G6P) entering it. If a fraction, *R*, of this F6P is recycled into the pentose shunt, the total hexose-phosphate (the sum of G6P and F6P) that enters the cycle is given by (Larrabee, 1989)

$$x_2\ (1+\tfrac{2}{3}R+(\tfrac{2}{3}R)^2+(\tfrac{2}{3}R)^3+.....) = x_2\ (\frac{3}{3-2R}) \qquad (1)$$

where x_2 is the flux through the oxidative branch of the pentose shunt of G6P that enters the shunt immediately after conversion from glucose, i.e., the amount determined under the assumption that all fluxes are unidirectional.

$^{13}CO_2$ yields from 1-^{13}C- and 6-^{13}C-glucose experiments

As shown in Figure 2, the carbon at the 1-C-position of glucose is released as CO_2 by the 6-phosphogluconate dehydrogenase reaction (flux 2) in the oxidative branch of the pentose shunt. Measurement of $^{13}CO_2$ derived from 1-^{13}C-glucose-incubated cells

Figure 2

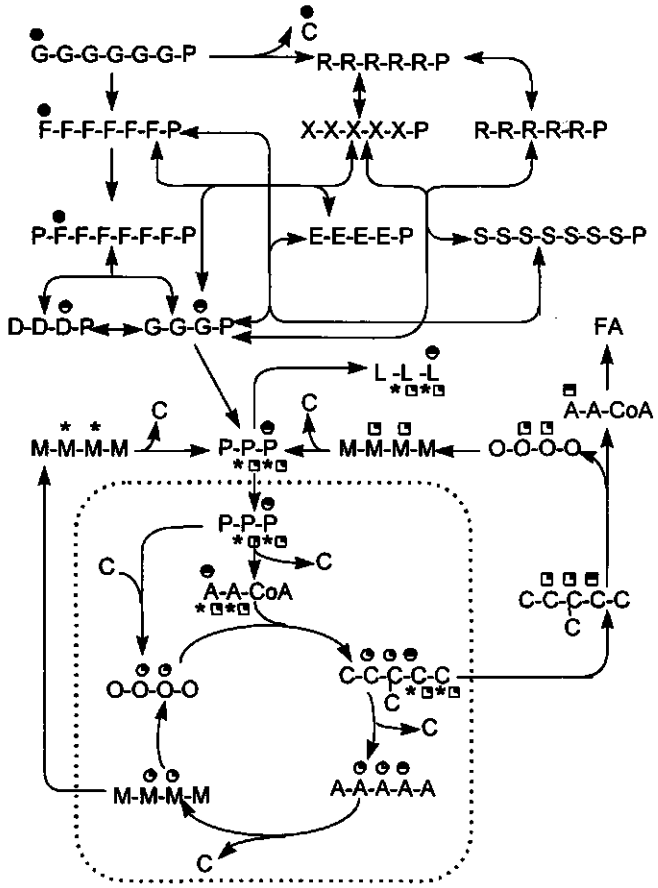

The metabolic fate of 1-^{13}C-glucose. Glycolytic labeling (circles), malate shunt labeling (stars), malate/pyruvate shuttle labeling (squares) are shown. Reductions (of 25 or 50 %) in filling of symbols indicate (25 or 50 %) reductions in labeling associated with reaction stoichiometry. Dashed line indicates mitochondrial membrane. Grey symbols indicate label transfer associated with interconnected pathways. Only labeling as a result of uni-directional fluxes are shown (Adapted from Mancuso et al. (1994).)

Capitals indicate C atoms of metabolites (except for the capital P which indicates phosphate groups and FA which denotes fatty acids). A acetyl-CoA, C carbon dioxide or citrate, D dihydroxyacetonephosphate, E erythrose-4-phosphate, F fructose-6-phophate or fructose 1,6-biphosphate, G glucose, glucose-6-phosphate, or glyceraldehyde 3-phosphate, L lactate, M malate, O oxaloactetate, P pyruvate (or phosphate group), R ribose-5-phosphate or ribulose-5-phosphate, S S7P sedoheptulose-7-phosphate, X xylulose-5-phosphate.

(or $^{14}CO_2$ derived from 1-^{14}C-glucose-incubated cells) can therefore be used to measure the pentose-shunt activity. This is however troubled by another fraction of the $^{13}CO_2$ from cells grown in 1-^{13}C-glucose-containing medium that is released by other decarboxylation reactions: When 1-^{13}C-glucose is not channeled through the pentose-phosphate pathway, but metabolized by the glycolysis and further oxidized in the TCA cycle and in the pyruvate/malate and malic shunt (see also Figure 2), $^{13}CO_2$ is released as well. It has been suggested that the $^{14}CO_2$ from 6-^{14}C-glucose can be used to correct for this fraction (Katz and Wood, 1963). In order to calculate the pentose-shunt flux Katz and Wood assumed that 3 moles of CO_2 were produced from each mole glucose-6-phosphate that entered the pentose cycle. Later, Larrabee (1989) argued that such an overall stoichiometry cannot be assumed. Instead, by applying a mass balance over $^{14}CO_2$, he showed that only a lower limit of the pentose-shunt flux can be attained from $^{14}CO_2$ (or $^{13}CO_2$) measurements. In this approach no assumptions with respect to a fixed overall stoichiometry of the pentose-phosphate pathway were made. For steady-state conditions it can be shown that (Larrabee, 1989)

$$x_2 \geq {}^*CO_2(1) - {}^*CO_2(6) \qquad (2)$$

where $^*CO_2(1)$ and $^*CO_2(6)$ are the measured $^{13}CO_2$ production rates from 1-^{13}C- and 6-^{13}C-glucose experiments, respectively. This expression does not set a unique value, but only provides lower limits for the pentose shunt, as it recognizes the fact that more CO_2 than the $^{13}CO_2$ from 1-^{13}C-glucose is generated by the pentose shunt due to recycling of F6P. The extra amount of F6P that enters the shunt due to the reversed phosphoglucose-isomerase flux (x_1) is estimated by Equation 1.

Another possible source of errors in the evaluation of $^{13}CO_2$ yields for the calculation of the pentose shunt, as discussed by Larrabee (1989), is the difference in time course of $^*CO_2(1)$ and $^*CO_2(6)$ during incubation of cells in medium containing 1-^{13}C- or 6-^{13}C-glucose. Here, such time-dependent errors are negligible because cells are grown in continuous culture.

Fractional labeling in lactate from 1-^{13}C, 2-^{13}C- and 6-^{13}C-glucose experiments

The determination of the fractional labeling of carbon in lactate by NMR spectroscopy has been proposed as an alternative to the measurement of the $^{13}CO_2$ or $^{14}CO_2$ production rate for the quantitation of the pentose-shunt activity (Willis et al., 1986; Kingsley-Hickman et al., 1990). In Figure 3 the fractional labeling of pyruvate (which is equal to the fractional labeling of lactate) is shown for both 100 % glycolytic and 100 % pentose-shunt labeling for the different types of glucose that are used in this work.

Figure 3

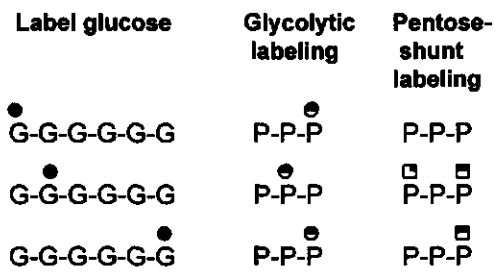

Label transfer from 1-^{13}C-, 2-^{13}C- and 6-^{13}C-glucose to pyruvate, shown for 100 % glycolytic and for 100 % pentose-phosphate shunt activity (assuming that all reactions are unidirectional). Capitals denote C atoms in glucose (G) and pyruvate (P).

Willis and co-authors (1986) derived the following equation to determine the shunt activity from the fractional labeling of 3-C-lactate after 1-^{13}C-glucose (100 % fractional enrichment) incubation:

$$PPS = \frac{(3 - 3r)}{(3 + 2r)} \qquad (3)$$

where r is the ratio of the sum of the ^{13}C satellite proton-resonance intensities to the non-coupled proton resonance intensity (3-^{13}C-lactate/3-^{12}C-lactate). This expression

applies only if there are no unlabeled lactate precursors (for example as a result of reactions 17, 19, and 41 in Figure 1). To correct for other, non-labeled carbon sources that dilute the label at 3-C-lactate, Kingsley-Hickman and coworkers (1990) suggested to use parallel 6-^{13}C-glucose experiments. The fraction of glucose that enters the pentose shunt is calculated as

$$PPS = 1 - \frac{*3\text{-}C\text{-}Lac(1)}{*3\text{-}C\text{-}Lac(6)} \qquad (4)$$

where *3-C-Lac(1) and *3-C-Lac(6) denote fractional labeling of the methyl carbon of lactate from a 1-^{13}C-glucose and a 6-^{13}C-glucose (100% fractional enrichment) experiment, respectively. Equation 4 neglects the fact that 3-C-lactate is not only diluted but also labeled via the malic enzyme (Figure 2). As can be seen in Figures 2 and 3, decarboxylation in the oxidative branch of the pentose pathway causes loss of label in *3-C-Lac(1). Correction for dilution of label by non-labeled carbon sources by applying Equation 4 is therefore dependent on the pentose-shunt flux. The higher x_2, the more *3-C-Lac(1) will be diluted via reactions 17 and 19. In contrast, this is not the case for *3-C-Lac(6).

Mancuso and co-authors (94) showed that the relative rates of glycolysis and pentose shunt can be derived from the fractional labeling in 1-C and 2-C-lactate from a 2-^{13}C-glucose experiment. Because the fractional labeling of 1-C-lactate can not be determined by ^{1}H-NMR, which is used here, and because the use of Equation 4 may result in overcorrecting of the dilution effect of endogenous carbon at high pentose-shunt activities (see also Results Section), an alternative calculation method is given. It can be shown that the label in 2-C-lactate from 2-^{13}C-glucose is diluted by the malic shunt (x_{17}), the pyruvate/malate shuttle (x_{19}), degradation of certain amino acids (x_{41}) and the pentose shunt. In contrast, the label of 3-C-lactate from 6-^{13}C-glucose is diluted by reactions 17, 19 and 41, but not by the pentose shunt. The relative pentose-shunt activity can therefore be calculated as follows:

$$PPS = \frac{*3\text{-}C\text{-}Lac(6)_{obs}}{*3\text{-}C\text{-}Lac(6)_{max}} - \frac{*2\text{-}C\text{-}Lac(2)_{obs}}{*2\text{-}C\text{-}Lac(2)_{max}} \qquad (5)$$

In Equation 5 subscripts *obs* and *max* indicate observed and maximum fractional labeling, respectively. The maximum fractional labeling of 2-C- and 3-C-lactate is 50 % of the fractional labeling of 2-^{13}C- and 6-^{13}C-glucose, respectively, as a result of the splitting of hexose into two triose units (This is indicated by the half filled circles in Figures 2 and 3). Similar to Equation 4, numbers between parentheses indicate which C-atom in glucose has been labeled.

Modeling of isotope distributions using atom-mapping matrices

The calculation methods described above only provide upper and/or lower limits of the fluxes to be determined. Further, two parallel experiments with different isotopic tracers have to be carried out, by which errors due to interexperiment variability are introduced. By combining isotopic-tracer experiments with mass-balance techniques absolute flux values can be calculated (Blum and Stein, 1982; Portais et al., 1993). Recently, Zupke and Stephanopoulos (1994) and Marx and co-authors (1996), developed non-invasive numerical algorithms for this purpose. In contrast to other methods, in which mass-balance equations for each single atom have to be derived (Blum and Stein, 1982), this approach only requires atom-mapping matrices (AMMs), in which the reaction stoichiometry is encapsulated. The resulting network is conveniently arranged, easier to understand, requires less algebraic manipulation, and modifications do not require new derivations of atom balances (Zupke and Stephanopoulos, 1994). Here, a slightly different algorithm is used that is described in Appendix B.

NAD(P)H mass balance

As an alternative to isotopic-tracer methods as described above, the NAD(P)H balance provides information on the split ratio of fluxes at the branchpoint at glucose-6-phosphate. By adding the NAD(P)H balance to the set of mass balances one singularity is removed (Bonarius et al., 1996). In theory, it should be possible to estimate the total shunt rate (including recycling of fructose-6-phosphate) using

metabolite balancing, provided that the NAD(P)H balance can be closed with sufficient accuracy.

MATERIAL AND METHODS

Cell line and culture medium

A murine hybridoma cell line that produces an IgG_{2A} antibody directed against human ferritin was grown in serum-free medium. A mixture of Dulbecco's, Ham's F12 and Iscove's powdered media (D:H:I = 1:1:2; Gibco, Grand Island, NY, USA) was used as the basal medium, which was supplemented with 5 mg/ml insulin (Sigma, St.Louis, MO, USA), 6 mg/ml transferrin (Boehringer Mannheim, Mannheim, FRG) and 0.35 % (w/v) Synperonic F68 (Serva, Heidelberg, FRG). The standard medium contained 5 mM glutamine and 2.73 g/l sodium bicarbonate. For each different steady state a different mixture of unlabeled glucose and 1-^{13}C-, 2-^{13}C, or 6-^{13}C-glucose (Cambridge Isotope Laboratories, Andover, MA, USA) was added.

Cell-culture bioreactor

A major practical drawback of using continuous cultures for labeling experiments is the requirement of large volumes of medium, making it expensive due to substantial requirements of ^{13}C-labeled substrates. To reduce costs, a small bioreactor made of polycarbonate (only 100 ml working volume) that can be operated in a continuous mode was designed and constructed (Figure 4). Despite its small size, temperature, pH and dissolved oxygen could be controlled and maintained at desired levels. The pH was maintained at 7.20 using 0.5 M NaOH. The dissolved-oxygen concentration was measured using a pO_2-electrode (Mettler-Toledo, Buchs, CH) and controlled at 30 % air saturation by adjusting the oxygen fraction in a nitrogen/oxygen gas mixture. pH, temperature and pO_2 were controlled using a process-control unit (Bioengineering, Wald, CH). Oxygen supply was via surface aeration only. The total gas flow was kept constant at 100 ml min^{-1} using mass-flow controllers (Brooks, Veenendaal, NL). The dilution rate was set at a value of 0.9 d^{-1} and measured four

times a day using a balance and adjusted manually when necessary. Despite the internal diameter of the silicone tube used for medium supply was small (0.5 mm), the dilution rate could only be kept constant with a maximum accuracy of ±10 %. A 5 ml sample was taken daily using the sampling device that is shown in Figure 4.

Figure 4

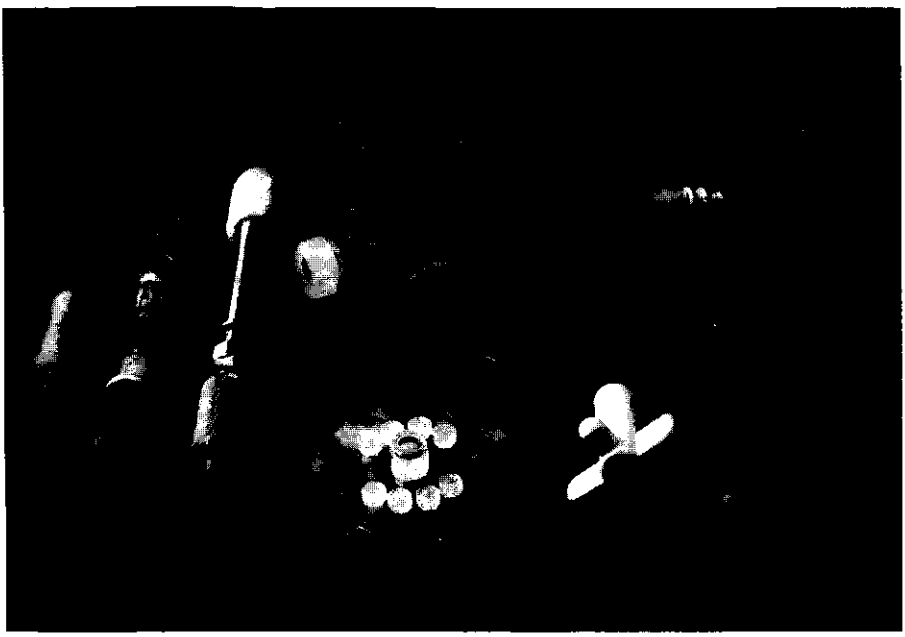

Bioreactor for isotopic-tracer experiments of mammalian-cell suspension culture. Although the polycarbonate bioreactor has a working volume of only 100 ml, temperature, pH, and pO_2 can be measured and controlled. From the left to the right: Pt-100 probe, pH electrode, oxygen electrode, bioreactor and lid, stirrer, and sampling unit.

This amount was used for cell counting and analysis of glucose, lactate, ammonia and amino acids. At the end of each steady state a 50 ml sample was taken for NMR analysis. Aliquots of 10 ml were freeze-dried and redissolved in D_2O in order to allow field stabilization on Deuterium and to increase sample concentrations for higher sensitivity in NMR spectrometry. Directly after taking the 50 ml samples, the

reactor volume was readjusted to 100 ml using culture medium without labeled substrates allowing the cell density to increase to its original steady-state value. After this "batch period", which took 36-48 hours, the continuous feeding, now using medium with a different type of labeled glucose was started again. After monitoring the cell density for three days, the analysis of the next steady-state period was initiated. During 2 to 3 days the in- and outgoing gas composition was analyzed, 5 ml samples were taken daily, and at the end a 50 ml sample was taken.

Oxygen uptake and carbon-dioxide evolution rates

Because the total gas flow is kept constant, and oxygen concentrations of the in- and out-going gas flow determined at high precision (ppm), the **oxygen uptake rate** (OUR) can be calculated according to (Eyer et al., 1995)

$$OUR = F_g^i \left(x_{O_2}^i - x_{O_2}^o \right) \quad (6)$$

In contrast to the determination of the OUR, the determination of the **carbon-dioxide evolution rate** (CER) of a bicarbonate-buffered mammalian-cell culture is complex because of several reasons. Since the medium contains bicarbonate, the measured carbon dioxide in the outlet gas comes from two sources: the medium and the respirating cells. Also, the accumulation in the liquid phase has to be taken into account. The liquid phase concentration can not be calculated by using Henry's law only, as a partial gradient for desorption is required (Royce and Thornhill, 1991). Moreover, during medium preparation and storage carbon dioxide evaporates from the bicarbonate-buffered medium. To account for these complications a method was developed to determine the CER under bicarbonate-buffered conditions (Bonarius et al., 1995a). It was shown that the CER can be determined by

$$V_l CER = x_{CO_2}^o \left[F_g^i + F_l \left(\frac{P}{H^{CO_2}} + \frac{F_g^o}{k_l^{CO_2} a V_l} \right) \left(1 + \frac{K_1}{10^{-pH}} \right) \right] - \beta F_l C_A^i(0) \quad (7)$$

where x_{CO2}^o is the measured CO_2 fraction in the outlet gas. For the calculation of $^{13}CO_2$ rates, the term $\beta F_l C_A^i(0)$ in Equation 7 is neglected, because the natural

abundance in bicarbonate is insignificant. ($C^{i}_{A}(0)$ denotes the concentration of bicarbonate in the culture medium directly after medium preparation.)

Values for $k_l^{CO2}a$ were determined as follows. The $k_l^{O2}a$ in cell-free medium was measured as described above. As the diffusion constants for CO_2 and O_2 are proportional to the square roots of their molecular weights, the $k_l^{CO2}a$ can subsequently be calculated, using

$$\frac{k_l^{CO_2}a}{k_l^{O_2}a} = \frac{\sqrt{M_{CO_2}}}{\sqrt{M_{O_2}}} = 0.89 \quad (8)$$

The gas composition of the in- and outgoing gas flow was determined using a quadropole mass spectrometer (PGM 407, Balzers AG, FL). Data acquisition was carried out as described by Eyer et al. (1995).

Analysis of cells and metabolites

Viable-cell concentrations were determined by the trypan-blue exclusion method using a haemacytometer. **Glucose** and **lactate** concentrations were determined with a YSI analyzer (YSI Incorp., Yellow Springs, OH, USA). **Ammonia** was measured with an ion-selective electrode (Orion, Boston, MA, USA). Primary and secondary **amino acids** were determined by HPLC (Amino Quant 1090, Hewlett-Packard, Palo Alto, CA) as described elsewhere (Schmid and Keller, 1992).

Since the bioreactor has only a 100 ml working volume, there was insufficient biomass available to determine its composition during each steady state. The **biomass** composition was therefore obtained as follows. It was found before that the average dry cell weight of the hybridoma cell line varies under different culture conditions. In contrast, the fractions of the different biomass components are assumed to remain constant (Xie and Wang, 1994; Bonarius et al., 1996). Therefore, the determination of the total cellular protein fraction was used to estimate the total biomass composition. The total protein fraction is the largest fraction of the total cell

biomass and its measurement requires relatively small amounts of material. **Total cellular protein** content was quantified using the Biuret method.

NMR analysis

^{1}H- and ^{13}C-NMR spectra were obtained on a Bruker AMX 500 spectrometer at 500.14 and 125.77 MHz, respectively. Typically 128 (^{1}H) and 512 (^{13}C) scans were accumulated. The relaxation delay D1 was 0.5s (^{1}H, long enough for ^{13}C satellite evaluation) and 1 or 15s (^{13}C). Resonance assignments are based on standard chemical shift (^{1}H, ^{13}C) and multiplicity (^{1}H) considerations as well as on DEPT-135 spectra (^{13}C). ^{13}C satellite evaluations in ^{1}H spectra were done by standard integration or when necessary by deconvolution (WIN-NMR,b-Vers. 5.1, Bruker-Franzen Analytik GmbH, Bremen, FRG). Quantitative evaluation of ^{13}C spectra (D1 15s, inverse gated sequence) was discarded because of insufficient signal/noise ratio (CO, ^{13}C satellites of 2-C lactate).

RESULTS AND DISCUSSION

Cell density, metabolic quotients and respiration quotient

Five steady states with various types of labeled ^{13}C-glucose in the culture medium were obtained. Table 1 shows the average values and standard deviations of viable-cell densities and the respiration parameters. The first two steady states were carried out without interruption. After finishing the two runs and inoculating again, the latter three steady state experiments were carried out. Therefore, steady states 1 and 2, and steady-states 3, 4 and 5 will be treated as two different experimental groups during the remainder of this section. These will be indicated as Group I and Group II. The measured extracellular metabolic rates and the calculated metabolic rates are shown in Table C1 and C2 (Appendix C), respectively.

Table 1

Viable cell densities (10^6 cells ml^{-1}), carbon-dioxide evolution and oxygen uptake rates (10^{-12} mol. $cell^{-1}.day^{-1}$), and respiration quotients (-). Numbers between square brackets refer to the fractional labeling of the (indicated) C atom in glucose. Numbers between parentheses indicate standard deviations.

Nr.	Type of glucose	Viable cell density	CER	^{13}CER	OUR	RQ
1.	1-^{13}C-glc [0.60]	2.40 (0.12)	11.3 (0.65)	0.82 (0.08)	16.9 (3.21)	0.73
2.	6-^{13}C-glc [0.60]	2.25 (0.15)	9.6 (1.01)	0.22 (0.05)	13.7 (6.02)	0.71
3.	2-^{13}C-glc [0.60]	2.11 (0.13)	12.3 (0.56)	0.64 (0.02)	18.1 (3.23)	0.72
4.	1-^{13}C-glc [0.35]	1.92 (0.10)	11.9 (1.77)	0.66 (0.04)	19.1 (2.98)	0.67
5.	6-^{13}C-glc [0.60]	1.88 (0.10)	13.1 (2.32)	0.45 (0.04)	19.5 (3.08)	0.70

Pentose-Phosphate Pathway

In the Theory Section various methods to determine the pentose-shunt flux are discussed. These rely either on isotopic-tracer studies, on mass balance equations or on both. In addition, different methods have been proposed to *evaluate* data from isotopic- tracer experiments (Katz and Wood, 1963; Larrabee, 1989; Willis et al., 1986; Kingsley-Hickman et al., 1990) or from metabolite balances (Zupke et al., 1995; Bonarius et al., 1996) to determine the pentose shunt in mammalian cells or tissue. In Table 2 pentose-shunt flux data determined using seven different methods are shown.

Estimating the pentose shunt from $^{13}CO_2$ yields

According to the evaluation method of $^{13}CO_2$ yields from 1-^{13}C- and 6-^{13}C-glucose experiments (Table 1) as proposed by Larrabee (Larrabee, 1989), at least 17 and 24 % of the glucose-6-phosphate pool in Group I and II, respectively, is channeled into the oxidative branch of the pentose cycle (Table 2). This is in agreement with flux values determined by other methods to calculate the pentose-cycle flux from ^{13}C data (Equations 3 and 5, and Appendix B) as will be shown below.

Table 2

Pentose-shunt activity calculated using different methods. Values are given as percentage of glucose uptake rate. Values between parentheses are absolute values in 10^{-12} mol G6P.cell^{-1}.day^{-1}.

Experimental Method	Group I	Group II
(1) $^{13}CO_2$ yields from 1-^{13}C- and 6-^{13}C-glucose experiments		
Larrabee (1989) (Eq. 2)	15.3 % (1.08)	20.8 % (1.41)
incl. 3/(3 - 2 *PPS*)	17.0 % (1.20)	24.1 % (1.63)
(2) Fractional labeling of 3-C- and 2-C-lactate from 1-^{13}C-, 2-^{13}C- and 6-^{13}C-glucose experiment		
Willis et al. (1986) (Eq. 3)	15.0 % (1.06)	20.4 % (1.38)
incl. 3/(3 - 2 *PPS*)	16.7 % (1.18)	23.6 % (1.60)
Kingsley-Hickman et al. (1990) (Eq.4)	12.1 % (0.85)	10.0 % (0.68)
incl. 3/(3 - 2 *PPS*)	13.2 % (0.92)	10.7 % (0.73)
This work (Eq. 5)	n.d.	19.3 % (1.29)
incl. 3/(3 - 2 *PPS*)	n.d.	22.2 % (1.48)
(3) Using mass balances and atomic mapping of isotopes (1-^{13}C-glucose)	Run 1	Run 4
Zupke and Stephanopoulos (1994)	17.3 % (1.22)	23.0 % (1.55)
incl. 3/(3 - 2 *PPS*)	19.6 % (1.38)	27.2 % (1.83)

(4) Using mass balances only

a. NAD(P)H balance

Exp. 1	Exp. 2	Exp. 3	Exp. 4	Exp. 5
75.4% (5.26)	59.0 % (3.57)	84.0 % (4.97)	98.3 % (6.58)	139 % (9.47)

b. Minimum-norm constraint

Exp. 1	Exp. 2	Exp. 3	Exp. 4	Exp. 5
89.9 %(6.34)	65.1 % (3.96)	106 % (6.28)	104 % (7.08)	118 % (8.29)

Estimating the pentose shunt from ^{13}C-lactate data

A typical example of the relevant regions in a ^{1}H-NMR spectrum from the culture medium from a 1-^{13}C-glucose experiment is shown in Figure 5. Both labeling on 3-C-lactate and 2-C-lactate protons give rise to satellites in the CH_3- and the C*H*(OH)-

region, respectively. The satellite peaks in the C*H*(OH)-region are relatively small and difficult to quantify (Figure 5, Bottom). Errors in the estimation of such low $^{13}C/(^{13}C+^{12}C)$ ratios may exceed 10 %. Therefore, in all methods to evaluate **C*-

Figure 5

^{1}H-NMR spectrogram of a typical steady-state from a 1-^{13}C-glucose experiment. (Top) CH_3-region with ^{13}C satellites. (Bottom) C*H*(OH)-region with mainly overlapped ^{13}C satellites.

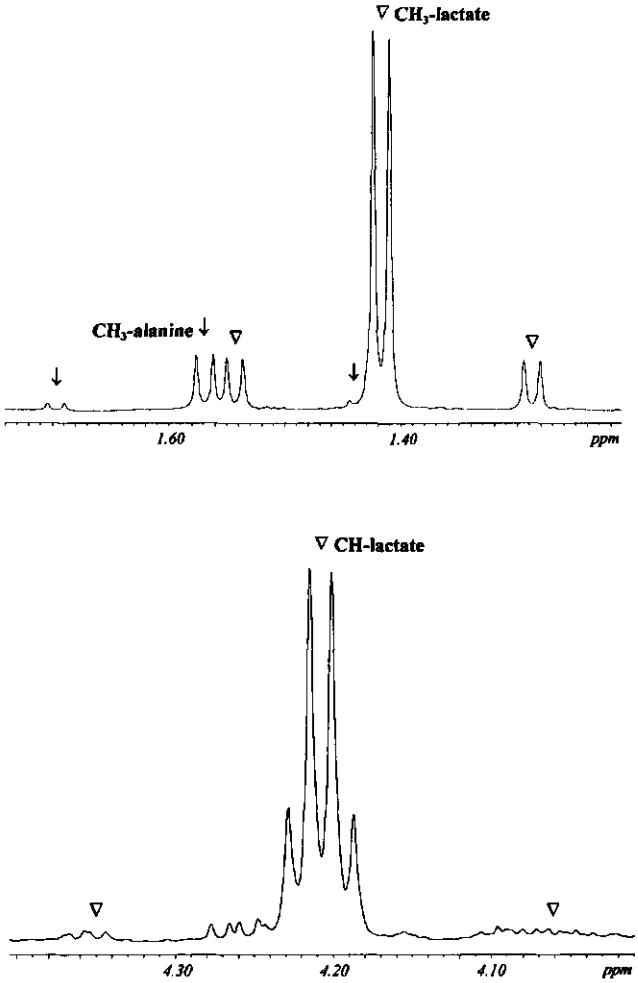

Lac(i) data to determine intracellular fluxes only higher measured $^{13}C/(^{13}C+^{12}C)$ ratios than 0.10 will be used. In Table 3 the fractional labeling of lactate and alanine as calculated from the relevant ^{1}H-NMR spectra of 5 different steady states are given.

Table 3

Fractional labeling of 3-C-lactate, 2-C-lactate and 3-C-alanine as determined using ^{1}H-proton NMR. Evaluations of the NMR spectograms have been done by integrations and when necessary by deconvolutions. Errors in evaluations are ca. 5 % for large values (>0.10) and minimal 10 % for small values (< 0.10). Values between parentheses indicate the fractional labeling of glucose. (b.a.= below accuracy required for flux analysis.)

Nr.	Type of glucose	CH_3 lactate	CH(OH) lactate	CH_3 alanine
1.	1-^{13}C-glc (0.60)	0.217	0.073 b.a.	0.219
	1-^{13}C-glc (0.60)	0.219	0.050 b.a.	0.216
2.	6-^{13}C-glc (0.60)	0.248	0.067 b.a.	0.210
3.	2-^{13}C-glc (0.60)	0.04 b.a.	0.205	n.d.
	2-^{13}C-glc (0.60)	0.04 b.a.	0.204	n.d.
4.	1-^{13}C-glc (0.35)	0.144	0.050 b.a.	0.144
	1-^{13}C-glc (0.35)	0.139	0.060 b.a.	0.138
5.	6-^{13}C-glc (0.60)	0.262	0.062 b.a.	0.248

As discussed in the Theory Section, various methods have been proposed to evaluate such NMR data for quantifying the pentose-shunt flux. Willis et al. (1986) derived a formulation to assess the pentose shunt in tissue culture from 3-^{13}C-lactate measurements after 1-^{13}C-glucose infusion (Equation 3). In this formulation the feed of other (unlabeled) metabolites into the pyruvate pool is neglected. To correct for other carbon sources than glucose, Kingsley-Hickman and co-authors (1990) suggested to use 6-^{13}C-glucose in parallel (Equation 4). However, this approach

neglects the fact that label on 3-C-lactate, that is transferred via the malate shunt (flux 17) and malate/pyruvate shuttle (flux 19), is always higher when 6-^{13}C-glucose is used compared to when 1-^{13}C-glucose is used. This is a result of ^{13}C loss in the oxidative branch of the pentose shunt (See Figure 2). Particularly at high pentose-shunt activities this can cause an overestimation of the correction for endogenous carbon sources (here, 'endogenous sources' refers to amino acids). In Table 2 it is shown that the pentose-shunt flux, when calculated by Equation 4, is significantly lower than the lower limits of the shunt obtained from $^{13}CO_2$ yields. This maybe a consequence of the relatively high pentose-shunt activity. In contrast, when a correction for dilution of label by endogenous carbon is not used (Equation 3), a better agreement is obtained.

In the Theory Section, an alternative approach to correct for endogenous carbon is proposed using 6-^{13}C-glucose in parallel to 2-^{13}C-glucose (Equation 6). In Figure 3 it is shown that at equal glycolytic/pentose-shunt ratios, 2-C-lactate from 2-^{13}C-glucose will be equally labeled as 3-C-lactate from 6-^{13}C-glucose experiment. Correction for the dilution of label from endogenous carbon will therefore not be influenced by ^{13}C loss in the pentose shunt. This suggests that particularly at relatively high pentose-shunt fluxes ($PPS > 0.15$) a correction for endogenous carbon in lactate should be carried out as according to Equation 5. A disadvantage of this method is that interference of label transfer via the reactions 17 and 19 is smaller in the case of 2-^{13}C-glucose, because the carbon at the second position of pyruvate, to which the majority of label will be transferred to (because flux 2 is smaller than flux 1), is decarboxylated by α-ketoglurate dehydrogenase (flux 15) before it reacts into malate. The values obtained by Equation 5, are in better agreement with pentose-flux values obtained from $^{13}CO_2$ measurements.

Estimating the pentose shunt using only mass balances

It has been suggested that the pentose-cycle activity can be estimated by adding theoretical constraints such as the minimum-norm constraint (Bonarius et al., 1996) or constraints determined by the NAD(P)H material balance (Zupke et al., 1995). In Table 2 it is shown that the use of either of these constraints results in different

values of the pentose flux as compared to the experimentally-determined values. Moreover, fluxes estimated using the NAD(P)H balance vary substantially, even under the same culture conditions. These observations can be a result of both measurement errors in the OUR, and of the fact that flux x_2 is very sensitive to small changes in the NADPH balance. Recently, it was shown that small deviations in the OUR do result in relatively large differences in the estimated pentose flux (Bonarius et al., 1998b). This is a consequence of the fact that the $r_{NAD(P)H}$ is large in comparison to other values in the vector **r**, and it has a relatively high weight in the least-squares solution. In mammalian-cell culture, the NAD(P)H balance should therefore not be used to estimate the split ratio of fluxes at the glucose-6-phosphate branchpoint.

Flux analysis by modeling isotope distributions

By combining the mass-balance equations of 18 metabolites, and the *$*CO_2(1)$* and **3-C-Lac(1)* data, 18 fluxes in the central carbon metabolism of mammalian cells can be determined using the algorithm described in Appendix B. In Table 4 and Figure 6 the fluxes in hybridoma cells of both 1-^{13}C-glucose experiments are given in 10^{-12} mole produced metabolite.cell^{-1}.day^{-1} (Table 4) and as a fraction of the glucose uptake (Figure 6).

The pyruvate-decarboxylase flux is negligible

In both experiments, the pyruvate-carboxylase flux is negligible (< 1 % on a Cmol basis) with respect to the glucose uptake rate. This implicates that under conditions such as investigated here, in contrast to what was suggested in the Theory Section, the singularity that is a result of flux 16, 17 and 18 does not necessarily have to affect flux analysis of mammalian cells based on metabolite balances. Also when hybridoma cells are grown in hollow-fiber bioreactors, it was shown using *in vivo* NMR that the pyruvate-carboxylase activity was negligible in hybridoma cells (Mancuso et al., 1994). This suggests that in theory, i.e. provided that the NAD(P)H balance can be closed at sufficient accuracy, the intracellular fluxes of the primary metabolism in mammalian cells can be quantified without using isotopic tracers.

Malic enzyme

The malic enzyme is both active in the pyruvate/malate shuttle (x_{19}) and in the malate shunt (x_{17}), i.e. 8 and 4 % on a Cmol basis of the glucose uptake rate, respectively (Table 4).

Table 4

Metabolic fluxes determined using modeling of isotope distributions using atomic mapping matrices and experiemental data from 1-^{13}C-glucose experiments. Values for two steady states are given in 10^{-12} mol product cell^{-1}.day^{-1}.

	Exp. 1	Exp. 4
1. G6P → F6P	5.76	5.18
2. G6P → Ru5P + CO2 + 2 NADPH	1.22	1.55
3. Ru5P → X5P	0.70	1.10
4. Ru5P → R5P	0.49	0.54
5. X5P + R5P → S7P + GAP	0.31	0.68
6. X5P + E4P → F6P + GAP	0.36	0.50
7. S7P + GAP → F6P + E4P	0.33	0.62
8. F6P + ATP → 2 GAP	12.62	13.14
9. GAP → G3P/SER + NADH + ATP	12.68	13.50
10. G3P/SER → PEP	12.68	13.31
11. PEP → PYR + ATP	12.67	13.36
12. PYR → ACoA + NADH + CO2	3.11	3.72
13. ACoA + OMA → CIT	3.64	4.45
14. CIT → AKG + NADH + CO2	2.55	3.45
15. AKG → MAL + 2 NADH + ATP + CO2	4.02	4.45
16. MAL → OAA + NADH	4.00	4.73
17. MAL → PYR + CO2 + NADPH	0.28	0.21
18. PYR + ATP + CO2 → OAA	0.02	0.13
19. 9 CIT + 9 NADH + 8 ATP + 7 NADPH → FA/CHOL + 9 PYR + 9 CO2	1.07	1.01
20. PYR + GLU → AKG + ALA	0.98	1.08
27. PYR + NADH → LAC	9.21	10.73

Flux through the pentose-phosphate pathway

The flow through the pentose-phosphate pathway relative to the glucose uptake rate

varies between 17 to 27 % in rapidly growing ($\mu = 0.9\ d^{-1}$), homogeneously-cultured hybridoma cells (Method 1 and 3, Table 2). This is considerably higher than results obtained with surface-attached-cultured hybridoma cells, as investigated by Mancuso and co-authors (1994), who found that only 4 % of the consumed glucose in hybridoma cells grown in hollow-fiber bioreactors was channeled to pyruvate via the pentose shunt. Apart from differences in methodology to determine the metabolic flux, the relatively high pentose-shunt flux observed here may be a result of mode of cultivation. At higher growth rates the requirements for NADPH are higher, and as a consequence the pentose-shunt activity increases (Stryer, 1988). Using Equation 2

Figure 6

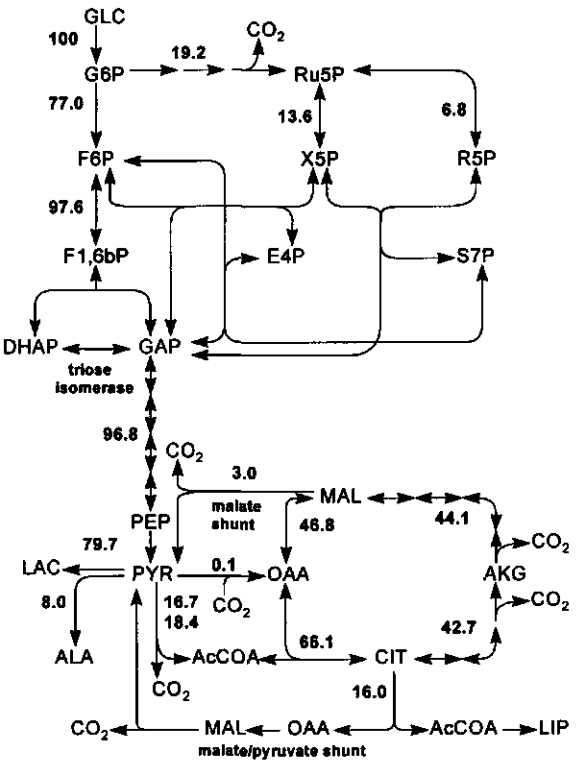

Fluxes of central carbon metabolism in continuously cultured hybridoma cells determined by mass-balance techniques combined with $^{13}CO_2$ mass spectrometry, ^{1}H-NMR spectro-metry. 1-^{13}C-glucose is used as isotopic source (steady state 4). Values are given in reaction product as fraction of glucose uptake ($Cmol.Cmol^{-1}$).

and off-line short-term radioactive assays, Jan et al. (1997) found pentose-shunt flux values of 10 % at a dilution rate of 1 d^{-1}.

TCA cycle

Only a relatively small amount of the pyruvate pool (23 % in both experiment 1 and 4) is oxidized in the TCA cycle. The majority (almost 77 %) is secreted as lactate and alanine in the culture medium. A significant fraction of carbon units in TCA-cycle intermediates has an endogenous source: approximately 40 % of the carbon that enters the cycle is derived from amino acids. The fraction of glucose that enters the TCA cycle can be estimated by the $^{13}CO_2$ produced by cells grown in 6-^{13}C-glucose-containing medium (Petch and Butler, 1994). Taking into account that the label on 3-C-pyruvate is diluted with a factor 2 due to the interconversion of triose phosphates (Figure 2), 12 and 22 % of the glucose is oxidized by α-ketoglutarate dehydrogenase (x_{15}) in experiment 1 and 4, respectively. Thus, on average 17 % of the consumed glucose is metabolized by the TCA cycle.

The TCA-cycle flux (the flux from isocitrate to α-ketoglutarate, x_{14}) in continuously cultured hybridoma cells is at least 40 % relative to the glucose uptake rate, which is relatively high compared to 25 % in the case of hybridoma cells cultured in a hollow-fiber bioreactor (Mancuso et al., 1994). Practically all of the glucose-derived carbon enters the TCA cycle through pyruvate dehydrogenase (x_{12}).

Implications for medium design

In contrast to non-tumorgenic mammalian cells, cancer cells such as hybridomas consume glucose independent of their requirement for energy or for building blocks for anabolic processes (Eigenbrodt, 1985). The surplus of the consumed glucose is secreted as lactate or alanine. Therefore, only by the accurate determination of the contribution of cyclic pathways, such as the pentose shunt and the TCA cycle, the minimum amount of glucose that cells require to produce NADPH and NADH (and in a lesser extent, precursors for nucleic acids and fatty acids), can be assessed.

A large amount of the NADH that is produced in the TCA cycle is "spilled" by lactate dehydrogenase (x_{27}). Of the 17.7 and 20.8 $*10^{-12}$ mol NADH.cell^{-1}.day^{-1} generated in the TCA cycle (the sum of fluxes 12, 14, 2*15 and 16, Table 4) 9.2 and 10.7 mol NADH.cell^{-1}.day^{-1}, in experiment 1 and 4, respectively (r_{LAC} in Table C1, Appendix C), is used for the reduction of pyruvate by lactate dehydrogenase. Only 8.5 and $10.1*10^{-12}$ mol NADH.cell^{-1}.day^{-1}, in experiment 1 and 4, respectively, is required for other processes. This corresponds to 48 and 49 % of the actual TCA-cycle flow. Taking into account that 40 % of the carbon in TCA-cycle intermediates derives from endogenous metabolism, these data suggest that only 8 to 9 % of the carbon derived from glucose is actually required for NADH generation. In contrast, the amount of glucose that is channeled through the pentose-shunt flux is much higher (20 %).

In both normal (Stryer, 1988) and tumorgenic (Eigenbrodt, 1985) cells, the key regulatory factor for glucose-6-phosphate dehydrogenase (x_2) is the $NADP^+$/NADPH ratio in order to ensure a tight coupling of the rate through the oxidative branch and reductive biosynthesis. Together with the flux data shown here this shows that the pentose-phosphate pathway, rather than the TCA cycle, determines the minimum requirement of glucose. The cells studied here require only an average of 23 % of the glucose consumption rate which equals to $1.5*10^{-12}$ mol glucose.cell^{-1}.day^{-1}. This is in very good agreement with the glucose uptake rate of cells cultured in optimal conditions with respect to glucose economy, as reported by Xie and Wang (1994b). By stoichiometric feeding a very efficient ratio of lactate to glucose of only 0.10 mol.mol^{-1} was obtained. The avarage glucose uptake rate in this study was $1.2*10^{-12}$ mol.cell^{-1}.day^{-1}. (The total protein per cell in the mentioned report is almost equal to the values measured here.) These data suggest that glucose uptake in the fed-batch culture as described by Xie and Wang (1994b) is close to the theoretical optimum.

Implications for metabolic engineering

From the above it is clear that the production of no lactate at all, by further decreasing the glucose consumption, is sub-optimal at pentose-shunt rates such as measured here. Assuming that hybridoma cells need all the NADPH produced in the pentose-phosphate pathway in amounts such as determined here, more pyruvate than necessary for NADH generation in the TCA cycle will be produced even at an optimal r_{GLC} of $1.3*10^{-12}$ mol $cell^{-1}.day^{-1}$. Lower availability of glucose will therefore result in glucose limitation. Instead of decreasing glucose concentrations to further reduce the ratio of lactate to glucose, the amount of fructose-6-phosphate that is recycled in the pentose-phosphate pathway should be increased, which results in higher NADPH yields per consumed glucose. Another possibility to decrease lactate/glucose yields, is the stimulation of the pyruvate-dehydrogenase reaction, of which the activity is negligibly small (Figure 6). A higher pyruvate-dehydrogenase flux could cause more pyruvate oxidation in the TCA cycle and therefore a reduction of lactate synthesis.

CONCLUSIONS

For continuously cultured hybridoma cells growing at high rates (μ=0.9 d^{-1}) the following can be concluded:

(i) The cells channel ~ 23 % of the consumed glucose through the pentose shunt.

(ii) Pyruvate-carboxylase activity is insignificant under the condition investigated here.

(iii) The malate-shunt flux and the flow through the TCA cycle is only 3 % and 40 % of the glucose uptake rate, respectively.

For medium design it has been shown that the pentose-shunt flux determines how much glucose is minimally required, which is ca.$1.5*10^{-12}$ mol glucose.$cell^{-1}.day^{-1}$ for the conditions investigated here.

ACKNOWLEDGEMENTS

We thank the following people from the Laboratorium für Technische Chemie, ETH Zentrum, Zürich, CH: Felix Bangert for carrying out the NMR analyses, Evelyn Blochilger for assistance with the lyophilization apparatus, Urs Seineke for designing and constructing the 100 ml polycarbonate bioreactor. We are also indebted to Dr. Ernst J. Schlaeger, Jean-Marie Vonach and Nathalie Schaub-Wild of the Department of PRP-Biotechnology, Hoffmann-La Roche AG, Basel, CH, for design and preparation of the culture medium and for amino-acid analysis, respectively. Pictures of the bioreactor were made by Ton Feyen (Repro Service, Agricultural University Wageningen). This work was supported both by the Department of PRP-Biotechnology, Hoffmann-La Roche AG and the Food and Bioengineering Group, Wageningen Agricultural University.

APPENDIX A

Table A1

Equations for the network that describes mammalian-cell glucose metabolism. These mass balances give the input vector **r** (1 x n, where n = 20) for the algorithm shown in Appendix A.

1. $r(G6P) = - x_{45}(GLC)$
2. $r(F6P) = x_{26}(TC)$
3. $r(Ru5P) = 0$
4. $r(X5P) = 0$
5. $r(R5P) = x_{28}(RNA) + x_{29}(DNA)$
6. $r(S7P) = 0$
7. $r(E4P) = 0$
8. $r(GAP) = x_{30}(PL)$
9. $r(G3P) = r_{nc,SER} + r_{nc,GLY}$
10. $r(PEP) = 0$
11. $r(PYR) = x_{27}(LAC) + r_{nc,ALA} + r_{nc,THR} + r_{nc,CYS} - 9*x_{19}(FA)$
12. $r(ACoA) = r_{nc,LEU} + r_{nc,ILE} + r_{nc,LYS} + r_{nc,PHE}$
13. $r(CIT) = 9*x_{19}(FA)$
14. $r(AKG) = r_{nc,PHE} - r_{nc,LEU} - r_{nc,ILE} - r_{nc,LYS} - r_{nc,ARG} - r_{nc,ALA} - r_{nc,MET} - x_{21} - x_{22}$
15. $r(MAL) = 0.8*x_{28}(RNA) + 0.8*x_{29}(DNA) + r_{nc,PHE} + r_{nc,MET}$
16. $r(OAA) = x_{21}$
17. $r(CO2) = r_{CO2} - (9*x_{19}(FA) + 0.015*x_{28}(RNA))$
18. $r(FA) = x_{19}(FA)$
19. $r(ALA) = r_{nc,ALA}$

Note: x_{21} and x_{22} are determined by mass-balancing techniques.

APPENDIX B

Numerical algorithm to calculate fluxes from isotopic tracers

For a detailed description of the numerical algorithm to determine metabolic fluxes using atom mapping matrices, as developed by Zupke and Stephanopoulos (1994), we refer to their work. In this appendix, the iteration process is briefly described and the different elements, terms and parameters are introduced.

The algorithm calculates the metabolic flux distribution as follows. First, a random solution **x(0)**, which satisfies the constraints of the underdetermined set of equations $\mathbf{Ax} = \mathbf{r}$, is calculated. From this arbitrary flux distribution **x(0)**, together with the fractional labeling of glucose, the fractional labeling of all metabolites is computed (using "atom-mapping matrices, **AMM**"). Out of the fractional labeling of all metabolites, a submatrix (the "specific activity matrix, **SAM**") is selected, which contains the fractional labeling (specific activity) of those C atoms that produce one of the C atoms of which the fractional labeling is actually measured (in this work, CO_2 and 3-C-lactate).

Together with the measured fractional labeling of CO_2 and 3-C-lactate, the **SAM** gives two mass balances, i.e. $\mathbf{SAM\ x} = \mathbf{r}_{SA}$. These two mass balances are added to the other mass balances, $\mathbf{Ax} = \mathbf{r}$, resulting in a determined system (Equation A8). The least-squares solution of this determined system, **x(1)**, has unacceptably high residual values, as **x(0)** has been chosen randomly. Subsequently, **x(1)** is used as input for the next iteration. The algorithm is repeated until the least-squares solution is stable.

The **atom-mapping matrix (AMM)** of a certain enzymatic reaction contains the carbon stoichiometry. The net stoichiometry of flux 8 which converts fructose-6-phosphate into glyceraldehyde-3-phosphate (by the action of phosphofructokinase, aldolase and triose-phosphate isomerase) is

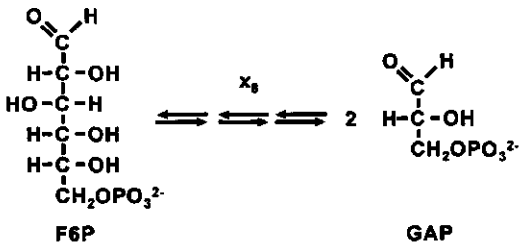

For example, due to reaction 8, 100 % label on 1-C-fructose-6-phosphate will be transferred to 3-C-glyceraldehyde-3-phosphate and diluted to 50 %. In the **AMM** associated with reaction 8 this results in one element with the value ½ (" ½^ " in Equation A1). In contrast, none of the 100 %

label on 1-C-fructose-6-phosphate will be transferred to 1-C-glyceraldehyde-3-phosphate by reaction 8, resulting in a 0 in $\mathbf{AMM}_8$ (" 0* " in Equation A1). The **AMM** that describes the label transfer of all C atoms of fructose-6-phosphate to all C atoms of glyceraldehyde-3-phosphate by flux xg is

$$[F6P > GAP]_8 = \begin{bmatrix} 0^* & 0 & ½ & ½ & 0 & 0 \\ 0 & ½ & 0 & 0 & ½ & 0 \\ ½^\wedge & 0 & 0 & 0 & 0 & ½ \end{bmatrix} \qquad (A1)$$

In Figure A1 the fluxes and metabolites that are used in the numerical process are shown.

Figure A1

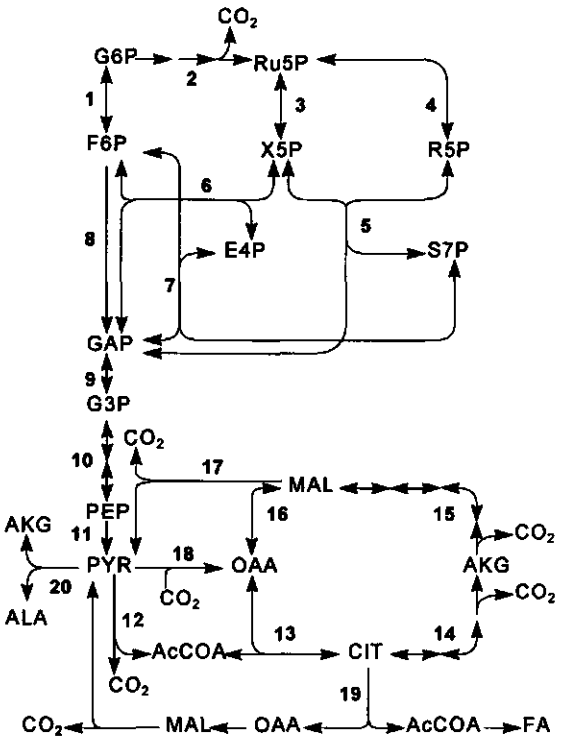

Metabolic network used for the calculation intracellular fluxes by modeling of isotopic distributions. The network contains 20 fluxes, 19 metabolite balances (Table A1) and 2 isotope balances (CO_2 and 3-C-lactate). Although flux 19 and 20 can be determined using mass balances alone (see also Figure 1), they have to be included in the algorithm because these reactions transfer label within the underdetermined network.

The **specific-activity vectors** (**SAVs**) represent the fractional labeling of the different carbon atoms. Some of the **SAVs** are known (glucose) or measured (lactate, CO_2 and alanine). The **SAVs** of other intermediates are calculated. For instance, when glucose is labeled for 50 % on the first carbon, the fractional labeling of CO_2 is 4 % and the specific activity of lactate is 22 %, 5 % and 1 % for 1-C-, 2-C- and 3-C-lactate respectively, the **SAVs** of these metabolites yield (neglecting natural abundance)

$$GLC = \begin{bmatrix} 0.50 \\ 0 \\ 0 \\ 0 \\ 0 \\ 0 \end{bmatrix}, \quad CO2 = [0.04], \quad LAC = \begin{bmatrix} 0.22 \\ 0.05 \\ 0.01 \end{bmatrix} \qquad (A2)$$

The **SAV** of a produced metabolite A is the product of the **AMM** that describes the reaction in which A is produced and the **SAV** of the substrate. For example, the oxidative branch of the pentose shunt (flux 2) yields two metabolites, ribulose-5-phosphate and CO_2. When 1-C-glucose-6-phosphate has a specific activity of 50 %, and the other C-atoms of glucose-6-phosphate do not have any activity, the transfer of label to ribulose-5-phosphate and CO_2 via flux 2 is calculated as

$$[G6P > R5P]_2 \bullet SAV_{G6P} = SAV_{R5P} \Leftrightarrow \begin{bmatrix} 0 & 1 & 0 & 0 & 0 & 0 \\ 0 & 0 & 1 & 0 & 0 & 0 \\ 0 & 0 & 0 & 1 & 0 & 0 \\ 0 & 0 & 0 & 0 & 1 & 0 \\ 0 & 0 & 0 & 0 & 0 & 1 \end{bmatrix} \bullet \begin{bmatrix} 0.50 \\ 0 \\ 0 \\ 0 \\ 0 \\ 0 \end{bmatrix} = \begin{bmatrix} 0 \\ 0 \\ 0 \\ 0 \\ 0 \end{bmatrix} \qquad (A3)$$

and

$$[G6P > CO2]_2 \bullet SAV_{G6P} = SAV_{CO2} \Leftrightarrow [1 \ 0 \ 0 \ 0 \ 0 \ 0] \bullet \begin{bmatrix} 0.50 \\ 0 \\ 0 \\ 0 \\ 0 \\ 0 \end{bmatrix} = [0.50] \qquad (A4)$$

respectively.

The examples above (Equations A3 and A4) suggest that the label of a produced metabolite is the result of one reaction. In reality, various reactions dilute label of or transfer label to a particular metabolite. To calculate the net label transfer of more than one flux to a particular metabolite, the fluxes have to be expressed as 'flux **fractions**'. For instance, the flux fraction of the malic enzyme to pyruvate, $f_{17} = x_{17}/(x_{11}+x_{17}+x_{19}+x_{41})$, is the fraction of pyruvate that is derived from the malic shunt. (This formulation recognizes the fact that only *ingoing* fluxes to the pool of metabolite Y determine the label distribution of Y.)

From the estimated **SAV**s and the flux fractions, the specific activity of those C-atoms that are determined experimentally is calculated. The output of this calculation is the so-called **Specific Activity Matrix**. The **SAM** contains m columns and o rows, where m refers to the number of fluxes and o to the number of measured specific activities. In this work $o = 2$, as only the fractional labeling of CO_2 and 3-C-lactate is used in the algorithm. After 3 iterations, the **SAM** yields for instance:

$$SAM(3) = \begin{bmatrix} 0 & 0.04 & 0 & 0 & 0 & 0 & 0 & 0 & 0 & 0 & 0.03 & 0 & 0.03 & 0.05 & 0 & 0.02 & -0.02 & 0.02 & 0 \\ 0 & 0 & 0 & 0 & 0 & 0 & 0 & 0 & 0 & 0.24 & -0.24 & 0 & 0 & 0 & 0 & 0.22 & -0.20 & 0.22 & -0.20 \end{bmatrix} \quad (A5)$$

Note that in this numerical example the iterative process is not stable yet. Typically, after 20 iterations the process will be stable and **SAM(3)** becomes:

$$SAM(20) = \begin{bmatrix} 0 & 0.04 & 0 & 0 & 0 & 0 & 0 & 0 & 0 & 0 & 0.04 & 0 & 0.04 & 0.04 & 0 & 0.04 & -0.04 & 0.04 & 0 \\ 0 & 0 & 0 & 0 & 0 & 0 & 0 & 0 & 0 & 0.22 & -0.22 & 0 & 0 & 0 & 0 & 0.22 & -0.22 & 0.22 & -0.22 \end{bmatrix} \quad (A6)$$

The (1,2) element of the specific activity matrix (numerical value 0.04 in Equations A5 and A6) represents the label distribution of CO_2 and is calculated by

$$SAM_{(1,2)} = [G6P > CO2]_2 \bullet SAV_{G6P} \quad (A7)$$

The elements of the **SAM** are dimensionless numbers. By multiplying the **SAM** elements with the measured production rates of the atoms of which the fractional labeling has been determined, their units can be adjusted to those of the final network, yielding:

$$\begin{bmatrix} A \\ SAM \end{bmatrix} \bullet [x] = \begin{bmatrix} r \\ r_{SA} \end{bmatrix} \quad (A8)$$

where $\mathbf{r}_{SA}$ represents an *l x o* vector with the measured production rates of the atoms of which the specific activity has been determined experimentally. In the example here $\mathbf{r}_{SA} = [\mathbf{r}_{CO2} ; \mathbf{r}_{LAC}]$ *1). Matrix A is the *m* x *n* stoichiometric matrix of the material balance equations and is rank deficient. Supplemented with the *o* x *n* **AMR** submatrix, the metabolic network finally becomes determined and x can be estimated by the least-squares method.

*1) This particular element of the final full rank network shows that it is of key importance to be able to measure both the CER and the ^{13}CER. Without these measurements, for which a method was developed earlier (Bonarius, et al. 1995), it is not possible to determine all fluxes of glucose metabolism in one independent experiment. The only alternative to this method is the measurement of the fractional labeling of intracellularly accumulated metabolites by *in vivo* NMR or by *ex situ* NMR of extracted metabolites.

APPENDIX C

Table C1

Metabolic rates. Values are given in 10^{-12} mol.cell^{-1}.day^{-1} and calculated using the mass balance equations given in ref. (Bonarius et al., 1996). Negative values indicate uptake rates. Total protein (TP) is given in 10^{-4} mg.cell^{-1}. (n.d. = not determined.)

Exp.nr.	1. 1-^{13}C-GLC	2. 6-^{13}C-GLC	3. 2-^{13}C-GLC	4. 1-^{13}C-GLC	5. 6-^{13}C-GLC
ASP	-0.049	-0.040	-0.143	-0.132	-0.109
GLU	0.176	0.146	-0.113	-0.111	-0.042
ASN	-0.086	-0.070	-0.097	-0.087	-0.094
SER	-0.266	-0.670	-0.184	-0.876	-0.143
GLN	-1.220	-1.141	-1.551	-1.501	-1.639
HIS	-0.054	-0.019	-0.110	-0.133	-0.108
GLY	0.137	0.087	-0.150	-0.112	-0.115
THR	-0.097	-0.090	-0.161	-0.121	-0.131
ALA	0.938	0.863	0.691	0.842	0.896
ARG	-0.115	-0.153	-0.172	-0.130	-0.138
TYR	-0.053	-0.037	-0.093	-0.077	-0.874
CYS	-0.075	-0.084	-0.096	-0.108	-0.093
VAL	-0.069	-0.046	-0.233	-0.165	-0.206
MET	-0.084	-0.099	-0.144	-0.115	-0.116
TRP	-0.035	-0.029	-0.044	-0.040	-0.024
PHE	-0.063	-0.086	-0.126	-0.094	-0.094
ILE	-0.255	-0.276	-0.353	-0.311	-0.334
LEU	-0.373	-0.442	-0.543	-0.529	-0.556
LYS	-0.349	-0.155	-0.116	-0.123	-0.115
HYP	0.235	0.350	0.210	0.250	0.252
PRO	0.314	0.262	0.652	0.782	0.868
GLC	-7.055	-6.124	-5.771	-6.692	-6.936
LAC	9.212	9.455	9.632	10.73	10.41
NH3	0.951	0.730	1.091	1.049	1.145
TP	2.73	3.12	n.d.	2.60	n.d.

Table C2

Metabolic rates calculated using the balance equations in Table A1. The values of Experiment 1 and 4 (1-^{13}C-glucose) are used as input data for the numerical algorithm described in Appendix B. (n.d.=not determined)

Exp.nr.	1. 1-^{13}C-GLC	2. 6-^{13}C-GLC	3. 2-^{13}C-GLC	4. 1-^{13}C-GLC	5. 6-^{13}C-GLC
G6P	-7.01	-6.08	-5.725	-6.647	-6.888
F6P	0.073	0.089	0.082	0.081	0.078
Ru5P	0.0	0.0	0.0	0.0	0.0
X5P	0.0	0.0	0.0	0.0	0.0
R5P	0.107	0.129	0.120	0.117	0.135
S7P	0.0	0.0	0.0	0.0	0.0
E4P	0.0	0.0	0.0	0.0	0.0
GAP	0.115	0.139	0.133	0.126	0.122
G3P	0.136	0.219	0.119	0.241	0.168
PEP	0.0	0.0	0.0	0.0	0.0
PYR	9.715	9.880	9.295	10.56	10.39
ACOA	-0.545	-0.226	-0.761	-0.693	-0.747
MAL	-0.085	-0.104	-0.094	-0.089	-0.091
CIT	1.056	1.285	1.191	1.159	1.124
AKG	-1.312	-1.212	-0.943	-0.891	-0.929
OAA	0.349	0.342	0.475	0.361	0.408
CO2	11.00	8.53	11.75	11.40	12.43
FA	0.117	0.143	0.132	0.129	0.125
ALA	1.041	0.990	0.924	1.070	1.117

Chapter 6

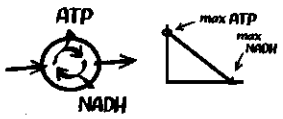

Metabolite-Balancing Techniques versus ^{13}C-tracer Experiments to Determine Metabolic Fluxes in Hybridoma Cells

Hendrik P.J. Bonarius, Bram Timmerarends,
Cornelis D. De Gooijer, and Johannes Tramper

ABSTRACT

The estimation of intracellular fluxes of mammalian cells using only mass balances of the relevant metabolites is not possible because the set of linear equations defined by these mass balances is underdetermined. In order to quantify fluxes in cyclic pathways the mass-balance equations can be complemented with several constraints: (1) the mass balances of co-metabolites, such as ATP or NAD(P)H, (2) linear objective functions, (3) flux data obtained by isotopic-tracer experiments. Here, these three methods are compared for the analysis of fluxes in the primary metabolism of continuously cultured hybridoma cells. The significance of different theoretical constraints and different objective functions is discussed after comparing their resulting flux distributions to the fluxes determined using $^{13}CO_2$ and ^{13}C-lactate measurements of 1-^{13}C-glucose-fed hybridoma cells. Metabolic fluxes estimated using the objective functions "maximize ATP" and "maximize NADH" are relatively similar to the experimentally determined fluxes. This is consistent with the

observation that cancer cells, such as hybridomas, are metabolically hyperactive, and produce ATP and NADH regardless of the need for these cofactors.

INTRODUCTION

A fundamental problem of the analysis of intracellular fluxes is caused by the presence of cyclic metabolic pathways in cell metabolism. Fluxes in these pathways cannot be quantitated solely by the measurement of the extracellular metabolic rates and the biomass composition, because their reaction stoichiometry is linearly dependent and thus generates singular (underdetermined) metabolic networks (Vallino and Stephanopoulos, 1990).

Fluxes in cyclic pathways are therefore determined by isotopic-tracer techniques. As the (carbon) stoichiometry of the reactions is known, it is possible to determine fluxes in cyclic pathways by tracing the metabolic fate of (carbon-)labeled substrates. Although isotopic-tracer techniques are well established and have been significantly improved, particularly since the application of NMR technology to biological systems (Shulman et al., 1979), they are laborious and expensive to conduct, and are not feasible at an industrial scale.

Metabolic-flux balancing techniques offer a possible alternative to isotopic-tracer studies. However, as mentioned above, a solution to the metabolite-balance equations generally does not exist because stoichiometric equations that describe cyclic metabolic pathways, contain linearly dependent reactions (Vallino and Stephanopoulos, 1990). Additional constaints are required to solve the linear set of equations determined by the mass-balance equations (Bonarius et al., 1997). This is explained in Figure 1A. The mass balances of metabolites A and B yield the same information, as a result fluxes 1 and 2 cannot be determined. Here, the solution space that contains all permissible solutions for both fluxes can be represented as a single line. In contrast, when a co-metabolite is produced or consumed in either flux 1 or 2 the three mass balances A, B, and C yield one unique solution (Figure 1B).

Figure 1

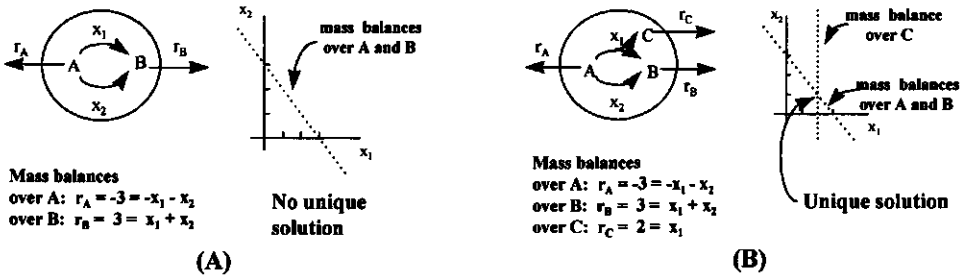

Fluxes in cyclic pathways without (A) and with (B) a co-metabolite. (Numerical values are chosen arbitrarily.)

In reality however, addition of the mass balance(s) of co-metabolites is generally not sufficient to generate an (over)determined system. In complex networks, co-metabolites are either produced in more than one cyclic pathway, or are not balanceable. For example, in mammalian cells carbon dioxide is co-produced in the pentose cycle, the TCA cycle and in the malate shunt (Figure 2). The addition of the carbon-dioxide balance to the metabolic network will therefore not remove the singularities that are a result of these cycles. (However, useful information can be obtained from the carbon-dioxide evolution rate as it provides additional information on the total flow in the three cycles mentioned above.) In contrast, the constraint that is imposed by the ATP balance theoretically can improve the observability of a metabolic network such as shown in Figure 2. However, the observability of the network can only theoretically be improved, because both ATP requirements for maintenance processes and the P/O ratio can only be approximately estimated (Pirt, 1965; Stouthamer, 1973).

In this article, various computational methods that were reported before (Fell and Small, 1986; Savinell and Palsson, 1992; Van Gulik and Heijnen, 1995; Bonarius et al., 1996) to estimate fluxes of underdetermined metabolic networks are compared and applied to measurement data of the primary metabolism of continuously cultured hybridoma cells. In addition, the flux values that are determined using these methods are compared to fluxes that are measured by ^{13}C-tracer experiments.

Figure 2

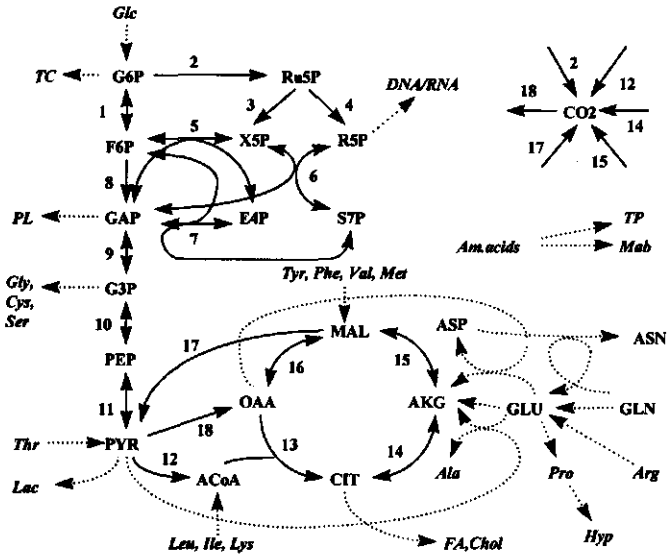

Metabolic fluxes of hybridoma cells. In this figure two combinations of reactions (Fluxes 1-16 and fluxes 16-18) are linearly dependent. In order to quantify these fluxes additional constraints are required. The fluxes indicated by dotted arrows can be determined soleley by mass-balance techniques.

MATERIALS AND METHODS

A detailed description of the experimental methods is published elsewhere (Bonarius et al., 1998d). Briefly, hybridoma cells were cultured in a continuous mode (D = 0.9 d^{-1}) on a 100 ml scale in defined serum-free, low-protein medium. Dissolved oxygen (30%), temperature (37°C) and pH (7.2) were controlled and kept constant during cultivation. Glucose and lactate were determined with automated enzymatic assays (YSI, Yellow Springs, OH), ammonia using an ion-selective electrode, and amino acids by HPLC (Amino Quant 1090, Hewlett-Packard, Palo Alto, CA). The cellular composition that was determined earlier was used to calculate the requirements for biosynthesis (Bonarius et al., 1996). 1-^{13}C-glucose (CIL, Inc. Andover, MA) was used as isotopic-tracer source and the fractional labeling of lactate was determined

by ^{1}H-NMR spectroscopy (Bruker AMX 500, Bruker-Franzen Analytik GmbH, Bremen, FRG). CO_2, $^{13}CO_2$ and O_2 in both the in- and outgoing gas flow were measured by mass spectrometry (Balzers Ag, FL) as described elsewhere (Eyer et al., 1995). The CO_2- and $^{13}CO_2$-production rate was determined using a method that was especially developed for mammalian-cell culture in bicarbonate-containing media (Bonarius et al., 1995a). The O_2 uptake rate was calculated from the O_2 concentrations in the in- and outgoing gas phase (Eyer et al., 1995). The intracellular metabolic fluxes were calculated by combining the mass-balance equations of the relevant metabolites (Figure 2) and the measured fractional labeling of CO_2 and lactate, based on the principles of the computational method described by Zupke and Stephanopoulos (1994).

RESULTS AND DISCUSSION

The minimum number of fluxes that must be measured using labeling techniques to determine the intracellular fluxes is equal to the number of fluxes minus the number of independent mass-balance equations. In Figure 2 metabolic pathways of the primary metabolism of mammalian cells are shown. The dotted arrows represent the fluxes that can be uniquely determined by the use of mass balances of the indicated metabolites only. The uninterrupted arrows indicate the fluxes that are linearly dependent. The network contains two combinations of linearly dependent reactions, i.e the coupled TCA cycle and the pentose shunt (one singularity) and the malate shunt. To determine all the fluxes in this network two fluxes, one flux out of each combination, must be determined independently using isotopic tracers.

Visual representation of the solution space

The solution space of the two mass balance equations in Figure 1A has one degree of freedom (*one* singularity) and can be represented by a *line*. Similarly, the solution space of the 18 fluxes in the metabolic network shown in Figure 2 (*two* singularities) can be visualized by a *two*-dimensional *plane*. For this purpose, the 18-dimensional

Figure 4

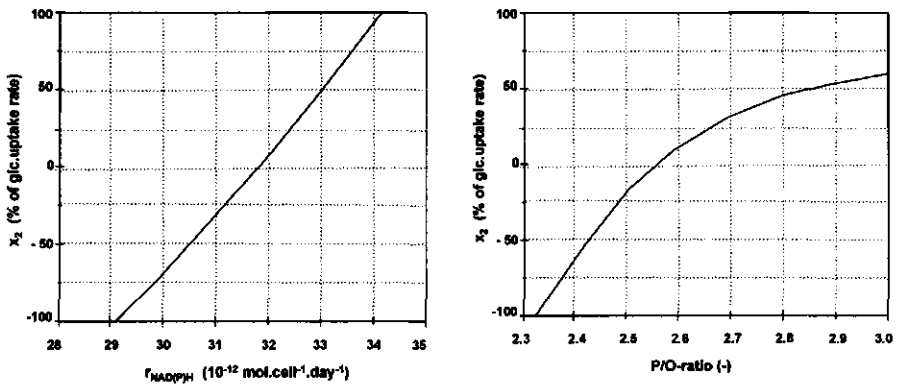

(A) (B)

Flux 2 (in % of glucose uptake rate) as a function of the P/O ratio (A) and the $r_{NAD(P)H}$ (B). Both sensitivity analyses were carried out using a metabolic network containing 17 fluxes (the pyruvate-carboxylase flux was assumed to be negligible) and 18 mass balances, including either the ATP (A) or NAD(P)H (B) mass balance. In both cases the network is nonsingular (Rank = 17). (In these calculations, flux 2 is assumed to be reversible.)

The flux distribution that is estimated using the NAD(P)H mass balance is considerably different from the one found using 1-^{13}C-glucose (See also Table 2). In continuously-cultured hybridoma cells, more than 75 % of NAD(P)H that is produced by the reactions shown in Table 2 is consumed during oxidative phosphorylation (Bonarius et al., 1996). The $r_{NAD(P)H}$ (Table 1) depends therefore largely on the oxygen uptake rate (OUR) measurement. Relatively small errors in this measurement may cause significant changes in the estimated flux distribution. In Figure 4B the estimated fraction of G6P that enters the pentose shunt is given as a function of $r_{NAD(P)H}$. In contrast to yeast or bacteria, for which the NAD(P)H balance can be used to determine the intracellular fluxes (Van Gulik and Heijnen, 1995), the accuracy with which the OUR can be measured is relatively small in low-density

mammalian-cell culture (Eyer et al., 1995) and under the conditions examined here, apperently not sufficient to estimate the metabolic fluxes.

(ii) Linear-optimization techniques

Instead of using the estimated NAD(P)H and ATP requirements as fixed values, the mass balances of these co-factors can be used to formulate objective functions for mammalian-cell metabolism (Fell and Small, 1986; Savinell and Palsson,1992). Flux distributions that are optimal with respect to these objective functions can subsequently be calculated by linear-optimization techniques. Table 1 shows some objective functions that reflect certain metabolic strategies with respect to energy metabolism. These objective functions are used here to estimate the fluxes 1-18. It is found in all cases that when a particular function (for example, maximize ATP) gives a feasible flux distribution, its opposite equivalent (minimize ATP) gives infinitely large fluxes. This is consistent with the solution plane shown in Figure 3 which is only finite on one particular side.

Table 1

Objective functions used to estimate fluxes 1-18. Each maximization problem has a "minimization counter-part" which is used as well.

Maximize ATP:	max $\{-x_8 + x_9 + x_{11} + x_{15} - x_{18}\}$
Maximize NADH:	max $\{x_9 + x_{12} + x_{14} + 2*x_{15} + x_{16}\}$
Maximize NADPH:	max $\{2*x_2 + x_{17}\}$
Maximize reducing equivalents:	max $\{2*x_2 + x_9 + x_{12} + x_{14} + 2*x_{15} + x_{16} + x_{17}\}$
Minimize norm	min $\{\Sigma x_i^2\}$

The following fluxes were assumed to be irreversible (≥ 0): x_2, x_{11}, x_{12}, x_{13}, x_{17}, and x_{18}.

Fluxes estimated using the minimum-norm constraint are considerably different from experimentally determined fluxes (Table 2). The suggestion that hybridoma cells have an efficient metabolism, and accordingly minimize the total flow of metabolites

(Bonarius et al., 1995a), seems therefore to be unlikely. In contrast, the flux distributions found using two other objective functions, i.e. maximize ATP and maximize NADH, are relatively similar to the distribution determined using 1-^{13}C-glucose (See also Table 2). This is consistent with the results obtained by Savinell

Table 2

Input vector **r** (metabolic rates) and various output vectors **x** (flux distribution). All values in 10^{-12} mol.cell^{-1}.day^{-1}. Metabolic rates are calculated as described elsewhere (Bonarius et al., 1998d). The same input vector (first column) is used to determine the bounds of the solution space (Figure 3) and to estimate the flux distribution using different constraints.

Input vector:		Output vectors:	Isotopic tracer	Min. norm constr.	Max. NADH
1. G6P	-6.647	1. G6P → F6P	5.18	-1.25	6.64
2. F6P	0.081	2. G6P → Ru5P + CO2 + 2 NADPH	1.55	8.04	0.0
3. Ru5P	0.0	3. Ru5P → X5P	1.10	5.50	0.55
4. X5P	0.0	4. Ru5P → R5P	0.54	2.66	0.39
5. R5P	0.117	5. X5P + R5P → S7P + GAP	0.68	2.96	0.28
6. S7P	0.0	6. X5P + E4P → F6P + GAP	0.50	2.67	0.28
7. E4P	0.0	7. S7P + GAP → F6P + E4P	0.62	2.85	0.28
8. GAP	0.126	8. F6P + ATP → 2 GAP	13.14	12.00	14.22
9. G3P	0.241	9. GAP → G3P/SER + NADH + ATP	13.50	12.00	14.37
10. PEP	0.0	10. G3P/SER → PEP	13.31	11.83	14.13
11. PYR	10.56	11. PEP → PYR + ATP	13.36	11.91	14.13
12. ACOA	-0.693	12. PYR → ACoA + NADH + CO2	3.72	1.38	3.03
13. MAL	-0.089	13. ACoA + OMA → CIT	4.45	2.12	5.79
14. CIT	-1.159	14. CIT → AKG + NADH + CO2	3.45	2.37	5.88
15. AKG[a]	-0.891	15. AKG → MAL + 2 NADH + ATP + CO2	4.45	1.33	4.73
16. OAA	0.361	16. MAL → OAA + NADH	4.73	2.38	5.61
17. CO2	11.40	17. MAL → PYR + CO2 + NADPH	0.30	0.54	0.54
18. NAD(P)H	30.54	18. PYR + ATP + CO2 → OAA	0.13	0.0	0.0
19. ATP	21.50				

(a) Glutamate feeds into the TCA cycle via α-ketoglutarate. The r_{AKG} is independent from the linear dependent reactions in glutaminolysis, and can be calculated without other constraints than the mass-balance equations. (b) r_{ATP} is determined using a P/O ratio of 2.0 and a m of 14.4*10^{-12} mol.cell^{-1}.day^{-1} (Martens et al., 1995, and references therein).

and Palsson (1992), who showed that hybridoma cells produce more ATP and NADH than the cells actually need. It appears that, similar to other cancer cells, hybridoma cells are metabolically hyperactive and consume nutrients regardless of energy requirements (Eigenbrodt et al., 1985). The biochemical strategy to maximize the ATP and NADH production, even in the case when these co-factors are sufficiently available, seems to be a realistic objective, which can be used to estimate metabolic fluxes in underdetermined networks describing hybridoma-cell metabolism.

ACKNOWLEDGEMENTS

H.P.J.B. acknowledges the Division of Biologics Development, (Novo Nordisk A/S, Gentofte, Denmark) for supporting the participation at the rDNA Biotechnology conference in Danvers, MA, at which this work was presented.

Chapter 7

Metabolic-Flux Analysis of Hybridoma Cells under Oxidative and Reductive Stress using Mass Balances and Physiologically Meaningful Constraints

Hendrik P.J. Bonarius, José H.M. Houtman,
Georg Schmid, Cornelis D. de Gooijer,
and Johannes Tramper

ABSTRACT

Hybridoma cells were grown at steady state under both reductive and oxidative stress and the intracellular fluxes were determined by mass-balancing techniques. By decreasing the dissolved oxygen pressure (pO_2) in the bioreactor, the reduced form of nicotinamide adenine nucleotide (NADH) was enhanced relative to the oxidized form (NAD^+). Oxidative stress, as a result of which the $NAD(P)^+$/NAD(P)H-ratio increases, was generated by both the enhancement of the pO_2 to 100 % air saturation and by the addition of the artificial electron acceptor phenazine methosulphate (PMS) to the culture medium. It was found that fluxes of dehydrogenase reactions by which NAD(P)H is *produced* decreased under hypoxic conditions, most likely to restore the disturbed $NAD(P)^+$/NAD(P)H balance. For example, the degradation rates of arginine, isoleucine, leucine, lysine and

the glutamate dehydrogenase flux were significantly lower at oxygen limitation, and increased at higher pO_2 levels and when PMS was added to the culture medium. In contrast, the proline synthesis reaction, which *requires* NADPH, decreased under PMS stress. The flux of the NADH-requiring lactate dehydrogenase reaction also strongly decreased from 19 to 3,4 pmol/cell/day, under oxygen limitation and under PMS stress, respectively.

Metabolic fluxes in cyclic pathways, such as the TCA cycle, the pentose and malate shunt were subsequently estimated by linear optimization techniques with appropriate objective functions, such as 'minimize NADH-producing reactions' or 'maximize NAD(P)H-producing reactions'. Although the estimated values were not in agreement with flux data determined by isotopic-tracer experiments, it is shown that various well-established physiological effects can be qualitatively estimated with this technique.

INTRODUCTION

The intracellular fluxes of microorganisms, animal cells or tissue culture can be determined if the extracellular production and uptake rates of the relevant metabolites and the reaction stoichiometry of fluxes are known (Vallino and Stephanopoulos, 1990). This methodology, referred to as 'metabolic-flux balancing' (Varma and Palsson, 1994) has been proposed as an alternative (or supplement) to isotopic-tracer studies for metabolic-flux analysis.

Although mass-balancing can be used to determine a large fraction of fluxes in metabolic networks, a number of pathways cannot be quantified due to the fact that the required set of linear mass-balance equations is underdetermined (Vallino and Stephanopoulos, 1990; Bonarius et al., 1997). This accounts in particular for linearly dependent reactions associated with cyclic metabolic pathways. Fluxes in cyclic pathways such as the TCA cycle, the pentose-phosphate shunt, or the malate shunt cannot be determined by measurement of the extracellular production and uptake rates of the relevant metabolites alone.

Additional constraints, usually obtained by isotopic-tracer experiments are required to solve underdetermined metabolic networks, and thus to quantify fluxes in cyclic pathways.
As an alternative to isotopic-tracer studies, which have practical limitations and are laborious to conduct, various 'theoretical constraints' have been proposed to supplement underdetermined metabolic networks. This approach has already been shown useful for many applications. For example, it was shown by linear-optimization techniques how fat synthesis constraints other metabolic pathways in adipose tissue (Fell and Small, 1986), and that the growth rate of hybridoma cells is neither limited by the ATP-maintenance demand nor by the antibody production rate (Savinell and Palsson, 1992). Metabolic-flux balances and linear optimization have also been used to determine capabilities of *Escherichia coli* for the biosynthesis of precursors (Varma and Palsson, 1993) and amino acids (Varma et al., 1993).

Metabolic-flux balancing has been used to analyse changes in intracellular flux distributions as a function of different culture conditions or differences in genotypes. Jørgensen and co-workers (1995) showed that the pentose-shunt activity in *Penicillium chrysogenum* decreases after addition of cysteine to the culture medium. Zupke and co-workers (1995) demonstrated using metabolite balances that the pyruvate-dehydrogenase flux decreases and the glutamate-dehydrogenase flux reverses in hybridoma cells cultured at low oxygen tension. We showed that the pentose-shunt activity in hybridoma cells increases after addition of a growth-stimulating hydrolysate (Bonarius et al., 1996), and that under ammonia stress hybridoma cells increase their glutamate-dehydrogenase flux, thus identifying glutamate dehydrogenase as a potential site for engineering ammonia-tolerant mammalian cells (Bonarius et al., 1998a). Sauer and co-workers (1996) estimated the pentose-shunt and TCA-cycle activity in both wild-type and riboflavin-producing *Bacillus subtilis* revealing an increase in the flux through the pentose-phosphate pathway in the strain engineered for riboflavin biosynthesis.

In all of the above-mentioned studies assumptions had to be made to estimate fluxes in linearly dependent (cyclic) subnetworks. Apart from some exceptions, many of the constraints used to estimate fluxes in metabolic pathways are a consequence of lack of information on the physiology of the organism under investigation. Only in some cases it is has been attempted to specify certain physiologically meaningful objectives. For example, the linear objective functions 'maximize the production of a certain metabolite' and 'maximize biomass synthesis' have been shown useful for analysis of metabolic capabilities and for the estimation of optimal growth patterns in *Escherichia coli*, respectively (Varma and Palsson, 1993). In contrast to constraints that are based on the principle of natural strive for optimality, such as optimal growth, other limitations imposed by culture conditions may also constrain the entire cellular physiology. For example, Fell and Small (1986) recognized the fact that adipose cells require relatively large amounts of NADPH for fatty acid synthesis and used the objective function 'maximize NADPH-producing reactions' as an additional constraint to estimate fluxes in these cells. Here, we apply this principle to continuously cultured hybridoma cells under different types of stress. Hybridoma cells are cultured under conditions that effect the availability of the electron carriers NAD and NADP. It shown for those metabolic fluxes that can be determined by mass-balancing techniques alone (that is, without additional constraints or assumptions), that NAD(P)H-producing reactions are activated under oxidative stress, and that the opposite occurs under reductive stress. These results suggest that physiologically meaningful constraints, such as 'minimize or maximize NAD(P)H-producing reactions' can be used to complement the underdetermined networks associated with cyclic pathways for the determination of the remaining metabolic fluxes of stressed hybridoma cells. Fluxes in cyclic pathways of stressed hybridomas are estimated by this technique and subsequently compared to data that have been obtained by isotopic-tracer techniques.

MATERIALS AND METHODS

Culture conditions and analyses

A detailed description of the various experimental procedures was published before (Bonarius et al., 1996). Briefly, hybridoma cells were cultured in a lab-scale bioreactor (Biostat MD, Braun, Melsungen, D) in a continuous mode at a dilution rate of 0.7 d^{-1}. A mixture of Dulbecco's, Ham's F12 and Iscove's powdered medium (Gibco, Grand Island, NY, USA) was supplemented with 5 µg/ml insulin (Sigma, St. Louis, MO, USA), 6µg/ml transferrin (Boehringer Mannheim, Mannheim, D), 0.35 % (w/v) Syperonic F68 (Serva, Heidelberg, FRG) and 1 % (w/v) Primatone RL (Sheffield Products, NY, USA). The medium contained 5.0 g/l glucose and 2.73 g/l sodium bicarbonate. PMS (Phenazine methosulphate, Sigma, St. Louis, MO, USA) was added at a concentration of $2*10^{-6}$ M.

A method developed to correct for the bicarbonate buffer in the culture medium (Bonarius et al., 1995) was applied for the determination of the CO_2 production rate (CER). The CO_2 in the outlet gas was measured by an infrared gas analyzer (Rosemount, Baar, CH). The O_2 uptake rate (OUR) was determined by the mass transfer coefficient $k_l^{O2}a$ and the fraction of oxygen in the inlet gas, as described before. Values for $k_l^{O2}a$ were determined by the dynamic method (Van 't Riet and Tramper, 1991).

Glucose and lactate were determined with automated enzymatic assays (YSI, Yellow Springs, OH), ammonia using an ion-selective electrode, and amino acids by HPLC (Amino Quant 1090, Hewlett-Packard, Paola Alto, CA, USA). Intracellular amino-acid pools were extracted by perchloric acid as described elsewhere (Schmid and Keller, 1992). The cellular composition was measured as described by Xie and Wang (1994): the total lipid fraction was determined by weight after chloroform/methanol extraction, total carbohydrates were analyzed by the phenol-reaction method, total cellular protein was estimated using the Biuret assay, and nucleic acids were quantitated by absorbance at 260 nm after

purification according to Chomczynski (1993). Cell size and number were determined using a Casy 1 instrument (Schärfe System, Reutlingen, D) and dry-cell weight was determined after dehydration under vacuum. Antibody titers were measured by a standard ELISA.

Metabolic-Flux Analysis

A model of the relevant pathways of hybridoma-cell metabolism is shown in Figure 1. Most of the fluxes in this model can be determined by mass-balancing techniques alone. Additional information is required for the quantification of fluxes in cyclic pathways. In Figure 1, these fluxes are indicated by solid arrows. It was previously shown that this 'underdetermined' metabolic subnetwork contains three sets of linearly dependent fluxes (Bonarius, et al. 1998b):
(i) the malate/pyruvate/oxaloacetate cycle (fluxes 16, 17 and 18),
(ii) glutamine degradation (fluxes 23, 24, and 25), and
(iii) the pentose shunt, glycolysis and TCA cycle (fluxes 1 to 16).
Therefore, three additional constraints are required to determine all fluxes by mass-balancing techniques alone:

(i) It was found by ^{13}C-NMR experiments that the flow through pyruvate carboxylase (flux 18) is negligible in hybridoma cells cultured in a hollow-fiber bioreactor (Mancuso et al., 1994). This was recently confirmed for the same hybridoma cell line, the same medium, and the same mode of cultivation as investigated here, by ^{1}H-NMR spectrometry analysis of 3-C-lactate (Bonarius et al., 1998c).

(ii) Although no direct evidence for hybridoma cells exists, it is assumed that the flow through asparagine synthetase (flux 23) is negligible. Street et al. (1993) could not detect labeled asparagine in the medium supernatant of 5-^{15}N-glutamine-fed HeLa and CHO cells, indicating that asparagine synthetase is not active. In cultured mammalian cells, the proposed pathway of glutamine degradation is via glutaminase, rather than via asparagine synthetase (For example: Reitzer et al., 1979, Ardawi and Newsholme, 1984, Mancuso et al.,

1994). Only when asparagine becomes limiting, asparagine synthetase may become active in mammalian cells (Kilberg et al., 1994).

(iii) Recently, we determined the pentose-phosphate shunt flux of continuously cultured hybridoma cells from $^{13}CO_2$ yields measured by mass spectrometry (Bonarius et al., 1998c). In contrast to the data of Mancuso and co-workers (1994), who showed that hybridoma cells cultured in hollow-fiber bioreactors direct only 5 % of the consumed glucose into the pentose shunt, up to 23 % of the glucose was channeled into the pentose shunt in rapidly growing cells ($\mu = 0.9$ day^{-1}) in continuous culture. Here, dependent on the particular culture conditions, different techniques are used to estimate the (linear

Figure 1

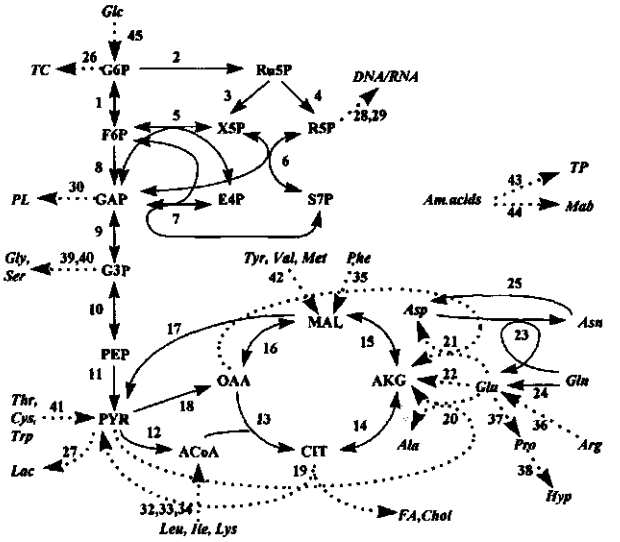

Network of mammalian-cell metabolism. Fluxes that can be quantified by mass balances alone are indicated as dashed lines. To measure the remaining fluxes (solid lines) additional constraints are required.

dependent) set of fluxes of the glycolytic and pentose-phosphate pathway (fluxes 1-16):

(A) For standard conditions, the flux ratio at the glucose-6-phosphate branchpoint is fitted to the flux distribution measured using isotopic-tracer techniques under the same standard conditions (Bonarius et al., 1998c). The

flux through the oxidative branch of the pentose shunt (flux 2) is assumed to be linearly dependent on the biomass requirements.

(B) For hybridoma cells it has been shown that both the mitochondrial and the cytosolic NAD^+/NADH ratios are relatively low under oxygen-limited conditions (Zupke et al., 1995). It is hypothesized here that under these conditions there will be less carbon channeled through fluxes catalyzed by NADH-producing dehydrogenases to restore the perturbed NAD^+/NADH balance. This metabolic strategy is simulated by applying the objective function 'minimize NADH-producing reactions'.

(C) In contrast to inhibiting NAD(P)H-producing reactions, these reactions can specifically be activated by using the oxidizing agent phenazine methosulfate (PMS) (Dickens and McIlwain, 1938). It has been established that the pentose- (fluxes 2-7) and the malic-shunt (flux 17) activity increase strongly by incubating cells or tissue with an artificial electron acceptor, such as PMS, (Greenbaum et al., 1971, Hothershall et al., 1979, Lin et al., 1993). The metabolic fluxes of hybridoma cells in PMS-containing medium are estimated using the linear objective function 'maximize NADH- and NADPH-producing reactions'.

(D) The fraction of the consumed glucose that enters the pentose-phosphate pathway is also compared to values obtained by isotopic-tracer methods. The pentose-shunt flux has been determined experimentally for lymphoblasts under PMS stress (Lin et al., 1993), and for hybridoma cells under different pO_2 levels (Jan et al., 1997; Bonarius et al., 1998c). Because these experimental data were obtained for different cell lines and different culture conditions, they are used for a qualitative comparison. Only the flux data from Bonarius et al. (1998c) have been measured for the same cell line and culture medium, however at a 100 ml-scale instead of a 1-L scale such as described here.

RESULTS AND DISCUSSION

Cell density

Hybridoma cells were cultivated in a continuous stirred-tank reactor at different oxygen concentrations. In addition, one experiment was conducted with the artificial electron acceptor PMS in the culture medium. Each time after changing to new culture conditions at least four days of continuous culture were used to dilute metabolites produced during the previous steady state and to

Table 1

Average viable-cell density (10^6 cells/ml) and average uptake and production rates of indicated metabolites (10^{-12} mol.cell^{-1}.day^{-1}) under different conditions. Values between parentheses indicate standard deviations.

pO_2	0.1 %	1.0 %	30 %	50 %	100 %	30 %/PMS
Viable cell density	1.16 (0.14)	1.78 (0.05)	1.46 (0.03)	1.58 (0.06)	1.47 (0.08)	1.30 (0.10)
Glucose uptake	12.3 (0.13)	7.27 (0.43)	6.34 (0.35)	5.37 (0.22)	5.82 (0.17)	4.02 (0.61)
Lactate production	19.1 (1.61)	10.7 (0.82)	7.48 (0.64)	5.27 (0.67)	7.03 (0.45)	3.43 (0.21)
$Y_{LAC/GLC}$	1.56	1.48	1.18	0.98	1.21	0.86
Glutamine uptake	2.02 (0.20)	1.40 (0.05)	1.52 (0.05)	1.62 (0.21)	1.90 (0.08)	1.03 (0.15)
Alanine production	1.15 (0.06)	0.77 (0.02)	1.23 (0.04)	0.98 (0.15)	1.23 (0.04)	1.36 (0.01)
Ammonia production	0.88 (0.13)	0.75 (0.05)	1.22 (0.11)	0.72 (0.14)	1.07 (0.12)	1.42 (0.09)
Specific Mab production (pg.cell^{-1}.day^{-1})	14.3 (1.25)	13.5 (0.59)	17.0 (0.49)	13.8 (0.61)	14.2 (0.13)	21.7 (2.05)

allow the viable-cell density to stabilize. Unless stated otherwise, each value presented below is an average of three data points, obtained by daily sampling during three days at steady-state conditions. The viable-cell and viability numbers of the entire experiment are shown in Figure 2 in an accompanying paper (Bonarius et al., 1998e).

Table 1 shows the average viable-cell densities, the average glucose and glutamine uptake rates and the average lactate, alanine, ammonia, and monoclonal antibody (Mab) production rates. Only at pO_2 of $\approx$ 0.1 %, the culture is oxygen limited and the cell density is significantly lower than cell densities at other oxygen tensions. Similar to data reported by Zupke et al. (1995), at low, albeit non-limiting oxygen tension (pO_2 = 1.0 %), the cell density is higher than at higher oxygen tensions. The reason for this is not clear.

PMS, an artificial electron acceptor which diffuses passively through cellular membranes (Hothershall et al., 1979) is toxic for mammalian cells. Sub-lethal concentrations have been found in the order of 10^{-4} M for fibroblasts (Lin et al., 1993) and in the 10^{-6} M range for glioma cells (Mitchell et al., 1989). In order to determine an effective but sub-lethal PMS concentration for hybridoma cells, T-flask experiments were conducted. Figure 2 shows that PMS is toxic above

Figure 2

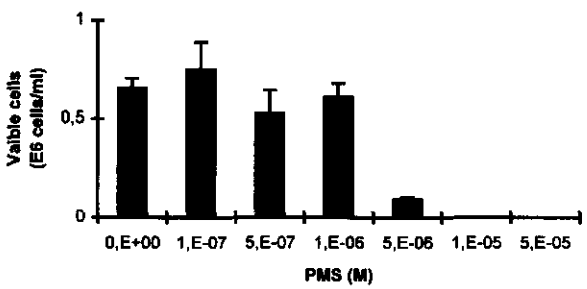

Viable-cell densities at different concentrations of PMS after two days of cultivation. Averages for two T-flask experiments are shown.

$5*10^{-6}$ M for hybridoma cells. Continuous-culture experiments are therefore conducted at a concentration of $2*10^{-6}$ M PMS. In Table 1 it is shown that the viable cell density is slightly lower at this concentration during this steady state ($1.30*10^{6}$ vs $1.46*10^{6}$ cells/ml, respectively).

Metabolic production and consumption rates

The extracellular production and consumption rates of amino acids, glucose, ammonia, lactate, oxygen, carbon dioxide and monoclonal antibody were determined. Also, the intracellular concentrations of amino acids, lactate, total cell protein, DNA, RNA, and the total lipid and carbohydrate contents were measured. Only a limited amount of the measured data are shown here in Tables 1-3 and in Figures 3-5. Complete tables with raw data are published in an

Table 2

Estimated fluxes (10^{-12} mol.cell^{-1}.day^{-1}) using metabolite balances and different theoretical constraints; pentose shunt fitted to biomass-synthesis rate (A), minimize NADH production (B), and maximize NAD(P)H production (C).

pO_2	0.1 %	1.0 %	30 %	50 %	100 %	PMS
Constraint	B	A	A	A	A	C
Oxidative branch pentose shunt (x_2)	7.11	1.63	1.76	1.81	1.65	5.61
Glycoclysis (x_8)	18.1	12.6	10.6	8.59	9.58	5.98
Pyruvate dehydrogenase (x_{12})	0.0	0.76	1.54	1.90	1.12	1.28
α-Ketoglutarate dehydrogenase (x_{15})	0.21	0.17	1.37	1.54	0.85	2.76
Isocitrate dehydrogenase (x_{16})	0.30	1.43	2.85	2.94	2.29	2.25
Malic enzyme (x_{17})	0.11	-0.04	0.06	0.05	0.10	0.14
Glutamate dehydrogenase (x_{22})[a]	-0.53	-0.31	-0.11	-0.17	-0.11	0.03
Lactate dehydrogenase (x_{27})[a]	19.1	10.7	7.48	5.27	7.03	3.43

[a] The value of the glutamate-dehydrogenase and the lactate-dehydrogenase flux is not influenced by any of the constraints A, B, or C, as it can determined by strictly using metabolite balances (See also Figure 1).

accompanying paper (Bonarius et al., 1998e), where it is demonstrated that the carbon and nitrogen balance over all metabolic rates are closed.

Glucose consumption and lactate production

It has been established that the specific glucose consumption and lactate production increase at low pO_2 levels (below ca. 10 % of air saturation) (Miller et al., 1987; Ozturk and Palsson, 1990; Zupke, et al., 1995). The data shown in Table 1 and Figure 3a are in agreement with these observations. In particular at oxygen-limiting conditions ($pO_2 \approx 0.1$ %) the glucose uptake and lactate production rate increase strikingly, as animal cells change from 'complete' oxidation of glucose to CO_2 to anaerobic glycolysis. The addition of PMS has an opposite effect on glucose metabolism: the glucose uptake decreases. In addition, the lactate yield per glucose decreases due to the artificial electron acceptor (Table 1), which is the consequence of competition between lactate dehydrogenase and PMS for NADH. Together, these two effects cause a decrease in the specific lactate production rate of more than 50 % compared to the control culture (pO_2 =30 %). This suggests that addition of PMS can be used to decrease lactate formation in mammalian-cell culture without affecting cell density, which may become significant for high-cell density cultures, where lactate inhibition constraints further cell growth. An additional beneficial effect of PMS is the increase in specific monoclonal-antibody production. Table 1 shows that the Mab production increases 27 % compared to the control culture.

In contrast to normal proliferating cells, which regulate glycolysis dependent on the requirement for ATP according to the Pasteur effect (Eigenbrodt et al., 1985), the glycolysis activity of tumor cells is insensitive to high concentrations of oxygen (Caroll et al., 1978; Simon et al., 1981). In Figure 3a it is shown that this also accounts for hybridoma cells.

Figure 3

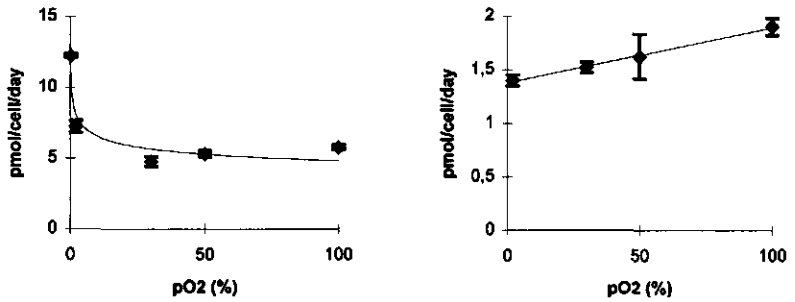

(A) (B)

Specific glucose (A) and glutamine (B) uptake rate (pmol.cell^{-1}.day^{-1}) of continuously cultured hybridoma cells as a function oxygen tension (% of air saturation). At oxygen limitation (pO_2 ≈ 0.1 %) the glutamine uptake increases to 2.02 pmol/cell/day (not shown in Figure B).

Oxidative degradation of amino acids

In mammalian-cell metabolism, a number of amino acids are not only used as building blocks for biomass, but also as fuel (Stryer, 1988). Other amino acids, such as glycine, proline, or alanine are produced by most continuous mammalian cell lines (Lanks and Li, 1988). Fluxes of amino-acid degradation and production pathways are determinable by mass-balancing techniques (Xie and Wang, 1996; Bonarius et al., 1996; Vriezen, 1998). Flux analysis of amino-acid metabolism is therefore an appropriate tool to test the hypothesis that under hypoxic conditions, when the NAD(P)$^+$/NAD(P)H-ratio is low (Zupke et al., 1995), steady state fluxes by which NAD(P)H are produced, *decrease* to restore NAD(P)$^+$ levels. At high pO_2 levels or during PMS-stress, the opposite may occur; steady state fluxes of reactions in which NAD(P)H is produced *increase* to regenerate NAD(P)H. The "net-catabolic rate of amino acid A" ($r_{nc,A}$) (Bonarius et al., 1996) is a measure for the conversion rate of amino acids corrected for biosynthesis requirements, and is used here to test this hypothesis. The $r_{nc,A}$ is determined from the consumption rate, the biomass synthesis rate (including Mab synthesis) and the fraction of each amino acid in biomass. A

negative value for $r_{nc,A}$ indicates that A is degraded, while a positive value indicates that A is produced.

In Table 3 the net catabolic rates of amino acids are shown for 6 different culture conditions. It appears that arginine, leucine, lysine, isoleucine, methionine, and cysteine are degraded at relatively high rates (~ 10^{-13}mol.cell^{-1}.day^{-1}). The net stoichiometric equations of the oxidative degradation of these amino acids are given in Table 4. During oxidation of arginine, (iso)leucine and

Table 3

Net catabolic rates of amino acids of continuous-cultured hybridoma cells at different dissolved oxygen concentration. pO_2 in % of air saturation, net catabolic rates in mol.cell^{-1}.day^{-1}. PMS indicates steady state with Phenazine Methosulfate ($2*10^{-6}$ M) in the culture medium. A negative value indicates that the amino acid is degraded. Amino acids are given in order of chromatographic separation.

PO_2	0,1 %	1 %	30 %	50 %	100 %	PMS
ASP	2,04E-13	1,65E-13	6,80E-14	1,65E-13	1,35E-13	2,07E-13
GLU	1,97E-13	1,54E-13	3,23E-14	1,94E-13	1,83E-13	2,16E-13
ASN	3,93E-14	3,06E-14	1,09E-13	2,61E-14	4,01E-14	1,33E-14
SER	8,29E-14	8,66E-14	2,08E-13	1,97E-13	2,26E-13	3,39E-13
GLN	-1,80E-12	-1,19E-12	-1,28E-12	-1,39E-12	-1,69E-12	-1,85E-12
HIS	-2,73E-14	-1,79E-14	-2,05E-14	-2,59E-14	-3,82E-14	-2,23E-14
GLY	1,16E-13	1,23E-13	1,38E-13	1,41E-13	1,23E-13	1,49E-13
THR	2,96E-14	4,46E-14	3,17E-14	4,12E-14	1,15E-14	2,22E-14
ALA	1,41E-12	1,07E-12	1,56E-12	1,30E-12	1,40E-12	1,73E-12
ARG	-2,64E-14	-1,87E-14	-8,46E-14	-2,37E-14	-4,67E-14	-1,17E-13
TYR	-2,90E-14	-1,96E-14	-2,39E-14	-2,04E-14	-3,16E-14	-3,14E-14
CYS	-1,10E-13	-6,43E-14	-7,16E-14	-6,17E-14	-7,30E-14	-8,55E-14
VAL	3,13E-14	3,12E-14	-4,20E-15	5,42E-15	-3,50E-14	-1,17E-14
MET	-6,71E-14	-5,45E-14	-6,35E-14	-6,44E-14	-7,79E-14	-9,36E-14
TRP	5,86E-16	-3,29E-15	-1,10E-14	-3,13E-15	6,84E-15	-1,86E-14
PHE	-6,08E-15	1,17E-16	3,48E-15	7,08E-16	-4,24E-15	-2,49E-14
ILE	-1,18E-13	-1,19E-13	-2,62E-13	-2,00E-13	-2,10E-13	-2,99E-13
LEU	-1,79E-13	-1,81E-13	-4,08E-13	-3,17E-13	-3,56E-13	-4,83E-13
LYS	-5,28E-14	-5,23E-14	-9,30E-14	-7,04E-14	-1,04E-13	-1,27E-13
PRO	3,41E-13	3,20E-13	2,34E-13	2,83E-13	2,80E-13	6,71E-14
HYP	3,04E-13	2,12E-13	2,53E-13	2,44E-13	2,54E-13	3,45E-13

Figure 4a

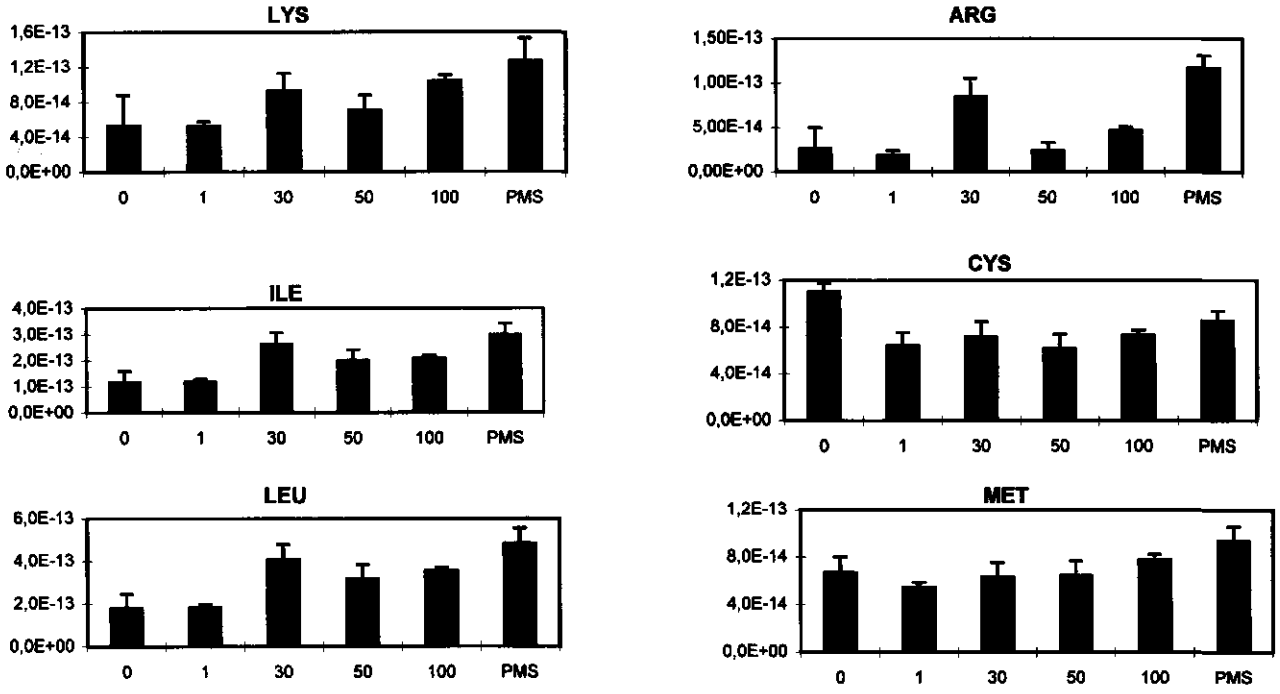

Degradation rates of lysine, isoleucine, leucine, arginine, cysteine, and methionine for 6 different steady states. Values are shown as absolute values of net catabolic rates, given in $mol.cell^{-1}.day^{-1}$, and are averages from 3 data points during each steady states. Standard deviations are shown as T-bars.

methionine, $NAD(P)^+$ is reduced to NAD(P)H. This is not the case for degradation of cysteine. Figure 4a shows the average values of the measured degradation rates of these amino acids, together with their standard deviations. At oxygen limitation ("0") and low pO_2 ("1") the steady state flux at which leucine, lysine, and isoleucine are catabolized are significantly lower than under standard conditions (30% or 50 % of air saturation). When the artificial electron acceptor PMS is added to the culture medium, the fluxes increase, which is particularly the case for lysine and arginine degradation. Methionine and arginine degradation increase slightly at higher pO_2 levels, but the differences are not as significant as for (iso)leucine and lysine. This may be a consequence of the fact that more oxidative power, that is more moles of NAD^+ per mole amino acid, is required for the degradation of (iso)leucine and lysine than for the degradation of methionine and arginine (See also Appendix A). In contrast to (iso)leucine, lysine, arginine and methionine, the degradation of cysteine does not require NAD^+. Figure 4a shows that the cysteine degradation rate does not increase at higher pO_2 and only slightly under PMS-stress.

Biosynthesis of proline, glycine, and serine

The "net catabolic rates" of proline, glycine, and serine are non-negative (Table 3), which indicates that these metabolites are produced from other amino acids in hybridoma cells. Figure 4b shows the average values of the measured production rates of these amino acids together with their standard deviations for 6 steady states. The serine production, which is dependent on the availability of NAD^+, is relatively low under oxygen limitation and low pO_2, which is consistent with the low NAD^+/NADH ratios under these conditions (Zupke and co-workers (1995)). It appears that the steady state proline-synthesis flux is independent of pO_2. This may be explained by the fact that in the proline synthesis pathway no NAD^+/NADH is co-metabolized. Instead, proline synthesis requires two moles of NADPH per one mole produced proline. When hybridoma cells are grown in medium supplemented with PMS, which oxidizes NADPH, the proline production decreases more than 3-fold.

Figure 4b

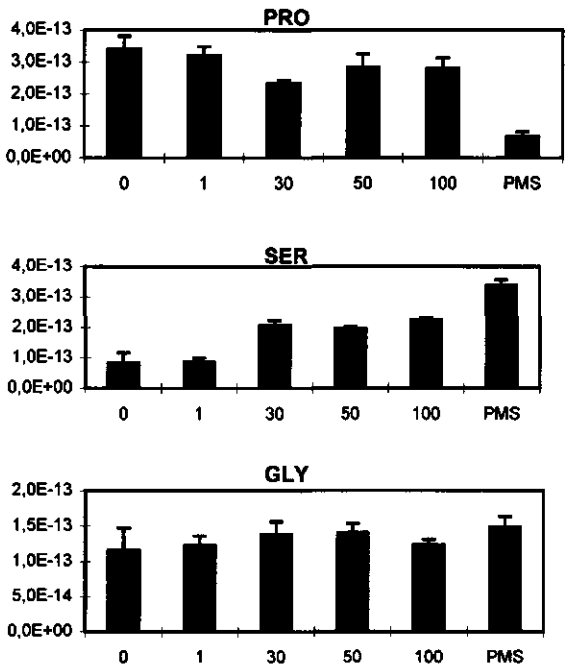

Net production rates of proline, serine, and glycine for 6 different steady states. Values are given as in mol.cell^{-1}.day^{-1} and are averages from 3 data points during each steady states. Standard deviations are shown as T-bars.

Glutamate dehydrogenase

Glutamate dehydrogenase (flux 22, Figure 1) catalyses the following oxidative deamination reaction:

$$\underset{}{\text{glutamate} + \underset{(\text{or NADP}^+)}{\text{NAD}^+} + \text{H}_2\text{O}} \Leftrightarrow \underset{}{\alpha\text{-ketoglutarate} + \text{NH}_4^+ + \underset{(\text{or NADPH})}{\text{NADH}} + \text{H}^+}$$

In contrast to fluxes in linearly dependent subnetworks, which require additional constraints for their quantification, flux 22 can be determined on the basis of mass-balance equations alone. Its value is therefore not influenced by any of the constraints A, B, or C mentioned in the Materials and Methods Section. Recently, we showed that glutamate dehydrogenase is activated in the

direction of α-ketoglutarate to glutamate in ammonia-stressed hybridoma cells (Bonarius et al., 1998a). Here it is shown that, in agreement with data reported by Zupke et al. (1995), also at lower oxygen tensions the glutamate-dehydrogenase flux reverses into the glutamate-producing direction (Table 2). The opposite is the case in PMS-stressed hybridoma cells: the glutamate-dehydrogenase flux increases towards the direction of α-ketoglutarate and NAD(P)H. This observation is similar to the stimulating effect of PMS on other NAD(P)H-producing fluxes such as the pentose- and malate-shunt flux (Greenbaum et al., 1971), the serine synthesis flux (Figure 4b) and the (iso)leucine degradation flux (Figure 4a).

Glutaminolysis and pyruvate oxidation

Similar to data reported by Miller et al. (1987) and Jan et al. (1997), the glutamine uptake decreases at lower oxygen levels (Figure 3b), probably because there is not sufficient oxygen available for complete glutamine oxidation. At oxygen-limiting conditions ($pO_2 \approx 0.1$ %) however, the glutamine uptake increases (Table 1). This may be explained by the fact that oxygen-limited hybridoma cells have to rely on glutaminolysis for energy production. Hornsby and Gill (1981) showed that when cells suffer a block in pyruvate oxidation, which was selectively achieved by cortisol treatment, the glutaminolysis activity increased (Eigenbrodt et al, 1985). This is in agreement with flux data shown in Table 2, and with flux data reported by Zupke et al. (1995). Both these results show that the pyruvate dehydrogenase is significantly smaller during oxygen limitation. Investigations with adrenocortical cells showed that the decrease in pyruvate oxidation and the simultaneous increase in glutamine respiration is not only associated with inhibition of pyruvate dehydrogenase, but also with a lower isocitrate-dehydrogenase flux (Hornsby and Gill, 1981). The same trend is found here for oxygen-limited hybridoma cells (Table 2). Other support for the low pyruvate- and isocitrate-dehydrogenase activity at low oxygen tension comes from the analysis of intracellular isocitrate and pyruvate pools, which were found to be significantly lower at low pO_2 (Zupke et al., 1995).

Pentose-phosphate pathway

Table 2 shows the estimated values of fluxes through NAD(P)H producing and consuming reactions. It has been shown before that the pentose-shunt flux (Flux 2, Figure 1) is sensitive to differences in the used theoretical constraint (Sauer et al., 1996; Bonarius et al., 1998b; Schmidt et al., 1998). Figure 5 shows the pentose-phosphate-shunt flux values (PPS) estimated by three different theoretical constraints for all investigated conditions. In addition, values obtained by isotopic-tracer experiments are shown. In all cases the relative PPS activity is estimated to be smaller at low oxygen tensions (pO_2 = 0 % and 1 %) and higher in PMS-containing culture medium compared to standard conditions (pO_2 = 30 % or 50 %). When the pentose-shunt flux is directly related to the rate of biomass synthesis (Constraint A) the estimated values using mass balances are relatively similar to fluxes determined by isotopic-tracer experiments. This is not surprising, as this constraint is a fit of

Figure 5

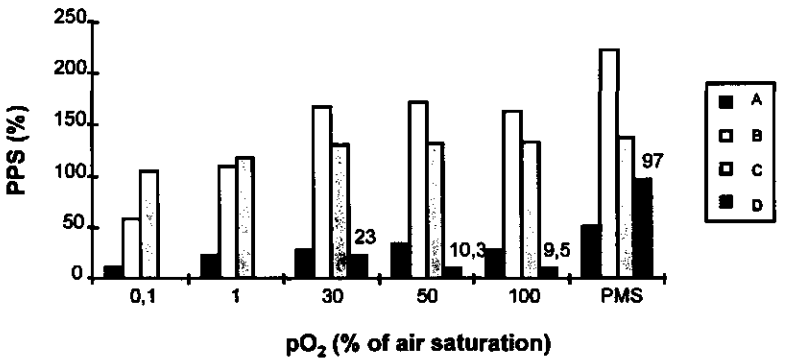

The flux through the oxidative branch of the pentose-phosphate shunt given as percentage of the glucose consumption. Values are estimated using different constraints: (A) linearized to biomass synthesis; (B) minimize NADH production; (C) maximize NAD(P)H production; (D, value added as label) determined by isotopic-tracer experiments. The experimentally-determined values (D) have been obtained from Bonarius et al., 1998d (pO_2 = 30 %); Jan et al., 1997 (pO_2 50 % and 100 %) and Lin et al., 1993 (PMS).

the experimentally obtained value to the biomass synthesis rate. It is noteworthy however, that the value for PMS-stressed cells is relatively high compared to the estimated values for the other culture conditions. This suggests that the well-established effect of PMS on the pentose-shunt activity is qualitatively measurable using mass-balancing techniques, even if the set of mass-balance equations is underdetermined.

The estimations of the pentose-shunt flux on the basis of linear objective functions (Constraints B and C) show overestimated values compared to the experimentally-determined fluxes (Figure 5). The objective function 'maximize NAD(P)H production' results in a particularly high value for the pentose-shunt flux of PMS-stressed cells. The trend is in agreement with the known effect of PMS (Hothershall et al. 1979), but the absolute value of flux 2 is significantly higher than the experiments of Lin and co-workers (1993) demonstrate. The overestimation is most likely a consequence of the fact that the linear optimization problem is not sufficiently constrained. There are only minimum values for a number of fluxes in the linear optimization problem (fluxes 2, 11, 12, 13, 17, and 18 in Figure 1). It has been shown before that the maximum value of the pentose-shunt flux in the linear-optimization problem is constrained by the irreversibility of pyruvate decarboxylase (flux 12) (Bonarius et al., 1998b). The solution suggests that the pentose-shunt flux is larger than the hexokinase flux (flux 45 in Figure 1). Indeed, when more NADPH is required than ribose-5-phosphate, glucose-6-phsophate is completely oxidized to CO_2 (Stryer, 1988), which means that flux 2 is larger than flux 45. Such conditions are artificially created with PMS in the culture medium. The cells have to regenerate therefore relatively large amounts of NADPH. However, according to Lin et al. (1993), this seems not be to the extent as estimated by linear programming techniques. For quantitative pentose-shunt flux data, isotopic-tracer experiments remain therefore indispensable.

CONCLUSIONS

The (steady-state) degradation rates of lysine, leucine, isoleucine, methionine, and arginine of hybridoma cells increase at higher pO_2 levels and under PMS stress. The proline synthesis flux decreases 3-fold in PMS-containing medium, and the serine production rate increases under oxidative stress.

Sub-lethal levels of the artificial electron acceptor PMS give 50 % lower lactate-production rates and 27 % higher Mab-production rates compared to the control in hybridoma-cell culture.

Under oxidative stress, the glutamate-dehydrogenase flux into the direction of α-ketoglutarate, and NH_4^+ increases. In contrast, under oxygen-limiting conditions the glutamate-dehydrogenase flux reverses into the direction of glutamate.

Physiologically meaningful objective functions can be added to underdetermined metabolic networks in order to estimate fluxes in cyclic pathways. Relative changes in metabolic fluxes, such as the decrease of the TCA flux under oxygen limitation or the increase of the pentose-shunt flux under PMS stress, can be detected with this technique. However, for quantitative values of fluxes in cyclic pathways, isotopic-tracer experiments remain indispensable.

APPENDIX A

Table A1

Net stoichiometric equations of amino acid metabolism (Only the reactions of amino acids that are discussed in the text are shown).

Amino acids that are degraded in hybridoma cells

Arginine	$ARG + 2\ H_2O + AKG + NAD^+ \rightarrow 2\ GLU + Urea + NADH$
Lysine	$LYS + H_2O + 3\ NAD^+ + 2\ FAD + 2\ AKG \rightarrow$ $ACoA + NH_3 + 2\ FADH_2 + 3\ NADH + 2\ GLU + 2\ CO_2$
Leucine	$LEU + AKG + 2H_2O + ATP + CoASH + NAD^+ + FAD \rightarrow$ $GLU + ADP + POH + ACoA + NADH + FADH + AAA$
Isoleucine	$ILE + AKG + 2H_2O + ATP + 2\ CoASH + 2\ NAD^+ + FAD \rightarrow$ $GLU + SuCoA + ADP + POH + ACoA + 2\ NADH + FADH$
Methionine	$MET + SER + CoASH + H_2O + NAD^+ + ATP + THF \rightarrow$ $CYS + SuCoA + methylene\text{-}THF + NH_3 + NADH + ADP + POH$
Cysteine	$CYS + AKG \rightarrow GLU + S + PYR$

Amino acids that are produced by hybridoma cells

Proline	$GLU + ATP + 2\ NADPH \rightarrow PRO + H_2O + ADP + POH + 2\ NADP^+$
Glycine	$SER + THF \rightarrow GLY + methyl\text{-}THF + H_2O$
Serine	$GLU + H_2O + 3PG + NAD^+ \rightarrow SER + AKG + POH + NADH$

Chapter 8

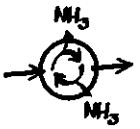

The Activity of Glutamate Dehydrogenase is Increased in Ammonia-Stressed Hybridoma Cells

Hendrik P.J. Bonarius, José H.M. Houtman,
Cornelis D. De Gooijer, Johannes Tramper,
and Georg Schmid

ABSTRACT

The effect of added ammonia on the intracellular fluxes in hybridoma cells was investigated by metabolic-flux balancing techniques. It was found that in ammonia-stressed hybridoma cells, the glutamate-dehydrogenase flux is in the reverse direction compared to control cells. This demonstrates that hybridoma cells are able to prevent the accumulation of ammonia by converting ammonia and α-ketoglutarate into glutamate. The additional glutamate that is produced by this flux, as compared to the control culture, is converted by the reactions catalyzed by alanine aminotransferase (45 % of the extra glutamate) and aspartate aminotransferase (37 %)., and small amount is used for the biosynthesis of proline (6 %) . The remaining 12 % of the extra glutamate is secreted into the culture medium. The data suggest that glutamate dehydrogenase is a potential target for metabolic engineering to prevent ammonia accumulation in high-cell-density culture.

INTRODUCTION

Amino acids, and glutamine in particular, are both used for biomass synthesis and energy generation in cultured mammalian cells (Reitzer et al., 1979). In contrast to normal proliferating tissue, that secretes its waste products from nitrogen metabolism in the form of urea, many tumor cell lines lack carbamyl phosphate synthase as a result of which they cannot synthesize urea (Eigenbrodt et al., 1985). Most of the cultured mammalian cells produce other nitrogen-sinks, such as alanine, aspartate, proline, glutamate and ammonia. These end products accumulate both intracellularly and in the culture medium (Lanks and Li, 1988).

Ammonia, the sum of non-ionized NH_3 and ionized NH_4^+, has various adverse effects on cultured mammalian cells as it inhibits cell growth and glycoprotein production (Glacken et al., 1986). It has been shown in many studies that ammonia inhibits cell growth (reviewed by Schneider, et al. 1996) and as a consequence, it can be the limiting factor for growth in high-cell-density cultures. In addition, ammonia influences glycosylation of (heterologuous) proteins (Anderson and Goochee, 1995), as a result of increased intracellular UDP aminohexoses (Ryll et al., 1994). Therefore, ammonia production and the metabolism of amino acids, in particular of glutamine, have received considerable attention in order to improve conditions for mammalian-cell culture used for the production of glycoproteins (Schneider et al., 1996). Several strategies have been proposed to overcome ammonia accumulation by manipulating mammalian-cell metabolism. These include substitution of glutamine by other nutrients such as glutamate (Darnell and Eagle, 1958), asparagine (Kurano et al., 1990) or α-ketoglutarate (Hassell and Butler, 1990), controlled addition of glutamine (Glacken et al., 1986; Ljunggren and Häggström, 1984), adaptation of cells to high ammonia concentrations (Schumpp and Schlaegger, 1992), reduction of glutamine in the cultured medium based on the exact requirements for biosynthesis (Xie and Wang, 1995), and transfection of a glutamine-synthetase gene to allow cells to grow in glutamine-free culture medium (Bell et al., 1995).

A better understanding of the metabolic mechanisms of adaptation to high ammonia concentrations may help to further modify cellular metabolism in order to enhance cell yields. In particular in high-cell-density cultures, where ammonia accumulation may become a limiting factor, a further reduction of the intracellular ammonia-producing reactions is desirable. By measuring the metabolic flows of the various pathways by which glutamine is degraded, bottle-necks in metabolic routes leading to other N-sinks than ammonia might be traced. Street and co-authors (1993) showed by $^{1}H/^{15}N$-NMR that most of the glutamate is transaminated, rather than deaminated by glutamate dehydrogenase in HeLa and CHO cells. This was recently confirmed for hybridoma cells by metabolic-flux balancing techniques (Zupke et al. 95; Bonarius et al., 1996). In continuously cultured hybridoma cells 55, 25 and 15 % of the produced glutamate was metabolized by alanine transaminase, aspartate transaminase and pyrroline-5-carboxylate reductase, respectively (Bonarius et al., 1996).

In this study, metabolic-flux balancing techniques are applied to further elucidate the metabolic strategy of hybridomas to avoid ammonia accumulation. By stressing continuously-cultured hybridoma cells with high ammonia concentrations (10mM), culture conditions with respect to N-metabolism that may occur in high-cell density cultures are simulated. Metabolic fluxes of both glutamine and glucose metabolism are determined using mass balances and are compared with intracellular fluxes of a control culture. The data show that at toxic levels, hybridoma cells reduce ammonia accumulation by converting ammonia and α-ketoglutarate into glutamate, which is subsequently metabolized by aminotranferases. These results suggest that glutamate dehydrogenase is a potential metabolic engineering site: not to inhibit its activity, as suggested before (Glacken, 1988), but in contrast, to increase its activity.

MATERIALS AND METHODS

Culture conditions and analyses

A detailed description of the various experimental procedures was published before (Bonarius et al., 1996). Briefly, hybridoma cells were cultured in a lab-scale bioreactor (1 L working volume, Biostat MD, Braun, Melsungen, FRG) in a continuous mode at a dilution rate of 0.7 d^{-1}. A mixture of Dulbecco's, Ham's F12 and Iscove's powdered media (DHI; 1:1:2) (Gibco, Grand Island, NY, USA) was used as the basal medium and was supplemented with 5 mg/ml insulin (Sigma, St.Louis, MO, USA), 6 mg/ml transferrin (Boehringer Mannheim, Mannheim, FRG), and 0.35 % (w/v) Synperonic F68 (Serva, Heidelberg, FRG). The medium contained 5 g/l glucose, 5 mM glutamine and 2.73 g/l sodium bicarbonate. After four days of continuous cultivation pseudo steady-state conditions were assumed. Samples for metabolite analyses were taken daily. At the end of each experiment, after three days of (pseudo) steady-state continuous culture, a large sample was taken for the analysis of the biomass composition.

A method developed to correct for the bicarbonate buffer in the culture medium (Bonarius et al., 1995) was applied for the determination of the **CO_2 production rate** (CER). The CO_2 in the outlet gas was measured by an infrared gas analyzer (Rosemount, Baar, CH). The **O_2 uptake rate** (OUR) was determined by the mass transfer coefficient $k_l^{O2}a$ and the fraction of oxygen in the inlet gas, as described before. Values for $k_l^{O2}a$ were by the dynamic method (Van 't Riet and Tramper, 1991).

Glucose and **lactate** were determined with automated enzymatic assays (YSI, Yellow Springs, OH), **ammonia** using an ion-selective electrode, and amino acids by HPLC (Amino Quant 1090, Hewlett-Packard, Paola Alto, CA). Intracellular **amino-acid** pools were extracted by perchloric acid as described elsewhere (Schmid and Keller, 1992). The cellular composition was measured as described by Xie and Wang (1994): the total **lipid** fraction was determined by weight after chloroform/methanol extraction, total **carbohydrates** were

analyzed by the phenol reaction method, total cellular **protein** was estimated using the Biuret assay, and nucleic acids were quantitated by absorbance at 260 nm after purification according to Chomczynski (1993). Cell **size** and **number** were determined using a Casy 1 instrument (Schärfe System, Reutlingen, FRG) and **dry cell weight** was determined after dehydration under vacuum. **Antibody** titers were measured by a standard ELISA.

Metabolic-Flux Analysis

Figure 1

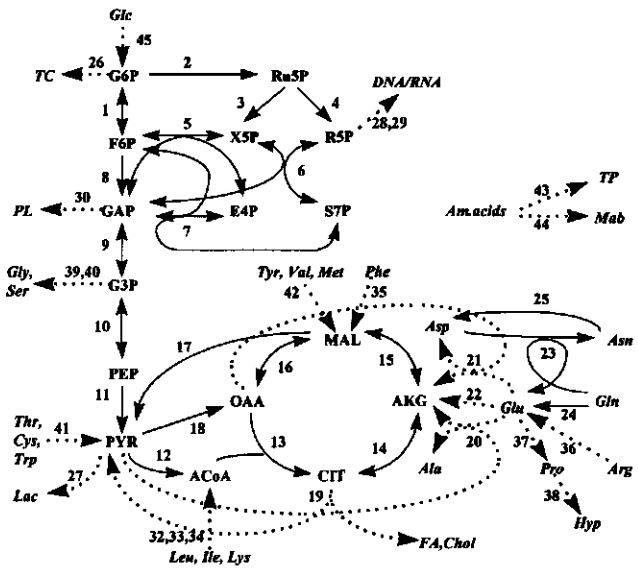

Network of mammalian-cell metabolism. Fluxes that can be quantified solely by mass-balancing techniques are indicated as dashed lines. To measure the remaining fluxes (solid lines) additional constraints are required.

ACoA acetyl-CoA, AKG α-ketoglutarate, ATP adenosine triphosphate, CHOL cholesterol, CIT citrate, DESM desmosterol, E4P erythrose-4-phosphate, GAP glyceraldehyde 3-phosphate, GLC glucose, GTP guanosine triphosphate, G6P glucose-6-phosphate, G3P 3-Phosphoglycerate, LAC lactate, MAB monoclonal antibody, MAL malate, OAA oxaloactetate, PEP phospho-enolpyruvate, PYR pyruvate, R5P ribose-5-phosphate, Ru5P ribulose-5-phosphate, S7P sedoheptulose-7-phosphate, TC total carbohydrates, TP total protein, X5P xylulose-5-phosphate.

The majority of the metabolic fluxes in mammalian cells, as depicted in Figure 1, can be determined by mass-balancing techniques without additional assumptions or isotopic-tracer experiments. In contrast, metabolic fluxes in cyclic pathways cannot be determined using the mass balances over the relevant metabolites (Vallino and Stephanopoulos, 1990; Bonarius et al., 1997). Reactions of the remaining underdetermined network are indicated by the solid lines in Figure 1. In this work, constraints based on experimental evidence (Street et al., 1993; Mancuso et al.,1994; Bonarius et al., 1998c) that was obtained by isotopic-tracer studies are used to estimate the flows through these reactions.

The metabolic network in Figure 1 contains three sets of linearly-dependent fluxes:
(i) the malate/pyruvate/oxaloacetate cycle (fluxes 16, 17 and 18),
(ii) glutamine degradation (fluxes 23, 24, and 25), and
(iii) the pentose shunt, glycolysis and TCA cycle (fluxes 1 to 16).
Therefore, three additional constraints are required to determine all fluxes by mass-balancing techniques alone.

(i) It was found by ^{13}C-NMR experiments that the flow through pyruvate carboxylase (flux 18) is negligible in hybridoma cells cultured in a hollow-fiber bioreactor (Mancuso, et al. 1994). This was recently confirmed for the same hybridoma cell line, the same medium, and the same mode of cultivation as investigated here, by ^{1}H-NMR techniques (Bonarius et al., 1998c).

(ii) Although no direct evidence for hybridoma cells exists, it is assumed that the flow through aspargine synthetase (flux 23) is negligible. Street et al. (1993) could not detect labeled asparagine in the medium supernatant of 5-^{15}N-glutamine-fed HeLa and CHO cells, indicating that asparagine synthetase is not active. In cultured mammalian cells, the proposed pathway of glutamine degradation is via glutaminase, rather than via asparagine synthetase (For example: Ardawi and Newsholme, 1984; Reitzer et al., 1979; Glacken, 1988; Mancuso et al., 1994). Only when asparagine becomes limiting, asparagine synthetase may become active in mammalian cells (Kilberg et al., 1994).

(iii) Recently, we showed by measuring $^{13}CO_2$ yields using mass spectrometry that the pentose-phosphate shunt is not negligible in hybridoma cells and dependent on the mode of cultivation (Bonarius et al., 1998c). In contrast to the data of Mancuso and co-workers (1994), showing that hybridoma cells cultured in hollow-fiber bioreactors direct only 5 % of the consumed glucose into the pentose shunt, up to 23 % of the glucose was channeled into the pentose shunt in rapidly growing cells ($\mu = 0.9$ day^{-1}) in continuous culture. In addition, we showed that both the constraint determined by the NAD(P)H mass balance and the minimum-norm constraint could not be used to estimate the pentose-shunt activity in hybridoma cells (Bonarius et al., 1998b). Although the NAD(P)H mass balance cannot be closed with sufficient accuracy to quantify the flow through reaction 2, the pentose-shunt activity is proportional to the NADPH requirements (Stryer, 1988). Therefore, we suggest that the best possible estimate for flux 2 is a linear fit to the pentose-shunt activity rate as determined earlier (Bonarius, et al. 1998c) to the measured biomass synthesis rate. For the cell line investigated here this assumption gives

$$\frac{x_2}{x_{2_o}} = \frac{\mu DCW}{\mu_o DCW_o} \qquad (1)$$

where μ is the measured growth rate, and DCW the dry cell weight. The subscript o denotes measured parameters of a standard culture to which x_2 is fitted (Bonarius et al., 1998c).

In addition to the three constraints mentioned above, directionality of irreversible fluxes is taken into account. In conclusion, this leads to the following set of constraints, which is solved using the least-squares method:

$$A\,x = r \qquad (2)$$

$$x_2 = x_{2_o}\frac{\mu\,DCW}{\mu_o\,DCW_o},\quad x_{18} = 0,\quad x_{23} = 0$$

It is stressed that the quantification of the reactions catalysed by alanine transaminase (flux 20), aspartate transaminase (flux 21) and glutamate dehydrogenase (flux 22) is not influenced by any of the above assumptions.

RESULTS AND DISCUSSION

Hybridoma cells appear to be more tolerant to ammonia than other cultured mammalian cells (Ozturk et al., 1992). To assess at which ammonia concentrations growth inhibition occurs for the cell line that was investigated in this study, experiments in T-flasks with various ammonia levels in the culture medium were done. It was found that growth inhibition occurred at concentrations of 5 mM ammonia (data not shown). In order to ensure significant effects on the intracellular metabolic fluxes, a continuous-culture experiment was carried out with 10 mM ammonia in the culture medium.

Table 1

Cell density, viability, respiration parameters for two steady states. Values are averages of three data points of samples taken daily from a continuous culture. Values between parentheses indicate standard deviations.

	Cell nr. (10^6 ml^{-1})	Viab. (-)	CER (10^{-12} mol.cell^{-1}.day^{-1})	OUR	RQ (-)	r_{GLC}	r_{LAC}	r_{NH3}
						(10^{-12} mol.cell^{-1}.day^{-1})		
Control	1.90 (0.31)	0.89	10.8 (0.15)	15.6 (0.17)	0.69	-4.681	4.775	1.143
NH_4^+	1.49 (0.17)	0.84	9.90 (0.17)	14.9 0.24)	0.66	-5.330	5.156	0.318

In Table 1 average cell densities, the viability, the respiration data, the metabolic qoutients of ammonia, glucose, and lactate of ammonia-stressed and control cells in continuous culture are shown. Under both conditions, lower values of the respiration qoutient (RQ) are found than reported before (Bonarius et al., 1995). This seems to be a result of a difference in OUR data, because the CER values are similar to those reported earlier. The reason for this discrepancy

is not evident, but it should be noted that OUR measurements on the basis of the liquid-phase O_2 balance have to be interpreted carefully due to possible inaccuracies associated with the determination of the $k_l^{O2}a$.

After ammonia addition the cell density decreases 21 %, the glucose uptake rate accelerates, and the specific Mab-production rate (Table 2) remains unaffected, which is similar as described elsewhere (Schneider et al., 1996), although the influence on the cell density is not as substantial as for instance reported by Glacken et al. (1986), Ozturk et al. (1992), and others.

In Table 2, the cellular composition for both (pseudo) steady states is given. Uptake and production rates of amino acids are shown in Table 3. It has been shown before that alanine production rates increase at elevated extracellular ammonia concentrations (Ozturk et al., 1992, Hansen and Emborg, 1994). In addition, similar to data reported by Ozturk et al. (1992), glutamine uptake rates increase at elevated ammonia. Most likely, the uptake rates of glucose and glutamine are higher under ammonia stress because of the increased

Table 2

Cellular composition. Values are given in 10^{-5} mg/cell and as a fraction of dry cell weight (DCW). Specific antibody production (r_{mab}) is given in 10^{-12} g.cell^{-1}.day^{-1} and as a fraction of the specific DCW production rate.

	Control		10 mM NH_4^+	
	Absolute value (10^{-5} mg/cell)	Fraction of DCW (%)	Absolute value (10^{-5} mg/cell)	Fraction of DCW (%)
Total carbohydrates	1.72	3.6	1.86	3.8
Total protein	37.7	79.4	37.5	76.0
Lipids	4.72	9.9	n.d.	-
RNA	2.14	4.5	2.34	4.7
DNA	1.19	2.5	1.53	3.1
DCW	47.5		49.5	
r_{Mab}	14.9	3.7	13.5	3.3

requirement for pyruvate. Both glucose and glutamine are carbon sources for pyruvate via the glycolysis and the malate enzyme, respectively (Rietzer et al.,1979).

Table 3

Total production rates (r_{tot}) and net catabolic rates (r_{nc}) of amino acids. The net catabolic rates are calculated as described before (Bonarius et al. 1996). The stoichiometric coefficients are calculated using the cellular composition (Table 2), the measured amino-acid composition in cellular protein (Table 5 in Bonarius et al., 1996) and the known amino-acid composition of Mab (Edelman et al., 69). A positive net catabolic rate indicates that the pertinent metabolite is produced in primary metabolism. Average values of three data points in each steady state (each data point *in duplo*) are given in 10^{-12} mol.cell^{-1}.day^{-1}.

	Production rates (10^{-12} mol.cell^{-1}.day^{-1})		Net catabolic rates (10^{-12} mol.cell^{-1}.day^{-1})		Intracellular pools (mM)	
	Control	10 mM NH_4^+	Control	10 mM NH_4^+	Control	10 mM NH_4^+
ASP	-0.173	-0.053	0.068	0.204	7.57	7.67
GLU	-0.208	-0.057	0.032	0.205	8.38	7.10
ASN	0.013	-0.503	0.109	0.045	1.04	1.23
SER	-0.023	0.065	0.208	0.292	3.62	5.91
GLN	-1.524	-2.005	-1.285	-1.742	1.33	3.48
HIS	-0.054	-0.065	-0.021	-0.032	0.25	0.60
GLY	-0.115	-0.121	0.138	0.134	3.41	5.04
THR	-0.134	-0.152	0.032	0.012	2.21	3.41
ALA	1.227	1.814	1.555	2.140	14.6	24.3
ARG	-0.158	-0.204	-0.085	-0.131	2.46	2.18
TYR	-0.075	-0.095	-0.024	-0.044	0.81	1.00
CYS	-0.101	-0.113	-0.072	-0.084	2.42	3.72
VAL	-0.198	-0.216	-0.004	-0.024	1.18	1.61
MET	-0.101	-0.129	-0.064	-0.092	1.22	1.51
TRP	-0.028	-0.022	-0.011	-0.004	1.37	1.47
PHE	-0.067	-0.096	0.004	-0.027	0.93	1.23
ILE	-0.377	-0.392	-0.262	-0.278	0.91	1.66
LEU	-0.596	-0.594	-0.408	-0.408	1.85	3.05
LYS	-0.189	-0.202	-0.093	-0.107	0.61	0.55
PRO	0.078	0.185	0.234	0.315	0.86	2.18
HYP	0.253	0.195	0.253	0.195	2.66	2.89

Table 3 shows some other significant effects on amino-acid metabolism. The net catabolic rates, i.e. the production rates after correction for biosynthesis

requirements (Bonarius, et al. 1996), of aspartate, proline and glutamate are higher under ammonia stress, demonstrating that these amino acids are used as alternative N-sinks. This already indicates that at elevated ammonia levels certain metabolic fluxes, which are not associated with biosynthesis, produce more aspartate, proline and glutamate than under normal conditions. The intracellular pools of several amino acids increase at high-ammonia conditions. In particular, the glutamine, alanine, serine, glycine, histidine, leucine, and proline pools are elevated. The most profound effect is on the ammonia-production rate, which decreases 72 %. (Table 1). In order to elucidate the mechanism by which hybridoma cells achieve this reduction, the intracellar fluxes are estimated.

Carbon and Nitrogen balances

The elemental balances of nitrogen and carbon provide a test for consistency of measured metabolic rates (Tables 1 and 3) and the measured cellular composition (Table 2) with respect to the law of mass conservation. Table 4 shows the total produced and consumed nitrogen and carbon of continuously cultured hybridoma cells. It is shown that both balances can be closed at an accuracy of less than 6 % of the net produced and consumed metabolites.

Table 4

Carbon and nitrogen balances. Values are in 10^{-12} Cmol.cell^{-1}.day^{-1} and 10^{-12} Nmol.cell^{-1}.day^{-1} for the total carbon and nitrogen production/consumption, respectively. The error is given both as an absolute value and as a percentage of the sum of produced and consumed carbon and nitrogen.

	Control		10mM NH_4^+	
	C	N	C	N
Total produced	59,91	7,30	50,26	7,00
Total consumed	62,50	7,56	56,34	7,59
Estimated error	2,59	0,25	6,08	0,59
Estimated error (%)	2,11	1,68	5,70	4,04

Intracellular fluxes

The intracellular fluxes of the two experiments are calculated as described in the Theory Section, and given in Table 5. Although it seems that fluxes 1-18 in control cells and ammonia-stressed cells are relatively similar, these values should be interpreted with care as they are calculated under the assumptions of the same stringent constraints with respect to flux 2 and 18 (Equation 2). The possibility that actual differences are masked due to these constraints can therefore not be ruled out.

Anaplerotic reactions

The malic-enzyme flux (x_{17}) appears to be negative in ammonia-stressed cells. Both the pyruvate-carboxylase (x_{18}) and the malic-enzyme reaction are important for the replenishment of TCA-cycle intermediates (Lehninger, 1977). The data shown in Table 5 suggest that at least one of these anaplerotic reactions is activated under ammonia stress. It is however not clear which of these two reactions is stimulated. Chauvin and co-workers (1994) showed by ^{13}C-NMR that the pyruvate-carboxylase flux increases in NH_4^+-stimulated kidney cells. If the same mechanism holds for the cell line investigated here, this suggests that the assumption that pyruvate carboxylase is inactive in hybridoma cells, is not valid for cells cultured under ammonia stress.

Glutamate-dehydrogenase flux is reversed

In contrast to fluxes 1-18, fluxes 19 to 22 are linearly independent and can be determined solely by mass-balancing techniques. It appears that the direction of the glutamate-dehydrogenase flux (reaction 22) reverses from an α-ketoglutarate-producing into a glutamate-producing reaction, i.e. from +0.02 to $-0.73 * 10^{-12}$ mol.cell.day^{-1}, when the ammonia concentration is increased (Table 5). Glutamate dehrydrogenase catalyzes the interconversion of L-glutamate and α-ketoglutarate:

$$\text{L-Glutamate} + \text{NAD(P)}^+ \Leftrightarrow \alpha\text{-Ketoglutarate} + \text{NAD(P)H} + H^+ + NH_4^+$$

At high levels, ammonia is consumed by this particular reaction, which results in a lower net ammonia production rate. Indeed, the chemical equilibrium of the

Table 5

Metabolic fluxes determined using the constraints given in Equation 2 and the measurement data of Tables 1, 2 and 3. Values are given in 10^{-12} mol product $cell^{-1}.day^{-1}$. (Co-factors, ATP and NAD(P)H, are not shown in stoichiometric equations.)

	Control	10 mM NH_4^+
1. G6P → F6P	2.95	3.66
2. G6P → Ru5P + CO2	1.85	1.84
3. Ru5P → X5P	0.92	0.94
4. Ru5P → R5P	0.96	0.96
5. X5P + R5P → S7P + GAP	0.52	0.57
6. X5P + E4P → F6P + GAP	0.44	0.43
7. S7P + GAP → F6P + E4P	0.49	0.52
8. F6P + ATP → 2 GAP	4.00	4.83
9. GAP → G3P/SER	8.32	10.0
10. G3P/SER → PEP	8.00	9.61
11. PEP → PYR	8.02	9.65
12. PYR → ACoA + CO2	2.50	2.30
13. ACoA + OAA → CIT	3.28	3.14
14. CIT → AKG + CO2	2.37	2.28
15. AKG → MAL + CO2	3.30	3.53
16. MAL → OAA	3.46	3.77
17. MAL → PYR + CO2	0.08	-0.55
18. PYR + CO2 → OAA	0.0	0.0
19. CIT → 1/9 FA/CHOL + PYR + CO2	1.04	1.04
20. PYR + GLU → AKG + ALA	1.56	2.14
21. GLU + OAA → ASP + AKG	0.21	0.70
22. GLU → AKG + NH3	0.02	-0.73
23.GLN + ASP → GLU + ASN	0.0	0.0
24.GLN → GLU + NH3	1.29	1.74
25. ASN → ASP + NH3	-0.14	-0.32
26. PYR → LAC	9.21	10.7

reaction catalyzed by glutamate dehydrogenase strongly favors glutamate production. The overall equilibrium constant (K) of the reaction,

$$K = \frac{[NAD(P)H][NH_4^+][\alpha - KG][H^+]}{[NAD(P)^+][GLU]} \qquad (3)$$

ranges from $1*10^{-14}$ to $1*10^{-15}$ M^2 (Fahien et al., 1965; Satlach and Fahien, 1969), yielding a ΔG^0 of ca. 20 kcal/mol at physiological conditions (Smith et al., 1976). In liver cells, this reaction may never reach equilibrium because the three products NAD(P)H, NH_4^+ and α-ketoglutarate can be rapidly metabolized (Satlach and Fahien, 1969). In hybridoma cells, certain conditions may drive the glutamate dehydrogenase reaction closer to equilibrium, favoring glutamate synthesis. Zupke et al. (1995) found by mass balancing techniques that the glutamate dehydrogenase flux reversed at low pO_2 in cultured hybridoma cells, as a result of the build-up of mitochondrial NAD(P)H at low oxygen levels.

Figure 3

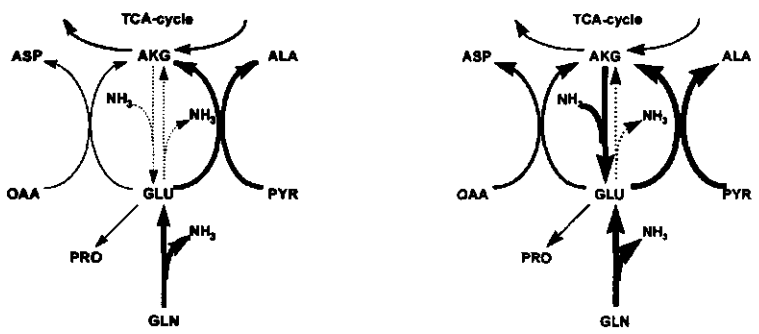

(A) (B)

Proposed mechanism of ammonia detoxification by cultured mammalian cells as analyzed by mass-balancing techniques. (A) Under normal conditions, the flux through glutamate dehydrogenase is insignificant relative to aminotransferases. (B) Under ammonia-stress, ammonia levels are reduced by converting it and α-ketoglurate into glutamate, which is subsequently channeled back into the TCA cycle by aminotransferases. Intensity of solid lines qualitatively represent magnitude of fluxes.

Here, it is shown that accumulated NH_4^+ drives the reaction into the direction of glutamate production. In contrast to liver cells, hybridoma cells lack the machinery to synthesize urea from NH_4^+ and CO_2. Glutamate dehydrogenase provides an alternative for the detoxification of NH_4^+ (See also Figure 2). The Michaelis constant for NH_4^+ as a substrate for glutamate dehydrogenase is in the order of 0,5 to 3,2 mM (Satlach and Fahien, 1965), which is well below the (extracellular) concentrations of cultured hybridoma cells under ammonia stress such as measured here (>10mM).

The produced glutamate, as compared to the control culture, is subsequently converted by alanine aminotransferase (45 % of the extra glutamate, flux 20), by aspartate aminotransferase (37 %, flux 21), and by pyrroline-5-carboxylate reductase (6 %, flux 37). The remaining 12 % of the extra glutamate that is produced by glumate dehydrogenase is secreted into the culture medium. This shows that under ammonia stress, more than 80 % of the α-ketoglutarate that is required for the detoxification of NH_4^+ is replenished into the TCA cycle by aminotransferases.

Implications for mammalian-cell culture

Setting the maximization of moles ATP produced per mole ammonia as an objective to improve bioreactor performance of mammalian cells, Glacken (1988) suggested to reduce ammonia formation by adding inhibitors of glutamate dehydrogenase to the medium, such as fumarate and pyroxidal phosphate. In the light of the data presented above, glutamate dehydrogenase should be stimulated rather than inhibited in order to reduce ammonia production rates. Apart from metabolic engineering techniques this can possibly be achieved by adding α-ketoglutarate in the culture medium (Hassel and Butler, 1990) and/or by lowering the glutamate concentrations. In addition, leucine concentrations should be kept low, as leucine stimulates the glutamate dehydrogenase reaction into the direction of α-ketoglutarate production (Glacken, 1988, referring to Smith et al., 1976). In particular at high-cell

density cultures, where ammonia accumulation may become a limiting factor, an increase of the glutamate-dehydrogenase flux may give higher cell yields.

ACKNOWLEDGMENTS

We would like to thank the following people at the Department PRP-Biotechnology, Hoffmann-La Roche AG. Christel Deuer and Agnes Weiss for ELISA analyses, Jean-Marie Vonach for medium preparation, Nathalie Schaub-Wild for assistance with amino-acid analysis and Dr. E.-J. Schlaeger for using the medium that was designed in his laboratory.

Chapter 9

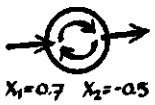

Flux Balances in Mammalian-Cell Culture: Methods & Applications

Hendrik P.J. Bonarius,
Cornelis D. De Gooijer,
and Johannes Tramper

ABSTRACT

Cultured mammalian cells do not regulate their glucose and amino-acid metabolism adequately for optimal bioprocess performance. Metabolic-flux balancing may provide quantitative data that can be used to design more efficient cell-culture processes. However, the estimation of fluxes in particular in cyclic metabolic pathways cannot be determined by mass-balancing techniques alone. Additional experimental flux data, which can be obtained by isotopic-tracer studies, are required to quantify these fluxes. Yet, flux-balance models have been shown useful for mammalian-cell culture. They have successfully been applied to estimate metabolite requirements for growth and energy, thus enabling to design significantly better media and feeding strategies. Further, metabolic-flux balances have been applied to assess various intracellular responses to changes in the extracellular environment. For example, it has been demonstrated how mammalian cells detoxify ammonia, thus providing guidance for the design

of ammonia-resistant cell lines. In the future, mass-balancing techniques may be used to analyze the synthesis of glycoproteins at a more detailed level.

INTRODUCTION

The metabolism of mammalian-cell lines that are used for the production of glycoproteins is inefficient and sub-optimal for industrial scale, because the nutrient uptake is not sufficiently tuned to the needs of biosynthesis. Mammalian cells take up more amino acids and glucose than they actually require for cellular processes. As a result waste products such as lactate, carbon dioxide and ammonia are secreted and their accumulation reduces process yields.

Although this is known for more than a decade (for a review see Glacken, 1988), it is surprising that only recently efforts have been undertaken to balance the medium composition to the actual growth and energy requirements of mammalian cells (Ljunggren and Häggström, 1990; Mather and Tsao, 1992; Messi, 1993; Xie and Wang, 1994; Adamson et al, 1995). Instead, mammalian cells have been cultivated since a long time in "minimal essential media" such as developed by Eagle (1959).

Here studies on glucose and amino-acid metabolism of mammalian cells are reviewed. First a brief survey is given on the metabolism of malignant cells, because their metabolism shares many characterisitics with the metabolism of mammalian cells in culture. It will be shown that these charateristics (which among others result in the above-mentioned problems in mammalian-cell culture) have certain selective advantages for metastatic tumor cells. Second reports on the metabolism of industrial cell lines will be discussed and similarities with tumor-cell metabolism are shown. Then the analysis of intracellular fluxes of mammalian-cell culture is surveyed. In particular methods and applications of flux balances are discussed. It is shown that flux-balancing techniques have successfully been applied to trace potential sites for

metabolic engineering, to determine metabolic capabilities, to study overflow metabolism and to design optimal medium compositions and feeding strategies. Finally an outlook is given on research that will lead to further improvement of low-cost, high-yield, cell-culture processes by the manipulation of cell metabolism.

Metabolic fluxes in cultured mammalian cells: some lessons from tumor-cell physiology

Most of our knowledge of carbohydrate and amino-acid metabolism of mammalian cells stems from physiological studies on malignant cells. Both tumor cells and cultured mammalian cells share, apart from the ability to proliferate continuously and the lack of differentiation, various properties with respect to their metabolism (Leist et al., 1990). In contrast to normally proliferating mammalian tissue, both tumor cells and cultured cells do not regulate the uptake of nutrients strictly to the needs of biosynthesis and maintenance processes. For example, the glucose uptake is high and not tuned to the requirements for energy and growth, which causes the production of lactate. The high rate of glycolysis combined with elevated lactate production observed in tumor cells initially gave rise to the postulation of impaired respiratory capabilities as a specific property of malignant cells (Warburg, 1956). Later, a number of observations led to the concept that the differences in carbohydrate metabolism in tumor cells compared to normal tissue were "selective" alterations that allowed tumor cells to proliferate under changing conditions with respect to glucose levels and oxygen tension and in the absence of sufficient metabolic control (For a review see Eigenbrodt et al., 1984). In Figure 1 several characteristics of the metabolism of tumor cells are shown and the proposed relevance for selection advantage is indicated.

For example, the high glycolytic activity allows tumor cells to generate energy in hypoxic areas (Epner et al., 1993). Also when sufficient oxygen is available, the glycolytic activity and lactate production rate in tumor cells remain high:

Figure 1

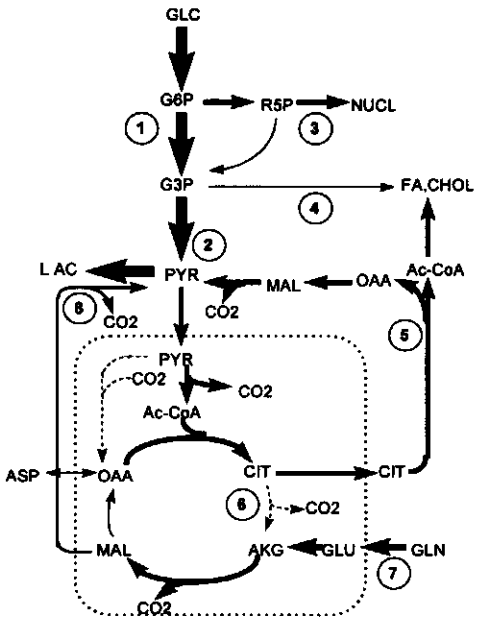

Selective advantages of tumor-cells metabolism. The regulation of glucose and amino-acid uptake in tumor cells is relatively poor compared to cells in normal tissue. Although this results in the secretion of toxic waste-products such as lactate and ammonia, several selective advantages are associated with the low level of metabolic control.

The high glycolytic rate enables tumor cells to proliferate in hypoxic areas (1). As a result, intracellular concentrations of the glycolytic intermediates between hexokinase and pyruvate kinase (2) remain high, and the availability of precursors for nucleic acid (3) and triglyceride synthesis (4) is ensured.

Tumor cells synthesize relatively high amounts of cholesterol (5), as a result of which the isocitrate-dehydrogenase flux (6) is low. This is an advantage for cells proliferating in areas with low concentrations of anti-oxidants, because isocitrate dehydrogenase is particularly sensitive to oxidative stress. TCA-cycle intermediates are replenished via glutamine degradation (7). If glucose levels are low, glutamine can be the major energy source. In that case, a relatively large amount of lactate will be derived from the malate shunt (8). (See also the main text for further details.)

The dotted line represents the mitochondrial membrane.

There is no feedback inhibition by ATP on phosphofructokinase (reaction 3, Figure 2a), as is the case in normal, non-malignant cells (Pasteur effect). Although this seems inefficient with respect to energy metabolism, it has been suggested that the high glycolytic rate ensures the availibity of precursors for biosynthesis: the intracellular pools of glycolytic intermediates between glucose-6-phosphate (G6P, Figure 1) and pyruvate (PYR) increase, thus supplying phosphometabolites for the biosynthesis of nucleotides, triglycerides and glycoproteins. This mechanism allows tumor cells to both proliferate (as precursors for biosynthesis are avaliable) and generate energy (as pyruvate kinase and pyruvate oxidation remain active) at a relatively high rate independetn of the oxygen tension (Eigenbrodt et al., 1992).

It has been established that lactate is not only generated by glycolysis, but also to a large extent from glutamine in malignant-cell lines (Reitzer et al, 1979). It is likely that in tumor cells not only the carbon of glutamine, but also that of other amino acids emerges in TCA-cyle intermediates and provides a significant amount of energy. Although this is both inefficient with respect to energy generation compared to the complete oxidation of glucose, and results in the secretion of ammonia, this allows tumor cells to proliferate in the absence of glucose (Wice et al., 1981).

In addition to enhanced glycolysis and glutaminolysis, tumor cells show little sensitivity to variation in oxygen concentrations, a lower requirement for anti-oxidants (Hornsby and Gill, 1981), a reduced (iso)citrate decarboxylation (x_{14} in Figure 2A) (Coleman and Lavietes, 1981), and enhanced nucleic acid (x_{28}, x_{29}) (Jackson et al., 1980) and lipid synthesis (x_{19}) (Engeser, 1982). The relevance of these characteristics for the metabolism of rapidly proliferating cells is outlined in Figure 1. The low isocitrate-dehydrogenase activity maybe an advantage for tumor cells, as isocitrate dehydrogenase is relatively sensitive to oxidative stress. Another possible advantage for a low isocitrate-dehydrogenase flux has been suggested by Coleman and Lavietes (1981). They hypothesized that the high lipid-synthesis rates 'truncate' the TCA cycle. In order to fuel lipid synthesis with carbon sources, the citrate-synthase reaction (x_{13}) is supplied

with oxaloacetate from TCA-cycle intermediates that are replenished by products from amino-acid degradation.

Metabolism of industrially relevant cell lines

From the early 80ies mammalian cells have been used for the production of heterologous glycoproteins. It appeared that their metabolism was similar to that of tumor cells: cultured mammalian cells do not adequately regulate the uptake of glucose and amino acids to the actual metabolic requirements for growth and energy. Therefore, cultured hybridoma, BHK and CHO cells produce large amounts of lactate, even if sufficient oxygen is available. At low oxygen concentrations glucose uptake rates increase to offset the reduced energy production from glutamine oxidation (Miller et al., 1987), resulting in more lactate production. At low glucose concentrations glutamine uptake rates and ammonia production rates increase (Miller et al., 1989; Meijer and Van Dijken, 1995). When adequate amounts of glucose are available, glutamine consumption is abundant, which results in the accumulation of various glutamate-derived amino acids (Ljunggren and Häggström, 1992; Schmid and Keller, 1992).

Because of the lack of metabolic regulation, the process engineer has to adjust the culture conditions in order to control nutrient uptake and to reduce waste-product formation. In the last Years, flux-balancing techniques have been applied to determine the actual nutrient requirements for energy, growth, and glycoprotein production, and to better understand the physiology of cultured mammalian cells. In the following sections different methods of flux-balance techniques are discussed, and applications to mammalian-cell culture are reviewed.

FLUX-BALANCE MODELS: METHODS

Metabolism is a large network of reaction pathways which enables (micro)organisms to convert substrates into biomass, energy and, in selected

cases, certain valuable products. The metabolic network of industrial microorganisms contains in the order of 10^3 enzymatic reactions for the degradation and synthesis of carbohydrates, fatty acids, lipids, amino acids, proteins and nucleic acids.

(i) Reduction of complexity

The first step in the formulation of a flux-balance model is to reduce the metabolic network to a manageable set of stoichiometric equations by selecting relevant pathways and by lumping complex subnetworks. For example, mammalian cells lack the pathway for synthesis of essential amino acids, and most cultured mammalian cells do neither generate glucogen nor urea, although the original species do possess the enzymes for glycogen and urea synthesis. These synthesis pathways are therefore omitted in a flux-balance model for cultured mammalian cells.

Lumping of linear reaction pathways is based on the assumption that the intracellular accumulation rate of intermediate metabolites is negligible with respect to the uptake rate of substrates and the accumulation of (end) products. For example, the complete fatty-acid synthesis machinery can be lumped into one reaction if the fractions of different fatty acids in triglycerides in mammalian cells are known. Figure 2a shows a flux model describing the metabolism of hybridoma cells after the above-mentioned reductions.

A problem in the estimation of biomass requirements is caused by the fact that most macromolecules can be synthesized via two different pathways, often designated as *de novo* and *salvage* pathways. *De novo* pathways refer to the biosynthesis of macromolecules via the complete biochemical pathways from basic nutrients, such as essential amino acids or (derivatives of) glucose to the end products. Salvage reactions are simpler and much less costly, and only include the assembly of pre-formed building blocks which accumulate as a result of turn-over of macromolecules. Implementation of both pathways in flux-balance models renders underdetermined networks: the different fluxes

cannot be determined by the measurement of the end product alone, because the reactions are linear dependent (See also below under Section *ii*). When the need for new biomass material is high, for example at high growth rates, *de novo* synthesis is most likely prevalent. Salvage pathways are therefore often neglected in metabolic-flux analysis of industrial microorganisms and mammalian cells (Xie and Wang, 1994b; Zupke and Stephanopoulos, 1995a; Bonarius et al., 1996; Vriezen, 1998). An exception is the metabolic model described by Savinell and Palsson (1992), in which the turn-over rate of RNA in hybridoma cells is estimated from mRNA and rRNA degradation rate constants. The re-use of the produced free bases can be can be calculated from these values. Preferably, the substrate requirements for macromolecules are determined experimentally. For example, Mancuso et al. (1994) determined the *de novo* synthesis of fatty acids by ^{13}C incorporation into triglycerides of cultured hybridoma cells.

Figure 2

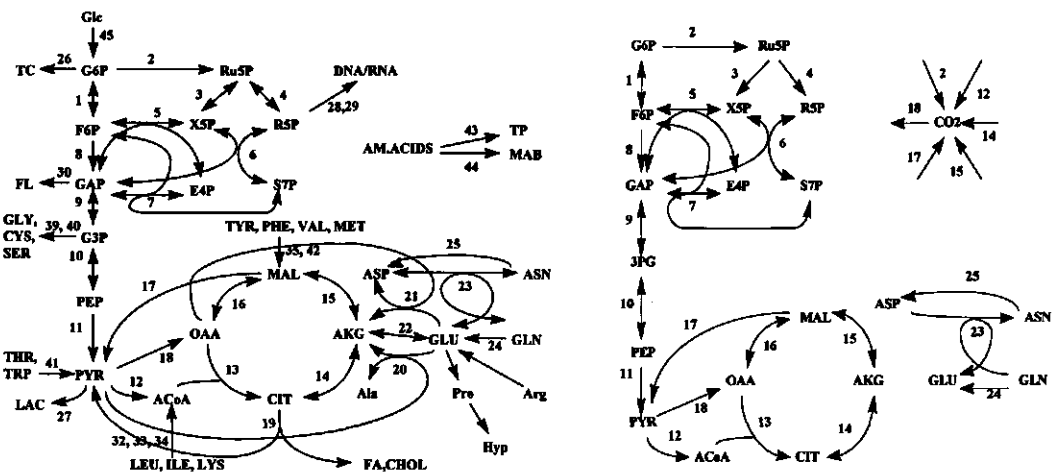

(A) (B)

Flux-balance models. The first step in the design of a flux-balance model is reduction, which leads from a complex to a simple network (2a). In the second step, linearly dependent fluxes are identified, which leads to a network such as shown in Figure 2b.

(ii) Identification of linear-dependent reactions

The second step in the formulation of flux-balance models involves the identification of determined and underdetermined subnetworks. Many fluxes can be estimated solely by metabolite-balancing techniques. For example, the alanine-aminotransferase flux (x_{20} in Figure 2a) is calculated from the extracellular alanine production rate and the (intracellular) alanine requirements for biomass. In contrast, most fluxes in cyclic pathways (for instance x_{14} and x_{15} in Figure 2a) cannot be determined independently by mass-balancing techniques alone. In the set of mass balance equations such fluxes cause linearly dependent relations (Vallino and Stephanopoulo, 1990).

In order to reduce the number of linearly dependent reactions, futile cycles are often neglected. The result of futile cycling is the dissipation of energy, while the net flux remains unchanged. For example, when flux-balance models are used to determine the requirement for carbon and nitrogen sources for anabolic processes, it is not necessary to include certain futile cycles. However, many cyclic pathways cannot be neglected for applications such as described here. Other constraints than the metabolite balances are required to estimate fluxes in a remaining underdetermined network, such as shown in Figure 2b. Examples of constraints that have been applied for flux analysis in mammalian-cell culture are reviewed in the following section.

(iii) Making the underdetermined determined

The minimal number of extra constraints that are necesarry to solve an underdetermind set of mass-balance equations, depends on how many sets of linear-dependent reactions are present. The metabolic network shown in Figure 2b contains three sets of linear-dependent reactions, for each of which an additional constraint is required. In this example these three sets are fluxes 1-16, fluxes 16-18, and fluxes 23-25. The determination of one flux out of each set is sufficient to solve the mass-balance equations. Preferably, these are derived from isotope balances (Mancuso et al, 1994; Sharfstein et al., 1994; Jan

et al. 1997; Bonarius et al., 1998c). If isotopic-tracer data are not available, other constraints which have been proposed for the estimation of fluxes in mammalian cells can be used instead (Fell and Small, 1986; Savinell and Palsson, 1992; Bonarius, et al. 1996). In Table 1 methods that have been applied for flux analysis in mammalian-cell culture are outlined.

Table 1

Determination of metabolic fluxes in mammalian-cell culture.

	Advantage	Disadvantage	When to use
1. Isotopic-tracer experiments			
a. Radioactive isotopes	-sensitive -small amounts sufficient	-radioactive -possible experimental bias because cells are incubated in new medium	-relative changes are sufficient
b. Stable isotopes NMR spectroscopy	-*in-situ* possible -*in vivo* possible -no experimental bias	-insensitive -metabolites/cells need to be concentrated	-absolute flux values are required
c. Stable isotopes mass spectroscopy	-*in-situ* possible -sensitive		-absolute flux values are required
2. Flux-balancing techniques			
a. Addition of mass balances - NAD(P) balance - ATP balance	-non-laborious	-error-sensitive	-estimation of relative changes is sufficient
b. Numerical methods - Linear optimization	-non-laborious	-error-sensitive -may give estimations when biochemical effects are well-established	-estimation of relative changes is sufficient

Radio-active isotopes

Katz and Wood (1963) and Bontemps et al. (1978) developed methods to determine metabolic fluxes of the pentose shunt, TCA cycle, and glycolysis in tumor-cell lines based on scintillation counting of labeled endproducts (CO_2 or H_2O). Recently, these methods were applied for the analysis of hybridoma-cell metabolism (Fitzpatricket al., 1993; Jan et al., 1997) and other industrially-relevant cell lines (Neermann and Wagner, 1997). Methods that apply radiolabeled isotopes are sensitive and have been proven useful to provide experimental evidence for certain (relative) biochemical effects. For example, Jan and co-workers (1997) showed that the relative flux of glucose through the pentose phosphate pathway increased at higher oxygen level. Jenkins and co-workers (1992) showed that a large fraction of glutamine (~ 36 %) was oxidized to CO_2, which emphasizes the importance of glutamine as an energy source. A disadvantage of assays based on radio-isotopic tracers for the analysis of metabolic fluxes in bioprocesses, is the fact that cells are sampled from the bioreactor and incubated in a new metabolic environment (that contains the ^{14}C- or ^{3}H-labeled substrate). Fluxes can thus not be assessed *in situ* with this method. When absolute flux values of cells cultured in bioreactors are required, data from scintillation experiments should therefore be interpreted carefully.

Stable isotopes

Stable isotopes that can be analyzed by NMR spectrometry or mass spectrometry (^{13}C or ^{15}N) have been applied to determine metabolic fluxes of cultured mammalian cells *in situ* in bioreactors. Zupke and Stephanopoulos (1994) used 1-^{13}C-glucose to assess the ratio of carbon entering the pyruvate branchpoint via the malate shunt by measuring the fractional labeling of lactate. Bonarius et al. (1998c) combined ^{1}H-NMR analysis of the ^{13}C-enrichment in secreted lactate and *on-line* $^{13}CO_2$-mass spectrometry to determine the pentose and malate shunt of continuously cultured hybridoma cells. These data were used to estimate the optimal glucose consumption rates, i.e., the minimum amount of glucose that should be consumed without limiting energy supplies. A step further to on-line flux analysis was taken by Sharfstein et al. (1994) and Mancuso et al. (1994), who exploited the fact that mammalian cells cultures in

hollow-fiber bioreactors are sufficiently dense to allow *in vivo* measurement of (labeled) metabolites by the relatively insensitive NMR spectroscopy. They showed for example that the high lipid-synthesis rates in hybridoma cells 'truncates' the TCA cycle (see also Figure 1), and that the pentose shunt activity was only 4 % of the glucose uptake, which is low compared to the pentose-shunt flux in cells grown in a CSTR (20 % of the glucose uptake, Bonarius et al. 1998c). In addition, NMR-spectrograms of hollow-fiber cultures can be used to assess the kinetics of uptake and incorporation of nutrients.

An alternative to the relative insensitive NMR spectrometry (Sharfstein et al. 1994; Mancuso et al., 1994), or mass spectrometry of volatile metabolites (Bonarius et al., 1998c) is GC-MS, which also can be applied to metabolites that are strictly dissolved in the liquid phase (Lin et al., 1993). This powerful technique has not been applied yet to study the metabolism of industrially-relevant cell lines.

NAD(P)H balance in metabolic-flux analysis

For industrial applications, it is desirable to determine intracellular fluxes by mass-balancing techniques alone. Various alternative constraints have been suggested to estimate fluxes without information from isotopic-tracer experiments. The NADH and NADPH balance has been used in flux-balance models for the determination of flux ratios at particular nodes in the metabolism of microorganisms (For example, Vallino and Stephanopoulos, 1990; Van Gulik and Heijnen, 1995; Jørgensen et al., 1995). The rank of stoichiometric networks increases after addition of the NAD(P)H balance, which allows the quantification of for example the flux ratio at the glucose-6-phosphate branch point (Goel et al., 1993; Bonarius et al., 1996; Fluxes 1 and 2 in Figure 2B). Although the requirements for NADPH for anabolic processes can be estimated and the amount of NADH that is oxidized can be approximated by measuring the oxygen uptake rate, certain fluxes appear to be overly sensitive to these mass balances. Even if the transhydrogenase activity -which generates a metabolic cycle in NADH and NADPH metabolism- is taken into account,

relatively small deviations in the NAD(P)H balance result in large differences in certain fluxes. For example, it has been shown for both *Bacillus subtilis* (Sauer et al., 1996) and hybridoma cells (Bonarius et al., 1998b) that the estimated pentose-shunt flux is very sensitive to changes in the NAD(P)H balance.

Linear-optimization techniques

Instead of assuming that the NAD(P)H balance can be closed, the NAD(P)H stoichiometry can be used to formulate biochemically meaningful objective functions (Fell and Small, 1986). In certain cases, the requirement for or surplus of one of these reduction equivalents may determine the metabolic-flux distribution of the cell. This is for instance the case for adipose tissue, which requires large amounts of NADPH for triglyceride synthesis (Fell and Small, 1986), oxygen-limited mammalian cells, which have NADH in surplus (Zupke et al., 1995), or artificially, for mammalian cells that are incubated with non-natural electron acceptors such as PMS, and as a result require large amounts of both NADH and NADPH (Bonarius et al., 1998d). Other objective functions were proposed by Savinell and Palsson (1992), who assumed that hybridoma cells maximize intracellular ATP levels, and by Bonarius et al (1996), who assumed that cell metabolism strives for the minimization of the net flow. Recently, a number of these objective functions were compared to flux values that were determined by isotopic-tracer experiments. The flux distributions found using two objective functions, i.e. maximize ATP and maximize NADH, were relatively similar to the distribution determined using 1-^{13}C-glucose (Bonarius et al., 1998c). This is consistent with the results obtained by Savinell and Palsson (1992), who estimated that hybridoma cells produce more ATP and NADH than the cells actually need. In addition, this suggests hybridoma cells are similar to other cancer cells, in being metabolically hyperactive and in the fact that they consume nutrients regardless of energy requirements.

FLUX-BALANCE MODELS: APPLICATIONS IN MAMMALIAN-CELL CULTURE

1. Balancing medium composition to requirements for biosynthesis

Metabolic-flux analysis has already been proven a useful tool to analyze the requirements for energy and biomass synthesis. Using linear optimization techniques to analyze data of hybridoma-cell metabolism, Savinell and Palsson (1992) calculated that neither the maintenance demand for ATP nor the antibody production rate limit the growth rate of these cells. They also estimated that hybridoma cells use their nutrients with only 57-78 % efficiency under normal conditions. Apart from this theoretical work, several experimental studies have been carried out to investigate 'overflow metabolism' of glucose and amino acids at an intracellular level. These will be discussed below.

Flux-balances have been used to improve the medium composition of cell culture. Ferrance and co-workers (1993) examined amino-acid balances for the development of insect-cell culture media. They distinguished "balanced" versus "unbalanced" amino acids in a batch-culture of Sf9 cells. A certain amino acid was designated "balanced" when the total amount measured amino acid after 10 days of cultivation (in the culture medium plus in the hydrolyzed cell extract) is less than 20 % different compared to the amount in the medium. In contrast, "unbalanced" amino acids are converted in catabolic processes for more than 20 %. It was found that the unbalanced amino acids were alanine and serine (which were produced in catabolism) and arginine, asparagine, glutamate, glutamine, glycine, and threonine (which were consumed in catabolism).

A similar concept is the determination of "net catabolic rates" (Bonarius et al., 1996). The net catabolic rates of metabolite X is the production rate of X corrected for the incorporation in biomass. The fraction of amino acids required for biosynthesis was determined by measuring amino acids in (hydrolyzed) cell protein, and measurement of nucleic-acid content. In hybridoma cells, the amino acids aspartate, asparagine, alanine, (hydroxy)proline, and serine were

found to be produced in catabolic processes. Arginine, glutamate, glutamine, isoleucine, leucine, and lysine were consumed and used to generate carbon for TCA-cycle intermediates. In other words, alanine, aspartate, asparine, proline, and serine are waste-products of amino acid catabolism, and their formation can be reduced by balancing arginine, glutamate, glutamine, etc., to the requirement for anabolic processes.

Sharfstein et al. (1994) used mass balances to complement ^{13}C-NMR data from hybridoma cells cultured in hollow-fiber bioreactors. It was found that both at low and high glutamine concentrations a significant fraction of amino acids entered the TCA-cycle at acetyl-CoA (f.e., isoleucine, leucine, lysine) and succinyl-CoA (isoleucine, methionine, and valine). At low glutamine concentrations, only 24 % of the amino acids entered the TCA-cycle via α-ketoglutarate (which is mainly glutamine). These data show that it is important not only to balance glutamine, but also other amino acids for optimal process conditions.

A systematic and successful approach to reduce the production of lactate, ammonia, and amino acids, while avoiding substrate limitation for biomass synthesis and energy generation has been proposed by Xie and Wang (1994, 1996). Based on stoichiometric analysis and mass-balancing techniques they designed a process-control strategy to meet the requirements for energy and growth of fed-batch-cultured hybridoma cells. The ratio of lactate to glucose and the ratio of ammonia to glutamine was only 0.067 and 0.15, respectively, compared to 1.33 and 0.40 in a conventional batch culture. As a result, the final antibody titer was 2.4 g/L, almost 50 times as high as in conventional batch cultivations (Xie and Wang 1996). It would be interesting to compare the efficiency of nutrient consumption of these optimized fed-batch cultures to the "non-balanced" cultures studied by Savinell and Palsson (1992), who reported that hybridomas metabolize nutrients with only 57-78 % efficiency.

2. Studying cellular physiology and finding sites for metabolic engineering

In addition to studies such as described above, mass balances have been used to estimate intracellular fluxes in mammalian-cell culture. For example, it has been shown that almost all glutamate enters the TCA cycle via transaminases (x_{20} and x_{21}) and not by the glutamate-dehydrogenase flux (x_{22}) in cultured hybridoma cells (Zupke et al., 1995; Bonarius et al., 1996), most likely to avoid production of additional ammonia. Indeed, when hybridoma cells are ammonia-stressed, the transaminase activity is higher and the glutamate-dehydrogenase flux is in the direction of glutamate production, thereby detoxifying a fraction of ammonia (See also Figure 3, and Bonarius et al,1998a). This suggests that ammonia-resistant cells can be engineered by the overexpression of glutamate dehydrogenase.

Figure 3

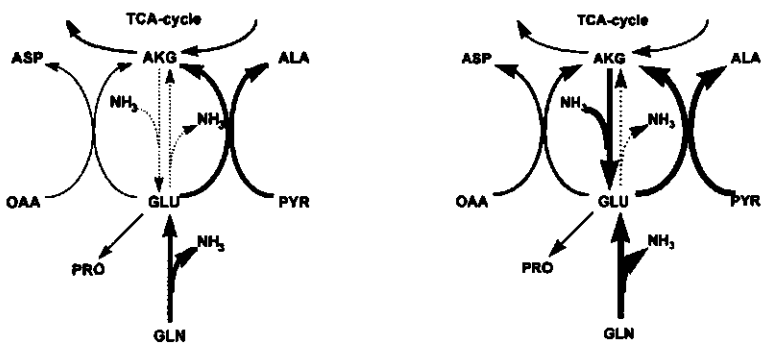

Mechanism of ammonia detoxification by cultured mammalian cells as elucidated by flux-balancing techniques. (A) Under normal conditions, the flux through glutamate dehydrogenase is insignificant relative to aminotransferases. (B) Under ammonia-stress, ammonia levels are reduced by converting it and a-ketoglurate into glutamate, which is subsequently channeled back into the TCA cycle by aminotransferases. Intensity of solid lines qualitatively represent magnitude of fluxes.

Another suggestion for a potential metabolic-engineering site to reduce the overflow metabolism of mammalian cells comes from the same above-mentioned study: the flux from the pyruvate-phospho-enol-pyruvate pool to the oxaloacetate-malate pool increases under ammonia-stress (Bonarius et al., 1998a). This is either due to an increased pyruvate-carboxylase flux (x_{18}), to a decreased malic-enzyme flux (x_{17}), or to a combination of both. Chauvin and co-workers (1994) showed that the pyruvate-carboxylase flux increased in ammonia-stressed kidney tissue. Further, it appears that at low ammonia levels, the pyruvate-carboxylase flux is negligibly small in hybridoma cells (Mancuso et al., 1994; Bonarius et al., 1998c). These data suggest that pyruvate carboxylase may be important for ammonia-resistant cell lines. Another effect of high pyruvate-carboxylase levels could be the reduction of glucose overflow metabolism (and thus lactate production), as this pathway channels pyruvate into the TCA cycle (R. Wagner, personal recommendation).

The effect of culture conditions on intracellular fluxes has been estimated with balancing techniques, even for underdetermined metabolic subnetworks. For instance, it has been shown that the TCA-cycle activity is low under oxygen-limiting conditions (Zupke et al., 1995). This is in agreement with the low pyruvate-oxidation activity found in other cultured cell lines (Hornsby and Gill, 1981). Recently, we demonstrated by metabolite-balancing techniques that the pentose-shunt flux (x_2) in hybridoma cells increases after addition of a growth-stimulating component (Bonarius et al., 1996), which is in agreement with the biochemical function of the oxidative branch of the shunt to supply NADPH for anabolic processes. These results suggest that mass-balancing techniques are useful for analyzing effects of toxic compounds on cellular physiology, even if the metabolic network under investigation is underdetermined.

OUTLOOK

In the near future, metabolite-balancing techniques may be used to study other areas of mammalian-cell metabolism than energy (Savinell and Palsson, 1992), glucose (Xie and Wang, 1994b; Zupke et al., 1995; Bonarius et al., 1996) or

amino-acid (Xie and Wang, 1994b; Bonarius et al., 1998a) metabolism. A few studies of those committed to the optimization of the production of glycoproteins by mammalian cells have already proceeded into this direction. Bibila and Flickinger (1992) used a structured model to study the pathway dynamics of antibody synthesis, and suggested that the antibody assembly in the ER may be rate-limiting in rapidly growing hybridoma cells. Recently, Umaña and Bailey (1997) used mass-balance techniques to predict the fraction of bi-antennary glycoforms of a glycoprotein product produced by CHO cells, as a function of β-N-acetyl glucosaminyl transferase III activity. Whiteley et al. (1997) described a model to quantify the effect of coexpression of the chaperone BiP on the secretion of IgG in insect cells. These studies consider only a fraction of the secretory pathway. When more quantitative *in vivo* data are available, it may be possible to determine rate-limiting steps in protein synthesis of mammalian cells by mass-balance techniques.

CONCLUSION

Flux-analysis techniques

It has been demonstrated that an important fraction of fluxes of large metabolic networks such as mammalian-cell metabolism can be estimated with only mass-balancing techniques. For the determination of fluxes in cyclic pathways isotopic-tracer experiments remain indispensable. However, relative trends in intracellular metabolic fluxes upon changes in extracellular conditions can be determined solely by mass-balancing techniques, even if the metabolic network is principally underdetermined. The *combination* of flux-balance models and isotopic-tracer studies will be the future tool of quantitative flux analysis of complex metabolic networks.

Flux analysis of mammalian-cell culture

Stoichiometric and flux analyses have been shown crucial for the optimization of cell-culture processes and in particular for the rational design of culture media. Flux-balancing techniques have led to almost a 2-log improvement of space-time yields and a significant reduction of waste-product secretion of mammalian cells. In addition, metabolic-flux analysis has been used to suggest genetic-engineering sites for the reduction of overflow metabolism. In the near future it will become clear whether the metabolism of mammalian cells can indeed be engineered into an efficient network for glycoprotein production.

List of Symbols

Symbol description

C	Concentration	($mol.l^{-1}$)
$C_A^i(0)$	Initial concentration of A (in Chapter 2, A = $CO_2 + HCO_3^-$) of the ingoing medium	($mol.l^{-1}$)
$C_{E,A}$	Extracellular concentration of metabolite A	(M)
$C_{E,A}^{med}$	Concentration of A in the ingoing medium	(M)
$C_{I,A}$	Intracellular concentration of metabolite A	($mol.cell^{-1}$)
$*CO_2(i)$	$^{13}CO_2$ or $^{14}CO_2$ production rate from a *i*-^{13}C- or *i*-^{14}C-glucose experiment, respectively.	($mol.l^{-1}.d^{-1}$)
CER	Volumetric carbon dioxide evolution rate	($mol.l^{-1}.d^{-1}$)
CSTR	Continuous stirred tank reactor	(-)
$*j$-C-Lac(i)	Fractional labeling of *j*-C-lactate from a *i*-^{13}C-glucose experiment	(-)
D	Dilution rate	(d^{-1})
DCW	Dry cell weight	($g.cell^{-1}$)
F_l^i	Medium feed rate (ingoing)	($l.d^{-1}$)
F_l^o	Medium feed rate (outgoing)	($l.d^{-1}$)
F_g^i	Gas flow rate (ingoing)	($mol.d^{-1}$)
F_g^o	Gas flow rate (outgoing)	($mol.d^{-1}$)
GC-MS	Gas chromatography mass spectrometry	(-)
H	Henry's constant	($Pa.l.mol^{-1}$)
h_ε	Test function	(-)
K_1	Reaction constant for CO_2/HCO_3^- equilibrium	($mol.l^{-1}$)
K_2	Reaction constant for the HCO_3^-/CO_3^{2-} equilibrium	($mol.l^{-1}$)
k	Number of relevant elements	(-)
k_la	Mass transfer coefficient	($1.d^{-1}$)
$k_l^{CO2}a$	Mass transfer coefficient for CO_2	(d^{-1})
$k_l^{O2}a$	Mass transfer coefficient for O_2	(d^{-1})
L	Hypothetical amount of CO_2 that evaporates from the medium tank	($mol.l^{-1}$)

M_i	Molecular weight of molecule *i*	($g.mol^{-1}$)
m	Number of metabolic reactions = number of fluxes	(-)
n	Number of metabolites	(-)
n_d	Concentration of dead cells	($cell.l^{-1}$)
n_v	Concentration of viable cells	($cell.l^{-1}$)
OUR	Volumetric oxygen uptake rate	($mol.l^{-1}d^{-1}$)
pH	pH in the bioreactor	(-)
pH^i	pH in the feed (ingoing medium)	(-)
$pH^{i,\varepsilon}$	Theoretical pH of the feed corrected by ε	(-)
PPS	Fraction of consumed glucose that is channeled through the pentose phosphate pathway	(-)
P	Pressure	(Pa)
q	Metabolic quotient	(mol/cells.d)
R	Molar gas constant	(J/mol.K)
RQ	Respiration quotient	(-)
r	Ratio of ^{13}C-satellite proton-resonance intensities to the non-coupled intensities in a ^1H-NMR spectrum of 3-C-lactate	(-)
$r_{nc,A}$	Net catabolic rate of metabolite A	($mol.cell^{-1}.d^{-1}$)
r_A	Extracellular production rate of metabolite A	($mol.cell^{-1}.d^{-1}$)
$r_{I,A}$	Intracellular production rate of metabolite A	($mol.cell^{-1}.d^{-1}$)
$r_{E,A}$	Extracellular production rate of metabolite A	($mol.cell^{-1}.d^{-1}$)
$r_{tot,A}$	Total production rate of metabolite A	($mol.cell^{-1}.d^{-1}$)
T	Temperature	(K)
V_l	Liquid reactor volume	(l)
V_g	Headspace volume	(l)
v_m, v_r	Synthesis rate of mRNA and rRNA, respectively	($mol.cell^{-1}.d^{-1}$)
x	Molar fraction	(-)
x_{CO2}^o	Fraction of CO_2 in the off-gas	(-)
x_i	Metabolic flux *i*	(mol (product).$cell^{-1}.d^{-1}$)
x_j	Metabolic flux through reaction *j*	($mol.cell^{-1}.d^{-1}$)
α_j	Stoichiometric coefficient of metabolite in reaction *j*	(-)
ß	Fraction of residual concentration of A (here $CO_2 + HCO_3^-$) of the ingoing medium as determined by its pH	(-)

ε	Ratio of buffer capacities	(-)
μ	Growth rate	(d^{-1})
$\Theta_{A,B}$	Stoichiometric coefficient of metabolite B for the biosynthesis of metabolite A	($mol.mol^{-1}$)

Matrices and vectors

A	Stoichiometric matrix (m x n)	(-)
$\mathbf{[A>B]_i}$	Atom mapping matrix that contains the carbon stoichiometry of reaction i from substrate A to product B	(-)
E	(k x n) Elemental composition matrix	(-)
r	Production rate vector (1 x n)	($mol.cell^{-1}.d^{-1}$)
$\mathbf{r_E}$	Extracellular production rate vector (1 x n)	($mol.cell^{-1}.d^{-1}$)
$\mathbf{r_I}$	Intracellular production rate vector (1 x n)	($mol.cell^{-1}.d^{-1}$)
$\mathbf{r_{tot}}$	Total production rate vector (1 x n)	($mol.cell^{-1}.d^{-1}$)
$\mathbf{r_{SA}}$	Production rate vector (1 x o) of metabolites of which the fractional labeling has been determined	($mol.cell^{-1}.d^{-1}$)
$\mathbf{SAV_A}$	Specific activity vector of metabolite A	(-)
SAM	Specific activity matrix (o x n)	(-)
x	Metabolic flux vector (1 x m)	(mol product.$cell^{-1}.d^{-1}$)
ε	(k x 1) Residual vector	($mol.cell^{-1}.d^{-1}$)

Metabolites

AAA Acetoacetate, ACoA acetyl-CoA, AKG a-ketoglutarate, ATP adenosine triphosphate, CHOL cholesterol, CIT citrate, DESM desmosterol, E4P erythrose-4-phosphate, FA Fatty acids, FAD flavin adenine dinucleotide, FAD^+ oxidized form of FAD, $FADH_2$ reduced form of FAD, GAP glyceraldehyde 3-phosphate, GLC glucose, GTP guanosine triphosphate, G6P glucose-6-phosphate, G3P 3-Phospho-glycerate, LAC lactate, MAB monoclonal antibody, MAL malate, NAD(P) nicotinamide adenine nucleotide (phosphate), $NAD(P)^+$ oxidized form of

NAD(P), NAD(P)H reduced form of NAD(P), OAA oxalo acetate, OMA malate plus oxaloactetate, PEP phosphoenolpyruvate, PMS phenazine methosulphate, PYR pyruvate, R5P ribose-5-phosphate, P5C pyrroline-5-carboxylate, Ru5P ribulose-5-phosphate, S7P sedoheptulose-7-phosphate, SuCoA Succinyl coenzyme A, TC total carbohydrates, THF tetrahydrofolate, TP total protein, X5P xylulose-5-phosphate.

References

A

Adamson, S.R., Drapeau, D., Luan, Y.-T., and Miller, D.A. 1995. Adaptation of mammalian cell lines to high cell densities. World International Property Organization, WO 95/12664.

Amos, H., Christopher, C.W., and Musliner, T.A.. 1976. Regulation of glucose transport in chick fibroblasts: bicarbonate, lactate and ascorbic acid. *J. Cell. Phys.* **89:** 669-676.

Andersen, D.C., and Goochee, C.F. 1995. The effect of ammonia on the O-linked glycosylation of granulyte colony-stimulating factor produced by Chinese Hamster Ovary cells. *Biotechnol. Bioeng.* **47**; 96-105.

Ardawi, M.S.M., and Newsholme, E.A. 1984. Glutamine metabolism in lymphoid tissues. *In:* Häussinger, D., and Sies, H. (Eds.), Glutamine metabolism in mammalian tissues. Springer-Verlag, Berlin. pp. 235-246.

B

Bailey, J.E., and Ollis, D.F.. 1986. *Biochemical engineering fundamentals.* Second Edition, McGraw-Hill, NY.

Bailey, J.E. 1991. Towards a science of metabolic engineering. *Science.* **252**: 1668-1675.

Bell, S.L., Bebbington, C., Scott, M.F., Wardell, J.N., Spier, R.E., Bushell, M.E., and Sanders, P.G. 1995. Genetic engineering of hybridoma glutamin metabolism. *Enzyme Microb. Technol.* **17**; 98-106.

Blum, J.J., and Stein, R.B. 1978. On the analysis of futile cycles in metabolism. *J.Theor. Biol.* **72**; 487-522.

Blum, J.J., and Stein, R.B. 1982. On the analysis of metabolic networks. In: Biological Regulation and Development. Goldberger R.F., Yamamoto, K.R. (Eds). Plenum Press, New York. pp. 99-125.

Bonarius, H.P.J., De Gooijer, C.D., Tramper, J., and Schmid, G. 1995a. Determination of the respiration quotient in mammalian cell culture in bicarbonate-buffered media. *Biotechnol. Bioeng.* **45**: 524-535 (Chapter 2 of this dissertation).

Bonarius, H.P.J., De Gooijer, C.D., Tramper, J., and Schmid, G. 1995b. Carbon dioxide evolution rates in animal cell culture in bicarbonate buffered and bicarbonate free medium. In: Animal Cell Technology. Proceedings of the 13th ESACT meeting. R.E. Spier, et al. (Eds), Butterworth-Heinemann Ltd, Wiltshire.

Bonarius, H.P.J., Hatzimanikatis, V., Meesters, K.P.H., De Gooijer, C.D., Schmid, G., and Tramper, J. 1996. Metabolic flux analysis of hybridoma cells in different culture media using mass balances. *Biotechnol. Bioeng.* **50**: 299-318 (Chapter 4 of this dissertation).

Bonarius, H.P.J., Schmid G., and Tramper, J. 1997. Flux analysis of underdetermined metabolic networks: The Quest for the Missing Constraint. *Trends in Biotechnol.* **15**: 308-314. (Chapter 1 of this dissertation)

Bonarius, H.P.J., Houtman, J.H.M., De Gooijer, C.D., Tramper, J., and Schmid, G. 1998a. Glutamate-dehydrogenase activity is increased in ammonia-stressed hybridoma cells. *Biotechnol. Bioeng.* 57: 447-453 (Chapter 8 of this dissertation).

Bonarius, H.P.J., Timmerarends, B., De Gooijer, C.D., and Tramper, J. 1998b. Metabolite balancing techniques versus ^{13}C tracer experiemtents to determine metabolic fluxes in hybridoma cells. *Biotechnol. Bioeng.* 58: 258-262 (Chapter 6 of this dissertation).

Bonarius, H.P.J., Özemre, A., Timmerarends, B., Skrabal, P., Heinzle, E., Schmid, G., and Tramper, J. 1998c. Metabolic-flux analysis of continuously cultured hybridoma cells using $^{13}CO_2$ mass spectrometry in combination with

NMR spectroscopy and metabolite balancing. *Submitted.* (Chapter 5 of this dissertation).

Bonarius, H.P.J., Houtman, J.H.M., Schmid, G., De Gooijer, C.D., and Tramper, J. 1998d. Metabolic-flux analysis of hybridoma cells under oxidative and reductive stress using mass balances and physiologically meaningful constraints. *Submitted.* (Chapter 7 of this dissertation).

Bonarius, H.P.J., Houtman, J.H.M., Schmid, G., De Gooijer, C.D., and Tramper, J. 1998e. Error analysis of metabolic-rate measurements in mammalian-cell culture by carbon and nitrogen balances. *Acc. for publication in Cytotechnol.* (Chapter 3 of this dissertation)

Box, G.E.P., Hunter, W.G., and Hunter, J.S. 1978. *Statistics for experimenters.* Wiley & Sons, Inc., NY.

C

Caroll, R.C., Ash, J.F., Vogt, P.K., and Singer, S.J. 1978. Reversion of transformed glycolysis to normal by inhibition of protein synthesis in rat liver kidney cells infected with temperature-sensitive mutant of Rous sarcoma virus. *Proc. Natl. Acad. Sci. USA.* 75: 5015-5021.

Chomczynski, P. 1993. A reagent for the single-step simultaneous isolation of RNA, DNA and proteins from cell and tissue samples. *Biotechniques* **15**; 532.

Cohen, D., Fallon, M., Popoloski, J.A., Pagano, S.A., and Adamson, S.R. 1989. CHO cell volume through a passage cycle. Presented at the 198th National Meeting of the American Chemical Society, Miami, Florida.

Coleman, P.S. and Lavietes, B.B. 1981. Membrane cholesterol, tumorigenesis and the biochemical phenotype of neoplasia. *CRC Crit.Rev.Biochem.* **11**: 341-393.

Creighton, T.E. 1984. Proteins: structures and molecular principles. W.H.Freeman, San Fransisco.

D

Darnell Jr., J.E., and Eagle, H. 1958. Glucose and glutamine in poliovirus production by HeLa cells. *Virology.* **6**: 556-566.

De Kok, H.E. and J.A. Roels. 1980. Method for the statistical treatment of elemental and energy balances with application to steady state continuous-culture growth of *S. cerevisiae CBS 426* in the respiratory region. *Biotechnol. Bioeng.* **22:** 1097-1104.

Dickens, F., and McIlwain, H. 1938. Phenazine compounds as carriers in the hexosemonophosphate system. *Biochem. J.* **32**: 1615-1625.

E

Edelman, G.M., Cunningham, B.A., Gall, W.E., Gottlieb, P.D., Rutishamer, U., and Waxdal, M.J. 1969. The covalent structure of an entire gammaG immunoglobuline molecule. *Proc. Nat. Acad. Sc.* **63**: 78-85.

Eigenbrodt, E., Fister, P., and Reinacher, M. 1985. New perspectives on carbohydrate metabolism in tumor cells, pp. 141-169. *In*: Breitner, R. (Ed.), Regulation of Carbohydrate Metabolism. Vol.2. CRC Press, Boca Raton.

Eigenbrodt, E., Reinacher, M., Scheefers-Borchel, U., Scheefers, H., and Friis, R. 1992. Double role for pyruvate kinase type M2 in the expansion of phosphometabolite pools found in tumor cells. *Crit. Rev.Oncog.* **3**: 91-115.

Engeser, H. 1982. Triglyceride and cholesterol ester metabolism of rat I cells and Rous sarcoma virus-transformed rat I cells. *Exp. Cell. Res.* **139**: 396-400

Epner, D.E., Partin, A.W., Schalken, J.A., Isaacs, J.T., and Coffey, D.S. 1993. Association of glyceraldehyde-3-phosphate dehydrogenase expression with cell motility and metastatic potential of rat prostatic adenocarcinoma. *Cancer Res.* **53**: 1995-1997.

Eyer, K., Oeggerli, A. and Heinzle, E. 1995. On-line gas analysis in animal cell cultivation: II. methods for oxygen uptake rate estimation and its application to controlled feeding of glutamine. *Biotechnol. Bioeng.* **45**: 54-62.

F

Fell, D.A. and Small, J.A. 1986. Fat synthesis in adipose tissue. An examination of stoichiometric constraints. *Biochem. J.* **238**, 781-786.

Fell, D.A. 1990. Substrate cycles: theoretical aspects of their role in metabolism. *Comments Theor. Biol.* **1**: 341-357.

Ferrance, J.P., Goel, A., and Ataai, M.M. 1993. Utilization of glucose and amino acids in insect cultures: quantifying the metabolic flows within primary pathways and medium development, *Biotechnol. Bioeng.* **42**: 697-707.

Ferrer, A., and Erickson, L.E.. 1980. Data consistency, yield, maintenance, and hysteresis in batch cultures of *Candida lipolytica* cultured on n-hexadecane. *Biotechnol. Bioeng.* **22**: 421-450.

Fitzpatrick, L., Jenkins, H.A., and Butler, M. 1993. Glucose and glutamine metabolism of a murine B-lymphocyte hybridoma grown in batch culture. *Appl. Biochem. Biotechnol.* **43**: 93-116.

G

Ganz, M.B., G. Boyarski, R.B. Sterzel and W.F. Boron. 1989. Arginine vasopressin enhances pH_i regulation in the presence of HCO_3^- by stimulating three acid-base transport systems. *Nature.* **337:** 648-651.

Glacken, M.W., Fleischaker, R.J., and Sinskey, A.J. 1986. Reduction of waste product excretion via nutrient control: possible strategies for maximizing product and cell yields on serum in cultures of mammalian cells. *Biotechnol. Bioeng.* **28**: 1376-1389.

Glacken, M.W. 1988a. Catabolic control of mammalian cell culture. *Bio/technol.* **6**: 1041-1050.

Glacken, M.W., Adema, E., and Sinskey, A.J. 1988b. Mathematical descriptions of hybridoma culture kinetics: I. Initial metabolic rates. *Biotechnol. Bioeng.* **32**: 491-506.

Goel, A., Ferrance, J., Jeong, J., and Ataai, M.M. 1993. Analysis of metabolic fluxes in batch and continuous cultures of *Bacillus subtilis*. *Biotechnol. Bioeng.* **42**: 686-696.

Golub, G.H., and Van Loan, C.F. 1989. Matrix computations. 2nd edition. John Hopkins University Press, Baltimore and London.

Greenbaum, A.L., Gumaa, K.A., and McLean, P. 1971. The distribution of hepatic metabolites and the control of pathways of carbohydrate metabolism in animals of different dietary and hormonal status. *Arch. Biochem. Biophys.* **143**: 617-663.

H

Hansen, H.H. and Emborg, C. 1994. Influence of ammonium ion on growth, metabolism, and productivity of a continuous suspension Chinese ovary cell culture. *Biotechnol. Prog.* **10**: 121-124.

Hassel, T., and Butler, M. 1990. Adaptation to non-ammoniagenic medium and selective substrate feeding lead to enhanced yields in animal cell culture. *J. Cell Sci.* **96**: 501-508.

Heinzle, E. 1992. Present and potential applications of mass spectometry for bioprocess research and control. *J. Biotechnol.* **25:** 81-114.

Hiller, A.G., Aeschlimann, A.D., Clark, D.S., and Blanch, H.W. 1991. A kinetic analysis of hybridoma cell growth and metabolism in continuous suspension culture in serum-free medium. *Biotechnol. Bioeng.* **38**: 733-741.

Hoffmann, E. 1983. Volume regulation in cultured cells. *Current topics in membranes and transport.* **30**: 125-180.

Hornsby, P.J. and Gill, G.N. 1981. Regulation of glutamine and pyruvate oxidation in cultured adrenocortical cells by cortisol, antioxidants, and oxygen: effects on cell proliferation. *J. Cell. Physiol.* 109: 111-123.

Hothershall, J.S., Baquer, N.Z., Greenbaum, A.L., and McLean, P. 1979. Alternative pathways of glucose utilization in brain. Changes in the pattern of glucose utilization in brain during development and the effect of phenazine methosulfate on the integration of metabolic routes. *Arch. Biochem. Biophys.* **198**: 478-492.

Hu, W.-S. and M.G. Oberg. 1990. Monitoring and control of animal cell bioreactors: Biochemical engineering considerations. In: *Large-scale mammalian cell culture technology.* Lubiniecki, A.S. (ed.) Marcel Dekker, Inc., NY, 451-481.

J

Jackson, R.C., Lui, M.S., Boritzki, T.J., Morris, H.P., and Weber, G. 1980. Purine and pyrimidine nucleotide patterns of normal, differentiating, and regenerating liver and of hepatomas in rats. *Cancer. Res.* **40**: 1286-1291.

Jeffrey, F.M.H., Rajagopal, A., Malloy, C.R., and Sherry, A.D. 1991. ^{13}C-NMR: a simple yet comprehensive method for analysis of intermediary metabolism. *Trends in Biochem. Sc.* **16**: 5-10.

Jenkins, H.A., Butler, M., and Dickson, A.J. 1992. Characterization of glutamine metabolism in two related murine hybridomas. *J. Biotechnol.* **23**: 167-182.

Jørgensen, H., Nielsen, J., Villadsen, J. and Møllgaard, H. 1995. Metabolic flux distributions in *Penicillium chrysogenum* during fed-batch cultivations. *Biotechnol. Bioeng.* **46**: 117-131.

K

Kacser, H., and Burns, J.A. 1973. Rate control of biological processes. *Symp. Soc. Exp. Biol.* **27**: 65-104.

Katz, J., and Wood, H.G. 1963. The use of $^{14}CO_2$ yields from glucose-1- and -6-^{14}C for the evaluation of the pathways of glucose metabolism. *J. Biol. Chem.* **238**: 517-523.

Kilberg, M.S., Hutson, R.G. and Laine, R.O. 1994. Amino acid-regulated gene-expression in eukaryotic cells. *FASEB J.* **8**: 13-19.

Kingsley-Hickman., P.B., Ross, B.D., and Krick, T. 1990. Hexose monophosphate shunt measurement in cultured cells with 1-^{13}C-glucose: correction for endogenous carbon using 6-^{13}C-glucose. *Anal. Biochem.* **185**: 235-237.

Kirkman, W.R., and Allfrey, V.G. 1972. Animal and plant cells and cell parts: chemical composition, pp. 387-392. *In:* Altman, P.L., and Dittmer, D.S. (eds.), Biology data book, 2nd ed., Vol. 1.

Kurano, N., Leist, C., Messi, F., and Fiechter, A. 1990. Growth of chinese hamster ovary cells in a compact loop reactor. 2. Effects of medium components and waste products. *J. Biotechnol.* **15**: 113-128.

L

Lanks, K.W., and Li, P.-W. 1988. End products of glucose and glutamine metabolism by cultured cell lines. *J. Cell. Phys.* **135**: 151-155.

Larrabee, M.G. 1989. The Pentose Cycle. Rigorous evaluation of limits to the flux from glucose using $^{14}CO_2$ data, with applications to peripherial ganglia of chicken embryos. *J. Biol. Chem.* **264**: 15875-15879.

Lazlo, P.A. 1981. Amino acids and glucose utilization by different metabolic pathways in ascites-tumour cells. *Eur. J. Biochem.* **117**: 19-25.

Leist, C.H., Meyer, H.P., and Fiechter, A. 1990. Potential and problems of animal cells in suspension culture. *J. Biotechnol.* **15**: 1-46.

Levering, P.R., Van Heijst, J.A.M., and Sünnen, C.M.G. 1992. Physiology of myeloma cells grown in glucose-limited chemostat cultures. *Cytotechnol.* **9**: 125-130.

Lin, Y.Y., Cheng, W.B., and Wright, C.E. 1993. Glucose metabolism in mammalian cells as determined by mass isotopomer analysis. *Anal. Biochem.* **209**: 267-273.

Ljunggren, J. and Häggström, L. 1992 Glutamine limited fed-batch cultures reduce the overflow metabolism of amino acids in myeloma cells. *Cytotechnol.* **8**: 45-56.

Loreck, D.J., Galarraga, J., Van der Veen, J., Phang, J., Smith, B.H., and Cummins, C.J. 1987. Regulation of the pentose phosphate pathway in human astrocytes and gliomas. *Metabol. Brain Dis.* **2**: 31-46.

Lust, W.P., Passoneau, J.V., and Crites, S.K. 1975. The measurement of glycogen in tissues by amyloglucosidase after the destruction of preexisting glucose. *Anal.Biochem.* **68**: 328-331.

M

Mancuso, A., Sharfstein, S.T., Tucker, S.N., Clark, D.S., and Blanch, H.W. 1994. Examination of primary metabolic pathways in a murine hybridoma with carbon-13 nuclear magnetic resonance spectroscopy. *Biotechnol. Bioeng.* **44**: 563-585.

Martens, D.E., De Gooijer, C.D., Van der Velden-de Groot, C.A.M., Beuvery, C.E., Tramper, J. 1993. Effect of dilution rate on growth, productivity, cell cycle and size, and shear stress sensitivity of hybridoma cells in continuous culture. *Biotechnol. Bioeng.* **41**: 421-439.

Martens, D.E., Sipkema, E.M., De Gooijer, C.D., Beuvery, E.C. and Tramper, J. 1995. A combined cell-cycle and metabolic model for the growth of hybridoma cells in steady-state continuous culture. *Biotechnol. Bioeng.* **48**: 49-65.

Marx, A., De Graaf, A.A., Weichert, W., Eggeling, L. and Sahm, H. 1996. Determination of the fluxes in the central metabolism of *Corynebacterium glutaminicum* by NMR spectroscopy combined with metabolite balancing. *Biotechnol. Bioeng.* **49**: 111-129

Mather, J.P., Tsao, M.C. 1992. Method for culturing chonese hamster ovary cells to improve production of recombinant proteins. United States Patent, US 005 122 469.

Messi, F. 1995. Serum- und proteinfrei wachsende Zellen. European Patent, EP 0 653 487 A1.

Miller, W.M., Wilke, C.R. and Blanch, H.W. 1987. Effects of dissolved oxygen concentration on hybridoma growth and metabolism in continuous culture. *J. Cell. Phys.* **132**: 524-533.

Miller, W.M., Wilke, C.R. and Blanch, H.W. 1989. Transient responses of hybridoma cells to nutrient additions in continuous culture: I. Glucose pulse and step changes. *Biotechnol. Bioeng.* **33**: 477-486.

Mitchell, S.L., Ross, B.D., Krick, T., and Garwood, M. 1989. Gas chromatographic-mass spectrometric analysis of hexose monophosphate shunt activity in cultured cells. *Biochem. Biophys. Res. Comm.* **158**: 474-479.

N

Newsholme, E.A., and Leech, A.R. 1983. pp. 409-410. Biochemistry for the medical sciences. Wiley, New York.

Noorman, H.J., Heijnen, J.J., and Luyben, K.Ch.A.M. 1991. Linear relations in miarobial reaction systems: a general overview of their origin, fosm, and use. *Biotechnol. Bioeng.* **38**: 603-618.

Nyiri, L.K., G.M. Toth and M. Charles. 1975. On-line measurement of gas-exchange conditions in fermentation processes. *Biotechnol. Bioeng.* **17:** 1663-1678.

O

Oeggerli, A. and E. Heinzle. 1994. On-line exhaust gas analysis of volatiles in fermentation using mass spectometry. *Biotechnol. Progr.* **10:** 284-290.

Ozturk, S.S., and Palsson, B.Ø. 1990. Effects of dissolved oxygen on cell growth, metabolism, and antibody production kinetics in continuous culture. *Biotechnol. Progr.* **6**:121-128.

Ozturk, S.S., and Palsson, B.Ø. 1991. Effect of medium osmolarity on hybridoma growth, metabolism, and antibody production. *Biotechnol. Bioeng.* **37**: 989-993.

Ozturk, S.S., Riley, M.R., and Palsson, B.Ø. 1992. Effects of ammonia and lactate on growth, metabolism, and antibody production. *Biotechnol. Bioeng.* **39**; 418-431.

P

Palsson, B.Ø. 1997. What lies beyond bioinformatics ? *Nature Biotechnol.* **15**: 3-4.

Papoutsakis, E.T., and Meyer, C.L. 1985. Equations and calculations of product yields and preferred pathways for Butanediol and mixed-acid fermentations. *Biotechnol. Bioeng.* **27**, 50-66.

Petch, D., and Butler, M. 1994. Profile of energy metabolism in a murine hybridoma: glucose and glutamine utilization. *J. Cell. Phys.* **161**: 71-76.

Phang, J.M., Cho Yeh, G., and Hagedorn, C.H. 1981. The intercellular proline cycle. *Life Sc.* **28**: 53-58.

Pirt, S.J. 1965. The maintenance energy of bacteria in growing cultures. *Proc. Roy. Soc. Lodon.* **193B**: 224-231.

Portais, J.-C., Schuster, R., Merle, M. and Canioni, P. 1993. Metabolic flux determination in C6 glioma cells using carbon-13 distribution upon [1-^{13}C]glucose incubation. *Eur. J. Biochem*: **217**: 457-468.

R

Reitzer, L.J., Wice, B.M., and Kennel, D. 1979. Evidence that glutamine, not sugar, is the major energy source for cultured HeLa cells. *J. Biol. Chem.* **254**; 2669-2676.

Reitzer, L.J., Wice, B.M., and Kennel, D. 1980. The pentose cycle. *J. Biol. Chem.* **255**: 5616-5626.

Ripps, D.L. 1965. Afjustment of experimental data. *Chem. Eng. Progr. Symp. Ser.* **55**: 8-13.

Ryll, T., Valley, U. and Wagner, R. 1994. Biochemistry of growth inhibition by ammonium ions in mammalian cells. *Biotechnol. Bioeng.* **44**: 184-193.

Roels, J.A. 1980. Applications of macroscopic principles to microbial metabolism. *Biotechnol. Bioeng.* **22**: 2457-2514.

Reff, E.R. 1993. High-level production of recombinant immunoglobulins in mammalian cells. *Curr. Opin. Biotechnol.* **4**: 573-576.

Royce, P.N., and Thornhill, N.F. 1991. Estimation of dissolved carbon dioxide concentrations in aerobic fermentations. *AIChE. J.* **37**: 1680-1686.

Royce, P.N. 1992. Effect of changes in the pH and carbon dioxide evolution rate on the measured respiratory quotient of fermentations. *Biotechnol. Bioeng.* **40:** 1129-1138.

S

Satlach, H.J., and Fahien, L.A. 1969. Nitrogen metabolism of amino acids, pp.1-79. *In*: Greenberg, D.M. (ed.), Metabolic Pathways. Vol.3. Academic Press, New York.

Sauer, U., Hatzimanikatis, V., Hohman, H.-P., Manneberg, M., Van Loon, A.P.G.M., and Bailey, J.E. 1996. Physiology and metabolic fluxes of wild-type and riboflavin-producing *Bacillus subtilis*. *Appl. Environ. Microbiol.* **62**: 3687-3696.

Savinell, J.M., and Palsson, B.Ø. 1992a. Network analysis of intermediary metabolism using linear optimization. *J. Theor. Biol.* **154**: 421-454.

Savinell, J.M., and Palsson, B.Ø. 1992b. Optimal selection of metabolic fluxes for *in vivo* measurements. II. Application to *E.coli* and hybridoma cell metabolism. *J. Theor. Biol.* **155**: 215-242.

Schmid, G., H.W. Blanch and C.R. Wilke. 1990. Hybridoma growth, metabolism, and product formation in HEPES-buffered medium. *Biotechnol. Lett.* **12**: 627-638.

Schmid, G., and Keller, T. 1992. Monitoring hybridoma metabolism in continuous suspension culture at the intracellular level. *Cytotechnol.* **9**: 217-229.

Schmidt, K., Marx, A., De Graaf, A.A., Wiecher, W., Sahm, H., Nielsen, J., and Villadsen, J. 1998. 13-C tracer experiments and metabolic balancing for metabolic flux analysis: comparing two approaches. *Biotechnol. Bioeng.* **58**: 254-257.

Schneider, M., Marison, I.W., and Von Stockar, U. 1996. The importance of ammonia in mammalian cell culture. *J. Biotechnology.* **46**: 161-185.

Schumpe, A., G. Quicker and W.-D. Deckwer. 1982. Gas solubilities in microbial culture media. *Adv. Biochem. Eng.* **24**: 1-83.

Schumpp, B. and Schlaeger, E.-J. 1992. Growth study of lactate and ammonia double resistant clones of HL-60 cells. *Cytotechnol.* **8**: 39-44.

Sharfstein, S.T., Tucker, S.N., Mancuso, A., Blanch, H.W., and Clark, D.S. 1994. Quantitative in vivo nuclear magnetic resonance studies of hybridoma metabolism. *Biotechnol. Bioeng.* **43**: 1059-1074.

Shulman, R.G., Brown, T.R., Ugurbil, S., Ogawa, S., Cohen, S.M., and Den Hollander, J.A. 1979. Cellular applications of ^{31}P and ^{13}C NMR. *Science* **205**: 160-166.

Schuster, R., and Schuster, S. 1993. Refined algorithm and computer program for calculating all non-negative fluxes admissable in steady states of biochemical reaction systems with or without some flux rates fixed. *Comp. Appl. Biosc.* **9**: 79-85.

Schuster, S., and Hilgetag, C. 1994. On elementary flux modes in biochemical reaction systems at steady state. *J. Biol. Syst.* **2**: 165-182.

Simon, L.M., Robin, E.D., and Theodore, J. 1981. Differences in oxygen dependent regulation of enzymes between tumor and normal cells in culture. *J. Cell. Physiol.* 108: 393-402.

Smith, E.L., Austin, B.M, Blumenthal, K.M., and Nye, J.F. 1976. Glutamate dehydrogenases. *In:* The enzymes, Boyer, P.B. (ed.), Academic Press, **11**: 294-366.

Srere, P.A. 1990. Citric acid cycle redux. *Trends in Biochem. Sc.* **10**: 411-412.

Stouthamer, A.H. 1973. A theoretical study on the amount of ATP required for synthesis of microbial cell material. *Antonie van Leeuwenhoek.* **39**: 545-565.

Street, J.C., Delort, A.M., Braddock, P.S., and Brindle, K.M. 1993. A $^{1}H/^{15}N$ NMR study of nitrogen metabolism in cultured mammalian cells. *Biochem. J.* **291**: 301-304.

Stryer, L. 1988. Biochemistry. 3rd edition. W.H. Freeman and Company, New York.

T

Thisted, R.A. 1989. Elements of statistical computing. Chapman and Hall, New York.

Tsai, P.S., Hatzimanikatis, V., and Bailey, J.E. 1996. Effect of *Vitreoscilla* hemoglobin dosage on microaerobic *Escherichia coli* carbon and energy metabolism. *Biotechnol. Bioeng.* **49**: 139-150.

U

Umaña, P., and Bailey, J.E. 1997. A mathematical model for N-linked glycoform biosynthesis. *Biotechnol. Bioeng.* **55**: 890-908.

V

Vallino, J.J. , and Stephanopoulos, G. 1990. Flux determination in cellular bioreaction networks: Applications to lysine fermenations. pp.205-219. *In:* S.K. Sikdar, M. Bier, and P.Todd (eds.), Frontiers in bioprocessing. CRC Press, Boca Rotan, FL.

Vallino, J.J., and Stephanopoulos, G. 1993. Metabolic flux distributions in *Coryne-bacterium glutamicum* during growth and lysine overproduction. *Biotechnol. Bioeng.* **41**: 633-646.

Van der Heijden, R.T.J.M., Romein, B., Heijnen,J.J., Hellinga, C., and Luyben, K.Ch.A. M.. 1994. Linear constraint relations in biochemical reaction systems. *Biotechnol Bioeng.* **43**: 1-20.

Van Gulik, W.M. and J.J. Heijnen. 1995. A metabolic network stoichiometry analysis of microbial growth and product formation. *Biotechnol. Bioeng.* **48**: 681-698.

Van 't Riet, K., and Tramper, J. 1991. Basic bioeactor design. Marcel Dekker, New York.

Varma, A., Boesch, B.W., and Palsson, B.Ø. 1993a. Biochemical production capabilities of *Escherichia coli*. *Biotechnol. Bioeng.* **42**: 59-73.

Varma, A, and Palsson, B.Ø. 1993b. Metabolic capabilities of *E.Coli*. I. Synthesis of biosynthetic precursors and cofactors. *J. Theor. Biol.* **165**: 477-502.

Varma, A., and Palsson, B.Ø. 1994. Metabolic flux balancing: Basic concepts, scientific and practical use. *Bio/Technol.* **12**: 994-998.

Varma, A., and Palsson, B.O. Stoichiometric flux balance models quantitavily predict growth and metabolic by-product secretion in wild type *Escherichia coli* W3110. *Appl. Environ. Microbiol.* **60**: 3724-3731.

Verduyn, C., Postma, E., Scheffers, W.A., Van Dijken, J.P. 1990. Energetics of *Saccharomyces cerevisiae* in anaerobic glucose-limited chemostat cultures. *J. Gen. Microbiol.* **136**: 405-412.

Von Stockar, U., and Auberson, L.C.M. 1992. Chemostat culture of yeast, continuous culture fundamentals and simple unstructured mathematical models. *J. Biotechnol.* **22**: 69-88.

Vriezen, N. 1998. *Physiology of mammalian cells in suspension culture.* PhD dissertation, Delft University, The Netherlands.

W

Wang, H.Y., Cooney, C.L. and Wang, D.I.C. 1977. Computer-aided baker's yeast fermentations. *Biotechnol. Bioeng.* **19:** 69-86.

Wang, H.Y., Cooney, C.L., and Wang, D.I.C. 1979. Computer control of bakers' yeast production. *Biotechnol. Bioeng.* **21**: 975-995.

Wang, N.S., and Stephanopoulos, G. 1983. Application of macroscopic balances to the identification of gross measurement errors. *Biotechnol. Bioeng.* **25**: 2177-2208.

Westerhoff, H. V., and Kell, D. B. 1996. What biotechnologists knew all along...? *J. Theor. Biol.* **182**: 411-420.

Wice, B.M., Reitzer, L.J., and Kennell, D. 1981. The continuous growth of vertebrate cells in the absence of sugar. *J. Biol. Chem.* **256**: 7812-7819.

Willis, A., Williams, W.F. and Schleich, T. 1986. Dynamic assesment of hexose monophosphate shunt activity in the intact rabit lens by proton NMR spectrometry. *Biochem. Biophys. Res. Comm.* **138**: 1068-1073.

Wiechert, W., and De Graaf, A.A. 1997. Bidirectional reaction steps in metabolic networks: I. Modeling and simulation of carbon isotope labeling experiments. *Biotechnol. and Bioeng.* **55**: 101-117.

Wu, W.-T. and P.-M. Wang. 1993. On-line optimal control for ethanol production. *J. Biotechnol.* **29:** 257-266.

X

Xie, L., and Wang, D.I.C. 1994a. Stoichiometric analysis of animal cell growth and its application in medium design. *Biotechnol. Bioeng.* **43**: 1164-1174.

Xie, L., and Wang, D.I.C. 1994b. Applications of improved stoichiometric model in medium design and fed-batch cultivation of animal cells in bioreactor. *Cytotechnol.* **15**:17-29.

Xie, L., and Wang, D.I.C. 1996. High cell-density and high monoclonal-antibody production through medium design and rational control in a bioreactor. *Biotechnol. Bioeng.* **51**: 725-729.

Xie; L., and Wang, D.I.C. 1997. Integrated approaches to the design of media and feeding strategies for fed-batch cultures of animal cells. *Trends in Biotechnol.* **15**: 109-113.

Y

Youmans, H.L. 1973. *Statistics for chemistry.* Bell & Howell Company, Columbus.

Z

Zubay, G. 1983. *Biochemistry.* Addison-Wesley Publishing Company, New York.

Zupke, C., and Stephanopoulos, G. 1994. Modeling of isotope distributions and intracellular fluxes in metabolic networks using atom mapping matrices. *Biotechnol. Prog.* **10**; 489-498.

Zupke, C. Sinskey, A.J., and Stephanopoulos, G. 1995a. Intracellular flux analysis applied to the effect of dissolved-oxygen on hybridomas. *Appl. Microbiol. Biotechnol.* **44**: 27-36.

Zupke, C., and Stephanopoulos, G. 1995b. Intracellular flux analysis in hybridomas using mass balances and in vitro ^{13}C NMR. *Biotechnol. Bioeng.* **45**: 292-303.

Abstract

In the biopharmaceutical industry mammalian cells are cultivated for the production of recombinant glycoproteins (for example EPO, tPA, and the blood factors FVII and FVIII) vaccines, and monoclonal antibodies. In contrast to other expression systems, such as prokaryotes or yeasts, mammalian cells are able to properly glycosylate and correctly fold therapeutic proteins. Therefore, in many cases, mammalian cells are the only possible production system for (recombinant) therapeutics.

Cultivated mammalian cells are similar to tumor cells: in contrast to normal cells in mammalian tissue they can proliferate continuously and are not differentiated to fulfill tissue-specific tasks. Cultivated cells and tumor cells also share other characteristics, for example parts of their metabolism. In general the metabolism of continuously-proliferating cells is not or only poorly regulated and controlled, and therefore inefficient. Cultivated mammalian cells show a high metabolic activity, and waste large amounts of nutrients and energy. Instead of tuning the consumption of glucose and certain amino acids to the requirements for growth, these nutrients are taken up whenever they are available. As a result waste products such as lactic acid, carbon dioxide, and bicarbonate accumulate, acidify the culture medium, and inhibit cell growth and protein production.

Another shared characteristic of tumor cells and cultured mammalian cells is the production of ammonia. Mammals normally produce urea, a waste product of the endogenous metabolism, in the liver. Mammalian cells cultivated for glycoprotein production, do not possess the machinery for the production of urea. Instead, they secrete ammonia into the culture medium, which accumulates at toxic levels.

It is thus apparent that the metabolism of mammalian cells is suboptimal for an efficient energy- and nutrient supply. To quantify the exact nutrient requirements for growth and energy, and to investigate which metabolic pathways should be optimized to reduce waste-product synthesis to increase

production yields, the intracellular reaction rates, i.e. "the metabolic fluxes", have to be determined. Intracellular fluxes can be quantified by incubating cells with isotope-labeled nutrients and measurement of the isotope distributions of end products. This method however, (i) has practical limitations since it is limited to the analysis of single metabolic pathways for each tracer experiment, (ii) is expensive, and (iii) is not feasible at an industrial scale. An alternative method is based on solving the linear set of equations that is determined by the mass balances of the relevant metabolites. In this dissertation this novel method, which is referred to as "metabolic-flux balancing", is applied to mammalian-cell culture.

Metabolic-flux balancing techniques are based on relatively simple linear algebra. If the stoichiometry of the relevant intracellular reactions and the cellular composition are known, and the uptake- and secretion rates of the relevant metabolites have been measured, the reaction rates can be determined using the appropriate mass-balance equations. Together, the mass-balance equations form a set of linear equations that can be solved by linear regression. However, in the metabolism of the cell there are a number of *cyclic* pathways which are linearly dependent within the set of mass-balance equations, which causes the metabolic network to be underdetermined. This is the central problem in this dissertation and is explained in detail in Chapter 1.

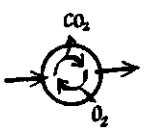

In most cyclic metabolic pathways certain co-metabolites are consumed or produced. For example, carbon dioxide, is a waste product of the TCA- and pentose cycle. The carbon-dioxide production rate is therefore an indication for the activity of the fluxes through these essential metabolic cycles. However, in mammalian-cell culture the measurement of the carbon-dioxide production rate is hampered by the use of bicarbonate as a buffer system and the accumulation carbon dioxide in the culture medium. In Chapter 2 a solution to this problem is given and a method is developed for the determination of the carbon-dioxide production rate in bicarbonate-buffered bioreactor systems.

In Chapter 3 it is shown that, if this method is used, it is possible to close the mass balance for total carbon in mammalian-cell culture. Together with the balance for nitrogen it is now possible to demonstrate statistically that there are no gross errors in the measurement data and there are not missing any relevant metabolites. Now, the metabolic-flux analysis can start.....

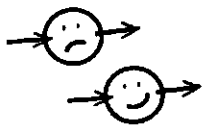

Unfortunately, the intracellular fluxes cannot be determined solely by flux-balancing techniques even when the mass balances of co-metabolites such as carbon dioxide are included in the metabolic network. This is both a result of the fact that mass balances of particular co-metabolites cannot be closed (*e.g.* the mass balance of ATP), and of the fact that co-metabolites are produced or consumed in more than one cyclic pathway. Such cyclic pathways remain therefore linearly dependent, and additional information is required to quantify the flows through these cycles. A solution is proposed in Chapter 4. It is assumed that hybridoma cells are efficient with respect to their metabolism (while taking into account the "inefficient" production and uptake rates mentioned above), and minimize the flow through the metabolic network. Within the set of all admissible solutions, the flux distribution with the minimum sum of squares is chosen. This assumption is referred to as the "minimum-norm constraint". The method is applied to hybridoma cells under both optimal and suboptimal conditions.

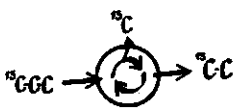

In Chapter 5 experiments are described that are conducted to test the assumption mentioned above. The metabolic fluxes in the TCA cycle, the pentose-phosphate cycle, and the malate shunt are determined by ^{13}C-tracer experiments. Hybridoma cells are cultured on a small scale and ^{13}C-labeled glucose is added to the culture medium. Subsequently, the isotopic distribution of lactate is determined by NMR spectrometry and the fraction of ^{13}C in carbon dioxide is measured by mass spectrometry. It appears that the actual fluxes in the mentioned cycles are significantly different from the fluxes estimated using the minimum-norm constraint.

In addition, it appears that rapidly proliferating hybridoma cells have a higher pentose-shunt activity than previously assumed. The reason for this high activity is probably the high need for NADPH (which is required for biomass synthesis). This also means that a larger part of glucose is consumed more efficiently than previously assumed on the basis of the amount of produced lactate alone. This allows to estimate the optimal amount of glucose that cells should consume per gram produced biomass.

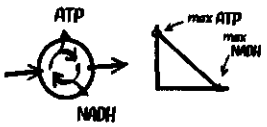

In Chapter 6 other theoretical methods to estimate metabolic fluxes in underdetermined networks are used to estimate fluxes in cyclic pathways. Linear optimization techniques are applied to determine solutions that are optimal with respect to particular "metabolic objectives". Various metabolic strategies that may be relevant for hybridoma cells are translated into so-called "linear objective functions" and used to estimate the metabolic flux distribution. It appears that the biochemical objective "maximize NADH-producing fluxes" gives flux values that approximate the values determined experimentally by isotopic-tracer studies (Chapter 5). It is speculated that this objective is in agreement with the uncontrolled oxidation of any available nutrients by continuously-growing mammalian cells, regardless of the need for ATP or NADH.

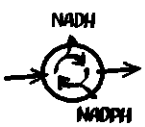

Under certain (extreme) culture conditions cells have to adapt their metabolism to the stress to which they are exposed. For example, cells in a bioreactor can be limited in oxygen supply, or certain toxic components can force the cell to redirect the fluxes into a particular direction. In Chapter 7 several experiments are described in which hybridoma cells are artificially stressed. It is shown that at oxygen limitation certain NAD(P)H-producing fluxes *decrease*, most likely to restore the disturbed $NAD(P)^+$/NADPH balance. Under oxidative stress the opposite occurs: NAD(P)H-producing fluxes *increase.* Other fluxes which -strictly speaken- cannot be determined by balancing techniques alone are subsequently estimated with "physiologically meaningful" objective functions. These objectives are associated with the metabolic strategy to adapt to the relevant

stress. For example, at oxygen limitation the objective function "minimize NADH-producing fluxes" applies.

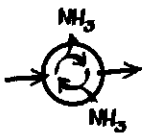

Ammonia is a waste product that is toxic for mammalian cells at relatively low concentrations and it limits the cell density in bioreactors. In Chapter 8 it is shown by flux-balancing techniques that hybridoma cells can reduce ammonia levels by converting ammonia and α-ketoglutarate into glutamate (a reaction catalyzed by the enzyme glutamate dehydrogenase). This suggests that overexpression of this enzyme may allow mammalian cells to survive higher concentrations of ammonia, which potentially enables high-cell density cultures.

It has been demonstrated that an important fraction of fluxes of large metabolic networks such as mammalian-cell metabolism can be estimated with only mass-balancing techniques. For the determination of fluxes in cyclic pathways isotopic-tracer experiments remain indispensable. However, relative trends in intracellular metabolic fluxes upon changes in extracellular conditions can be determined solely by mass-balancing techniques even if the metabolic network is principally underdetermined. The *combination* of flux-balance models and isotopic-tracer studies, of which an example is given in Chapter 5, will be the future tool of quantitative flux analysis of complex metabolic networks.

Samenvatting

In de biofarmaceutische industrie worden dierlijke cellen gekweekt als produktiesystemen voor recombinante eiwitten (zoals bijvoorbeeld EPO, tPA, en de bloedfactoren FVII and FVIII), vaccins, en monoclonale antilichamen. Dierlijke cellen zijn de enige cellen die geschikt zijn als expressiesysteem van veel therapeutische eiwitten, omdat ze in staat zijn deze correct te vouwen en te glycosileren. In tegenstelling tot normale cellen in dierlijk weefsel hebben gekweekte dierlijke cellen de eigenschap dat ze niet gedifferentieerd zijn en zich ongeremd kunnen vermenigvuldigen. Dit maakt ze sterk verwant aan tumorcellen. Ook wat betreft de stofwisseling komen gekweekte cellen en tumorcellen sterk overeen. In het algemeen kan worden gesteld dat de stofwisseling van continu groeiende cellen slecht gecontroleerd is: er is een hoge metabole activititeit en een grote verkwisting van energie en nutriënten. De opname van suiker en verschillende aminozuren is niet afgestemd op de behoefte voor groei en energie. Daardoor worden er onnodig afvalstoffen opgehoopt, zoals melkzuur, kooldioxide en koolzuur, die het kweekmedium verzuren. Bovendien zijn beide celtypen niet in staat om ureum (een afvalprodukt van het stikstofmetabolisme) te maken, een functie die in zoogdieren normaal door levercellen wordt vervuld. Gevolg is dat ze ammoniak uitscheiden, dat ophoopt tot toxische concentraties.

Uit een en ander is duidelijk dat de stofwisseling van gecultiveerde dierlijke cellen verre van optimaal is om ze te gebruiken als efficiënt produktiesysteem van eiwitten. Optimalisatie van de stofwisseling van dierlijke cellen is daarom een interessante optie om de opbrengst te verhogen en de produktiekosten te verlagen. Het is daarvoor gewenst om de stofwisseling nader te analyseren en eventuele knelpunten op te sporen. Hiervoor dienen de relevante intracellulaire omzettingssnelheden, oftewel "de metabole fluxen", te worden bepaald. Intracellulaire metabole fluxen kunnen worden bepaald door cellen met isotoop-gelabelde substraten te incuberen en de isotopenverdeling van eindprodukten te meten. Deze methode is echter (i) onpraktisch omdat slecht één metabolische route per tracerexperiment kan worden geanalyseerd, (ii) zeer duur en (iii) niet toepasbaar op industriële schaal. Een alternatieve methode is gebaseerd op het

oplossen van een set van lineaire vergelijkingen die de massabalansen van de verschillende metabolieten voorstellen. In dit proefschrift wordt deze nieuwe methode toegepast op dierlijke celkweek.

Intracellulaire metabole fluxen kunnen worden berekend als de extracellulaire produktie- en consumptie-snelheden van de relevante metabolieten en de reactiestoichiometrie (de molaire verhouding tussen de substraten en produkten bij stofwisselingsreacties) bekend zijn. Echter, in de stofwisseling van dierlijke cellen komt een aantal cyclische metabole routes voor waardoor het stelsel van vergelijkingen niet meer oplosbaar is; hoewel er evenveel 'vergelijkingen' (massabalansen voor de metabolieten) als 'onbekenden' (metabole fluxen) zijn, kunnen metabole fluxen in *cyclische* routes niet worden berekend omdat ze lineair afhankelijk zijn. Dit is de centrale probleemstelling van dit proefschrift en wordt nader uitgelegd in Hoofdstuk 1. Bovendien wordt opgemerkt dat, hoewel er geen unieke oplossing is voor de intracellulaire fluxen, er wèl een oplossingsgebied is waarbinnen alle toegelaten oplossingen vallen.

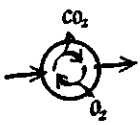

In alle cyclische stofwisselingsroutes worden co-metabolieten geproduceerd of opgenomen. Zo is bijvoorbeeld kooldioxide (en koolzuur) een afvalprodukt van de citroenzuur- en pentosephosphaatcyclus. Door de kooldioxideproduktiesnelheid te bepalen zou het daarom mogelijk kunnen zijn om de stroom door deze essentiële cyclische routes te schatten. Echter, het was tot voor kort niet mogelijk om de kooldioxideproduktie in dierlijke celkweek te bepalen, omdat in het kweekmedium kooldioxide en koolzuur worden gebruikt als buffersysteem om de zuurtegraad constant te houden. In hoofdstuk 2 wordt hiervoor een oplossing gegeven: door massabalansen op te stellen voor zowel kooldioxide (in de gasfase van bioreaktor) als kooldioxide en koolzuur (in de vloeistoffase) kon een methode worden ontwikkeld om de kooldioxide produktiesnelheid te bepalen.

In hoofdstuk 3 wordt vervolgens aangetoond dat deze methode correct is: de totale koolstofbalans voor gekweekte dierlijke cellen is sluitend als deze methode wordt toegepast. Tevens wordt in combinatie met de stikstofbalans een statische analyse toegepast waarmee wordt laten zien dat er geen grove meetfouten in de metabolieten-analyse voorkomen, en dat alle relevante metabolieten zjin meegenomen. Nu kan de fluxanalyse beginnen....

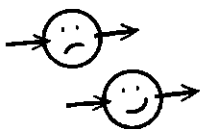

De intracellulaire fluxen kunnen echter nog niet worden bepaald, ook als de kooldioxide-produktiesnelheid bekend is. Dit komt omdat kooldioxide, net zoals andere co-metabolieten, niet slechts in één maar in meerdere cyclische routes wordt geproduceerd. Fluxen in verschillende cyclische metabole routes die dezelfde co-metabolieten produceren, blijven daardoor lineair afhankelijk. Er is dus meer informatie nodig om de werkelijke metabole fluxverdeling te berekenen uit het toegelaten oplossingsgebied dat bepaald wordt door de massabalansen. In hoofdstuk 4 wordt een enigszins kunstmatige oplossing voorgesteld: de oplossing waarvoor geldt dat de som van het kwadraat van de fluxen het kleinst is, wordt geselecteerd. Deze methode gaat van de aanname uit dat fluxen in cyclische routes de meest efficiënte weg (met de kleinste netto flux) kiezen. Deze methode wordt toegepast op hybridoma cellen onder zowel optimale als suboptimale kweekomstandigheden.

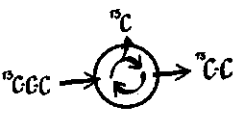

De extra aanname uit hoofdstuk 4 blijkt voor de onderzochte hybridomacellen niet te kloppen. In hoofdstuk 5 worden de fluxen in cyclische routes experimenteel gemeten met ^{13}C-gelabelde substraten. Daar gelabelde substraten zeer kostbaar zijn, is om dit experiment uit te voeren een mini-reaktor ontworpen (met een volume van 100 ml) waarin de cellen onder condities die vergelijkbaar zijn met industriële omstandigheden kunnen worden gekweekt. De hoeveelheid ^{13}C in koolzuurgas wordt gemeten met massa spectrometrie, en de ^{13}C in melkzuur wordt geanalyseerd met NMR spectrometrie. Door middel van een algoritme is de informatie van massabalansen en van het isotopenexperiment samengevoegd, waardoor het mogelijk is om uit één enkel ^{13}C-experiment

fluxen uit drie verschillende cyclische routes te bepalen. Dit maakt de onpraktische isotoop-experimenten eenvoudiger en minder foutgevoelig. De in hoofdstuk 2 ontwikkelde methode om de kooldioxideproduktiesnelheid te bepalen bleek overigens essentieel te zijn voor het correct berekenen van fluxen met behulp van het genoemde algoritme.

Het blijkt dat snelgroeiende hybridoma cellen een hogere activiteit van de pentose-phosphate cyclus hebben dan algemeen verondersteld werd. Aangenomen dat deze activiteit als doel heeft de cel van NADPH te voorzien (een co-metaboliet noodzakelijk voor biosynthese van verschillende macromoleculen), betekent dit onder andere dat tenminste een deel van de suikeropname efficiënt gebruikt wordt, ookal wordt er uiteindelijk het afvalproduct melkzuur gemaakt.

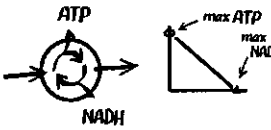

Omdat met behulp van de theoretische methode, voorgesteld in hoofdstuk 4, de fluxen in cyclische routes niet correct geschat kunnen werden, worden enkele andere methoden beproefd. Deze zijn gebaseerd op lineaire programmeringstechnieken, ook wel 'optimaleringstechnieken' genoemd. (Het principe van deze methode is gevisualiseerd in Figuur 3 van Hoofstuk 1). Hierbij wordt aan een onderbepaald stelsel vergelijkingen een bepaalde doelfunctie toegevoegd, waarmee uit het toegelaten oplossingsgebied de voor die doelfunctie optimale oplossing berekend wordt. Verschillende doelfuncties die biochemisch gezien relevant lijken voor hybridomacellen zijn vervolgens gebruikt om fluxen in cyclische routes te schatten. Het blijkt dat de doelfunctie "maximaliseer NADH-producerende fluxen" het best de experimenteel gevonden fluxen (uit Hoofdstuk 5) benadert. Deze doelfunctie komt overeen met het feit dat continu-groeiende dierlijke cellen op ongecontroleerde wijze metabolieten verbranden, ongeacht de behoefte voor energie.

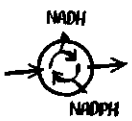

Soms veranderen kweekcondities zodanig dat de metabole strategie van de cellen aangepast moet worden. In de dierlijke celkweek kan bijvoorbeeld zuurstoflimitatie optreden. Ook kunnen bepaalde toxische stoffen de cel ertoe dwingen de stofwisselings-

strategie aan te passen. In hoofdstuk 7 worden verschillende kweken beschreven waarbij de cellen aan bepaalde vormen van stress worden blootgesteld. Het blijkt dat bij zuurstoflimitatie de NAD(P)H-producerende fluxen relatief hoog zijn, terwijl het omgekeerde gebeurt bij hoge zuurstofspanning. De fluxen die strikt genomen niet met behulp van massabalansen kunnen worden bepaald, worden vervolgens geschat met doelfuncties die overeenkomen met de strategie die de cellen nodig hebben om zich aan de opgelegde stress aan te passen. Zo past bij zuurstoflimitatie bijvoorbeeld de doelfunctie "minimaliseer NADH-producerende reacties".

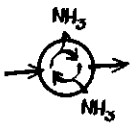

Ammonia is een afvalprodukt van de stofwisseling dat bij voorcelkweek-gangbare concentraties giftig is, en verdere groei remt. In hoofdstuk 8 wordt met behulp van de massabalansen aangetoond dat hybridomacellen ammonia detoxificeren door het met α-ketoglutaraat te laten reageren tot glutamaat (een reactie die wordt gecatalyseerd door het enzym glutamaatdehydrogenase). Dit betekent dat het mogelijk zou zijn om dierlijke cellen in cultuurmedium met hogere concentraties ammonia te laten overleven, als glutamaatdehydrogenase tot over-expressie wordt gebracht. Hierdoor zijn theoretisch celkweken met een hogere celdichtheid mogelijk.

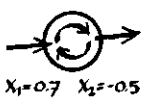

Dit proefschrift laat zien dat een groot deel van de metabole fluxen in dierlijke celkweek kan worden geschat met behulp van massabalansen. Om fluxen in cyclische stofwisselingsroutes the bepalen blijven experimenten met isotopisch gelabelde substraten echter onontbeerlijk. Relatieve trends in intracellulaire fluxen kunnen wel worden aangetoond, zelfs als het netwerk in principe onderbepaald is. De *combinatie* van massabalansen en isotoopexperimenten, waarvan een voorbeeld is gegeven in hoofdstuk 5, is *de* methode van de toekomst om fluxen in complexe stofwisselingssytemen te kwantificeren.

Bibliography

Publications

Van der Pol, L., Bonarius, H.P.J., Van de Wouw, G., and Tramper, J. 1993. The effect of silicone antifoam on the shear-stress sensivity of hybridoma cells in sparged cultures. *Biotechnol. Progr.* **9**: 504-509.

Ibba, M., Bonarius, H.P.J., Kuhla, J., and Kuenzi, M. 1993. Mode of cultivation is critical for the optimal expression of recombinant Hirudin in *S.cerevisiae*. *Biotechnol. Lett.*: **15**: 667-672.

Bonarius, H.P.J., De Gooijer, C.D., Tramper, J., and Schmid, G. 1995. Determination of the respiration quotient in mammalian cell culture in bicarbonate-buffered media. *Biotechnol. Bioeng.* **45**: 524-535 (Chapter 2 of this dissertation).

Bonarius, H.P.J., Meesters, K.P.H., Schmid, G. and Tramper, J. 1995. Determination of metabolic fluxes in animal cells. pp. 111-115. *In:* Beuvery, E.C., Griffiths, B., and Zeijlemaker, W.P. Animal Cell Technology. Kluwer Academic Publishers, Dordrecht, NL.

Bonarius, H.P.J., De Gooijer, C.D., Tramper, J., and Schmid, G. 1995. Carbon dioxide evolution rates in animal cell culture in bicarbonate buffered and bicarbonate free medium. *In:* Animal Cell Technology. Proceedings of the 13th ESACT meeting. R.E. Spier, et al. (Eds), Butterworth-Heinemann Ltd, Wiltshire.

Bonarius, H.P.J., Hatzimanikatis, V., Meesters, K.P.H., De Gooijer, C.D., Schmid, G., and Tramper, J. 1996. Metabolic flux analysis of hybridoma cells in different culture media using mass balances. *Biotechnol. Bioeng.* **50**: 299-318 (Chapter 4 of this dissertation).

Bonarius H.P.J., Özemre, A., Timmerarends, B., Skrabal, P., Heinzle, E., De Gooijer, C.D., Tramper J., and Schmid, G. 1997. Metabolite flux analysis of hybridoma cells using mass balances, $^{13}CO_2$ mass spectrometry and NMR spectrometry, pp. 633-638. *In:* Carrondo, M.J.T., Griffiths, B., and Moreira, J.L.P. Animal Cell Technology. Kluwer Academic Publishers, Dordrecht, NL.

spectrometry, pp. 633-638. *In:* Carrondo, M.J.T., Griffiths, B., and Moreira, J.L.P. Animal Cell Technology. Kluwer Academic Publishers, Dordrecht, NL.

Bonarius, H.P.J., Schmid G., and Tramper, J. 1997. Flux analysis of underdetermined metabolic networks: The Quest for the Missing Constraint. *Trends in Biotechnol.* **15**: 308-314. (Chapter 1 of this dissertation)

Bonarius, H.P.J., Nielsen, N.V., and Kongerslev, L. 1997. Optimal image analysis software for rapid and reliable determination of cell numbers in mammalian-cell culture. *Abstr. Am. Chem. Soc.* **213**: 206.

Bonarius, H.P.J., Houtman, J.H.M., De Gooijer, C.D., Tramper, J., and Schmid, G. 1998. Glutamate-dehydrogenase activity is increased in ammonia-stressed hybridoma cells. *Biotechnol. Bioeng.* **57**: 447-453 (Chapter 8 of this dissertation).

Bonarius, H.P.J., Timmerarends, B., De Gooijer, C.D., and Tramper, J. 1998. Metabolite balancing techniques versus ^{13}C tracer experiemtents to determine metabolic fluxes in hybridoma cells. *Biotechnol. Bioeng.* **58**: 258-262 (Chapter 6 of this dissertation).

Bonarius, H.P.J., Özemre, A., Timmerarends, B., Skrabal, P., Heinzle, E., Schmid, G., and Tramper, J. 1998. Metabolic-flux analysis of continuously cultured hybridoma cells using $^{13}CO_2$ mass spectrometry in combination with NMR spectroscopy and metabolite balancing. *Submitted.* (Chapter 5 of this dissertation).

Bonarius, H.P.J., Houtman, J.H.M., Schmid, G., De Gooijer, C.D., and Tramper, J. 1998. Metabolic-flux analysis of hybridoma cells under oxidative and reductive stress using mass balances and physiologically meaningful constraints. (Chapter 7 of this dissertation).

Bonarius, H.P.J., Houtman, J.H.M., Schmid, G., De Gooijer, C.D., and Tramper, J. 1998. Error analysis of metabolic-rate measurements in mammalian-cell culture by carbon and nitrogen balances. *Acc. for publication in Cytotechnol.* (Chapter 3 of this dissertation)

Bonarius, H.P.J., De Gooijer, C.D., and Tramper, J. 199?. Flux balances in mammalian-cell culture: Methods & applications. *To be published in:* The Encyclopedia of Cell Culture Technology. Spier, R. (Ed.) (Chapter 9 of this dissertation).

Patent

Bonarius, H.P.J. 1997. Proliferation control of eukaryotic cells producing heterologous proteins by nucleotide-manipulating agents. Danish Patent Application No. DK 1490/97.

Bibiography

Curriculum Vitae

In 1986 Hendrik Bonarius started studying Food Science at the Agricultural University in Wageningen, The Netherlands, after a stay at Leiden University (1983-1986), where he studied Psychology. In 1990 he visited the laboratory of Drs L. Van der Pol at Bio-Intermediar BV (currently DSM BV), Groningen to explore the shear-stress sensitivity of hybridoma cells in sparged bioreactors. A year later he worked at the laboratory of Dr. M. Griot., Department of Biotechnology at Ciba-Geigy AG (currently Novartis AG), Basel, Switzerland, on a project to improve plasmid stability in *Saccharomyces cerevisiae* for the production of β-interferon. In 1992, he received his first degree at the Agricultural University of Wageningen, in Food technology, specialization in Bioprocess Engineering.

The same year, he started a PhD project on metabolic-flux analysis of mammalian-cell culture in the laboratory of Dr. G. Schmid, Department of Biotechnology, Hoffmann-La Roche AG, Basel, Switzerland, which is reported in this dissertation. The project was also supervised by Dr. J. Tramper (Agricultural University Wageningen, The Netherlands). He visited the laboratory of Dr. E. Heinzle, Department of Chemical Engineering, Eidgenössische Hochschule Zürich, Switzerland, in 1995, to analyse metabolic fluxes of mammalian-cell culture with mass and NMR spectrometry (Chapter 5 of this thesis).

Since 1996, Hendrik Bonarius works at the Department of Cell Biology, Novo Nordisk AS, Gentofte, Denmark, on the development of production processes of glycoproteins based on cell-culture technology.